"THIN WALLED STRUCTURAL FORMS UNDER ECCENTRIC COMPRESSIVE LOAD ACTIONS".

A Thesis presented for the Degree of Doctor of Philosophy of the University of Glasgow.

by

Alastair C. Walker M.Sc., A.R.C.S.T.

11 Kelvin Drive,
Kirkintilloch,
GLASGOW.

June 1964.

ProQuest LLC.
789 East Eisenhower Parkway
P.O. Box 1346
Ann Arbor, MI 48106 – 1346

CONTENTS.

A B S T R A C T

ABSTRACT.

The investigation was carried out to determine the load bearing characteristics of flat rectangular plates and structural shapes when they are subjected to eccentric end compressive load actions.

A short review of relevant published literature is presented in Chapter I of the thesis. This reveals that the bulk of the research in the field of thin walled structural forms has been concerned with uniform loading. In structures such as those found in aircraft and light civil engineering applications the resultant of the direct compressive load is often offset from the centroid of the component cross-section leading to non-uniform load distribu-:tions. It is to provide information into this condition of loading that this investigation was designed.

The subject matter of the thesis is divided into two main sections, the first, which comprises Chapters II - V, deals analytically and experimentally with individual plates while the second section, comprising Chapters VI - VIII, is similarly concerned with certain structural shapes.

Chapter II begins with a brief derivation of the general large deflection equations appliable to all types of end compressive loading; this is followed by an outline of the Galerkin method of solving differential equations. The chapter then presents the derivation of a series solution developed by the author specifically suitable for the solution of the basic equations in the case of a variety of non-uniform load applications.

In the first part of Chapter III this generalised solution is applied to the determination of the elastic instability loads for a range of eccentricities.

In the second part of the chapter the basic large deflection equations are then solved for the post-buckling behaviour and, with the introduction of a simple yield criterion, the collapse load values for single plates under a variety of load conditions are derived. The values presented have been arrived at by matrix formulation of the appropriate equations and the design of computer programmes of general application.

The plate experimental investigations are described in Chapter IV, these took the form of some forty tests to collapse on plates of varying thicknesses. For this purpose special loading and photogrammetric equipment was designed and built.

These experimental and theoretical results are compared and fully discussed in Chapter V. It is generally shown that good agreement is obtained and the findings also sub-:stantiate the assumptions made of the mechanics of collapse.

In Chapter VI an original approximate analytical treatment of short thin walled structural forms subjected to eccentric compressive load action is presented. This is based on the assumption that such sections may be considered as being composed of individually compressed plates which can then be treated as indicated in the earlier chapters of this thesis. Compatibility of boundary conditions along the unloaded adjoining edges is obtained using geometrical

constructions.

To determine the efficacy of the above analysis a special test rig was designed and built. This is described in Chapter VII in which results of approx-:imately forty tests to collapse of lipped and plain thin walled channel sections of various thicknesses are also presented.

In Chapter VIII these experimental results are compared to the predictions of the theoretical analysis. The agreements are seen to be good thus indicating that the assumptions are rational and that the method developed here may be used to give good engineering forecasts of the initial instability and collapse loads of eccentrically loaded plain and lipped short thin walled channels.

This chapter is followed by a summary of the find-:ings of the whole investigation. The thesis is con-:cluded by six appendices which enlarge on various aspects of the analysis and also present the character-:istics of the materials used in the tests.

N O M E N C L A T U R E

NOMENCLATURE.

The following symbols are used throughout the text. Any additional symbols are defined where they first appear.

D	flexural rigidity of the plate.
E	Young's Modulus of elasticity of the plate material.
F	Airy's stress function.
F'	Airy's stress function in non-dimensional terms.
H	channel shape factor.
N_x, N_y	normal forces per unit length in the middle plane of the plate in the x and y directions, respectively.
N_{xy}	shearing force in direction of y axis per unit length of a section of the plate perpendicular to x axis.
M_x, M_y	bending moments per unit length of sections of the plate perpendicular to the x and y axes, respectively.
N_o	the value of N_x at $y = b/2$, $x = o$ and $x = a$

N_o'	non-dimensional form of N_o.
N_{crit}	the value of N_o which causes initial instability.
P	total load applied to plate or channel in x direction.
$P_{cr.}$	plate, or channel, instability load.
P_{max}	plate, or channel, maximum load.
a	plate, or channel, length.
b	plate width.
b_f	flange width of a channel section.
b_w	web width of a channel section.
h	plate thickness.
$b_{oo}, b_{o1},$	coefficients in the Galerkin series for stress function.
i, j, k, n	integers used in the Galerkin series for deflection.
l	limit in deflection series.
m	number of half sine waves in the x direction.

r, s, p, q integers used in the Galerkin series for stress function.

t, u limits in the stress function series.

r_0, r_1 degree of rotational restraint per unit distance in x direction as plate edges $y = b/2$ and $y = -\frac{b}{2}$ respectively.

$q_0, q_1,$ coefficients in the Galerkin series for deflection.

u, v deformation of the plate middle plane in the x and y directions, respectively.

w deflection of a point in the middle plane of the plate in a direction normal to the undeformed plate.

x, y, z plate cartesian co-ordinates.

z'', z', z distances measured on photographic plate.

α load eccentricity parameter.

β an angle in the photogrammetric optical system.

ϕ ratio of plate length to width.

ϕ_f length to width ratio for flange of a channel section.

ϕ_w length to width ratio for web of a channel section.

K_0, K_1 degree of rotational restraint per unit distance in x direction at plate edges $y = b/2$ and $y = -b/2$, respectively, in non-dimensional form.

K_f degree of rotational restraint per unit distance in x direction at the edge of a flange which adjoins the web.

K_w degree of rotational restraint per unit distance in x direction at the unloaded edges of the web of a channel section.

ν Poisson's ratio for plate and channel material.

ξ, η plate cartesian co-ordinates in non-:dimensional form.

θ an angle in the photogrammetric optical system.

ω deflection of a point on the middle surface of the plate in a direction normal to the undeformed plate, in non-dimensional form.

σ_x, σ_y direct stresses in the x and y directions, respectively.

σ_{yield} yield stress of the plate and channel material.

σ_{max} maximum applied stress in the x direction for channel sections.

$\bar{\sigma}, \tilde{\sigma}$ maximum applied stress in the x direction for lipped and plain channel sections, respectively, in non-dimensional form.

σ_ξ, σ_η direct stresses in the ξ and η directions, respectively, in non-dimensional form.

σ_{ξ_2} direct stress in the direction in the middle plane of the plate at $\eta = 0.5$, in non-dimensional form.

τ_{xy} shear stress in the x-y plane.

$\tau_{\xi\eta}$ shear stress in the ξ-η plane, in non-:dimensional form.

ϵ_x, ϵ_y direct strains in the x and y directions, respectively.

$\epsilon_\xi, \epsilon_\eta$ direct strains in the ξ and η directions, respectively.

γ_{xy} shear strain in the x-y plane.

$\gamma_{\xi\eta}$ shear strain in the ξ-η plane, in non-dimensional terms.

The chapters, section and equations have been numbered in accordance with the decimal system of reference. In this the first figure denotes the chapter, the second the section and the subsequent figures give the appropriate equation number. For example, III.3.16 should be read as Chapter three, section three and equation sixteen.

C H A P T E R I

CHAPTER I.

INTRODUCTION AND REVIEW OF RELEVANT PUBLISHED LITERATURE.

The use of thin plates and structural sections composed of thin plates as load bearing elements is widespread in Aeronautical and Civil Engineering. There are two main phases in the behaviour of these flat plate elements when they are compressed longitudinally in their own plane. The first to be encountered as the load is increased is instability, also known as buckling. At this load the original flat plate shape is no longer tenable and from energy considerations a deflected configuration must be taken up.

When the plates are formed into thin-walled structural components buckling can take two forms, i.e. overall instability and local instability. In the former the element is usually in the form of a column in which the length is very much greater than any of the cross-sectional dimensions. This type of buckling is characterised by a lateral movement of the cross-section, or twisting of the cross-section about the column axis, or a combination of these effects. In any of these cases the cross-sectional shape is substantially unaltered. Local buckling, however, is characterised by a change in the shape of the cross-section. This phenomenon occurs in columns where the length is of the same order as the cross-sectional dimensions and it is this type of buckling which is

considered in this thesis.

The second important phase in the load bearing behaviour is collapse. It is one of the important features of short thin plate structures that this phase may follow the preceding one after a significant load increase.

In aircraft structures, where the elements are more fully utilised than in similar Civil Engineering applications, it was common at one time for the plates to be loaded into the post-buckling region. However, with the advent of supersonic aircraft this is no longer the case. Now the prime necessity is for the maintenance of the designed aerodynamic shape of the vehicle. Thus once more accurate knowledge of buckling loads is important.

This is not to say that post-buckling characteristics and collapse loads are neglected by designers. Some factor of load reserve must be employed and it is from such information that it can be calculated. This is equally the case in Civil Engineering applications.

Since the beginning of this century considerable research has been carried out into the problem of thin flat plates longitudinally loaded in compression. In this chapter the more important of the published results of this research are briefly reviewed. For simplicity of presentation the review is made under two headings:

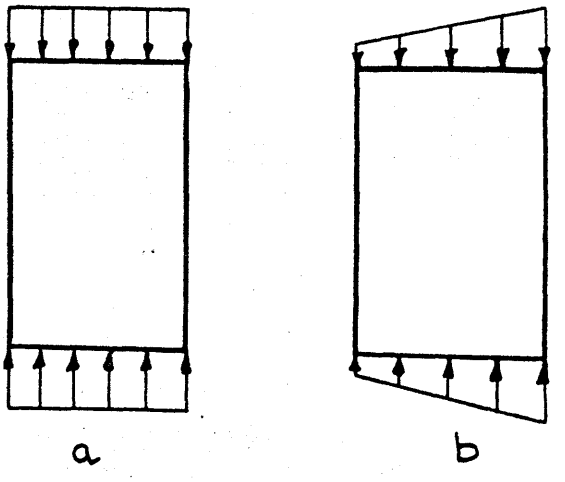

FIG. I.1.

1. Instability.
2. Post-buckling and collapse.

Each heading is further sub-divided into:

a. Plates.
b. Structural shapes.

I.1a Instability of Thin Flat Plates.

The differential equation of equilibrium for a flat plate under compressive load actions in its own plane was first presented by St. Venant (1883). An exact solution to this equation is available if the plate is compressed along two opposite simply supported edges by a uniform load distribution. Such a plate is shown in Figure I.1a; the unloaded edges may have any compatible boundary conditions. No exact analytical solution has yet been published when the load distribution is other than uniform, for example, the important case of a linear distribution (Figure I.1b).

In such conditions the energy method presented by Bryan (1891) is of considerable value. This utilises the phenomenon of neutral equilibrium which exists at the instability load. This method was extensively developed by Timoshenko (1961) to obtain the elastic instability loads for plates with linear load distribution. A Fourier series was used to represent the deflected shape and results were

presented for simply supported loaded edges and simply supported or built-in unloaded edges. Much the same approach was used by Johnson and Noel (1953); in this case the eccentricity of the load distribution was such as to cause one unloaded edge to be in tension. This edge was considered to be simply supported while the other was subject to an elastic rotational restraint.

I.1b Local Instability of Open Structural Shapes.

Bleich (1924) was the first to present an analytical approach to the local elastic instability of thin walled channel sections. He considered the channel as a collection of single thin plate elements which have a degree of elastic rotational restraint at their common edges. Since use was made of the analytical solution to St. Venant's equation the results were restricted to sections subjected to a uniform load distribution and with simply supported loaded edges. (These conditions apply similarly to all the published literature on structural component instability reviewed herein.) The rotational restraint was considered to be applied by the neighbouring element and could theoret-:ically vary between the simply supported condition and built-in.

Lundquist, Stowell and Shuette (1943) developed a method based on the principle of moment distribution. In order to obtain the instability of a section it was necessary to know the stiffness and carry-over factors as defined in the principle. In two collections of tables and charts Kroll (1943) presented these factors for a

collection of plates in such a way as to minimise interpolation for designers.

Chilver (1951) provided a more direct method of solution in which the general solutions to St. Venant's equation for the constituent plates were solved simul-:taneously with the relevant boundary conditions using determinant theory. This facilitated the evaluation of the local instability load of any section composed of plate elements; the number of elements involved was only limited by the unwieldiness of the resulting algebra. Experimental results showed excellent agreement when the method of Southwell (1932) was used to analyse the experi-:mental observations.

Harvey (1953) obtained the boundary rotational restraint factor in the form of a transcendental equation. For any chosen value of web to flange width ratio and web aspect ratio the instability load of the section could be obtained from this equation by trial and error approximation procedures.

I.2a Post-buckling Characteristics and Collapse Loads of Thin Plates.

The region of loading subsequent to buckling is characterised by a rapid increase in the lateral deflections. of the plate. This is accompanied by change of the stress pattern due to the stretching of the plate middle plane

surface. These two effects taken together complicate considerably the mathematical study of this loading region.

Although Von Karman (1910) some time ago developed the differential equations describing the interaction of the lateral deflection and stress distribution it is only in recent years that any great success has been enjoyed in obtaining a solution to them. Levy (1942) using a Fourier series for each of the unknown functions, i.e. deflection and stress distributions, developed an approximate solution for a plate simply supported on all edges and uniformly compressed along two opposite edges. All the edges were constrained to remain straight and results were presented for square plates only. Levy's method has since been adapted to investigate the load bearing characteristics of plates subject to other boundary conditions. Coan (1951) set out to obtain a more realistic picture of the true experimental conditions. The edges of the plate were free to translate in the plane of the plate and the plate was considered to have a small initial curvature. The loaded edges could be subject to uniform displacements, uniform stress or uniform strain distributions. The direct use of Levy's method to predict the effect of small initial deviations from initial flatness, with boundary conditions similar to those of the plate in Levy's study, was studied by Hu et al. (1946). A more generalised approach was given by Yamaki (1959). Here again a Fourier series was used but in this case the stress function equation was solved using Galerkin's method. Results were presented for square plates with uniform displacement of loaded edges in the

plane of the plate and the unloaded edges simply supported or built-in.

These three last mentioned contributions are extremely important from a practical point of view as no plate is truly flat. Since buckles begin to grow with the beginn-:ing of loading for a plate that has an initial deviation from flatness, there can be no buckling stress for an actual plate in the strictly theoretical sense; however, just as a defined yield stress has been found useful for materials that have no actual yield stress, so a defined buckling or critical stress for a plate can convey much meaning when designing plate structures or interpreting experimental results. Both Coan and Hu concluded that the commonly used method of "top-of-the-knee" and "strain reversal" underestimated the theoretical flat plate criti-:cal load. In the latter paper it was shown that while, in general, the "Southwell Plot" method might not be expected to give satisfactory results it could be used in the loading region well below the critical load for plates with only slight initial deviations from flatness.

The theory developed by Levy and subsequently modified has been used only for square plates which buckle into one half wave in the direction of loading. For plates in which the length, i.e. the dimension taken in the direction of loading, is greater than the breadth it is possible for two or more half waves to develop at the buckling load. Also, depending on the magnitude of the length to breadth ratio, it is possible for this number to increase as the loading proceeds. This phenomenon was

indicated in a theoretical study carried out by Stein (1959). Wave length was considered as being closely related to the strain energy content of the plate. As the loading increased there could come a point at which the energy contained in a deflected shape of say one half wave was greater than if the plate was deflected in two half waves. Theoretically, therefore, a change of wave length was indicated. In practice this change might be delayed or advanced by slight deviations of the actual plate condition from the ideal. The expression for the strain energy contained in a plate with large deflections is extremely complicated so that, in order to maintain clarity of study, a simplified mathematical model was used instead. With this it could be shown that there are several paths of loading and unloading which might be followed. Some led to conditions of continuous change of wavelength whereas others led to snapping or "explosive" changes. The path which was followed by the plate could be dictated by the initial conditions of the plate and also whether the loading was induced by controlled end thrust or controlled end movement.

In a subsequent paper Stein (1959) presented a solution of the Von Karman equations by using a modified perturbation method. The non-linear differential equations were convert-:ed to an infinite set of linear differential equations by expanding the displacements into a power series in terms of an arbitrary parameter. The analytical treatment of a finite selection of these equations gave an approximate solution to the problem. Continuous wave length change was not tackled here; the plate was assumed to have deflected in a specific

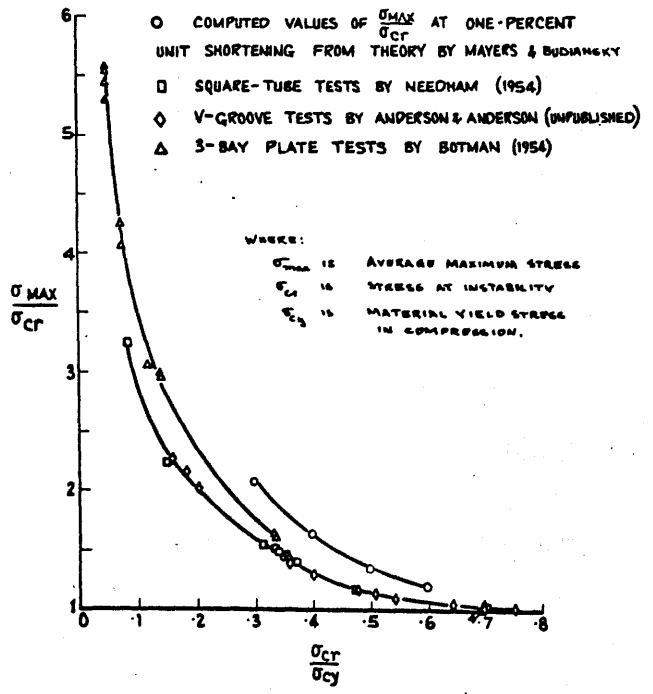
O COMPUTED VALUES OF $\frac{\sigma_{MAX}}{\sigma_{cr}}$ AT ONE-PERCENT UNIT SHORTENING FROM THEORY BY MAYERS & BUDIANSKY
□ SQUARE-TUBE TESTS BY NEEDHAM (1954)
◇ V-GROOVE TESTS BY ANDERSON & ANDERSON (UNPUBLISHED)
△ 3-BAY PLATE TESTS BY BOTMAN (1954)
WHERE:
σ_{max} IS AVERAGE MAXIMUM STRESS
σ_{cr} IS STRESS AT INSTABILITY
σ_{cy} IS MATERIAL YIELD STRESS IN COMPRESSION.
$\frac{\sigma_{MAX}}{\sigma_{cr}}$
$\frac{\sigma_{cr}}{\sigma_{cy}}$
6
5
4
3
2
1
0
·1
·2
·3
·4
·5
·6
·7
·8

FIG. I 2.

wave length. Results of an experimental investigation also carried out by Stein showed good agreement with his theoretical conclusions.

The ultimate load bearing capacity of a plate is intimately bound up with the characteristics of the material involved. The study of collapse therefore must include not only the non-linearity of the large deflection equations but also the non-linearity of the material beyond the elastic region. This extremely difficult problem has, to date, only been fully tackled by Mayers and Budiansky (1955). Their analysis involved the application of a variational principle of the deform-:ation theory of plasticity in conjunction with computations carried out on a high speed calculating machine. The plate was assumed to consist of two stress-carrying faces only, the stress being constant through the thickness of each face. Numerical results were given for four square flat aluminium plates with straight edges compressed uniformly beyond the buckling load into the plastic range. Within the range of calculations the average applied stress did not reach a maximum, but by assuming collapse to have occurred at the large unit shortening of 0.01 an approximate maximum load was obtained. The comparison given in Figure I.2 of these theoretical results, in terms of non-:dimensional parameters, with the experimental results of Needham (1954) and Botman (1954) showed the theoretical predictions to have been high. The tests, however, were conducted on plates which did not entirely satisfy the straight edge conditions and also on multi-panel plates.

Although it was shown by Mayers and Budiansky that

CRUCIFORM & ANGLE SECTIONS

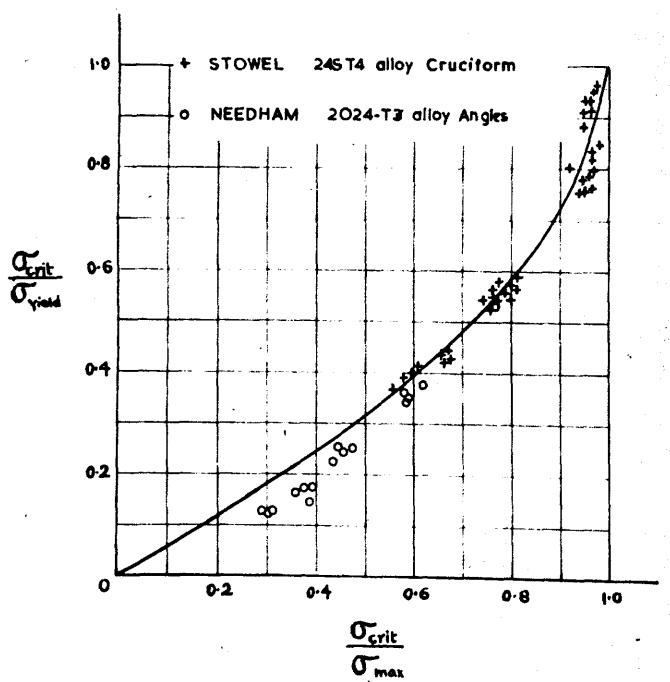

FIG. I.3

plastic stresses calculated from elastic displacements differed markedly, in their case, from the stresses calculated from purely plastic considerations, this method of mixing elastic and plastic considerations was used with some success by Stowell(1951). By extending the differential equation of equilibrium of a compressed open column, derived by Wagner (1936), it was possible to obtain the large deflection elastic behaviour of a long flat plate having one edge straight and simply supported and the other free; the loaded edges were uniformly compressed and straight. The elastic deformations so obtained were then used to evaluate the relevant plastic longitudinal direct stresses from the deformation theory of plasticity and the stress-strain curve of the material (24S-T aluminium alloy). By numerically integrating these stresses across the plate width the load was found; the process was repeated for increasing deflection until the maximum load was reached. The ultimate load was found to coincide with the stress intensity at the hinged edge attaining the yield value for the material. Experimental results showed good agreement with the predictions of this method, these are presented in Figure I.3 in non-dimensional terms.

As well as the theoretical analyses outlined above there have been several important semi-empirical approaches to plate collapse. Paramount among these is the concept of effective width proposed by Von Karman et al. (1932) and further developed by Marguerre (1942) for plates supported along both edges. In this the centre portion of the plate, i.e. the part most deflected, was considered to carry no

load. The load was carried by two outside strips, when the stress in these strips reached the yield value of the material the plate was considered to have collapsed. The empirical factor in the derived equation was supplied by Sechler (1933). Another approach, Gerard (1957), was a development of the results of Stowell (1951). This was based on the fact that collapse was closely associated with the highest attainable value of the edge stress - in this method account was taken of the unloaded edge conditions.

I.2b Collapse Loads of Structural Sections.

Up to the present time workers in this field have limited themselves to presenting design data on the collapse load alone. This data may be obtained either from consider-:ation of the section as a collection of plate elements or from empirical laws derived from tests on complete sections.

Among the first to present the former method were Sechler and Dunn (1942). Here the section was taken to be composed of individual plates which were assumed to be hinged at the common edges. The collapse load was calculated as the sum of the instability loads of the plates. These design criteria were soon shown to be inadequate by Winter (1946). In this paper the compression flanges of thin walled lipped and plain channel sections loaded as beams were studied. By noting the similarity of section test results with those of Sechler (1933) on flat plates it was concluded that the compression flange could be treated as an individual plate.

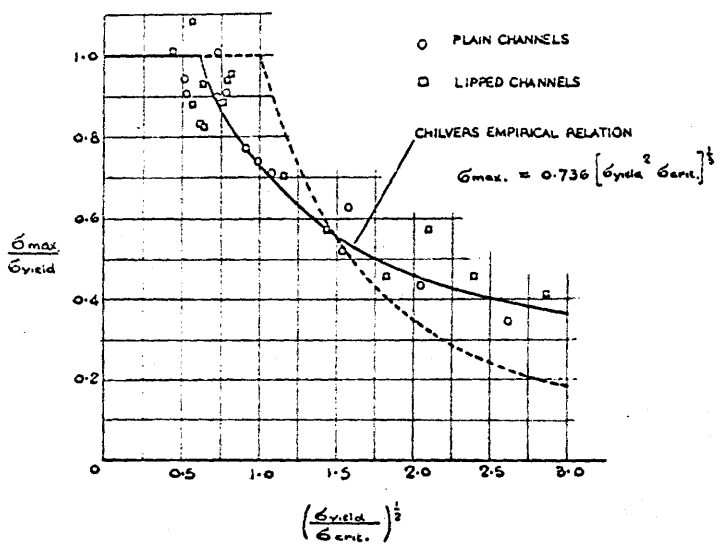
PLAIN CHANNELS
LIPPED CHANNELS
CHILVERS EMPIRICAL RELATION
$\sigma_{max.} = 0.736 \left[\sigma_{yield}^{2}\, \sigma_{crit.}\right]^{\frac{1}{3}}$
$\frac{\sigma_{max}}{\sigma_{yield}}$
1·0
0·8
0·6
0·4
0·2
0
0·5
1·0
1·5
2·0
2·5
3·0
$\left(\frac{\sigma_{yield}}{\sigma_{crit.}}\right)^{\frac{1}{2}}$

FIG. I. 4

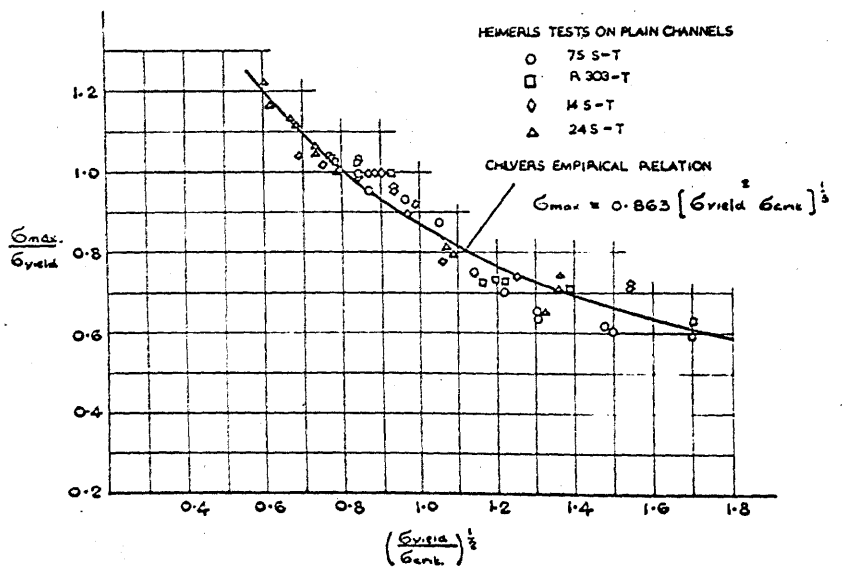
HEIMERLS TESTS ON PLAIN CHANNELS
75 S-T
R 303-T
14 S-T
24 S-T
CHILVERS EMPIRICAL RELATION
$\sigma_{max} = 0.863 \left[\sigma_{yield}^{2}\, \sigma_{crit.}\right]^{\frac{1}{3}}$
$\frac{\sigma_{max.}}{\sigma_{yield}}$
1·2
1·0
0·8
0·6
0·4
0·2
0·4
0·6
0·8
1·0
1·2
1·4
1·6
1·8
$\left(\frac{\sigma_{yield}}{\sigma_{crit.}}\right)^{\frac{1}{2}}$

FIG. I.5

In this way a design method was formulated using the effective width concept.

Needham (1954) presented a method of predicting the collapse loads of complicated structural shapes which gave good comparison with experimental results. The sections were divided not into plates but into angle elements. The collapse loads of these elements could, for any practical case, be obtained by interpolation from the results on a great number of angle geometries. The section maximum load was taken to be the sum of these loads. The method was to some extent suggested by the paper of Heimerl and Woods (1946). This showed that the tensile strength of aluminium alloy can be raised by as much as 25% by cold working when the sections are made by brake forming.

By intuitive reasoning the governing parameters for describing the ultimate load variation of open channel sections are: maximum average stress, instability stress and the material yield stress. Design criteria have been formulated from empirical relationships of these factors. To obtain the values of the constants in these relationships a great number of tests on steel and aluminium sections were carried out by Heimerl (1947), Schuette (1949) and Chilver (1953). Results are shown in Figures I.4 and I.5 with the laws derived from them.

Kenedi et al. (1955) determined various semi-empirical relations as a basis of design from a large number of tests on cold rolled plain and lipped channel sections.

C H A P T E R I I

CHAPTER II.

THE GENERALISED PLATE EQUATIONS AND THE FORMULATION OF THE GALERKIN SERIES FOR THEIR SOLUTION FOR A LINEARLY VARYING COMPRESSIVE LOAD DISTRIBUTION.

This chapter begins with an outline of the derivation of the "Von Karman" elastic large deflection equations. These are then transposed into non-dimensional terms in order to facilitate their solution and maintain clarity of presentation. This is followed by a description of the series method of solving differential equations developed by V. G. Galerkin (1915) with an indication of the advantages, and disadvantages, of the use of the method in the solution of the present problem.

The chapter finishes with a detailed derivation of the relevant boundary conditions and the resulting Galerkin Series associated with them.

II.1 Elastic Large Deflection Equations.

Considering an incremental segment of the plate and assuming no body forces present the forces and moments on it can be represented as shown in Figures II.1 and II.2. These give rise to the following equations of equilibrium

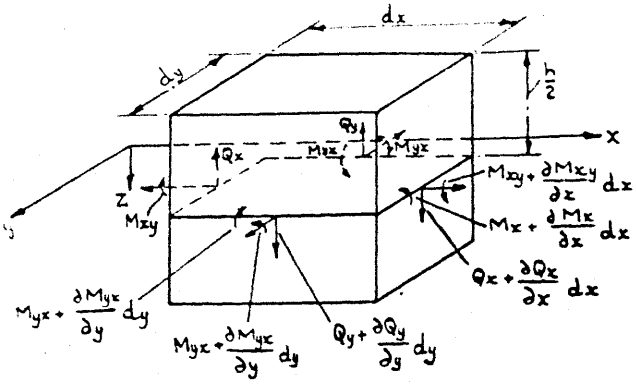

FIG II. 1.

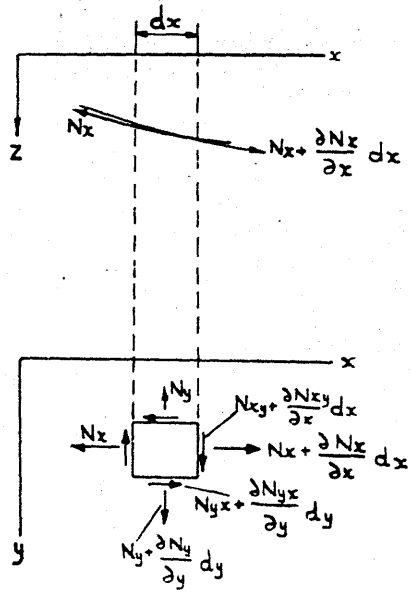

FIG. II. 2.

$$\frac{\partial N_x}{\partial x} + \frac{\partial N_{xy}}{\partial y} = 0 \qquad \text{II.1.1a.}$$

$$\frac{\partial N_y}{\partial y} + \frac{\partial N_{xy}}{\partial x} = 0 \qquad \text{II.1.1b.}$$

$$\frac{\partial^2 M_x}{\partial x^2} - 2\frac{\partial^2 M_{xy}}{\partial x \partial y} + \frac{\partial^2 M_y}{\partial y^2} = -\left(N_x \frac{\partial^2 w}{\partial x^2} + N_y \frac{\partial^2 w}{\partial y^2} + 2 N_{xy} \frac{\partial^2 w}{\partial x \partial y}\right) \qquad \text{II.1.1c.}$$

The solution of these equations is facilitated by introducing a stress function (F). It is seen that equations II.1.1a and 1.b are identically satisfied if

$$N_x = h\frac{\partial^2 F}{\partial y^2} \qquad N_y = h\frac{\partial^2 F}{\partial x^2} \qquad N_{xy} = -h\frac{\partial^2 F}{\partial x \partial y} \qquad \text{II.1.2.}$$

It can be shown (Timoshenko, 1961. chap. 8) that if the curvatures of the plate in the x and y directions are approximated to by $-\frac{\partial^2 w}{\partial x^2}$ and $-\frac{\partial^2 w}{\partial y^2}$ respectively then

$$M_x = -D\left[\frac{\partial^2 w}{\partial x^2} + \nu \frac{\partial^2 w}{\partial y^2}\right]$$

$$M_y = -D\left[\frac{\partial^2 w}{\partial y^2} + \nu \frac{\partial^2 w}{\partial x^2}\right]$$

Thus equation II.1.1c becomes

$$\frac{\partial^4 w}{\partial x^4} + 2\frac{\partial^4 w}{\partial x^2 \partial y^2} + \frac{\partial^4 w}{\partial y^4} = \frac{h}{D}\left[\frac{\partial^2 F}{\partial y^2}\cdot\frac{\partial^2 w}{\partial x^2} + \frac{\partial^2 F}{\partial x^2}\cdot\frac{\partial^2 w}{\partial y^2} - 2\frac{\partial^2 F}{\partial x \partial y}\cdot\frac{\partial^2 w}{\partial x \partial y}\right] \qquad \text{II.1.3.}$$

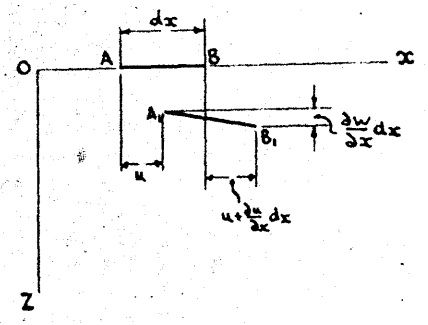

FIG. II. 3.

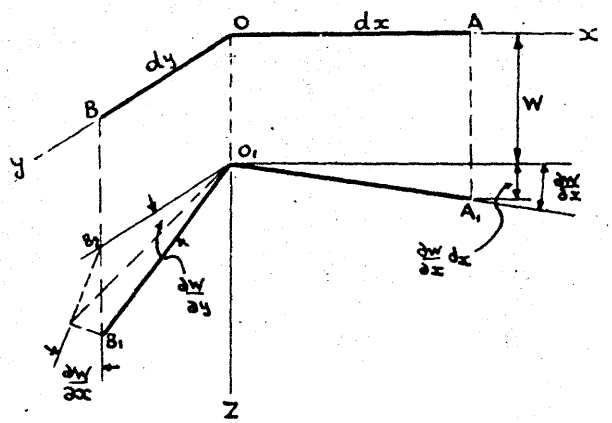

FIG. II. 4

Since in the case being considered the movement in the Z direction is very much greater than in the x and y directions the strain of an element of the middle plane of the plate can be shown from figures II.3 and II.4 to be

$$\epsilon_x = \frac{\partial u}{\partial x} + \frac{1}{2}\left(\frac{\partial w}{\partial x}\right)^2 \quad \text{II.1.4a.}$$

$$\epsilon_y = \frac{\partial v}{\partial y} + \frac{1}{2}\left(\frac{\partial w}{\partial y}\right)^2 \quad \text{II.1.4b.}$$

$$\gamma_{xy} = \frac{\partial u}{\partial y} + \frac{\partial v}{\partial x} + \frac{\partial w}{\partial x}\cdot\frac{\partial w}{\partial y} \quad \text{II.1.4c.}$$

By differentiating these expressions it can be seen that

$$\frac{\partial^2 \epsilon_x}{\partial y^2} + \frac{\partial^2 \epsilon_y}{\partial x^2} + \frac{\partial^2 \gamma_{xy}}{\partial x \partial y} = \left(\frac{\partial^2 w}{\partial x \partial y}\right)^2 - \frac{\partial^2 w}{\partial x^2}\cdot\frac{\partial^2 w}{\partial y^2} \quad \text{II.1.5.}$$

However,

$$\epsilon_x = \frac{1}{hE}\left[N_x - \nu N_y\right] = \frac{1}{E}\left[\frac{\partial^2 F}{\partial y^2} - \nu \frac{\partial^2 F}{\partial x^2}\right]$$

$$\epsilon_y = \frac{1}{hE}\left[N_y - \nu N_x\right] = \frac{1}{E}\left[\frac{\partial^2 F}{\partial x^2} - \nu \frac{\partial^2 F}{\partial y^2}\right]$$

$$\gamma_{xy} = \frac{1}{hG} N_{xy} = -\frac{2(1+\nu)}{E}\cdot\frac{\partial^2 F}{\partial x \partial y}$$

Thus equation II.1.5 can be written as

$$\frac{\partial^4 F}{\partial x^4} + 2\frac{\partial^4 F}{\partial x^2 \partial y^2} + \frac{\partial^4 F}{\partial y^4} = E\left[\left(\frac{\partial^2 w}{\partial x \partial y}\right)^2 - \frac{\partial^2 w}{\partial x^2}\cdot\frac{\partial^2 w}{\partial y^2}\right] \quad \text{.... II.1.6.}$$

II.2 Formulation of Large Deflection Equations in Non-dimensional Terms.

Taking

$$\xi = \frac{x}{a} \qquad \eta = \frac{y}{b} \qquad \phi = \frac{a}{b} \qquad \omega = \frac{w}{h} \qquad F' = \frac{F}{Eh^2}$$

then equation II.1.3 can be written as

$$\frac{\partial^4 (h\omega)}{\partial (a\xi)^4} + 2\frac{\partial^4 (h\omega)}{\partial (a\xi)^2 \partial (b\eta)^2} + \frac{\partial^4 (h\omega)}{\partial (b\eta)^4} =$$

$$= \frac{h}{D}\left[\frac{\partial^2 (F'Eh^2)}{\partial (a\xi)^2}\cdot\frac{\partial^2 (h\omega)}{\partial (b\eta)^2} + \frac{\partial^2 (F'Eh^2)}{\partial (b\eta)^2}\cdot\frac{\partial^2 (h\omega)}{\partial (a\xi)^2} - 2\frac{\partial^2 (F'Eh^2)}{\partial (b\eta)\,\partial (a\xi)}\cdot\frac{\partial^2 (\omega h)}{\partial (b\eta)\partial (a\xi)}\right]$$

where $D = \frac{Eh^3}{12(1-\nu^2)}$

$$\therefore \frac{1}{\phi^2}\cdot\frac{\partial^4 \omega}{\partial \xi^4} + 2\frac{\partial^4 \omega}{\partial \xi^2 \partial \eta^2} + \phi^2\cdot\frac{\partial^4 \omega}{\partial \eta^4} =$$

$$= 12(1-\nu^2)\left[\frac{\partial^2 F'}{\partial \xi^2}\cdot\frac{\partial^2 \omega}{\partial \eta^2} + \frac{\partial^2 F'}{\partial \eta^2}\cdot\frac{\partial^2 \omega}{\partial \xi^2} - 2\frac{\partial^2 F'}{\partial \xi\,\partial \eta}\cdot\frac{\partial^2 \omega}{\partial \xi\,\partial \eta}\right] \quad \text{II.2.1.}$$

Similarly equation II.1.6 can be written as

$$\frac{\partial^4(FEh^2)}{\partial(a\xi)^4} + 2\frac{\partial^4(FEh^2)}{\partial(a\xi)^2\,\partial(b\eta)^2} + \frac{\partial^4(FEh^2)}{\partial(b\eta)^4} =$$

$$= E\left[\left(\frac{\partial^2(\omega h)}{\partial(a\xi)\partial(b\eta)}\right)^2 - \frac{\partial^2(\omega h)}{\partial(a\xi)^2}\cdot\frac{\partial^2(\omega h)}{\partial(b\eta)^2}\right]$$

$$\therefore \frac{1}{\phi^2}\frac{\partial^4F'}{\partial\xi^4} + 2\frac{\partial^4F'}{\partial\xi^2\partial\eta^2} + \phi^2\frac{\partial^4F'}{\partial\eta^4} = \left(\frac{\partial^2\omega}{\partial\xi\,\partial\eta}\right)^2 - \frac{\partial^2\omega}{\partial\xi^2}\cdot\frac{\partial^2\omega}{\partial\eta^2} \quad \ldots\ldots \text{II.2.2.}$$

In the same manner

$$\sigma_\eta = \sigma_y\frac{a}{Eh^2} \qquad \sigma_\xi = \sigma_x\frac{a^2}{\phi^2Eh^2} \qquad \tau_{\xi\eta} = \tau_{xy}\frac{a^2}{\phi Eh^2}$$

II.3 Brief Description of Galerkin's Method.

To the author's knowledge so far no exact solutions to the problem formulated in equations II.1.3 and II.1.6 together with the appropriate boundary conditions have been published. The approximate solutions presented usually start by assuming some series function representing the deflection (w). Apart from preference for mathematical reasons it is the more easily observed and measured parameter in tests and therefore the least difficult one to describe mathematically. The series for w should contain at least

one and preferably more terms, each qualified by an undetermined coefficient.

The deflection function is then substituted into equation II.1.6 and the stress function (F) obtained, either by analytical or approximate methods, in terms of the deflection coefficients from the resulting linear differential equation. Now w and F are substituted into equation II.1.3 to determine the absolute value of these coefficients; since the assumption for w is an approx-:imation the resulting differential equation cannot be solved analytically. By using a method such as that developed by Galerkin, however, it is possible to determine the coefficients such that equation II.1.3 is on the average closely satisfied over the range of interest.

The method of solution being presented in this thesis closely follows the above outline but, since the series chosen for w is of necessity a complicated one, the differential equation for F cannot be solved exactly and Galerkin's method is used for this also.

The method of Galerkin (Duncan, 1937) belongs to the same general class as those of Rayleigh and Ritz. It seeks to obtain an approximate solution of a differential equation with stated boundary conditions by taking an assumed series function and specialising it in such a manner as to secure approximate satisfaction of the differ-:ential equation. Each term of the chosen series satisfies the relevant boundary conditions exactly and is qualified by an unknown coefficient. The degree of accuracy with which the Galerkin series fits the differential equation

improves as the number of terms included in the assumed series is increased.

Suppose the solution is required of the linear ordinary differential equation

$$P_0(x)\frac{d^n y}{dx^n} + P_1(x)\frac{d^{n-1} y}{dx^{n-1}} + \cdots\cdots P_{n-1}(x)\frac{dy}{dx} + P_n(x)y + Q(x) = 0 \qquad \text{II.3.1.}$$

for the range $a \leq x \leq b$ of the independent variable. The Galerkin method is essentially as follows: if Y is a function of x which satisfies the prescribed boundary conditions exactly and $Y_1, Y_2, \ldots\ldots Y_m$ is a sequence of linearly independent functions which satisfy the homogeneous boundary conditions then it can be seen that

$$y = Y + \sum_{r=1}^{r=m} c_r Y_r \qquad \text{II.3.2.}$$

will also satisfy the boundary conditions if the coefficients c_r are independent of x. The determination of these coefficients is obtained by substituting equation II.3.2 into equation II.3.1, multiplying by Y_s, integrating the result over the range of interest and equating to zero. As s is made $1, 2, \ldots m$ in succession, m linear algebraic equations are obtained, the simultaneous solution of which yields the coefficients c_r.

It can be seen that if instead of II.3.1 a non-linear differential equation had been chosen then the resulting algebraic equations would also have been non-linear and to the same degree as the differential equation.

Galerkin's method has a major drawback in its use in applied elasticity in that the boundary conditions of these problems may lead to large and complicated expressions in the appropriate assumed series. This results in an enormous amount of arithmetic work for the inclusion of even a few terms in the series. This feature has been to some extent overcome in the solution presented in this dissertation by making use of an automatic digital computer which, if it is programmed for a generalised term in the Galerkin series, will perform all the arithmetic operations quickly and accurately. No extra work is required of the operator for an increase in the number of terms in the series and the limitations are now imposed merely by the machine speed and available storage space.

When the method of Galerkin is used to obtain a solution to a problem which can be described by a single differential equation then it may be shown that the results are identical with those obtained by using the energy method of Rayleigh and Ritz for the problem, provided that the same series is used in each case. This is advantageous since it is known that an approximate solution of a problem obtained by the Rayleigh-Ritz method approaches the exact solution of that problem in such a way that with increasing numbers of terms included in the chosen series the strain energy of the system is monotonically reduced. Thus it is possible to make an analytical estimate of the probable error incurred by using only a finite number of terms in the series.

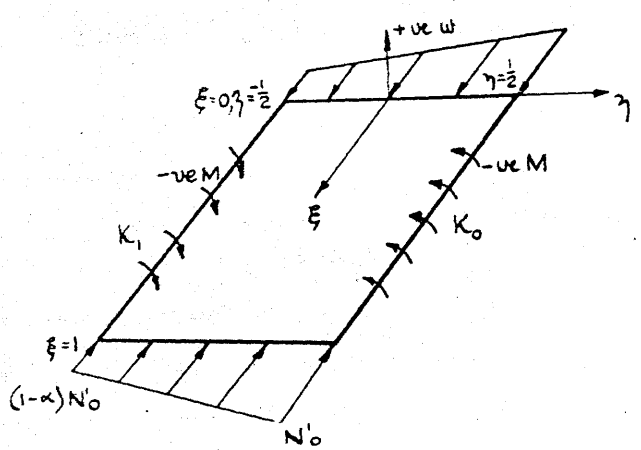
+ve w
$\xi=0, \eta=\frac{-1}{2}$
$\eta=\frac{1}{2}$
η
-ve M
-ve M
ξ
K_1
K_0
$\xi=1$
$(1-\alpha)N'_0$
N'_0

FIG II.5

This property is shown clearly in the next chapter when the instability condition, which mathematically is described by only one differential equation, is considered. However, for the post-buckling condition the problem is formulated as two simultaneous differential equations and, since it is proposed to solve both of these using Galerkin's method, no similar direct method is available for estimating the nature of the approximation. This, to a large extent, is overcome by using an adequately large number of terms in the Galerkin series and by investigating the convergence individually for the conditions considered.

II.4 Derivation of the Galerkin series for the Stress and Deflection Functions for Selected Cases.

As stated in Section 2 of this chapter, it is proposed to obtain an approximate solution to the non-dimensional equations II.2.1 and II.2.2 for selected cases by using the Galerkin series method. The first step in this process is the derivation of the series to be used; this is described in detail below.

Case a. Initially flat rectangular plate compressed by a linearly varying load action along two simply supported opposite edges and having equal or unequal rotational restraint along the other two edges (Figure II.5).

For the Stress Function (F') the boundary conditions

are given by the stress resultants considered at the plate edges in the plate middle plane.

Hence at $x=0$ and a with the imposed loading and for zero shear stress the mathematical conditions are

$$\left[\sigma_x\right]_{x=0,a} = \frac{N_0}{h}\left[(1-\tfrac{\alpha}{2}) + \alpha\,\frac{y}{b}\right]$$

$$\left[\gamma_{xy}\right]_{x=0,a} = 0$$

in non-dimensional terms these become

$$\left[\sigma_\xi\right]_{\xi=0,1} = \left[\frac{\partial^2 F'}{\partial \xi^2}\right]_{\xi=0,1} = N_0'\left[(1-\tfrac{\alpha}{2}) + \alpha\,\eta\right]$$

$$\left[\gamma_{\xi\eta}\right]_{\xi=0,1} = \left[\frac{\partial^2 F'}{\partial \xi\,\partial \eta}\right]_{\xi=0,1} = 0$$

where $N_0' = \dfrac{N_0 a^2}{\phi^2 E h^3}$

Along the edges $y=-\frac{b}{2}$ and $y=\frac{b}{2}$ there is considered to be no direct stress acting in the y direction nor any shear stress, i.e.

$$\left[\sigma_y\right]_{y=-\frac{b}{2},\frac{b}{2}} = 0$$

$$\left[\gamma_{xy}\right]_{y=-\frac{b}{2},\frac{b}{2}} = 0$$

Again in non-dimensional terms these become

$$\left[\sigma_\eta\right]_{\eta=-\frac{1}{2},\frac{1}{2}} = \left[\frac{\partial^2 F'}{\partial \xi^2}\right]_{\eta=-\frac{1}{2},\frac{1}{2}} = 0$$

$$\left[\gamma_{\eta\xi}\right]_{\eta=-\frac{1}{2},\frac{1}{2}} = \left[\frac{\partial^2 F'}{\partial \xi\,\partial \eta}\right]_{\eta=-\frac{1}{2},\frac{1}{2}} = 0$$

Assuming the Stress Function to be represented by

$$F' = A\left[(1-\tfrac{\alpha}{2}) + \tfrac{\alpha}{3}\eta\right]\eta^2 + \sum_r \sum_s b_{rs} f_r(\xi)\, g_s(\eta) \quad \ldots\ldots \text{II.4.1.}$$

where A is a constant, b_{rs} are constants, $f_r(\xi)$ is a function of ξ only and $g_s(\eta)$ is a function of η only.

Now $$\frac{\partial^2 F'}{\partial \eta^2} = 2A\left[(1-\tfrac{\alpha}{2}) + \alpha\eta\right] + \sum_r \sum_s b_{rs} \frac{\partial^2}{\partial \eta^2} f_r(\xi)\, g_s(\eta)$$

thus if $$\left[\sum_r \sum_s b_{rs} \frac{\partial^2}{\partial \eta^2} f_r(\xi) g_s(\eta)\right]_{\xi=0,1} = 0$$ then

$A = \frac{N_0'}{2}$ and the assumed form of the Stress Function can be given by

$$F' = \frac{N_0'}{2}\left[(1-\tfrac{\alpha}{2}) + \tfrac{\alpha}{3}\eta\right]\eta^2 + \sum_r \sum_s b_{rs} f_r(\xi)\, g_s(\eta) \quad \ldots\ldots \text{II.4.2.}$$

For each term in the series part of equation II.4.2 the boundary conditions can now be written as

$$\left[\frac{\partial^2 f_r(\xi)}{\partial \xi^2} g_s(\eta)\right]_{\eta=-\frac{1}{2},\frac{1}{2}} = 0$$

$$\left[\frac{\partial^2}{\partial \xi \partial \eta} f_r(\xi) g_s(\eta)\right]_{\eta=-\frac{1}{2},\frac{1}{2}} = 0$$

$$\left[f_r(\xi)\, \frac{\partial^2 g_s(\eta)}{\partial \eta^2}\right]_{\xi=0,1} = 0$$

$$\left[\frac{\partial^2}{\partial \xi \partial \eta} f_r(\xi) g_s(\eta)\right]_{\xi=0,1} = 0$$

which in essence are

$$\left[g_s(\eta)\right]_{\eta=-\frac{1}{2},\frac{1}{2}} = 0$$

$$\left[\frac{dg_s(\eta)}{d\eta}\right]_{\eta=-\frac{1}{2},\frac{1}{2}} = 0$$

$$\left[f_r(\xi)\right]_{\xi=0,1} = 0$$

$$\left[\frac{df_r(\xi)}{d\xi}\right]_{\xi=0,1} = 0$$

One possible form for $f_r(\xi)$ is

$$f_r(\xi) = \sin^2 r\pi\xi \quad \ldots\ldots\ldots \text{II.4.3.}$$

where $r = 1, 2, 3,$ etc.

Testing this for the appropriate boundary conditions it is seen that

$$\left[f_r(\xi)\right]_{\xi=0,1} = 0$$

$$\left[\frac{df_r(\xi)}{d\xi}\right]_{\xi=0,1} = \left[\sin 2\pi r\xi\right]_{\xi=0,1} = 0$$

thus the function given by equation II.4.3 is admissable for use in the Galerkin series.

For $g_s(\eta)$ a polynomial form is chosen, viz.

$$g_s(\eta) = \eta^{s+4} + A_s\eta^{s+3} + B_s\eta^{s+2} + C_s\eta^{s+1} + D_s\eta^s$$

where $s = 0, 1, 2,$ etc. and A_s, B_s, etc. are constants. Substitution of this form into the relevant boundary conditions yields the following,

at $\eta = -\frac{1}{2}$, $g_s(\eta) = 0$

$$\therefore \left(-\tfrac{1}{2}\right)^{s+4} + A_s\left(-\tfrac{1}{2}\right)^{s+3} + B_s\left(-\tfrac{1}{2}\right)^{s+2} + C_s\left(-\tfrac{1}{2}\right)^{s+1} + D_s\left(-\tfrac{1}{2}\right)^s = 0$$

$$\therefore \quad 1 - 2A_s + 4B_s - 8C_s + 16D_s = 0$$

at $\eta = \frac{1}{2}$, $g_s(\eta) = 0$

$$\therefore 1 + 2A_s + 4B_s + 8C_s + 16D_s = 0$$

$$\therefore \quad D_s = -\frac{1}{16}(1 + 4B_s)$$

$$\text{and} \quad C_s = -\frac{A_s}{4}$$

at $\eta = -\frac{1}{2}$, $\frac{dg_s(\eta)}{d\eta} = 0$

$$\therefore 2(s+3)A_s - 4(s+2)B_s + 8(s+1)C_s - 16sD_s = (s+4)$$

at $\eta = \frac{1}{2}$, $\frac{dg_s(\eta)}{d\eta} = 0$

$$\therefore\ 2(s+3)A_s + 4(s+2)B_s + 8(s+1)C_s + 16\,s\,D_s = -(s+4)$$

$$\therefore A_s = 0 \quad \text{and} \quad B_s = -\tfrac{1}{2}$$

Hence

$$g_s(\eta) = \eta^{s+4} - \tfrac{1}{2}\eta^{s+2} + \tfrac{1}{16}\eta^s$$

The Galerkin series for the Stress Function for this case can therefore be written as:

$$F' = \frac{N_0'}{2}\left[(1-\tfrac{\alpha}{2}) + \tfrac{\alpha}{3}\eta\right]\eta^2 + \sum_{r=1,2,}\sum_{s=0,1,} b_{rs}\sin^2 r\pi\xi\,.\left(\eta^{s+4} - \tfrac{1}{2}\eta^{s+2} + \tfrac{1}{16}\eta^s\right) \qquad \text{II.4.4.}$$

Derivation of the series for Deflection (ω).

The loaded edges of the plate are considered to be simply supported; mathematically this can be formulated as

$$\left[M_x\right]_{x=0,a} = \left[-D\left(\frac{\partial^2 w}{\partial x^2} + \nu\frac{\partial^2 w}{\partial y^2}\right)\right]_{x=0,a} = 0$$

$$\left[w\right]_{x=0,a} = 0$$

or in non-dimensional terms as

$$\left[\frac{\partial^2\omega}{\partial\xi^2} + \nu\phi^2\frac{\partial^2\omega}{\partial\eta^2}\right]_{\xi=0,1} = 0 \qquad \text{II.4.5a.}$$

$$\left[\omega\right]_{\xi=0,1} = 0 \qquad \text{II.4.5b.}$$

The unloaded edges are fully restrained against lateral deflection and elastically restrained against rotation, i.e.

$$\left[w\right]_{y=-\frac{b}{2},\frac{b}{2}} = 0$$

$$\left[M_y + r_0\phi\right]_{y=+\frac{b}{2}} = 0$$

$$\left[M_y - r_1\phi\right]_{y=-\frac{b}{2}} = 0$$

where τ_0, τ_1 are the degree of rotational restraint and ϕ is the slope of the plate middle plane in the y direction. Again transposing to non-dimensional terms these conditions become

$$\left[\omega\right]_{\eta=-\frac{1}{2},\frac{1}{2}} = 0 \quad \text{II.4.5c.}$$

$$\left[\frac{\partial^2\omega}{\partial\eta^2} + \frac{\nu}{\phi^2}\frac{\partial^2\omega}{\partial\xi^2}\right]_{\eta=+\frac{1}{2}} = -K_0\left[\frac{\partial\omega}{\partial\eta}\right]_{\eta=+\frac{1}{2}} \quad \text{II.4.5d.}$$

$$\left[\frac{\partial^2\omega}{\partial\eta^2} + \frac{\nu}{\phi^2}\frac{\partial^2\omega}{\partial\xi^2}\right]_{\eta=-\frac{1}{2}} = K_1\left[\frac{\partial\omega}{\partial\eta}\right]_{\eta=-\frac{1}{2}} \quad \text{II.4.5e.}$$

where $K_0 = -\frac{b\tau_0}{D}$ and $K_1 = -\frac{b\tau_1}{D}$

The series form for the deflection is assumed to be

$$\omega = \sum_m \sum_n q_{mn} \cdot f_m(\xi)\, g_n(\eta)$$

where q_{mn} are constants, $f_m(\xi)$ is a function of ξ only and $g_n(\eta)$ is a function of η only.

A possible function for $f_m(\xi)$ is

$$f_m(\xi) = \sin m\pi\xi \quad \text{where } m = 1, 2, 3, \text{ etc.} \quad \text{II.4.6.}$$

This function satisfies equations II.4.5a and II.4.5b thus may be used in the Galerkin series.

A polynomial function is chosen for $g_n(\eta)$, viz.,

$$g_n(\eta) = \eta^{n+4} + A_n\eta^{n+3} + B_n\eta^{n+2} + C_n\eta^{n+1} + D_n\eta^n \quad \text{II.4.7.}$$

where $n = 0, 1, 2$, etc.

To obtain the values of the coefficients A_n, B_n, etc. equations II.4.6 and II.4.7 are substituted into equations II.4.5c, d and e in turn. Thus: $\omega = 0$ at $\eta = \frac{1}{2}, -\frac{1}{2}$ becomes on substitution of equation II.4.6 $g_n(\eta) = 0$ which in turn becomes, after substitution of equation II.4.7 and

simplification,

$$A_n + 2B_n + 4C_n + 8D_n = -\tfrac{1}{2}$$

and

$$A_n - 2B_n + 4C_n - 8D_n = \tfrac{1}{2}$$

When equation II.4.6 is substituted in equation II.4.5d and equation II.4.5c is considered then

$$\frac{\partial^2\omega}{\partial\eta^2} + \frac{\nu}{\phi^2}\frac{\partial^2\omega}{\partial\xi^2} = -K_o\frac{\partial\omega}{\partial\eta} \quad \text{at} \quad \eta = \tfrac{1}{2} \quad \text{becomes}$$

$$\frac{d^2 g_n(\eta)}{d\eta^2} = -K_o\frac{dg_n(\eta)}{d\eta} \quad \text{at} \quad \eta = \tfrac{1}{2}$$

which on the substitution of equation II.4.7 becomes

$$2(n+4)(n+3) + 4(n+3)(n+2)A_n + 8(n+2)(n+1)B_n + 16n(n+1)C_n + 32(n-1)n D_n =$$
$$= -K_o\left[(n+4) + 2(n+3)A_n + 4(n+2)B_n + 8(n+1)C_n + 16n D_n\right]$$

$$\therefore\ 2(n+3)\left[(n+2)+\frac{K_o}{2}\right]A_n + 4(n+2)\left[(n+1)+\frac{K_o}{2}\right]B_n + 8(n+1)\left[n+\frac{K_o}{2}\right]C_n + 16n\left[(n-1)+\frac{K_o}{2}\right] =$$
$$= -(n+4)\left[(n+3)+\frac{K_o}{2}\right]$$

Similarly

$$\frac{\partial^2\omega}{\partial\eta^2} + \frac{\nu}{\phi^2}\frac{\partial^2\omega}{\partial\xi^2} = K_1\frac{\partial\omega}{\partial\eta} \quad \text{at} \quad \eta = -\tfrac{1}{2} \quad \text{becomes}$$

$$\frac{d^2 g_n(\eta)}{d\eta^2} = K_1\frac{dg_n(\eta)}{d\eta} \quad \text{at} \quad \eta = -\tfrac{1}{2} \quad \text{leading to}$$

$$2(n+3)\left[(n+2)+\frac{K_1}{2}\right]A_n - 4(n+2)\left[(n+1)+\frac{K_1}{2}\right]B_n + 8(n+1)\left[n+\frac{K_1}{2}\right]C_n - 16n\left[(n-1)+\frac{K_1}{2}\right]D_n = (n+4)\left[(n+3)+\frac{K_1}{2}\right]$$

Since, as was stated before, all arithmetic operations involved in the Galerkin method as used in this solution were performed on a digital computer (see Appendix I for details of the machine) the above equations were not solved explicitly to give A_n, B_n, etc. in terms of n, K_1, etc. but were programmed in the matrix form shown below. This speeded up computing time by permitting the use of

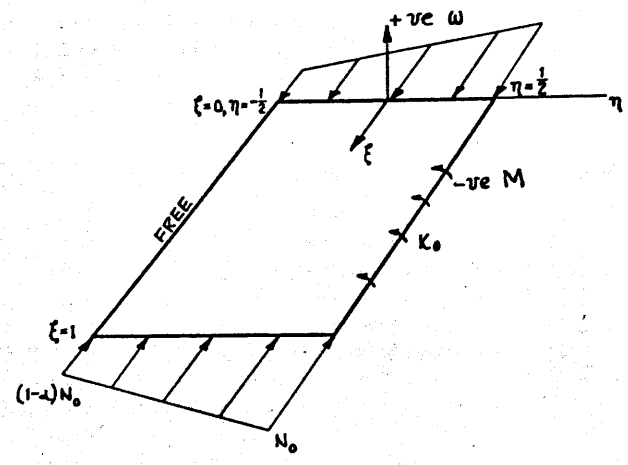

FIG. II.6

the extremely fast sub-routines available for the machine.

$$\begin{bmatrix} 1 & 2 & 4 & 8 \\ 1 & -2 & 4 & -8 \\ 2(n+3)\left[(n+2)+\frac{K_2}{2}\right] & 4(n+2)\left[(n+1)+\frac{K_2}{2}\right] & 8(n+1)\left[n+\frac{K_2}{2}\right] & 16n\left[(n-1)+\frac{K_2}{2}\right] \\ 2(n+3)\left[(n+2)+\frac{K_1}{2}\right] & -4(n+2)\left[(n+1)+\frac{K_1}{2}\right] & 8(n+1)\left[n+\frac{K_1}{2}\right] & -16n\left[(n-1)+\frac{K_1}{2}\right] \end{bmatrix} \begin{bmatrix} A_n \\ B_n \\ C_n \\ D_n \end{bmatrix} = \begin{bmatrix} -\frac{1}{2} \\ \frac{1}{2} \\ -(n+4)\left[(n+3)+\frac{K_2}{2}\right] \\ (n+4)\left[(n+3)+\frac{K_1}{2}\right] \end{bmatrix}$$

Thus the deflection series can be written as

$$\omega = \sum_{m=1,2,} \sum_{n=0,1} q_{mn} \sin m\pi\xi \left[\eta^{n+4} + A_n \eta^{n+3} + B_n \eta^{n+2} + C_n \eta^{n+1} + D_n \eta^n\right] \qquad \text{II.4.8.}$$

with the coefficients A_n, B_n, etc. obtained from the solution of the above matrix equation.

Case b. Initially flat rectangular plate compressed by a linearly varying load action along two simply supported opposite edges and having one unloaded edge rotationally restrained and the other free (Figure II.6).

The boundary conditions for the Stress Function for this type of plate are identical to those for the plate in Case a. So that the series approximation for the Stress Function can again be given by equation II.4.2.

Derivation of the series for Deflection (ω).

As in Case a the derivation of the Galerkin series

for the Deflection starts with the loaded edges which are again considered to be simply supported, i.e.

$$\left[\frac{\partial^2\omega}{\partial\xi^2} + \nu\phi^2\frac{\partial^2\omega}{\partial\eta^2}\right]_{\xi=0,1} = 0 \quad \ldots\ldots \text{II.4.8a.}$$

$$\left[\omega\right]_{\xi=0,1} = 0 \quad \ldots\ldots \text{II.4.8b.}$$

As before the conditions for the rotationally restrained edge are given by

$$\left[\omega\right]_{\eta=\frac{1}{2}} = 0 \quad \ldots\ldots \text{II.4.9a.}$$

and $$\left[\frac{\partial^2\omega}{\partial\eta^2} + \frac{\nu}{\phi^2}\frac{\partial^2\omega}{\partial\xi^2}\right]_{\eta=\frac{1}{2}} = -K_o\left[\frac{\partial\omega}{\partial\eta}\right]_{\eta=\frac{1}{2}} \quad \ldots\ldots \text{II.4.9b.}$$

while for the free unloaded edge the mathematical con-:ditions are shown by Timoshenko (1961, Chap. 8) to be

$$\left[M_y\right]_{y=-\frac{b}{2}} = -D\left[\frac{\partial^2 w}{\partial y^2} + \nu\frac{\partial^2 w}{\partial x^2}\right]_{y=-\frac{b}{2}} = 0$$

$$\left[Q_x - \frac{\partial M_{xy}}{\partial y}\right]_{y=-\frac{b}{2}} = \left[\frac{\partial^3 w}{\partial y^3} + (2-\nu)\frac{\partial^3 w}{\partial y\,\partial x^2}\right]_{y=-\frac{b}{2}} = 0$$

which in non-dimensional terms are given by

$$\left[\frac{\partial^2\omega}{\partial\eta^2} + \frac{\nu}{\phi^2}\frac{\partial^2\omega}{\partial\xi^2}\right]_{\eta=-\frac{1}{2}} = 0 \quad \ldots\ldots \text{II.4.9c.}$$

$$\left[\frac{\partial^3\omega}{\partial\eta^3} + \frac{(2-\nu)}{\phi^2}\frac{\partial^3\omega}{\partial\eta\,\partial\xi^2}\right]_{\eta=-\frac{1}{2}} = 0 \quad \ldots\ldots \text{II.4.9d.}$$

Once more the series for the deflection can be represented by

$$\omega = \sum_m \sum_n q_{mn} f_m(\xi) g_n(\eta)$$

and $f_m(\xi) = \sin m\pi\xi$ and $m = 1, 2,$ etc. . . II.4.10.

also $g_n(\eta) = \eta^{n+4} + A_n\eta^{n+3} + B_n\eta^{n+2} + C_n\eta^{n+1} + D_n\eta^n$ where $n = 0, 1, 2,$ etc. II.4.11.

To obtain the values of the coefficients A_n, B_n, etc. equations II.4.10 and II.4.11 are substituted into equations II.4.9a, b, c and d in turn.

Hence $\left[\omega\right]_{\eta=\frac{1}{2}} = 0$ gives $\left[g_n(\eta)\right]_{\eta=\frac{1}{2}} = 0$

and when this condition is applied to equation II.4.11 the result is

$$A_n + 2B_n + 4C_n + 8D_n = -\tfrac{1}{2}$$

Similarly using equations II.4.10 and II.4.9b

$$\left[\frac{\partial^2\omega}{\partial\eta^2} + \frac{\nu}{\phi^2}\frac{\partial^2\omega}{\partial\xi^2}\right]_{\eta=\frac{1}{2}} = -K_0\left[\frac{\partial\omega}{\partial\eta}\right]_{\eta=\frac{1}{2}} \quad \text{becomes}$$

$$\left[\frac{d^2g_n(\eta)}{d\eta^2}\right]_{\eta=\frac{1}{2}} = -K_0\left[\frac{dg_n(\eta)}{d\eta}\right]_{\eta=\frac{1}{2}}$$

which when applied to equation II.4.11 gives

$$2(n+3)\left[(n+2) + \frac{K_0}{2}\right]A_n + 4(n+2)\left[(n+1) + \frac{K_0}{2}\right]B_n + 8(n+1)\left[n + \frac{K_0}{2}\right]C_n +$$
$$+ 16n\left[(n-1) + \frac{K_0}{2}\right]D_n = -(n+4)\left[(n+3) + \frac{K_0}{2}\right]$$

By substitution of equation II.4.10

$$\left[\frac{\partial^2\omega}{\partial\eta^2} + \frac{\nu}{\phi^2}\frac{\partial^2\omega}{\partial\xi^2}\right]_{\eta=-\frac{1}{2}} = 0 \quad \text{becomes}$$

$$\left[\frac{d^2g_n(\eta)}{d\eta^2} - \frac{\nu m^2\pi^2}{\phi^2}g(\eta)\right]_{\eta=-\frac{1}{2}} = 0$$

Application of the condition to equation II.4.11 gives

$$\frac{(n+4)(n+3)}{(-2)^{n+2}} + \frac{(n+3)(n+2)}{(-2)^{n+1}}A_n + \frac{(n+2)(n+1)}{(-2)^n}B_n + \frac{(n+1)n}{(-2)^{n-1}}C_n + \frac{n(n-1)}{(-2)^{n-2}}D_n -$$

$$- \frac{\nu m^2\pi^2}{\phi^2}\left[\frac{1}{(-2)^{n+4}} + \frac{A_n}{(-2)^{n+3}} + \frac{B_n}{(-2)^{n+2}} + \frac{C_n}{(-2)^{n+1}} + \frac{D_n}{(-2)^n}\right] = 0$$

$$\therefore \left[2\frac{\nu m^2\pi^2}{\phi^2} - 8(n+3)(n+2)\right]A_n + \left[16(n+2)(n+1) - 4\frac{\nu m^2\pi^2}{\phi^2}\right]B_n + \left[8\frac{\nu m^2\pi^2}{\phi^2} - 32(n+1)n\right]C_n +$$

$$+\left[64n(n-1) - 16\,\frac{\nu m^2\pi^2}{\phi^2}\right]D_n = \left[\frac{\nu m^2\pi^2}{\phi^2} - 4(n+4)(n+3)\right]$$

On the substitution of equation II.4.10 in equation II.4.9d. and simplification

$$\left[\frac{\partial^3\omega}{\partial\eta^3} + \frac{(2-\nu)}{\phi^2}\,\frac{\partial^3\omega}{\partial\eta\,\partial\xi^2}\right]_{\eta=-\frac{1}{2}} = 0 \quad \text{becomes}$$

$$\left[\frac{d^3 g_n(\eta)}{d\eta^3} - \frac{(2-\nu)}{\phi^2}\,m^2\pi^2\,\frac{dg_n(\eta)}{d\eta}\right]_{\eta=-\frac{1}{2}} = 0$$

which when applied to equation II.4.11 results in

$$\frac{(n+4)(n+3)(n+2)}{(-2)^{n+1}} + \frac{(n+3)(n+2)(n+1)}{(-2)^n}A_n + \frac{(n+2)(n+1)n}{(-2)^{n-1}}B_n + \frac{(n+1)n(n-1)}{(-2)^{n-2}}C_n +$$

$$+\frac{n(n-1)(n-2)}{(-2)^{n-3}}D_n - \beta\left[\frac{(n+4)}{(-2)^{n+3}} + \frac{(n+3)}{(-2)^{n+2}}A_n + \frac{(n+2)}{(-2)^{n+1}}B_n + \frac{(n+1)}{(-2)^n}C_n + \frac{n}{(-2)^{n-1}}D_n = 0\right.$$

where $\beta = (2-\nu)\,\frac{m^2\pi^2}{\phi^2}$

$$\left[2\beta(n+3) - 8(n+3)(n+2)(n+1)\right]A_n + \left[16(n+2)(n+1)n - 4\beta(n+2)\right]B_n + \left[8\beta(n+1) -\right.$$

$$\left.-32(n+1)n(n-1)\right]C_n + \left[64n(n-1)(n-2) - 16\beta n\right]D_n = \left[\beta(n+4) - 4(n+4)(n+3)(n+2)\right]$$

Thus for this case the matrix equation is:

$$\begin{matrix} & 1 & 2 & 4 & 8 \end{matrix}$$

$$\begin{bmatrix} 2(n+3)\left[(n+2)+\frac{K_0}{2}\right] & 4(n+2)\left[(n+1)+\frac{K_0}{2}\right] & 8(n+1)\left[n+\frac{K_0}{2}\right] & 16n\left[(n-1)+\frac{K_0}{2}\right] \\ \left[2\,\frac{\nu m^2\pi^2}{\phi^2} - 8(n+3)(n+2)\right] & \left[16(n+2)(n+1) - \frac{4\nu m^2\pi^2}{\phi^2}\right] & \left[8\,\frac{\nu m^2\pi^2}{\phi^2} - 32(n+1)n\right] & \left[64n(n-1) - 16\,\frac{\nu m^2\pi^2}{\phi^2}\right] \\ \left[2\beta(n+3) - 8(n+3)(n+2)(n+1)\right] & \left[16(n+2)(n+1)n - 4\beta(n+2)\right] & \left[8\beta(n+1) - 32(n+1)n(n-1)\right] & \left[64n(n-1)(n-2) - 16n\beta\right] \end{bmatrix} \begin{bmatrix} A_n \\ B_n \\ C_n \\ D_n \end{bmatrix} = \begin{bmatrix} -\frac{1}{2} \\ -(n+4)\left[(n+3)+\frac{K_0}{2}\right] \\ \left[\frac{\nu m^2\pi^2}{\phi^2} - 4(n+4)(n+3)\right] \\ \left[\beta(n+4) - 4(n+4)(n+3)(n+2)\right] \end{bmatrix}$$

C H A P T E R I I I

CHAPTER III.

SOLUTION OF THE VON KARMAN EQUATIONS BY MEANS OF THE GALERKIN METHOD TO DETERMINE THE INSTABILITY LOADS, THE POST-BUCKLING BEHAVIOUR AND THE MAXIMUM LOADS OF PLATES FOR SPECIFIC BOUNDARY CONDITIONS.

In this chapter the biharmonic equation is derived from the generalised elastic plate equations and solved, by use of the Galerkin method, to give the initial elastic instability loads for flat plates subjected to a linearly varying compressive load action. The complete form of the large deflection equations is then used together with the Galerkin series derived in Chapter II to give the post-buckling behaviour of these plates.

The chapter ends by the introduction of a simple yield criterion which permits the development of a simple and effective method for determining the maximum load which the plates may sustain.

III.1 Evaluation of the Elastic Instability Load.

The elastic instability load is considered to be that load at which the flat plate first develops deflect-:ions out of the plane of the plate. Of course this is a purely theoretical concept, since every practical plate will have some deviation from flatness buckles will begin to grow from the beginning of load application. It has

been shown, however, by Coan (1951) and Hu et al. (1946) and others that for a plate with a small initial deviation from flatness the buckles grow very much more quickly in the region of the equivalent flat plate instability region.

For this reason therefore the elastic instability load is of considerable use to a designer when the stiff-:ness of a structure is to be considered.

The theoretical assumptions made for the plate are that (i) the plate is perfectly flat at a load slightly less than the instability load;
and (ii) at loads slightly greater than the instability load the deflections are sufficiently small for the stress distribution to be substantially unaltered from that in the flat plate.

Thus in equation II.4.2 the coefficients b_{rs} are zero and the equation becomes

$$F' = \frac{N_0'}{2}\left[(1-\tfrac{\alpha}{2}) + \tfrac{\alpha}{2}\eta\right]\eta^2$$

and equation II.2.1 reduces to the biharmonic equation

$$\frac{1}{\phi^2}\frac{\partial^4\omega}{\partial\xi^4} + 2\frac{\partial^4\omega}{\partial\xi^2\partial\eta^2} + \phi^2\frac{\partial^4\omega}{\partial\eta^4} = 12(1-\nu^2)N_0'\left[(1-\tfrac{\alpha}{2}) + \alpha\eta\right]\frac{\partial^2\omega}{\partial\xi^2}$$

$$= \frac{N_0 b^2}{D\phi^2}\left[(1-\tfrac{\alpha}{2}) + \alpha\eta\right]\frac{\partial^2\omega}{\partial\xi^2} \quad \ldots\ldots \text{III.1.1.}$$

It is now possible to reduce equation III.1.1 to an ordinary differential equation by letting m, in equation II.4.12, take a specific value.

Hence equation II.4.12 becomes

$$\omega = \sum_{n=0,1} q_n \sin m\pi\xi\left[\eta^{n+4} + A_n\eta^{n+3} + B_n\eta^{n+2} + C_n\eta^{n+1} + D_n\eta^n\right]$$

which for simplicity can be rewritten as

$$\omega = \sin m\pi\xi \cdot Y \quad \text{III.1.2.}$$

where $$Y = \sum_{n=0,1,} q_n \left[\eta^{n+4} + A_n \eta^{n+3} + B_n \eta^{n+2} + C_n \eta^{n+1} + D_n \eta^n\right]$$

or a similar function of η. Substituting now equation II.1.2 into equation II.1.1 gives

$$\frac{d^4Y}{d\eta^4} - 2\frac{m^2\pi^2}{\phi^2}\frac{d^2Y}{d\eta^2} + \frac{m^4\pi^4}{\phi^4}Y = -k\frac{m^2\pi^2}{\phi^2}\left[(1-\tfrac{\alpha}{2}) + \alpha\eta\right]Y \quad \text{III.1.3.}$$

where $-k = -\frac{N_o b}{D}$ and $N_o \equiv N_{crit.}$

A detailed outline of the solution of equation III.1.3 by the Galerkin method now follows. An alternative method of solution involving finite difference techniques is presented in Appendix III.

The Galerkin method of solution is obtained by expanding the following integral and obtaining its roots.

$$\int_{-\frac{1}{2}}^{\frac{1}{2}} \left\{ \frac{d^4Y}{d\eta^4} - 2\frac{m^2\pi^2}{\phi^2}\frac{d^2Y}{d\eta^2} + \frac{m^4\pi^4}{\phi^4}Y - k\frac{m^2\pi^2}{\phi^2}\left[(1-\tfrac{\alpha}{2}) + \alpha\eta\right]Y \right\} \frac{\partial Y}{\partial q_n} d\eta = 0 \quad \text{III.1.4.}$$

The form of this expansion is probably clearer if the following method of presentation is used. A typical term of the Galerkin series Y is taken as $q_i Y_i$ and the Galerkin expansion can then be written as

$$\sum_{n=0,1,}^{n=l} \int_{-\frac{1}{2}}^{\frac{1}{2}} \left\{ \frac{d^4Y_n}{d\eta^4} - 2\frac{m^2\pi^2}{\phi^2}\frac{d^2Y_n}{d\eta^2} + \frac{m^4\pi^4}{\phi^4}Y_n - k\frac{m^2\pi^2}{\phi^2}\left[(1-\tfrac{\alpha}{2}) + \alpha\eta\right]Y_n \right\} \frac{dY_i}{dq_i} d\eta = 0$$

where l is the limit of the number of terms included in the series. A detailed expansion of this equation is given in Appendix IV. It will be seen from equation III.1.4 that as n and i vary over the range $0 \leq n, i \leq l$ a square matrix of the coefficients q_n will be built up.

This matrix can be represented by

$$\begin{bmatrix} (L_{oo} - k M_{oo}) & (L_{o1} - k M_{o1}) \dots\dots\dots & (L_{ol} - k M_{ol}) \\ (L_{o1} - k M_{o1}) & & \vdots \\ \vdots & & \\ (L_{lo} - k M_{lo}) \dots\dots\dots\dots & & (L_{ll} - k M_{ll}) \end{bmatrix} \begin{bmatrix} q_o \\ \vdots \\ q_n \\ \vdots \\ q_l \end{bmatrix} = 0$$

The values of k only have practical meaning for the non-trivial values of q_n, i.e. if the determinant of the above matrix is zero. It is thus possible to obtain the required range of eigenvalues by equating the determinant to zero, expanding it and solving the resultant polynomial. The only value which is of relevance, however, in this investigation is the lowest real one. An alternative method of the matrix therefore is to assume that the required eigenvalue is unique and to arrange the matrix as follows:

$$\begin{bmatrix} L_{oo} \dots\dots L_{ol} \\ \vdots \quad\quad \vdots \\ L_{lo} \dots\dots L_{ll} \end{bmatrix} \begin{bmatrix} q_o \\ \vdots \\ q_l \end{bmatrix} = k \cdot \begin{bmatrix} M_{oo} \dots\dots M_{ol} \\ \vdots \quad\quad \vdots \\ M_{lo} \dots\dots M_{ll} \end{bmatrix}$$

$$\text{i.e.} \quad [L][q] = k\,[M][q]$$

$$[q]\frac{1}{k} = [L^{-1}.M][q]$$

If now a trial vector is chosen arbitrarily, operated on using $[L^{-1}.M]$ and then normalised, the resulting value of $\frac{1}{k}$ will be closer to the highest eigenvalue than the chosen one. Thus an iterative cycle can be set up, viz.,

$$\frac{1}{k}[q]_{r+1} = [L^{-1}.M][q]_r$$

so that k converges to the lowest eigenvalue and the buckling mode is given by the normalised vector. This procedure was programmed for the computer and convergence was found to be very rapid.

It was stated in an earlier chapter that the rate of convergence of this solution can be indicated merely by increasing the number of terms included in the series. Two examples of this property are given below.

(a) Uniformly compressed square plate, simply supported along one unloaded edge, free along the other. $\alpha = 0 \quad \phi = 1 \quad K_0 = 0$

Terms included	Eigenvalue
q_0	14.52005
$q_0 \quad q_1$	14.16723
$q_0 \quad q_1 \quad q_2$	14.15520
$q_0 \quad q_1 \quad q_2 \quad q_3$	14.15485
$q_0 \quad q_1 \quad q_2 \quad q_3 \quad q_4$	14.15484
$q_0 \quad q_1 \quad q_2 \quad q_3 \quad q_4 \quad q_5$	14.15484

(b) Eccentrically compressed ($\alpha = 1$) square plate, simply supported along one edge, built-in along the other. $\phi = 1 \quad K_1 = 0 \quad K_0 = \infty$

Terms included	Eigenvalue
q_0	130.8019
$q_0 \quad q_1$	125.2303
$q_0 \quad q_1 \quad q_2$	125.2001
$q_0 \quad q_1 \quad q_2 \quad q_3$	125.1820
$q_0 \quad q_1 \quad q_2 \quad q_3 \quad q_4$	125.1800
$q_0 \quad q_1 \quad q_2 \quad q_3 \quad q_4 \quad q_5$	125.1797
$q_0 \quad q_1 \quad q_2 \quad q_3 \quad q_4 \quad q_5 \quad q_6$	125.1797

The convergence is thus seen to be very rapid. Given below are examples of comparisons of the results of the method developed here and those of previous workers. Four terms were used in the Galerkin series.

k' values derived by the author.
k'' values given by Timoshenko (1961, Chap. 8).
k^* values given by Lundquist & Stowell (1942).

Table 1 Comparison of values of k for a uniformly compressed plate, simply supported along the unloaded edges. $\alpha = 0 \quad K_1 = K_0 = 0$

ϕ	0.4	0.8	1.1
k^*	83.003	41.468	39.834
k'	83.003	41.477	39.838

Table 2 Comparison of values of k for eccentrically compressed plate, simply supported along the unloaded edges. $\alpha = 1 \quad K_1 = K_0 = 0$

ϕ	0.4	0.6	0.8	1.0
k''	149.030	95.735	79.944	76.938
k'	149.536	96.164	80.255	77.101

Table 3 Comparison of values of k for eccentrically compressed plate, built-in along one unloaded edge and simply supported along the other. $\alpha = 2 \quad K_1 = \infty \quad K_0 = 0$

ϕ	0.6	0.8	1.0
k''	243.285	249.701	279.309
k'	238.339	243.347	273.072

Table 4 Comparison of values of k for concentrically compressed plate, simply supported along one unloaded edge and free along the other.
$\alpha = 0 \quad K_o = 0$

ϕ	1.0	1.4	1.5	2.0
k''	14.222	9.396	8.751	6.889
k'	14.154	9.400	8.764	6.888

Table 5 Comparison of values of k for concentrically compressed plate, rotationally restrained along one unloaded edge and free along the other. $\alpha = 0 \quad K_o = a$

ϕ	1.0	1.5	2.0
k''	15.596	11.448	11.054
k'	15.573	11.411	11.099

Table 6 Comparison of values of k for concentrically compressed plate, built-in along one unloaded edge, free along the other.
$\alpha = 0 \quad K_o = \infty$

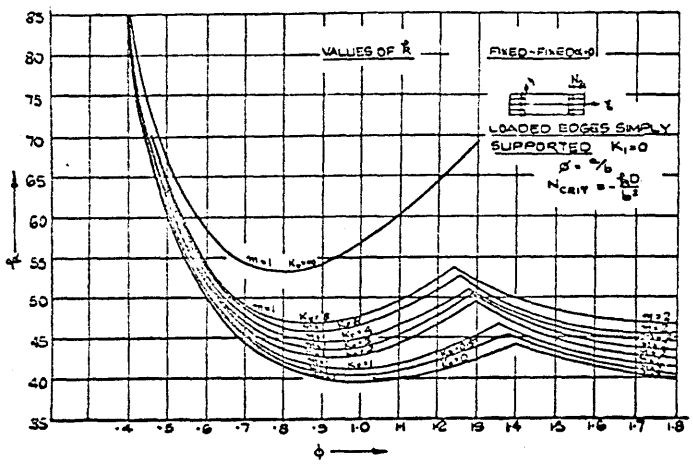

FIG. III.1 BUCKLING CONSTANT Vs. ASPECT RATIO.

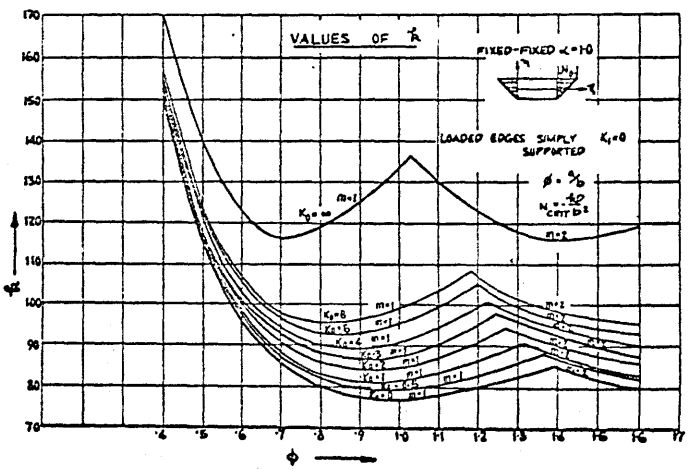

FIG. III.2 BUCKLING CONSTANT Vs. ASPECT RATIO

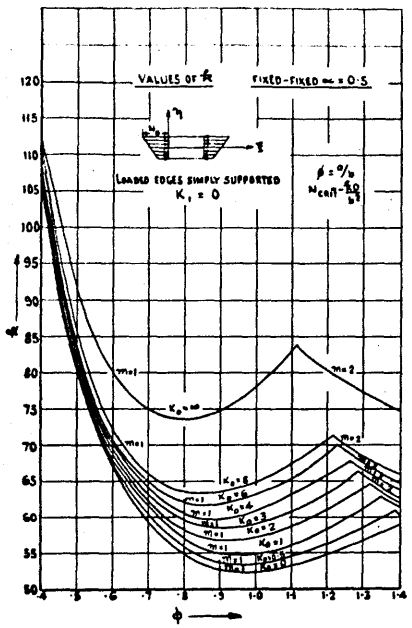

FIG III.3 BUCKLING CONSTANT Vs. ASPECT RATIO.

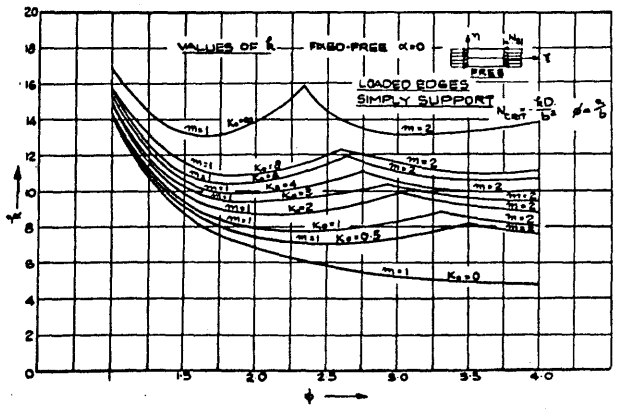

FIG. III.4 BUCKLING CONSTANT Vs. ASPECT RATIO

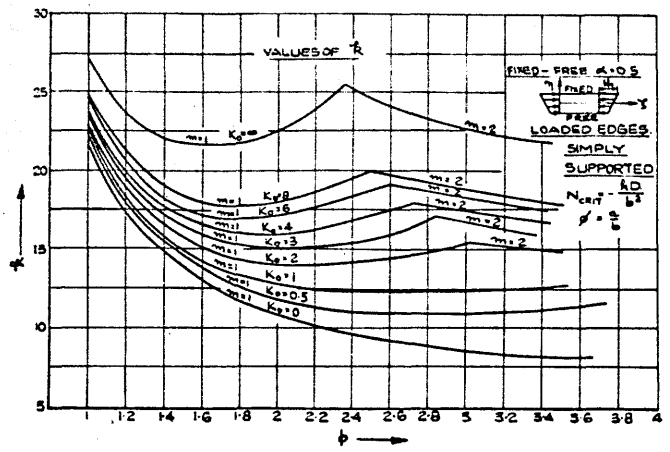

FIG. III.5 BUCKLING CONSTANT VS. ASPECT RATIO.

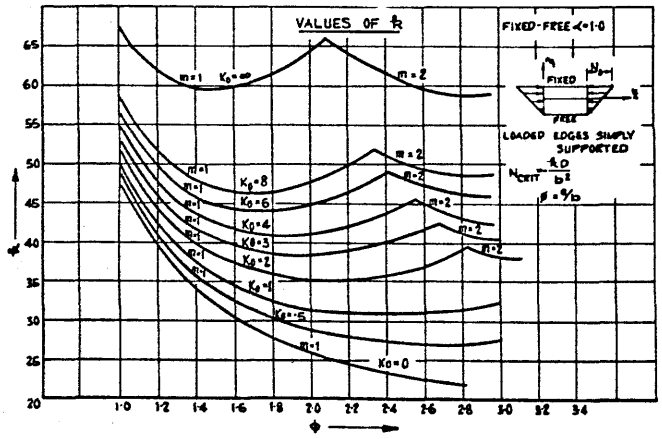

FIG. III.6 BUCKLING CONSTANT VS. ASPECT RATIO

ϕ	1.0	1.5	2.0
k''	16.679	13.230	13.620
k'	16.761	13.217	13.681

In Figures III.1 - III.6 sample results of the calculations outlined above are given, again four terms were used in the Galerkin series. All calculations were carried out with $\frac{m}{\phi}$ equal to unity and the range presented was extended merely by treating this parameter as a constant.

From these figures the buckling load can be calcul-:ated as

$$P_{crit.} = -\frac{k D}{b}\left(1-\frac{\alpha}{2}\right)$$

III.2 Post-buckling Behaviour.

One characteristic often observed in plates compress-:ed beyond the buckling load is change of wavelength. That is, depending on the length to breadth ratio of the plate and the edge conditions it is possible for the number of buckles to increase as the loading proceeds. This phenomenon was the subject of a theoretical study carried out by Stein (1959). Practice has shown, however, that the change in wavelength may be delayed or advanced by even slight deviations of the actual from the ideal theoretical plate conditions. For this reason the post-buckling behaviour presented in this chapter is for plates which maintain the same wavelength from instab-

:ility to collapse.

In Chapter II the Galerkin series were derived as

$$F' = \frac{N_0'}{2}\left[(1-\tfrac{\alpha}{2})+\tfrac{\alpha}{2}\eta\right]\eta^2+\sum_{r=1,2,}\sum_{s=0,1,} b_{rs}\sin^2 r\pi\xi\left[\eta^{s+4}-\tfrac{1}{2}\eta^{s+2}+\tfrac{1}{16}\eta^s\right] \quad \text{II.4.4.bis.}$$

$$\omega = \sum_{m=1,2,}\sum_{n=0,1,} q_{mn}\sin m\pi\xi\left[\eta^{n+4}+A_n\eta^{n+3}+B_n\eta^{n+2}+C_n\eta^{n+1}+D_n\eta^n\right] \quad \text{II.4.8.bis.}$$

For obvious reasons the summations cannot be taken to infinity, the limits are in fact imposed by the avail-:ability of storage space in the particular computer used. After programming it was found that $r \times s$ could not be more than twelve and $m \times n$ could not be more than three for the Ferranti "Sirius" used. For this reason it was decided to limit the approximation to the deflected shape in the ξ direction by letting m equal 1 or 2 or 3, etc. This leads to a more accurate solution than limiting the approx-:imation in the η direction. Thus equations II.4.4 and II.4.8 become

$$F' = \frac{N_0'}{2}\left[(1-\tfrac{\alpha}{2})+\tfrac{\alpha}{3}\eta\right]\eta^2+\sum_{r=1,2}^{r=t}\sum_{s=0,1}^{s=u} b_{rs}\sin^2 r\pi\xi\left[\eta^{s+4}-\tfrac{1}{2}\eta^{s+2}+\tfrac{1}{16}\eta^s\right] \quad \text{III.2.1.}$$

$$\omega = \sin m\pi\xi\sum_{n=0,1,}^{n=l} q_n\left[\eta^{n+4}+A_n\eta^{n+3}+B_n\eta^{n+2}+C_n\eta^{n+1}+D_n\eta^n\right] \quad \text{III.2.2.}$$

where $r \times u \neq 12$; $l \neq 3$

If $$F'_{pq} = b_{pq}\sin^2 p\pi\xi\left[\eta^{q+4}-\tfrac{1}{2}\eta^{q+2}+\tfrac{1}{16}\eta^q\right]$$

and $$\omega_i = q_i\sin m\pi\xi\left[\eta^{i+4}+A_i\eta^{i+3}+B_i\eta^{i+2}+C_i\eta^{i+1}+D_i\eta^i\right]$$

are specific terms of equations III.2.1 and III.2.2 respectively, then by Galerkin's method

$$\sum_{n=0,1,}^{n=l}\sum_{r=1,2,}^{r=t}\sum_{s=0,1,}^{s=\mu}\int_{0}^{1}\int_{-\frac{1}{2}}^{\frac{1}{2}}\left[\frac{1}{\phi^2}\frac{\partial^4 F'}{\partial\xi^4}+2\frac{\partial^4 F'}{\partial\xi^2\partial\eta^2}+\phi^2\frac{\partial^4 F'}{\partial\eta^4}-\left(\frac{\partial^2\omega}{\partial\xi\partial\eta}\right)^2-\frac{\partial^2\omega}{\partial\xi^2}\cdot\frac{\partial^2\omega}{\partial\eta^2}\right]\frac{dF'_{pq}}{db_{rs}}\,d\eta\,d\xi=0 \qquad \text{III.2.3}$$

$$\sum_{n=0,1,}^{n=l}\sum_{r=1,2,}^{r=t}\sum_{s=0,1}^{s=\mu}\int_{0}^{1}\int_{-\frac{1}{2}}^{\frac{1}{2}}\left[\frac{1}{\phi^2}\frac{\partial^4\omega}{\partial\xi^4}+2\frac{\partial^4\omega}{\partial\xi^2\partial\eta^2}+\phi^2\frac{\partial^4\omega}{\partial\eta^4}-12(1-\nu^2)\left(\frac{\partial^2 F'}{\partial\xi^2}\cdot\frac{\partial^2\omega}{\partial\eta^2}+\right.\right.$$

$$\left.\left.+\frac{\partial^2 F'}{\partial\eta^2}\cdot\frac{\partial^2\omega}{\partial\xi^2}-2\frac{\partial^2 F'}{\partial\xi\partial\eta}\cdot\frac{\partial^2\omega}{\partial\xi\partial\eta}\right)\right]\frac{d\omega_i}{dq_i}\,d\eta\,d\xi=0 \qquad \text{III.2.4}$$

As the ranges $1\leq p,r\leq t$; $0\leq q,s\leq\mu$ and $0\leq n,i\leq l$ are covered two systems of simultaneous non-linear algebraic equations are built-up, viz:

$$\begin{aligned}
&A_{1010}b_{10}+\cdots+A_{101\mu}b_{1\mu}+\cdots+A_{10t\mu}b_{t\mu}+B_{1000}q_0^2+B_{1010}q_0q_1+\cdots+B_{10ll}q_l^2=0\\
&\vdots\qquad\qquad\vdots\qquad\qquad\vdots\qquad\qquad\vdots\qquad\qquad\vdots\\
&A_{t\mu10}b_{10}+\cdots+A_{t\mu1\mu}b_{1\mu}+\cdots+A_{t\mu t\mu}b_{t\mu}+B_{t\mu00}q_0^2\cdots\cdots+B_{t\mu ll}q_l^2=0
\end{aligned}$$

$$\begin{aligned}
&C_{00}q_0+C_{01}q_1+\cdots+C_{0l}q_l+D_{1000}b_{10}q_0+\cdots+D_{t\mu0l}b_{t\mu}q_l=0\\
&\vdots\qquad\vdots\qquad\qquad\vdots\qquad\vdots\qquad\qquad\vdots\\
&C_{l0}q_0+C_{l1}q_1+\cdots+C_{ll}q_l+D_{10l0}b_{10}q_0+\cdots+D_{t\mu ll}b_{t\mu}q_l=0
\end{aligned}$$

where the constants A, B, C and D are obtained from equations III.2.3 and III.2.4 the expansions of which are given in Appendix IV.

In matrix form the above system of equation becomes

$$\begin{bmatrix}A_{1010}&\cdots&A_{10t\mu}\\ \vdots&&\vdots\\ A_{t\mu10}&\cdots&A_{t\mu t\mu}\end{bmatrix}\begin{bmatrix}b_{10}\\ \vdots\\ b_{t\mu}\end{bmatrix}=-\begin{bmatrix}B_{1000}&\cdots&B_{10ll}\\ \vdots&&\vdots\\ B_{t\mu00}&\cdots&B_{t\mu ll}\end{bmatrix}\begin{bmatrix}q_0q_0\\ \vdots\\ q_lq_l\end{bmatrix} \qquad \text{III.2.5}$$

$$\begin{bmatrix}C_{00}&\cdots&C_{0l}\\ \vdots&&\vdots\\ C_{l0}&\cdots&C_{ll}\end{bmatrix}\begin{bmatrix}q_0\\ \vdots\\ q_l\end{bmatrix}=-\begin{bmatrix}D_{1010}&\cdots&D_{t\mu0l}\\ \vdots&&\vdots\\ D_{10l0}&\cdots&D_{t\mu ll}\end{bmatrix}\begin{bmatrix}b_{10}q_0\\ \vdots\\ b_{t\mu}q_l\end{bmatrix} \qquad \text{III.2.6}$$

In equation II.2.6 C_{oo} can be divided into its components, i.e.

$$C_{oo} = C'_{oo} - N'_o C''_{oo}$$

An example of the coefficients is taken with

$$\phi = 2 \qquad K_1 = K_o = 0 \qquad \alpha = 1 \qquad m = 2 \qquad t = u = l = 1$$

$$2344.5\, b_{10} = -234.7\, q_o^2 \quad \ldots\ldots \text{III.2.7.}$$

$$(76.7 + 10.9\, N'_o) q_o = 26.4\, b_{10} q_o \quad \ldots\ldots \text{III.2.8.}$$

One way to solve these equations is to obtain b_{10} in terms of q_o^2 from equation III.2.7, i.e.

$$b_{10} = -0.102\, q_o^2$$

and hence by substitution and for $N_o = -30$ equation III.2.8 becomes

$$-2\,51.2\, q_o = -2.62\, q_o^2 \quad \ldots\ldots \text{III.2.9.}$$

An obvious but trivial solution to equation III.2.9 is $q_o = 0$ and therefore $b_{10} = 0$. The other two solutions are obtained by assuming q_o to be other than zero and cancelling in equation III.2.9 to give $q_o = \pm 9.7$, $b_{10} = -9.8$.

This simple example illustrates the fundamental characteristics of equations III.2.6 and III.2.5 and shows that the solution for the deflection series can have three real roots, one zero and the other two equal in magnitude but opposite in sign. These respectively correspond to the plate remaining flat or deflecting laterally in either direction, both of equal significance. For the stress function the roots are identical for the laterally deflected plate irrespective of the sign of the deflection.

If this procedure is applied to equations III.2.5

and III.2.6 it is possible to solve these to give the required series. Thus, if equation III.2.5 is written for simplicity as

$$[A][b_{rs}] = [B][q_i q_j] \quad \text{where} \quad 0 \leq i,j \leq l \qquad \text{III.2.10.}$$

then

$$[b_{rs}] = [A^{-1}.B][q_i q_j] \qquad \text{III.2.11.}$$

Similarly equation III.2.6 can be written as

$$\{[C'] + N_0'[C'']\}[q_k] = [D][b_{rs}\, q_k] \quad \text{where} \quad 0 \leq k \leq l \qquad \text{III.2.12.}$$

and by substitution of the individual elements of equation III.2.11 into equation III.2.12 it becomes

$$\{[C'] - N_0'[C'']\}[q_k] = [E][q_i q_j q_k] \qquad \text{III.2.13.}$$

Equation III.2.13 is now the matrix equivalent of equation III.2.9 but if $l \geq 2$ then some iterative cycle must be set up to obtain q_0, q_1, etc. This involves a lot of arithmetical operations and was found to be slow to converge. If, instead of a load, a value of deflection (q_0) is chosen and substituted into equation III.2.13 then an iterative cycle need only be set up if $l \geq 3$ and this was found to converge very much more quickly. This was the procedure which was programmed for the computer.

The convergence of the solution of the Von Karman equations by Galerkin's method can only be obtained for each individual case of boundary and loading conditions by comparison of the relevant parameters for varying

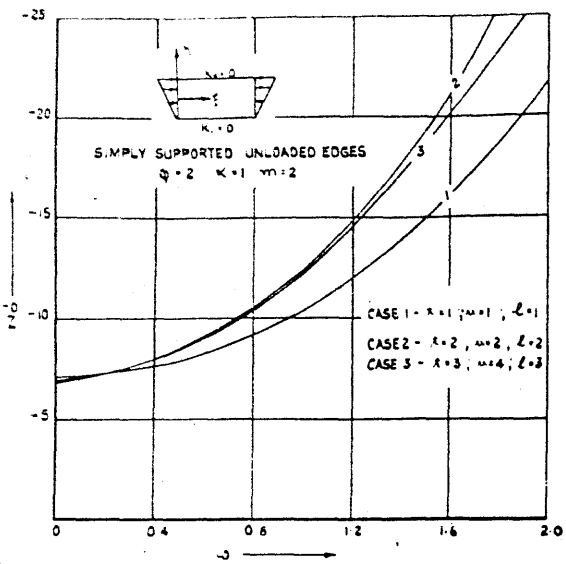

FIG III 7 COMPARISON OF LOAD Vs DEFLECTION FOR VARYING NUMBERS OF TERMS INCLUDED IN SERIES.

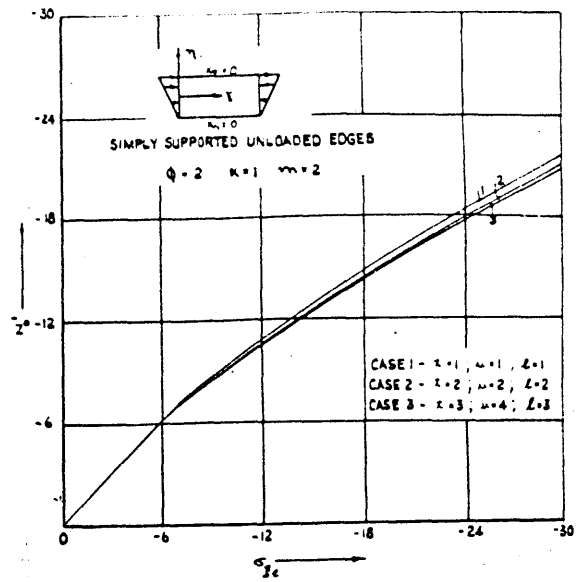

FIG. III 8 COMPARISON OF LOAD Vs EDGE STRESS FOR VARYING NUMBERS OF TERMS INCLUDED IN SERIES.

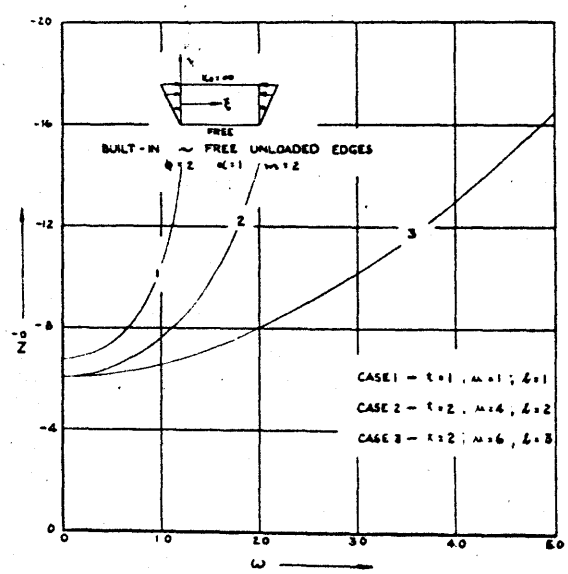

FIG III 9 COMPARISON OF LOAD Vs. DEFLECTION FOR VARYING NUMBERS OF TERMS INCLUDED IN SERIES.

limits in the series. Samples of these comparisons are shown in Figures III.7,8 and III.9; convergence of these parameters is further discussed in a later chapter of this thesis when the results of the experi-:mental investigation are compared to the corresponding theoretical predictions. Conclusions are then drawn from these comparisons as to the probable rate of con-:vergence of the series solution.

III.3 Maximum Load Carrying Capacity.

The ultimate load which a plate can carry must be deduced not only from a consideration of large deflection theory but also from plasticity theory. If the metal was to remain linearly elastic, increasing load would merely cause increasing deflection and deformation and there would be no maximum load. So far to the author's knowledge only one attempt has been made to solve the extremely complicated non-linear problem posed by the inclusion of the deformation theory of plasticity on the consideration of the large deflection of plates. This reference (Budiansky and Mayers, 1955) has already been reviewed fully in Chapter I and it is only necessary to note here that in order to proceed at all, a coarse physical model had to be postulated to the plate, thus limiting from the outset the accuracy of the method. Until some method is presented to overcome this difficulty, however, considerable information can be obtained from a study of the elastic equations together with some simple criterion for the onset of plastic flow.

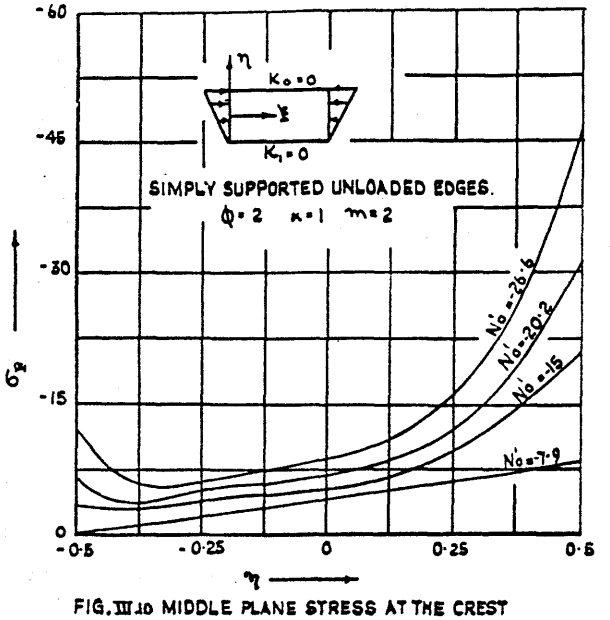

FIG. III.10 MIDDLE PLANE STRESS AT THE CREST OF A BUCKLE.

The solution to the elastic equations developed herein indicates that in the post-buckling region the direct stresses in the ξ direction are greater than the other stresses and, as loading proceeds, become concentrated at the plate edges near the crest of a buckle.

A sample distribution of these stresses across a section at the crest of a buckle on the middle plane of the plate is shown in Figure III.10. For a plate with a free edge the stresses are similarly concentrated at the edge, but in this case the maximum values occur on the plate skin due to bending. This concentration of direct stresses has led to the formulation of a collapse criterion based on Rankine's yield criterion. Thus it is considered that when the stress in the ξ direction at any section of the plate reaches the yield value for the plate material then the plate has collapsed.

This is of course only applicable to those materials which exhibit sudden and extensive yielding at a specific load. Examples of such materials are to be found in the high grade mild steel used in light civil engineering structures and the new titanium alloys which are being introduced into aircraft construction. Employment of this criterion leads to a simple and practically useful method for determining the collapse loads of eccentrically loaded thin plates and, as will be shown later, gives values which are in good agreement with those found experi-:mentally.

An example is now given of the method of obtaining

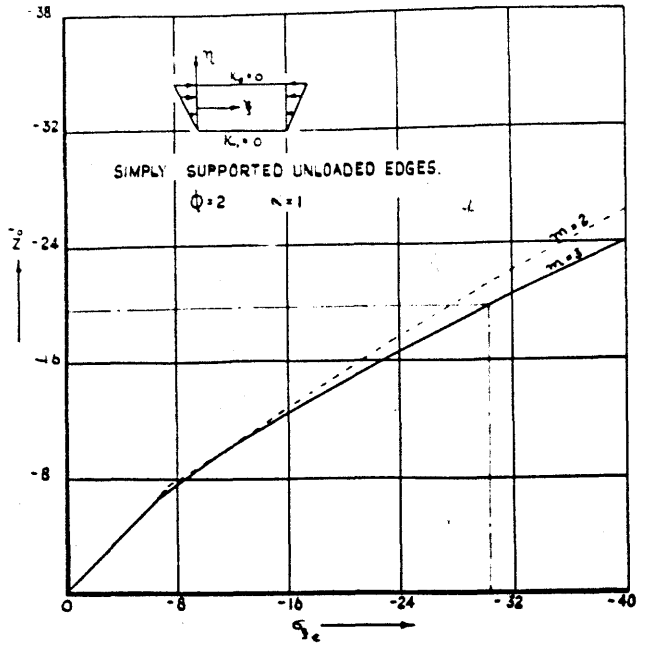

FIG. III.11 LOAD Vs. EDGE STRESS

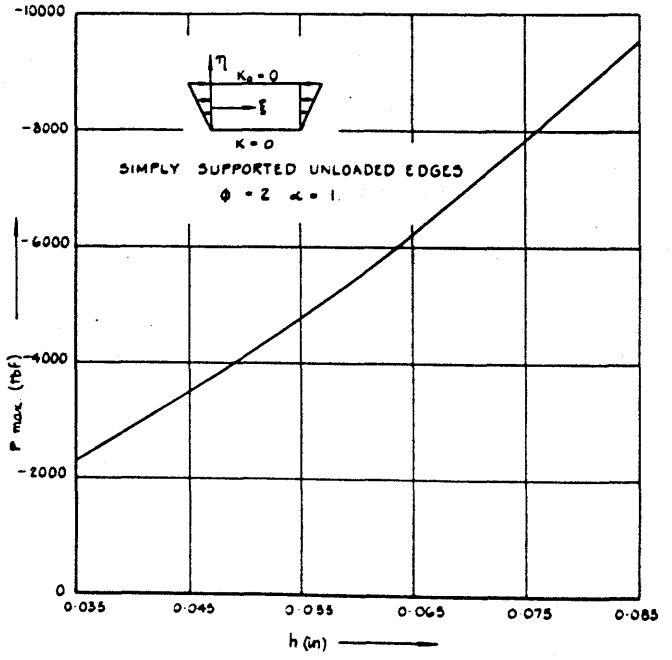

FIG III 12 COLLAPSE LOAD V. PLATE THICKNESS.

the plot of "collapse load vs. plate thickness" for a plate simply supported along both unloaded edges. The non-dimensional stress at $\eta = 0.5$ at the crest of a buckle is plotted against the non-dimensional load parameter in Figure III.11 in which it will be seen that values have been calculated with $m=2$ and $m=3$. The reason for this is that in tests on such plates, described later, the initial buckling pattern of two half waves in the ξ direction sometimes changed to three half waves. Thus collapse loads were calculated using the values in Figure III.11 which gave the lower theoretical collapse load and so providing a theoretically conservative value for those plates which did not have a change of wavelength.

From tensile tests on specimens taken from the test plates the average values of yield stress and Young's Modulus were $\sigma_{yield} = 25.5 \times 10^3$ tf/in^2 and $E = 33 \times 10^6$ tf/in^2 respect-:ively. Assuming these values to hold in compression, the stress at the edge at collapse is given by

$$\sigma_{\xi_e} = \frac{\phi^2 E h^2}{a^2} \times -25.5 \times 10^3$$

taking $\phi = 2$ $h = 0.05$ $a = 20$" this gives $\sigma_{\xi_e} = -30.9$

The corresponding value of N_o' from Figure III.10 is $N_o' = -19.8$

Now $N_o' = \frac{Pb}{Eh^3(1-\frac{\alpha}{2})}$ hence the collapse load $(P_{max}) = -4080$ tf.

Thus by choosing other values of thickness the theoretical curve in Figure III.12 was constructed.

C H A P T E R I V

CHAPTER IV.

EXPERIMENTAL INVESTIGATIONS INTO THE LOAD BEARING BEHAVIOUR OF INDIVIDUAL PLATES.

An extensive experimental investigation has been carried out by the author into the problem of the post-:buckling behaviour of single plates subjected to eccen-:tric edge compression. In this chapter the aims and organisation of the test programmes conducted in this investigation are presented together with detailed descriptions of the special equipment designed and built for the purposes of these tests. The chapter ends with a presentation of typical results obtained from this experimental investigation.

IV.1 Test Programmes.

The tests were organised in two main categories according to the type of information to be derived from them. The first dealt with the overall characteristics of plate behaviour, i.e. instability and collapse loads; in connection with this about forty plates were loaded to collapse under various conditions of edge support and loading geometry. These plates varied in thickness from 0".036 to 0".083 but all had the same width and length of 10" and 20" respectively. Tensile test specimens were taken from various locations on typical plates, and the resulting values for the material properties are given in Appendix VI..

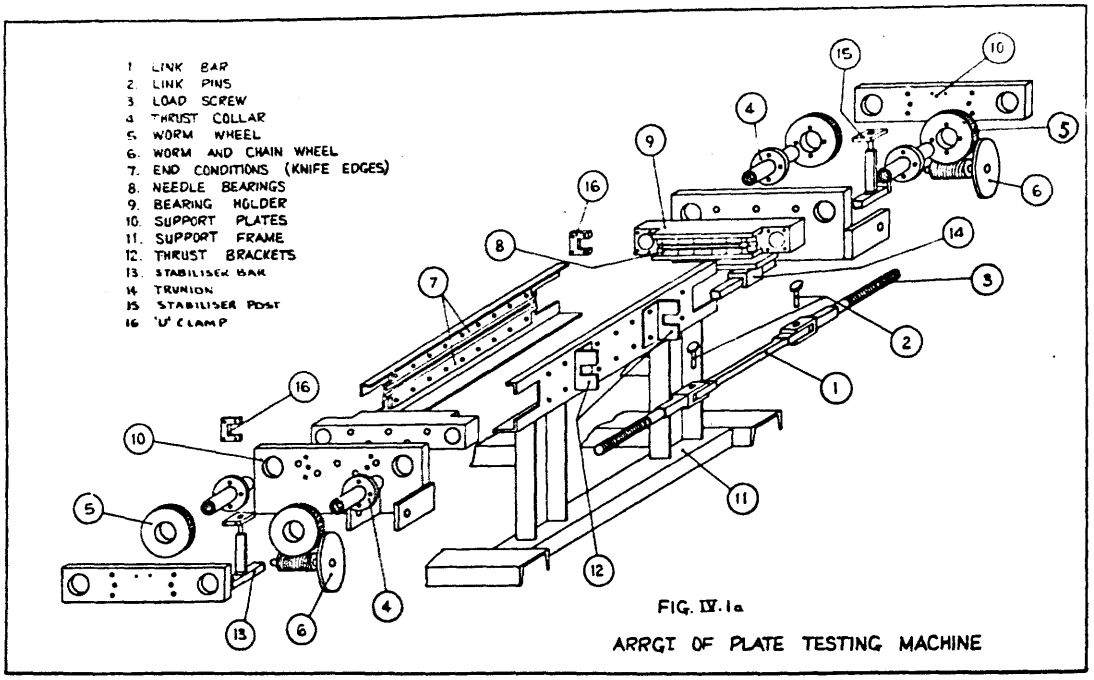

FIG. IV.1a

ARRGT OF PLATE TESTING MACHINE

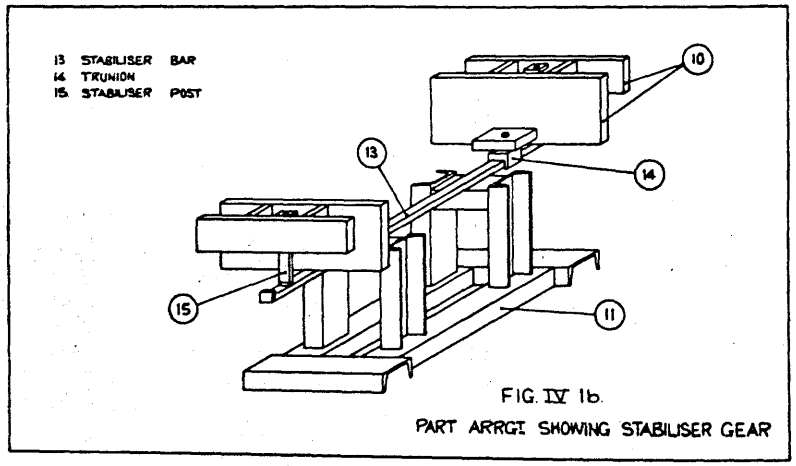

FIG. IV 1b.

PART ARRGT SHOWING STABILISER GEAR

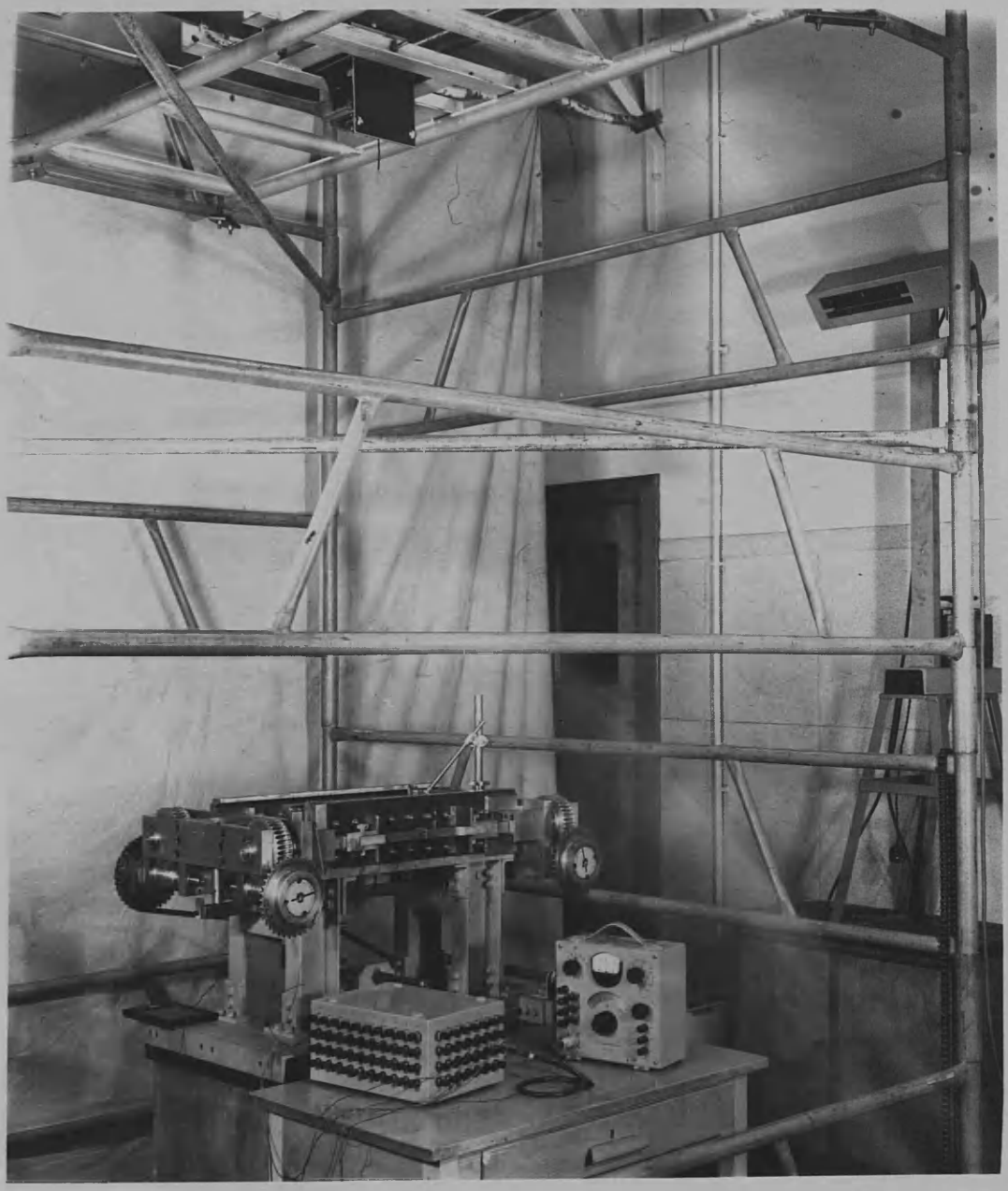

FIG. IV.2a

The second category of tests was designed to provide information on the more detailed aspects of the problem such as strain and deflection distributions. To facilitate the determination of the out-of-plane deflections over the whole plate surface photogrammetric equipment was designed and built; this is described briefly in the next section of this chapter, and much more fully in Appendix V.

IV.2 Special Test Equipment.

a. Loading Rig.

This rig was specially designed for this series of tests with the aim that the specimen plate could be subjected to a compressive loading of carefully controlled eccentricity. The length to width ratio chosen for the specimen plate was two, for the reason that this ratio gave many variations of half wave patterns with change of edge conditions and loading geometry, i.e. with $\phi < 2$ one half wave tends to predominate and for $\phi > 2$ tests conducted by previous workers on concentrically compressed plates show that the plates tend to buckle into square panels and the collapse loads are thus broadly unaffected by change in length.

The rig is shown schematically in Figures IV.1a and IV.1b and in situ in Figure IV.2a. The frame consisted mainly of two channels rigidly mounted parallel to each other on a pedestal (11). The inside faces of these

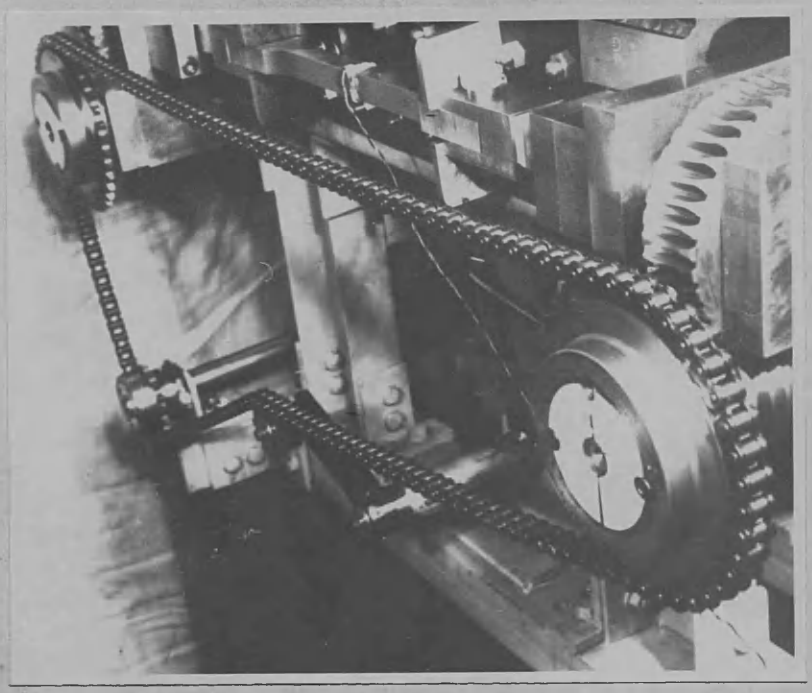

Fig. IV.2b.

channels were machined smooth to carry the unloaded edge conditions (7) and the ends, having been reinforced with welded pads, were machined to receive the end load-:ing beams. The loading beams, when mounted in these bearing slots directly opposed each other both vertically and horizontally; the horizontal position being maintained by the trunnion arrangement (14). The faces of parts 9 were carefully ground to size so that very little clear-:ance resulted on assembly with the channels.

The end assemblies consisted of two sets of worms and wheels, the wheels being attached to a collar which was screwed 1" B.S.F. along the full length of its bore. When the load screw (3) was assembled to this and locked against rotation by a 'U' clamp (16) the result was a loading arrangement with a very high mechanical advantage. The two end assemblies were identical so that the load screws opposed each other and could be joined by a link bar (1). The holes shown in items 1 and 3 were bored out together and bushes fitted; the hardened pin which fitted in the bushes thus provided a strong but rotationally free joint.

Rotation of the handwheels (6) caused the end assemblies to approach each other thus inducing a load in the plate placed in position between the end loading beams. Eccentric loading was obtained by differential rotation of one side from the other. These handwheels were in fact chain sprocket wheels and the rig was fitted with a chain drive (Figure IV.2b) for fast traverse during the setting-up period while during an actual test the wheels were turned

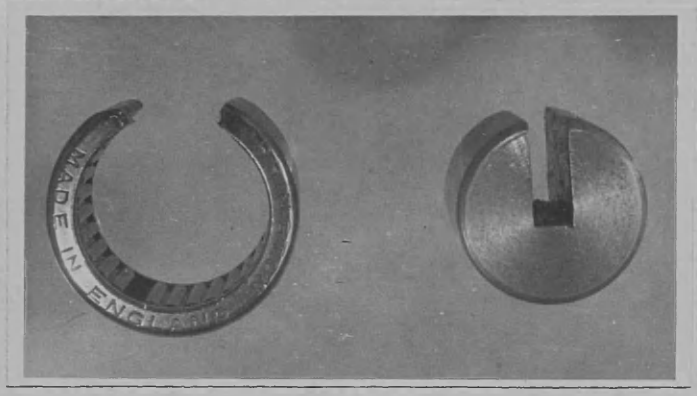

Fig. IV.3.

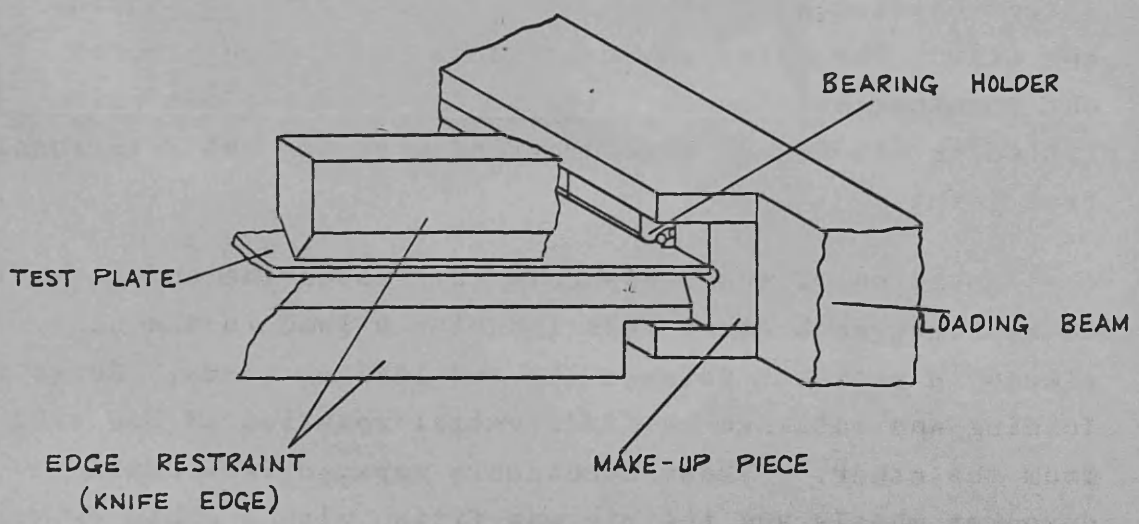

FIG. IV.4

manually, this was found to give a very sensitive arrangement. The magnitude of the load was indicated by electrical resistance foil strain gauges bonded to the link bars and connected to a Huggenberger switch box and strain bridge. Each bar assemply (1 and 3) was calibrated on an Avery tensile testing machine and gave a linear response of 16.91 μin/in up to the maximum calibrated load of four tons.

The loaded edge condition of "simple support" was obtained by using slotted rollers (Figure IV.3) in needle bearings which were mounted in groups of four in blocks (8) which in turn were mounted in the loading beams. A segment of 40^{o} was cut from the needle bear-:ing and with two extra needles removed the ends were resealed. To maintain the loading right up to the edge of the plate, i.e. to where the edge conditions were located, grooved blocks were fitted in the load bar in place of the bearing and rollers (Figure IV.4).

The general theoretical condition of rotational restraint at the unloaded edges is extremely difficult to reproduce experimentally. For this reason only the limiting cases of this condition were studied, i.e. "simple support" and "built-in". The "free edge" condition was obtained simply as the name implies by having no form of restraint on the plate at that edge. The "built-in" edge restraint is shown in Figure IV.5a, these were bolted to the main runners by 3/8" diameter bolts as were the knife edges (Figure IV.5b) which simulated the "simple support" condition. As shown in

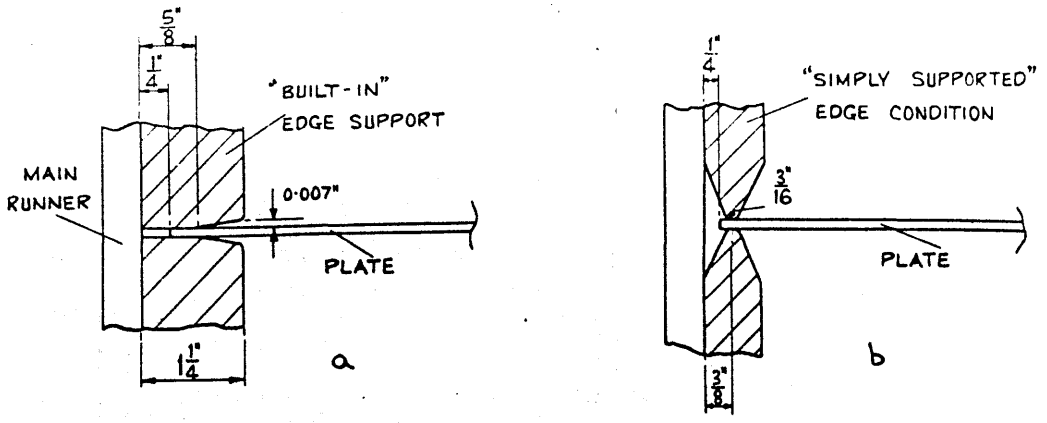

FIG. IV. 5

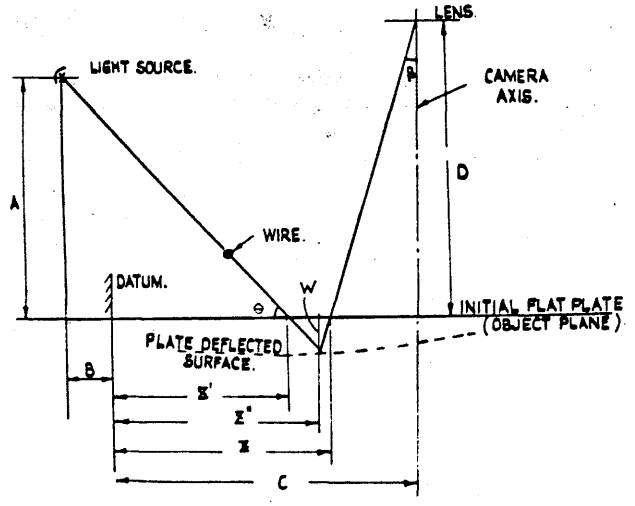

REQUIRED : W & Z'

MEASURED ON PHOTOGRAPHS : Z' & Z

CONSTANT DIMENSIONS : A (56'.25) ; B (47'.875) ; C (9'.4) ; D (18'.875) ; PHOTO. SCALE (7·14.)

FIG. IV.6 OPTICAL SYSTEM GEOMETRY.

Figure IV.5a the edges of the restraining bars were washed away in an attempt to make the acting width as close to the actual width as possible.

b. Photogrammetric Equipment.

This equipment was developed to obtain the distri-:bution of the out-of-plane deflections over the plate surface. The principle of the method, which was first successfully applied by Jackson (1947), was very simple and was essentially as follows.

Light from a line source fell on to a series of thin straight wires stretched above the plate and parallel to the lamp element. The sharp shadow thus cast on the plate surface was straight and parallel to the wire so long as the plate was flat, but when a vertical plate movement took place the shadows were displaced horizontally. This displacement was recorded by a camera mounted verti-:cally above the test rig and by accurate measurement of the photographic plate and application of the known system geometry the required deflections were obtained.

Figure IV.6 gives an example of the geometry of the system for a typical wire, the transforming of the horiz-:ontal photographic measurements to the corresponding vertical plate movements was programmed by the author for the computer thus eliminating tedious and trivial calcul-:ations.

IV.3 Test Procedure.

The following is an example of the procedure which was carried out during a test to collapse in which the "wire-shadow" technique was also used.

The test plate was first cleaned and examined for burrs and flaws, these possibly being caused during the machining of the edges. The plate dimensions were then noted, the thickness variation was usually about ±0".0005 (see Appendix VI) and the edges were parallel to within ±0".002. The plate was then mounted in the rig with longitudinal edge supports loosely bolted in place. The loading beams were each brought into a central posi-:tion using the fast traverse gear until they were lightly bearing on the ends of the plate. To maintain centrality during this and other operations in the setting up routine the screws in the thrust angles (12) were pinched lightly against the shoulders of the load screws. These thrust angles also took the load caused by the friction between the plate and the restraining bars until the load was fully developed when the arrangement was self balancing.

The width of the slot in the rollers at each loaded end was 0".110 and it was thus necessary to shim the plate to keep it central; these shims were as short and narrow as possible to avoid stiffening the end of the plate. This operation completed, the surfaces between the edge restraints and the plate were smeared with a mixture of oil and molybdenum disulphide paste which formed a high pressure lubricant. The edge supports were centralised to the loading beams using feeler gauges and, after

pinching on to the plate surface to obtain good contact, were then firmly bolted in place. A measure of the initial flatness of the plate was obtained using a clock comparator mounted on a bar running the length of the plate, this of course varied from plate to plate but was generally small, within 10% of the plate thickness.

The wire carriers were then screwed into place and the wire laced tightly round the pegs and secured. To obtain a good shadow on the plate surface a thin film of opaque grease was smeared on the plate surface prior to this operation. After taking a photograph of the initial unloaded plate and recording the initial reading on the link bar strain gauges as zero load the test was ready to proceed.

The loading was applied simultaneously on both ends of the plate in the ratio calculated to produce the required loading geometry. The value of this loading was recorded at intervals and photographs taken. Collapse was taken to have occurred when a slight reduction of the load was indicated for an inward movement of the loading beams.

IV.4 Test Results.

(i) First Series.

There have been several methods suggested for obtaining that load in actual plates which is equivalent to the

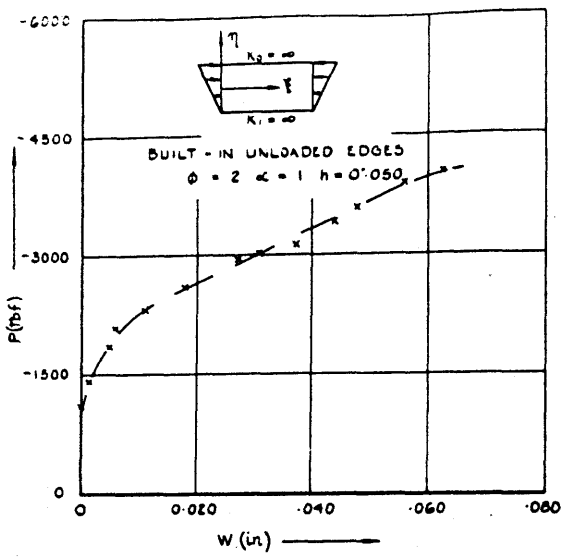

FIG. IV 7 LOAD Vs DEFLECTION.

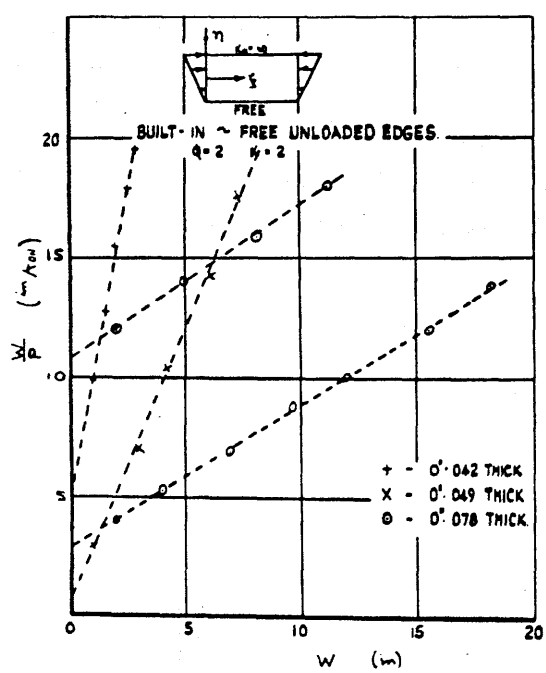

FIG. IV.8 EXAMPLE SOUTHWELL PLOTS.

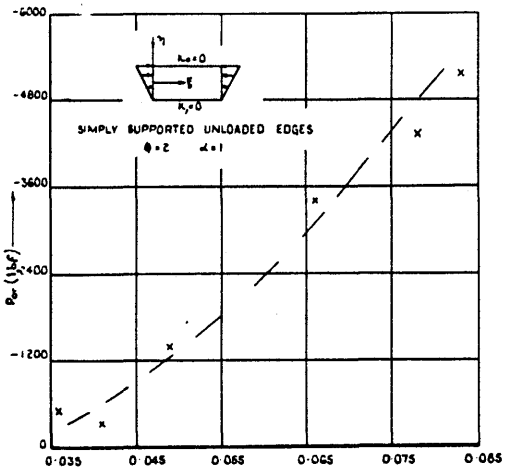

FIG. IV.9 INSTABILITY LOAD V. PLATE THICKNESS

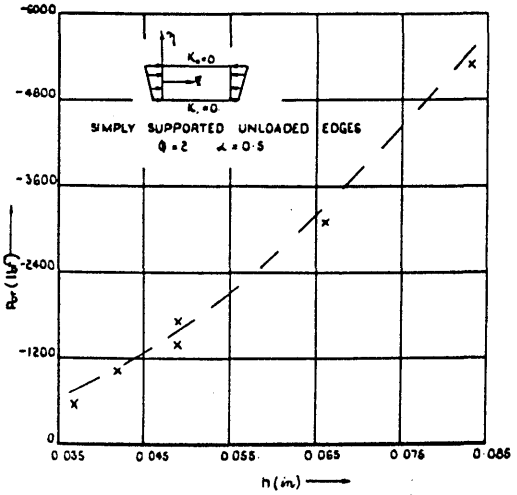

FIG. IV.10 INSTABILITY LOAD V. PLATE THICKNESS

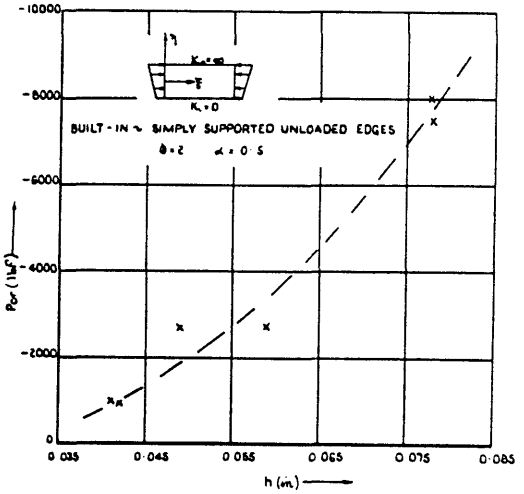

FIG. IV.11 INSTABILITY LOAD V. PLATE THICKNESS

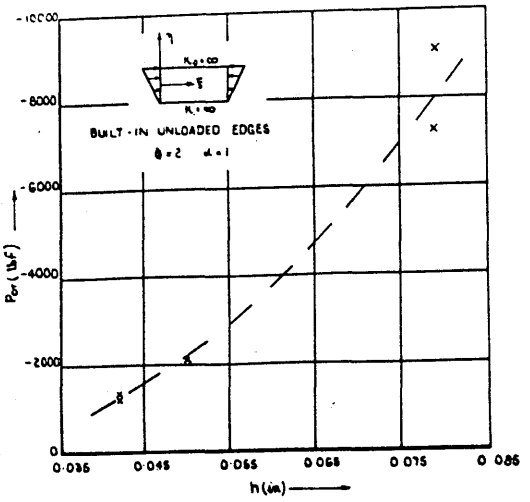

FIG. IV.12 INSTABILITY LOAD V. PLATE THICKNESS

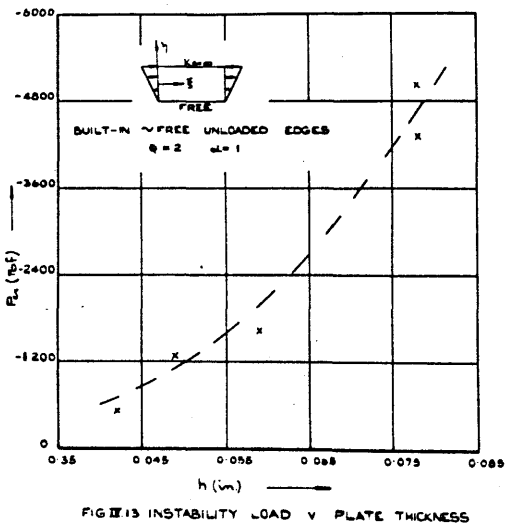

FIG IV.13 INSTABILITY LOAD V PLATE THICKNESS

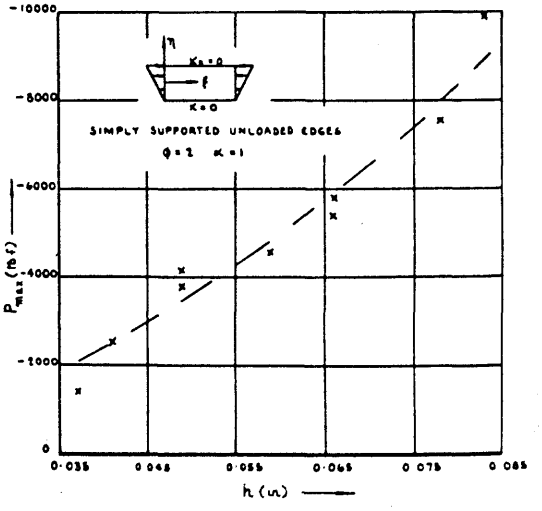

FIG. IV.14 COLLAPSE LOAD V PLATE THICKNESS

instability loads in an ideally flat plate. The need for such a process may be illustrated here by a consideration of Figure IV.7; this figure, which may be taken as typical of the results from this series of tests, shows that deflections began to grow very soon after the application of loading. This was of course due mainly to the initial imperfections present in the plate in the unloaded state.

Among the more widely used of the methods so far suggested for concentrically compressed plates are "top-of-the-knee" of the load vs. deflection plot and the "point of inflection" of the same plot. In the case of eccentrically compressed plates considered in this thesis, however, neither of these methods proved to be completely satisfactory, due mainly to the fact that the wavelength sometimes changed as the loading increased. If the "Southwell Plot" method was employed using values of the load vs. deflection plots at low loads then it was found that good straight lines were obtained. Examples of these are given in Figure IV.8. This then was the procedure used throughout this investigation to infer the experimental "instability loads" and values of these are shown plotted in Figures IV.9 - IV.13 for the combinations of edge conditions and loading geometries chosen for study here.

These combinations were:

(i) simply supported unloaded edges with loading eccentricity $\alpha = 1$

(ii) simply supported unloaded edges with loading eccentricity $\alpha = 0.5$

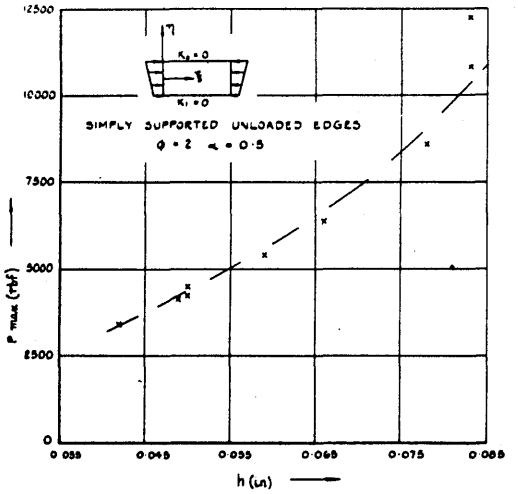

FIG. IV.15 COLLAPSE LOAD v. PLATE THICKNESS.

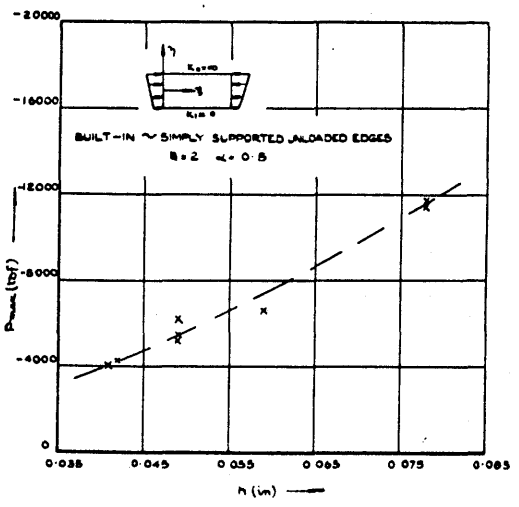

FIG IV.16 COLLAPSE LOAD v PLATE THICKNESS

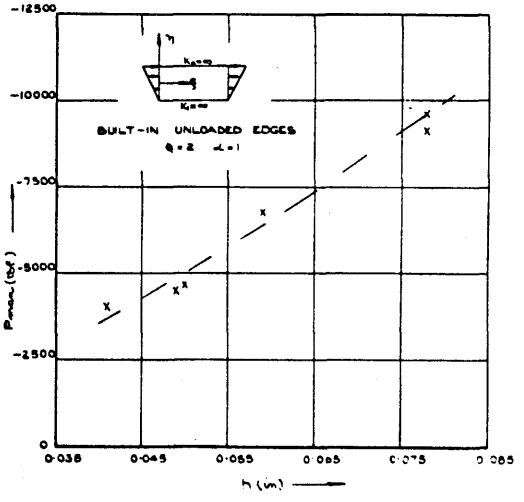

FIG IV.17 COLLAPSE LOAD v. PLATE THICKNESS

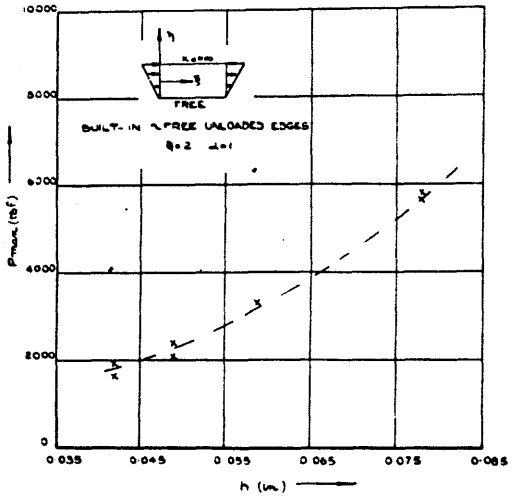

FIG IV 18 COLLAPSE LOAD v PLATE THICKNESS

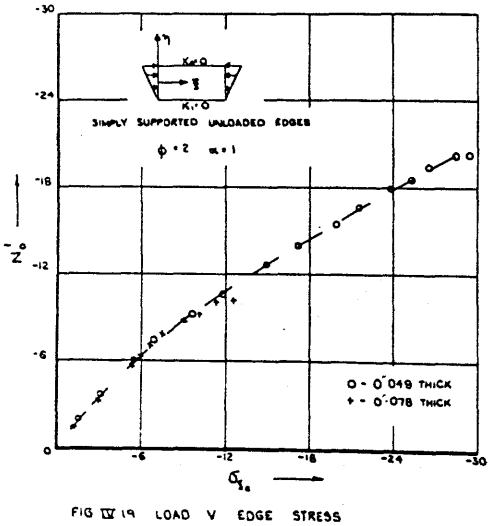

FIG IV 19 LOAD V EDGE STRESS

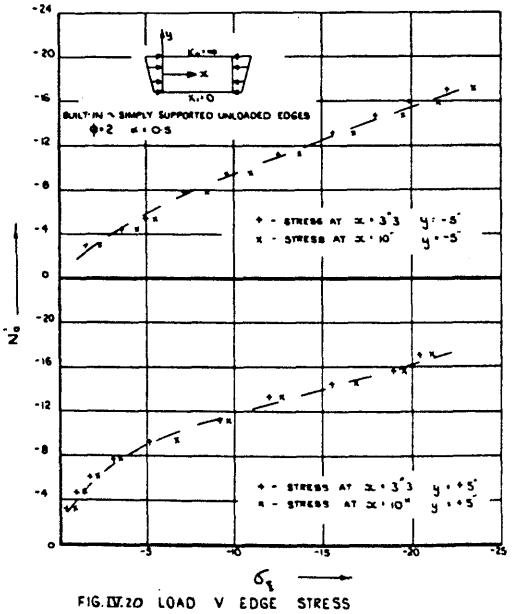

FIG. IV.20 LOAD V EDGE STRESS

(iii) one unloaded edge built-in, the other simply supported with loading eccentricity $\alpha = 0.5$

(iv) built-in unloaded edges with loading eccentricity $\alpha = 1$

(v) one unloaded edge built-in, the other free with loading eccentricity $\alpha = 1$

The thicknesses of the plates tested varied from 0".036 - 0".083 with five different values within that range.

The collapse loads corresponding to the tests are shown plotted in Figures IV.14 - IV.18.

(ii) Second Series.

As stated earlier this series of tests was designed to study the strain distributions and overall deflection patterns for specimen test plates.

One of the important relationships in the development of the theory for collapse is the load vs. edge stress in the ξ direction. In Figures IV.19 and IV.20 experimentally obtained values of this relationship are given for two types of loading and edge condition. The strain values from which these plots were inferred were obtained using electric resistance foil strain gauges bonded as closely to the plate edge as possible. One set was placed on the top surface and another directly opposite on the under surface and by connecting these in series the middle surface strains were obtained. The values are plotted

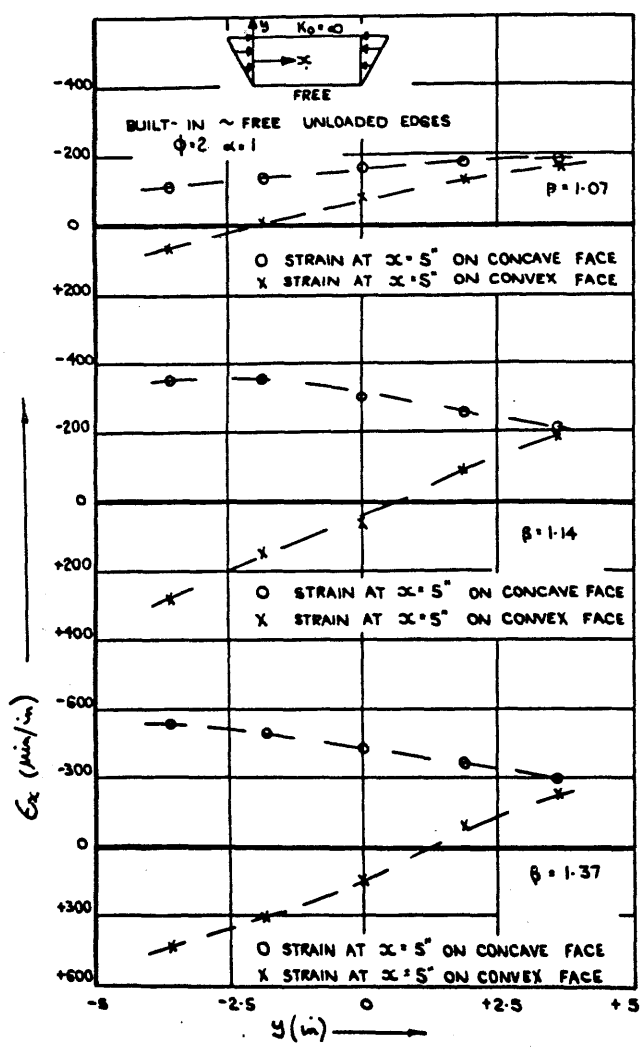

FIG. XI 21 PLATE SURFACE STRAIN V. PLATE WIDTH.

→ Direction of light.

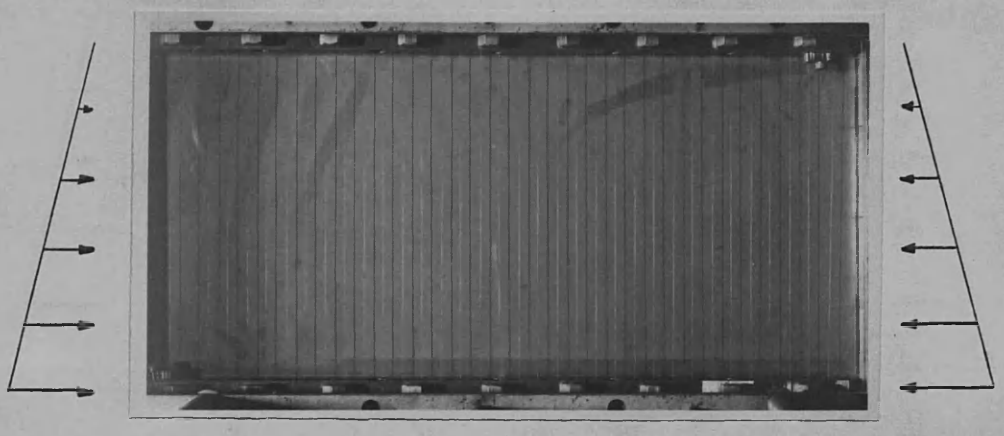

Fig. IV.22 Load = 0 lbf.

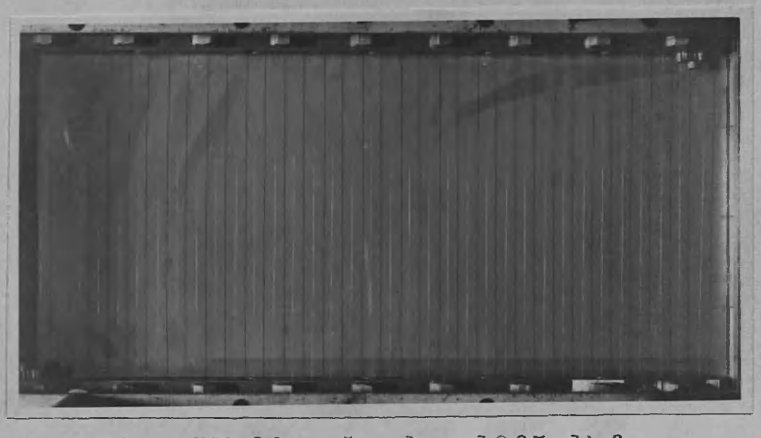

Fig. IV.23 Load = 1965 lbf.

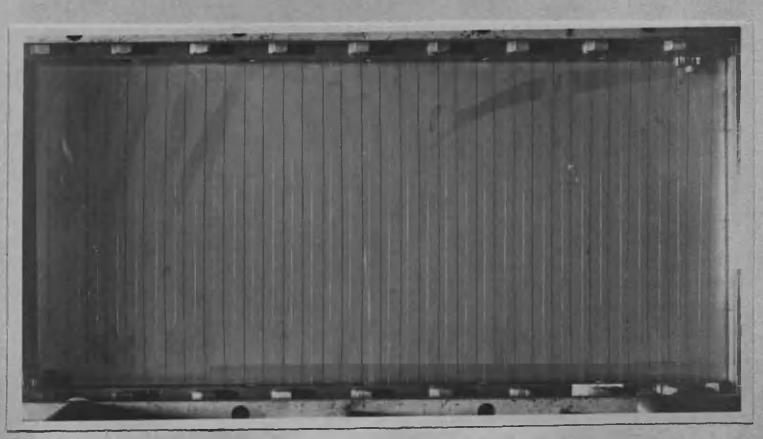

Fig. IV.24 Load = 2520 lbf.

Direction of light.

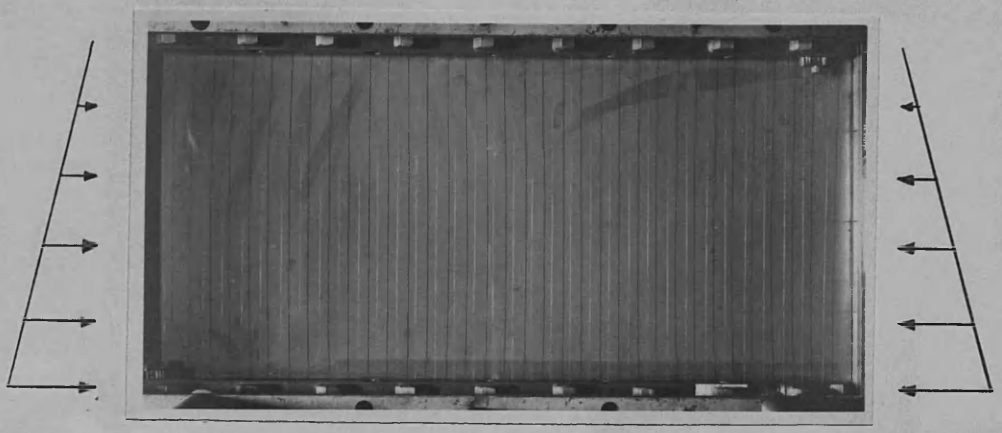

Fig. IV.25 Load = 2980 lbf.

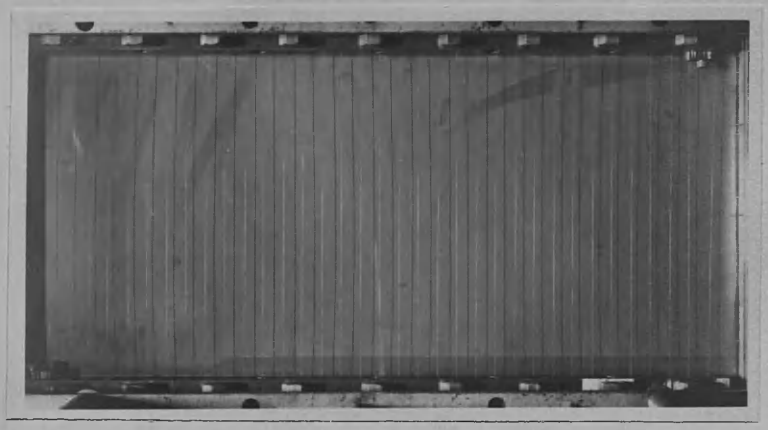

Fig. IV.26 Load = 3460 lbf.

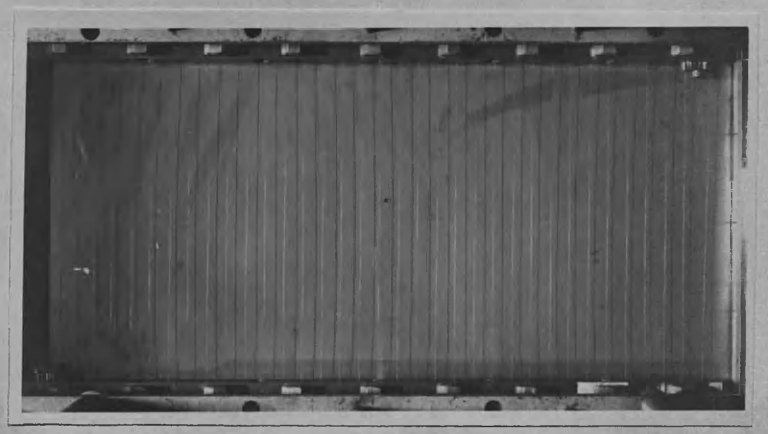

Fig. IV.27 Load = 3970 lbf.

Direction of light.

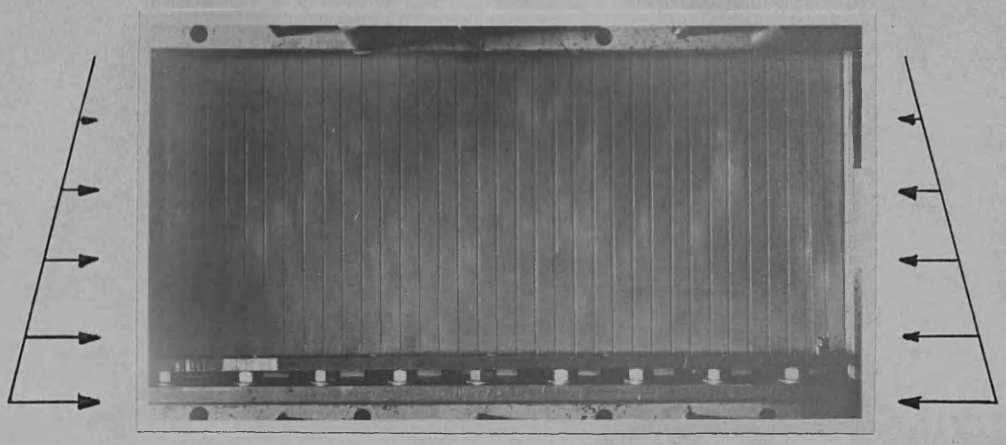

Fig. IV.28 Load = 0 lbf.

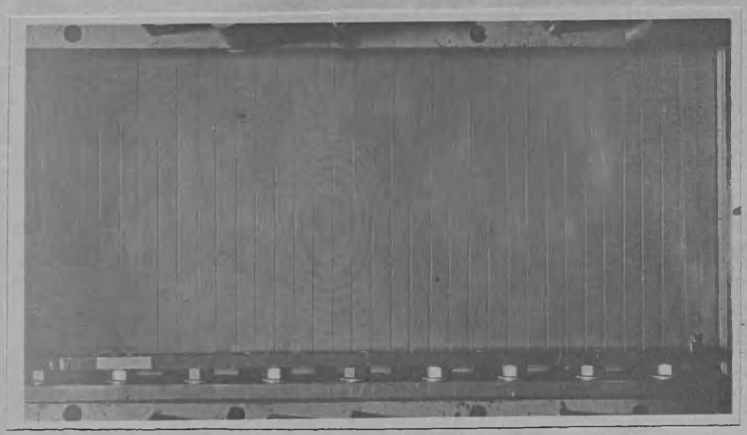

Fig. IV.29 Load = 1075 lbf.

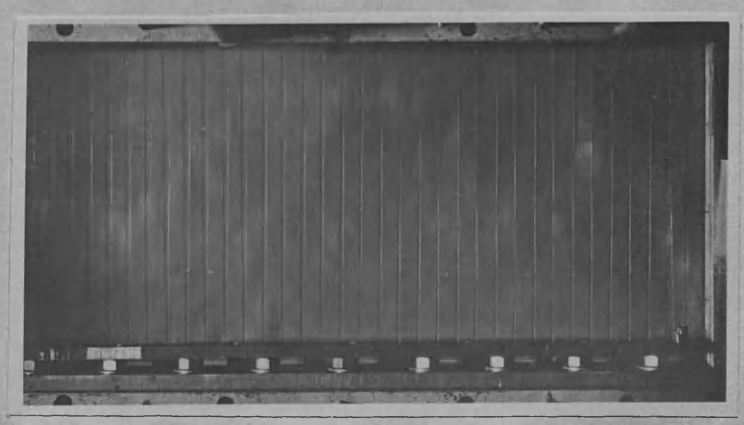

Fig. IV.30 Load = 1395 lbf.

Direction of light.

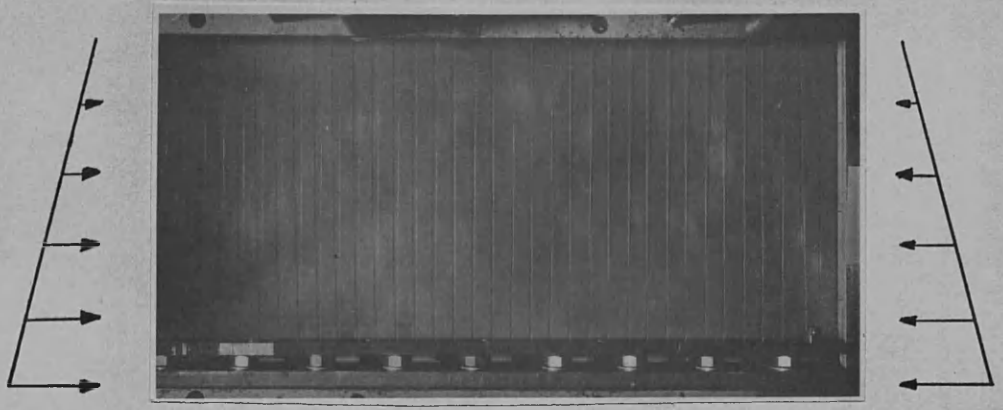

Fig. IV.31 Load = 1700 lbf.

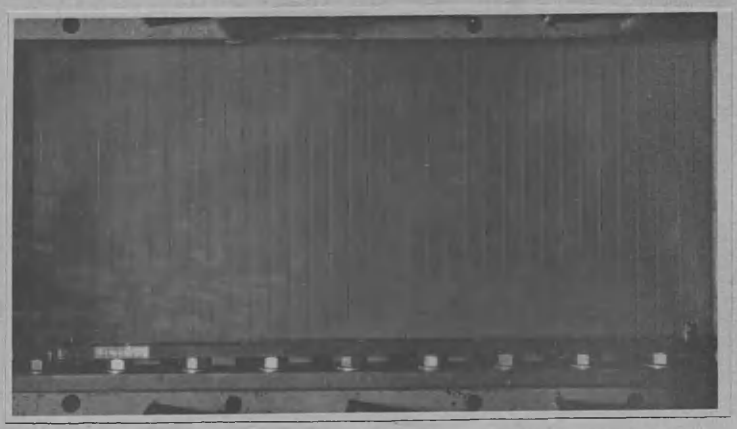

Fig. IV.32 Load = 2000 lbf.

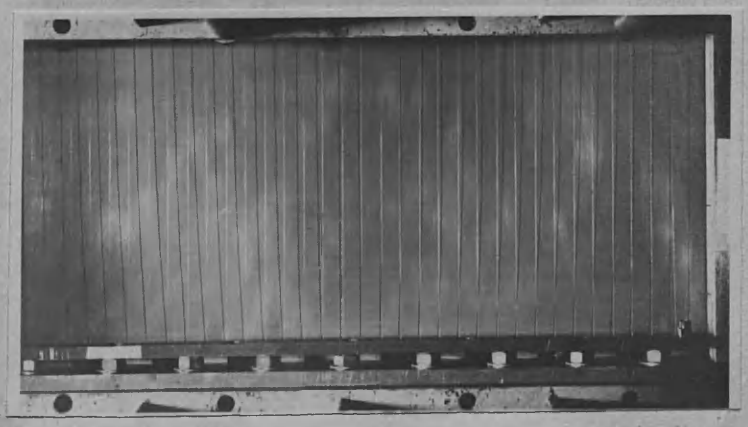

Fig. IV.33 Load = 2180 lbf.

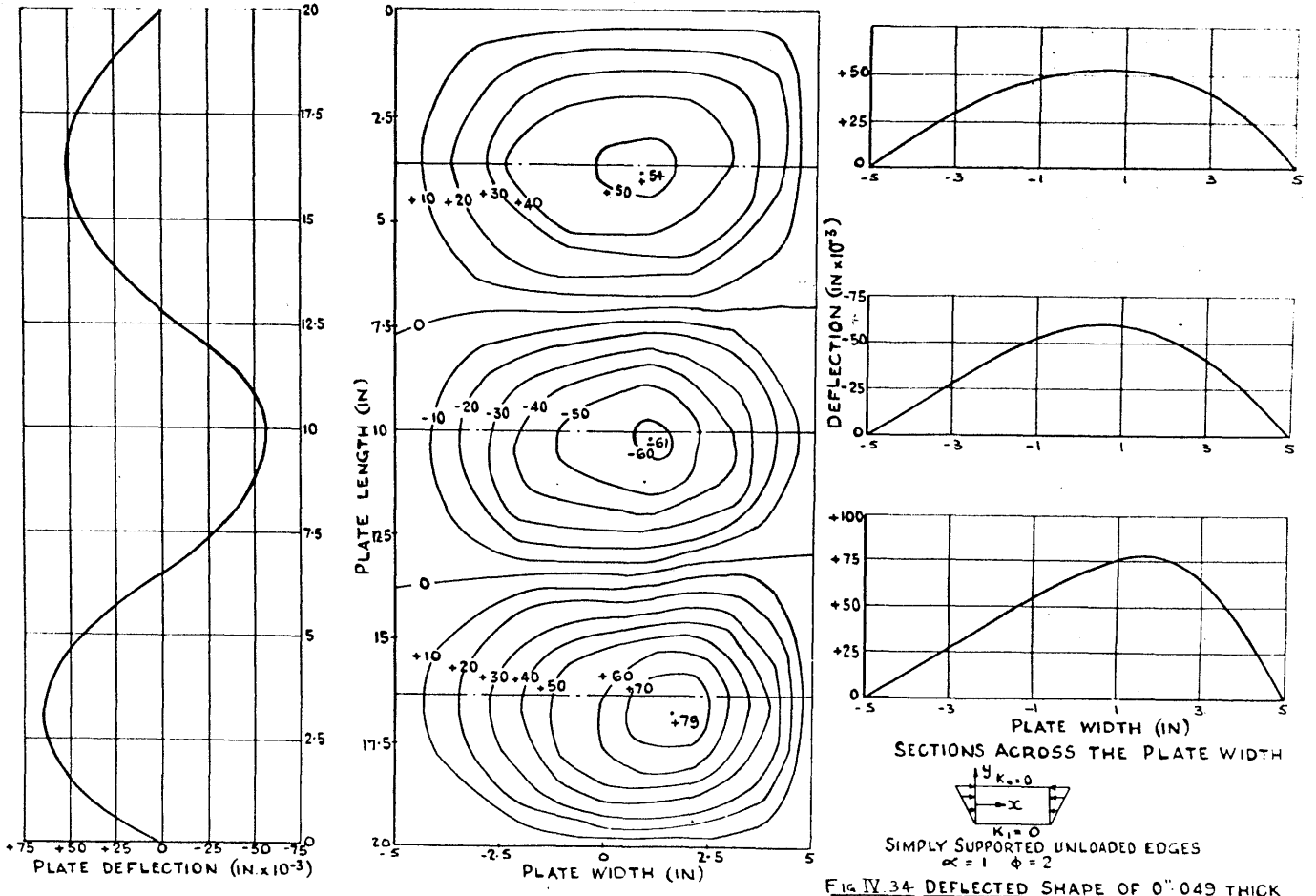

LONGITUDINAL SECTION THROUGH PLATE AT y=0"

FIG IV 34 DEFLECTED SHAPE OF 0".049 THICK PLATE AT A LOAD OF 2520 lb f.

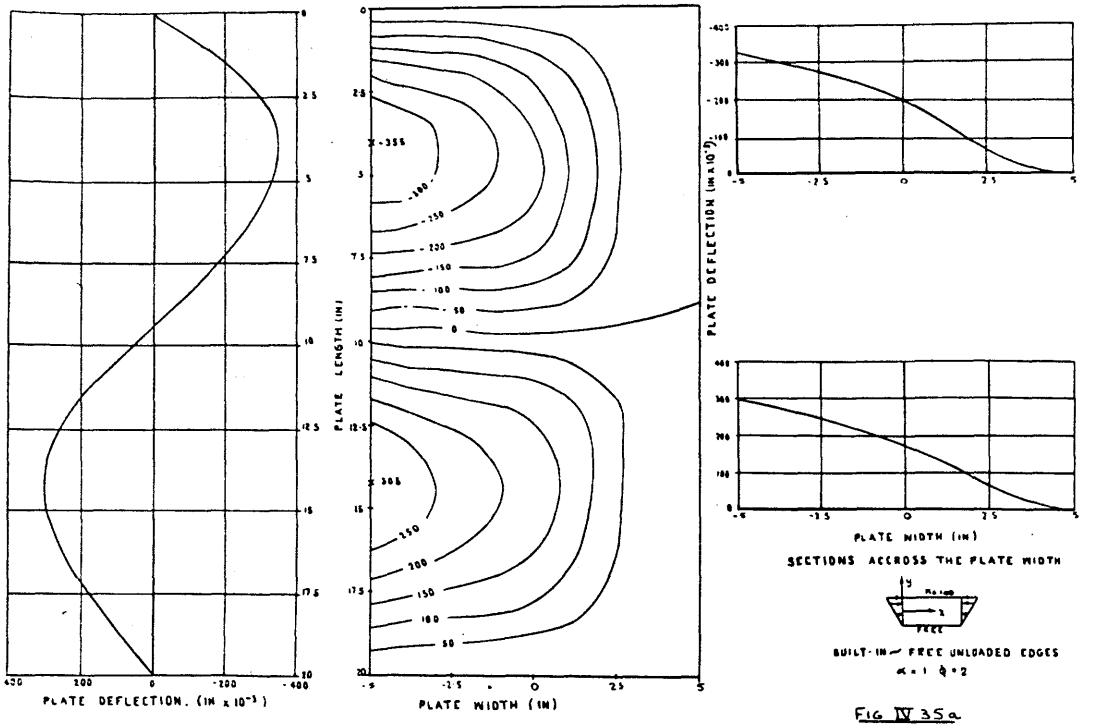

LONGITUDINAL SECTION THROUGH PLATE AT y = 5"

Fig IV 35a

DEFLECTED SHAPE OF 0·049 THICK PLATE AT A LOAD OF 2180 LB f.

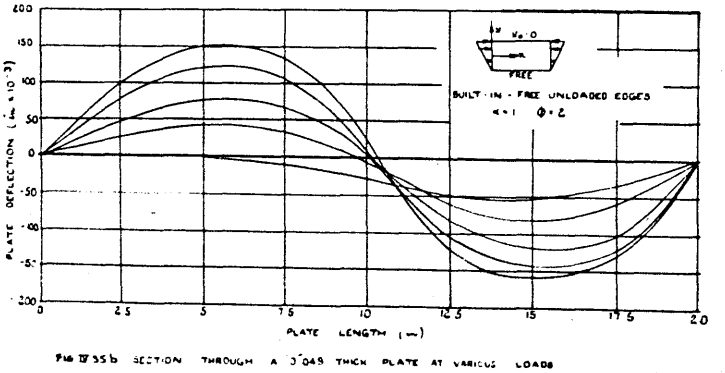

Fig IV 35b SECTION THROUGH A 0·049 THICK PLATE AT VARIOUS LOADS

in terms of the non-dimensional parameters developed in Chapter II for ease of comparison.

Figure IV.21 gives the strain distributions on the plate surfaces at various stages of loading for a built-in~free plate with loading eccentricity $\alpha=1$. Again the strain values were obtained using foil strain gauges bonded to the plate surfaces. The gauges were connected through a switch box to a Huggenberger Strain Bridge.

Sample results of the photogrammetric method described earlier in this chapter are now presented. Figures IV.22 - IV.33 are prints of the actual photo-:graphic plates taken during tests on two specimen plates, one simply supported ~ simply supported with $\alpha=1$ and the other built-in ~ free with $\alpha=1$. The results of the analyses of these photographic plates are shown in Figures IV.34 and IV.35 in the form of contour maps of the test plate surface and sections through the plate at various loads. These show the detail which can be extracted from such a simple method.

C H A P T E R V

CHAPTER V.

COMPARISONS OF PLATE EXPERIMENTAL AND THEORETICAL RESULTS.

In this chapter the test results presented in Chapter IV are compared to the relevant predictions of the theoretical approach developed in Chapters II and III. Such comparisons are held to test not only the suitability of this theory to the problem in hand but also the capabilities of the test equipment to reproduce the required conditions of loading and edge support. It is only in the light of these comparisons that conclusions can be drawn as to the success of this portion of the investigation. In the figures which illustrate the comments in this chapter the full lines were derived theoretically while the points were experi-:mentally obtained; full size prints of these diagrams may be found in the section following Part II of this thesis.

V.1 Strain and Stress Distributions.

It was stated in Chapter II that because the Galerkin method was used in this present theoretical approach to solve the generalised elastic equations for both the stress function and deflection distributions then no analytical

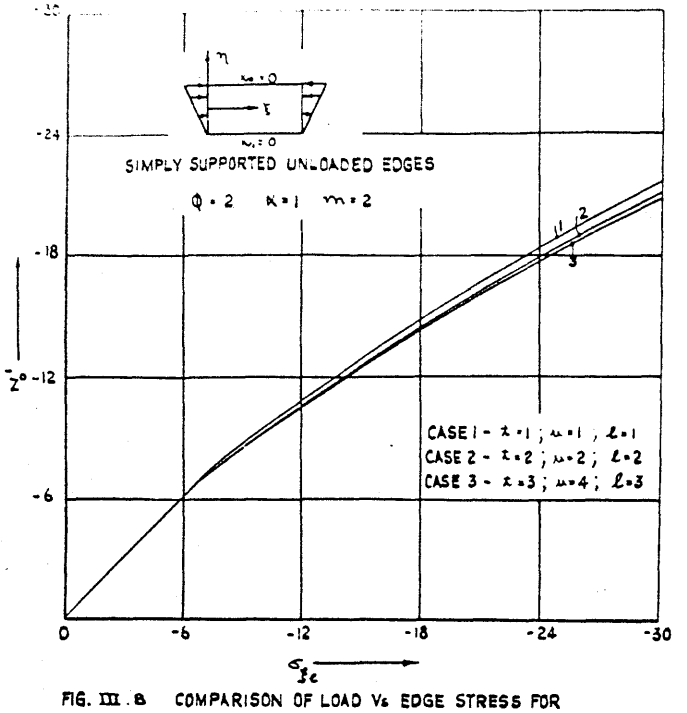

FIG. III.8 COMPARISON OF LOAD Vs EDGE STRESS FOR VARYING NUMBERS OF TERMS INCLUDED IN SERIES.

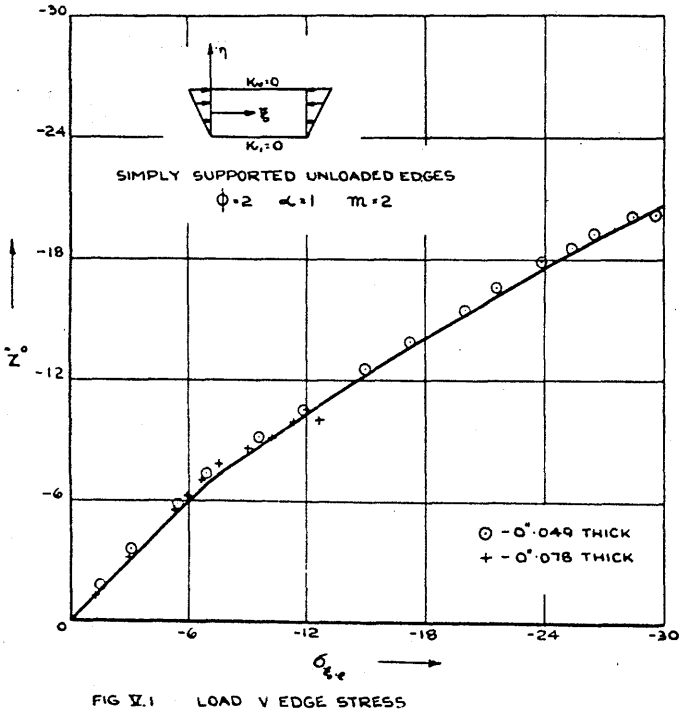

FIG V.1 LOAD V EDGE STRESS

estimate could be made to the probable rate of con-:vergence of the series solution. It is possible, however, by comparing the relevant parameter values for varying number of terms included in the series, to obtain a measure of this convergence for specific cases. An example of this is given in Figure III.8 which shows the variation of the plot of theoretical edge stress in the ξ direction vs. load parameter with various series limits. It is seen that this curve was not greatly affected by such variations but that for the inclusion of more terms the edge stress for a given load tended to become larger. From the similarity of the three values shown in Figure III.8 it would appear that convergence for this parameter was fairly rapid and monotonic, a conclusion which is confirmed by Figure V.1. This shows the curve derived using the maximum number of terms in the series compared to the relevant experimental points taken at the crest of a buckle, the values being plotted in terms of the non-dimensional parameters previously developed in order that the results of tests on two different thicknesses could be superimposed. The experimental values of edge stress in Figure V.1 were slightly low due to the fact that the strain gauges from which they were inferred were placed a little way back from the edge of the plate.

Agreement, however, is good which confirms that for this combination of boundary and loading conditions sufficient terms had been used in the series to provide a good convergence. It is one of the features of the Galerkin method that the solution is convergent irrespect-

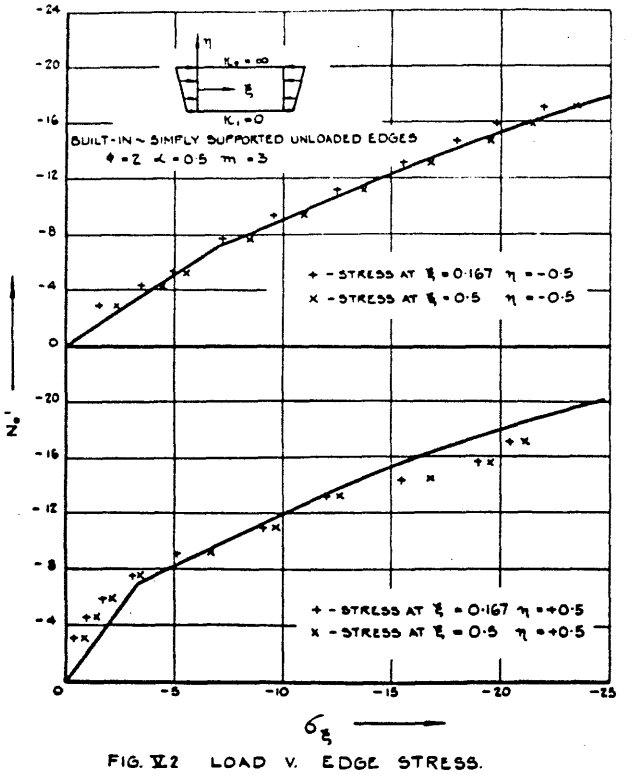

FIG. V.2 LOAD V. EDGE STRESS.

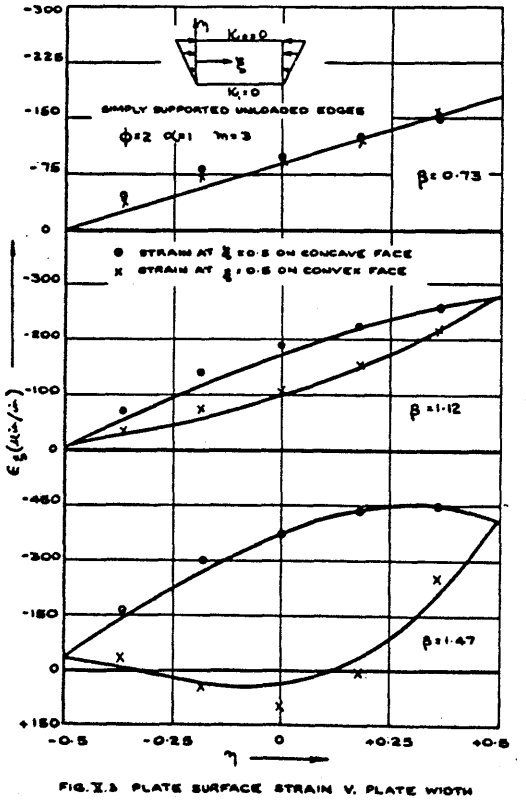

FIG. V.3 PLATE SURFACE STRAIN V. PLATE WIDTH

:ive of the functions chosen for the approximate series provided that they fulfil the boundary conditions exactly. An example of this property is given by taking two assumed functions, one trig-:onometric the other a polynomial, for the stress function distribution in the ξ direction. Some sample results of these two series are shown compared in Appendix II where it is seen that in a plot of load vs. edge stress for a simply supported plate the edge stress obtained by the trigonometric function was higher than that at the corresponding load obtained using the polynomial function.

In view of the remarks made in an earlier para-:graph of this chapter therefore it would appear that the results obtained from the trigonometric function were more accurate but the closeness of the comparison gives further emphasis to the power of Galerkin's method.

Figure V.2 shows the same parameters as in Figure V.1 plotted now for a plate 0"049 thick built-in along one unloaded edge, simply supported along the other and with loading eccentricity $\alpha = 0.5$. Here again fair agreement is observed, the divergence at the simply supported edge was caused by a slight local deformation in the plate, so that once more it may be concluded that the elastic equations had been solved to sufficient accuracy.

The comparisons of experimentally obtained strain values and the corresponding theoretical distributions

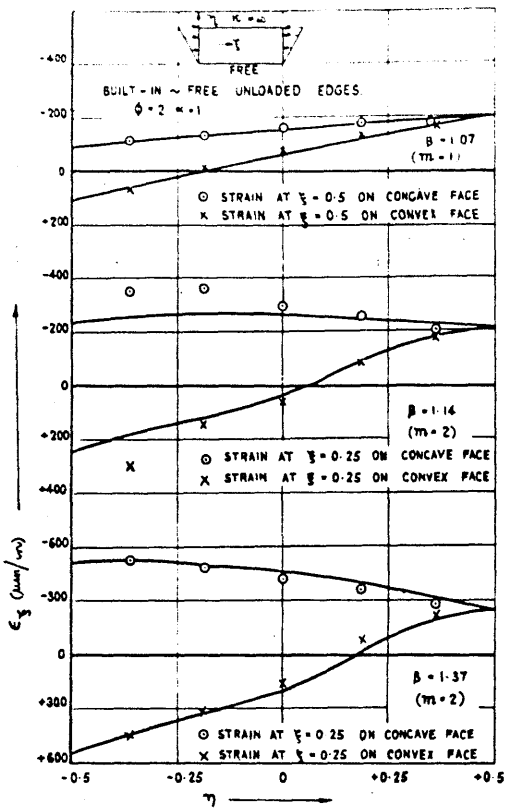

FIG. V.4 PLATE SURFACE STRAIN V PLATE WIDTH

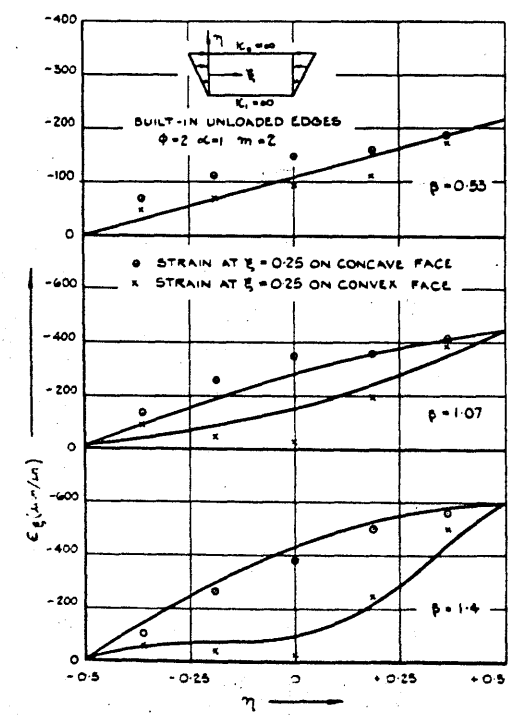

FIG V.5 PLATE SURFACE STRAIN V PLATE WIDTH

shown in Figures V.3 - V.5 may be taken not only as a test of the accuracy of the mathematical solution but also as a test of the loading rig to produce the correct loaded boundary conditions. The actual surface strains were evaluated at the crest of a buckle from tests on plates 0"059 thick subjected to the same type of loading, i.e. $\alpha = 1$, but with various unloaded edge conditions. Figure V.3 shows values for a plate simply supported along both unloaded edges which had buckled into three half waves. The examples given were for loads below and just above the theoretical critical load, also one close to the collapse load. It is seen that good agreement was obtained in each case.

In Figure V.4 similar comparisons are given for a plate built-in along one unloaded edge and free along the other. Agreement here is also good; the deviation at $\beta = 1.14$ (here $\beta = \frac{\text{actual load}}{\text{theoretical instability load}}$) was caused by the number of buckle half waves changing from one to two. This change was slow and for a time the plate was highly asymmetric with respect to $x = 10"$ with the deflections at one end, the end at which the strains were measured, being very much greater than at the other. By the time the load had increased to $\beta = 1.37$, however, the two half wave pattern was fully developed and agreement with the theory was once more good.

In Figure V.5 which gives comparison of surface strains for a plate built-in along both unloaded edges, it may be noted that at the load of $\beta = 0.53$ there was

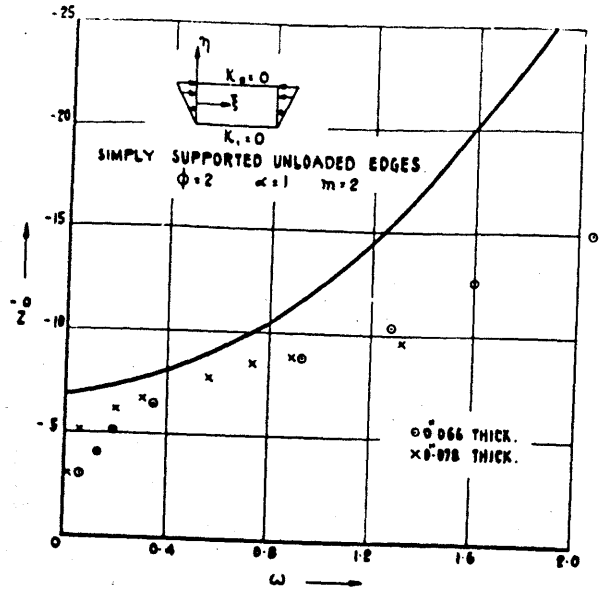

FIG V.6 LOAD V DEFLECTION.

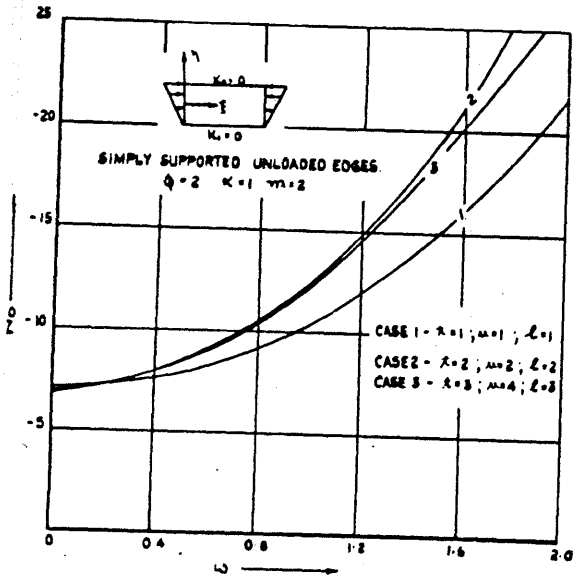

FIG. III.7 COMPARISON OF LOAD Vs DEFLECTION FOR VARYING NUMBERS OF TERMS INCLUDED IN SERIES.

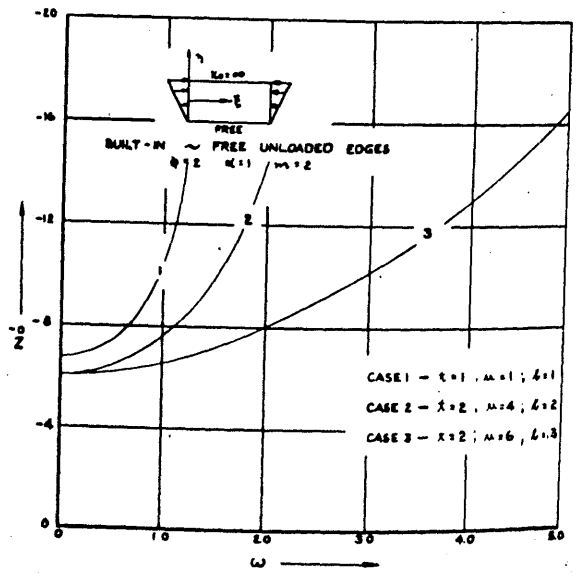

FIG III.9 COMPARISON OF LOAD Vs. DEFLECTION FOR VARYING NUMBERS OF TERMS INCLUDED IN SERIES.

already a divergence of the strains on the upper surface from those on the lower surface. This was due mainly to initial deviations from flatness in the plate causing deflections to occur at loads below the theoretical instability load. This phenomenon is further discussed in the next section of this chapter but it is shown in Figure V.5 that although the deviations from the theoretical values remained, their relative magnitudes decreased as the loading proceeded.

Hence it may be concluded from the comparisons presented in this section that not only had the elastic equations been solved to give the stress function to sufficient accuracy but the loading rig was competent to produce the required load distributions.

V.2. Deflection Distributions.

In the previous section of this chapter the accuracy of the mathematical solution of the elastic equations for the stress function and the loading capa-:bilities of the test rig were discussed with reference to typical stress and strain distributions. In this section deflection values from tests are used to provide information on the accuracy of the mathematical predict-:ions for deflection distributions and on the efficacy of the experimental boundary conditions.

Figure III.7 shows the variation of the plot of

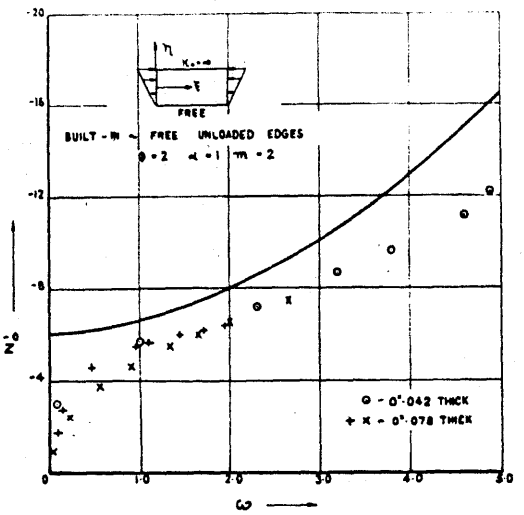

FIG. V 7 LOAD V DEFLECTION.

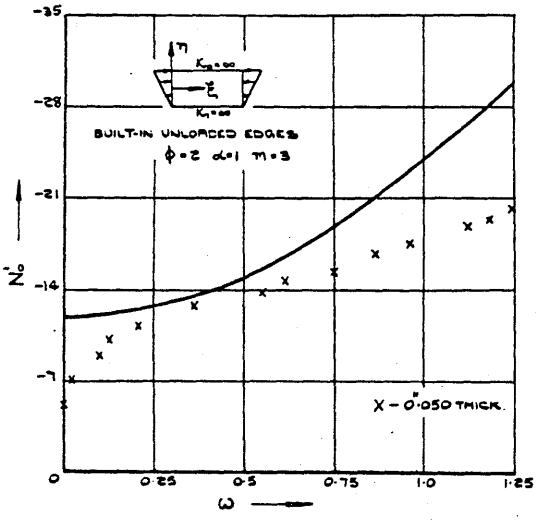

FIG. V 8 LOAD V DEFLECTION.

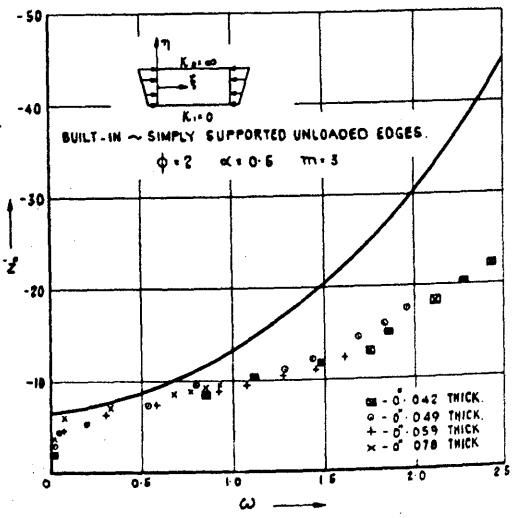

FIG. V 9 LOAD V DEFLECTION.

load vs. deflection, at the mid-width of a simply supported plate on the crest of a buckle, with changes in the limits of the assumed series. A feature of this is that the theoretical deflection at this point for any given load was far more sensitive to change of limits than was the corresponding stress function value. When, in Figure V.6, corresponding experimental values are compared to the theoretical curve it is seen that the tendency of the theoretical deflection to increase as the limits were increased was augmented by the anticipated growth of the deflections at loads below the theoretical instability load. This was of course caused by the initial lack of flatness in the plate and is common in some degree to all plates loaded in edge compression.

Figure III.9 shows a theoretical plot of the same parameter for a built-in ~ free plate and again it can be seen that, for a given load, as the limits were increased the deflection at the crest of a buckle was also increased. When the values obtained using the maximum limits are compared in Figure V.7 with those obtained experimentally it is found once more that the deflections started to grow from the beginning of load application and that this emphasises the lack of agreement at the higher loads. Two further examples of this type of plot are given in Figure V.8, for a plate built-in along both unloaded edges, and in Figure V.9, where the plate was simply supported along one unloaded edge and built-in along the other.

The experimental values shown in Figures V.6 - V.9 were obtained from tests in which no change of wavelength was observed, by plotting these in terms of the non-dimensional parameters it is indicated that there was good consistency in the various plots between the different plate thicknesses in that they appear to define a single curve. Thus it may be concluded that there was some lack of agreement between the theoretical and corresponding experimental values of deflection at the crest of a buckle and that this is probably attributed in some degree to both the theoretical solution and the initial imperfections of the plate. It will be shown in a later section of this chapter, however, that the accuracy of the collapse load predictions was not greatly affected by such inaccuracies in deflection prediction.

The "wire-shadow" method proved very successful in providing a means of determining the deflection distri-:bution over the plate surface; examples of the results are given in Chapter IV and Appendix V. One interesting feature in Figure IV.35 is the change of wavelength as the loading progressed. In this figure longitudinal sections of the plate, which was built-in ~ free, are given at various loads and it is seen that at the lowest of these the plate was in the process of changing from one half wave to a full wave. In the subsequent loads the shape is seen to be slightly asymmetric but this reduced as the load approached the collapse load. This confirms the argument put forward in Section 1 of this chapter on the reason for divergence of the actual strain distribution from that predicted for this type of plate.

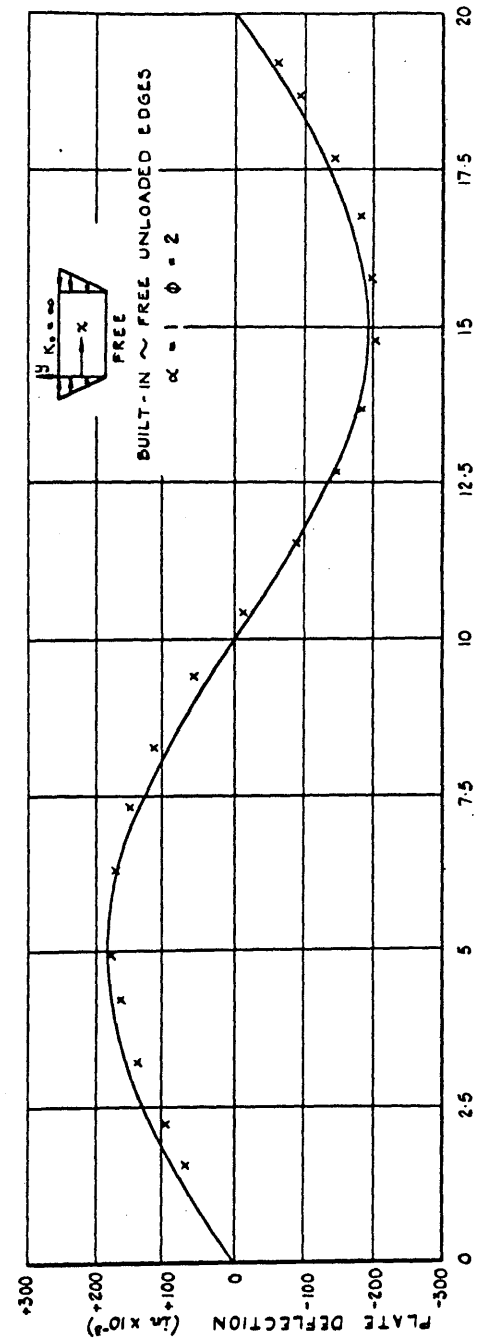

FIG. V.10 SECTION THROUGH 0'.049 THICK PLATE AT y = 0.

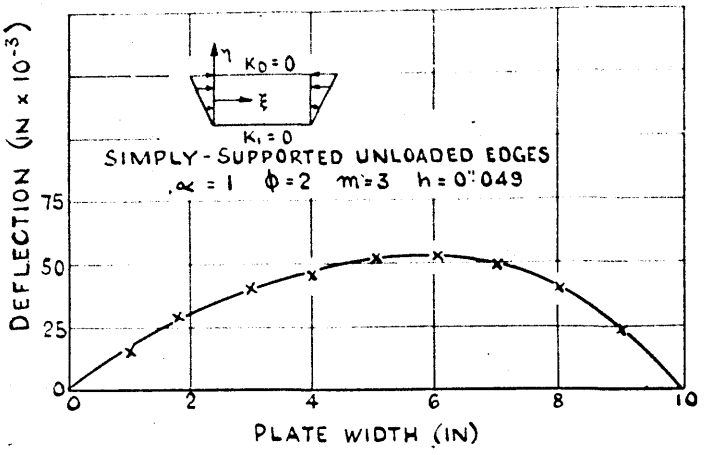

FIG V.11 DEFLECTED SHAPE ACROSS THE PLATE AT THE CREST OF A BUCKLE.

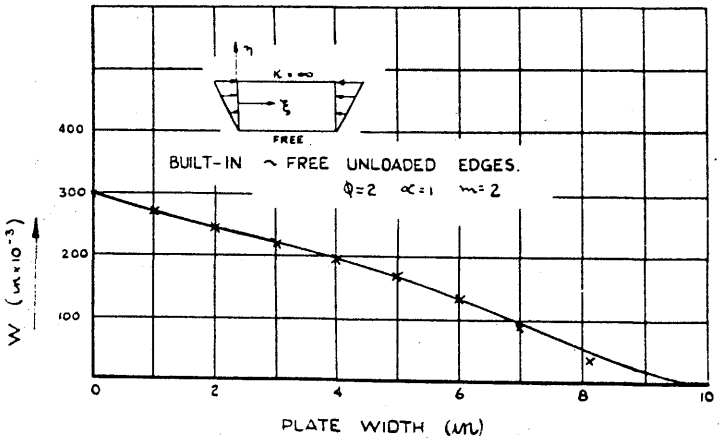

FIG V.12 COMPARISON OF THEORETICAL AND EXPERIMENTAL DEFLECTION DISTRIBUTION ACROSS THE PLATE AT THE CREST OF A BUCKLE.

Comparisons of the deflected shapes from test with the relevant theoretical values are given in Figures V.10 - V.12. In Figure V.10 the longitudinal section of a built-in ~ free plate near collapse is considered; this shows that good agreement was obtained. The theoretical shape was computed with the peak deflect-:ions equal to the average of the experimental values. A point of value is that the experimental loaded edge conditions were a very good approximation to the theoret-:ical condition of simple support. This comment is substantiated by Figures IV.34, IV.35 and AV.7, it is also supported by observations made during the test that at no time did crinkles, which would have been indicative of rotational restraint, appear at the loaded edges of the plates.

Figures V.11 and V.12 show comparisons of experi-:mental and theoretical deflection values along sections taken through the crest of a buckle of a simply supported plate and a built-in ~ free plate, respectively. Again the theoretical values were computed to coincide with the test results at mid-section. It may be seen that very good agreement was obtained in both cases from which it can be concluded that at these loads the restraints on the unloaded boundaries also provided good approximations to the theoretical conditions of simple support and complete rotational fixity, i.e. built-in. It may also be concluded that although, as was indicated earlier in this section, the magnitudes of the deflections were not accurately predicted by the theory the deflected shapes were given very closely.

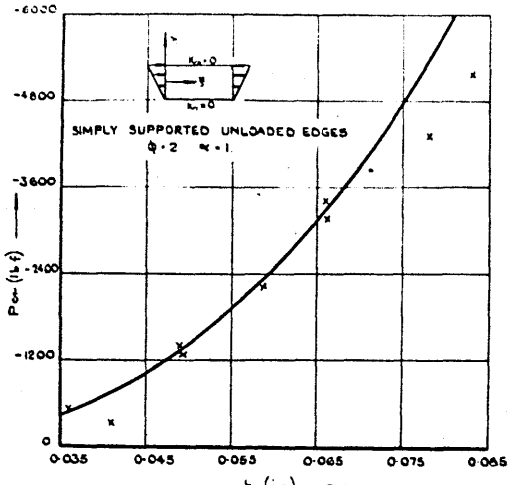

FIG. V.13 INSTABILITY LOAD V PLATE THICKNESS

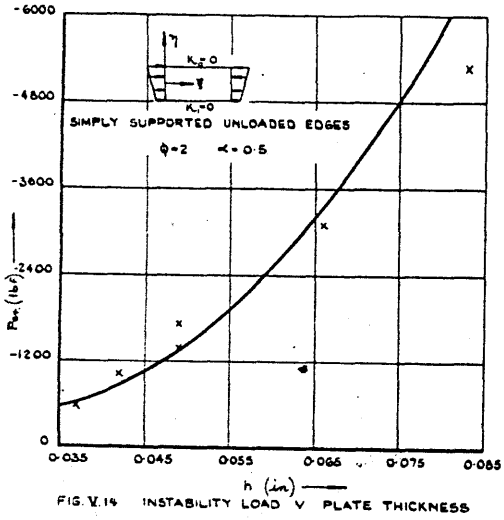

FIG. V.14 INSTABILITY LOAD V PLATE THICKNESS

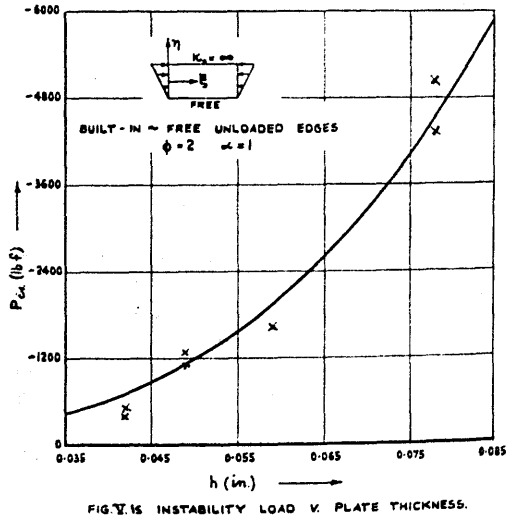

FIG. V.15 INSTABILITY LOAD V. PLATE THICKNESS.

V.3 Instability Loads.

The experimental critical loads were calculated using the "Southwell Plot" method of analysis. Other methods of estimation, e.g. "top-of-the-knee" and point of inflection of the load vs. deflection graph, were also examined but were found to be not as consistent as the method used here. The reason for this was that as the load was increased there was, in general, a tendency for the plate buckle shape to change. This affected considerably the shape of the load vs. deflection curve for the plate at loads near, and above, the theoretical critical load. This in turn gave rise to errors in the methods inferring the critical load which use these portions of the experimental curves. If, however, the lower regions of the loading were used in the Southwell Plot then the influences of the wavelength change were less marked and greater accuracy was obtained.

The comparisons are given in Figures V.13 - V.17 of the experimental loads thus calculated and the corresponding theoretical flat plate buckling loads. Good agreement has been obtained for all the curves. Figure V.16 shows that the test points for the plates with built-in edges fell below the theoretical values. This was attributed mainly to the experimental edge conditions not fully simulating the required built-in conditions at the low deflections at which the values were taken for the Southwell Plot. This was true only for a plate with

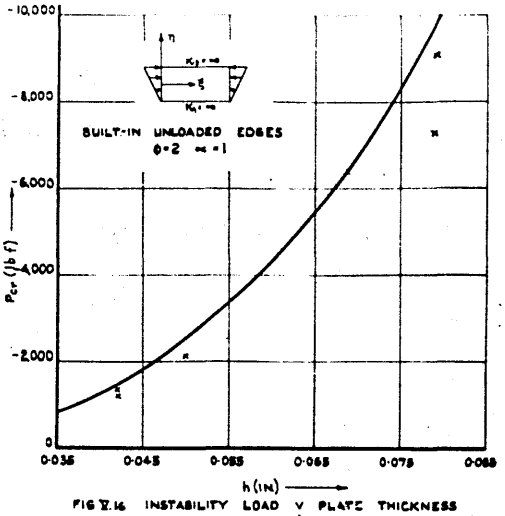

FIG V.16 INSTABILITY LOAD V PLATE THICKNESS

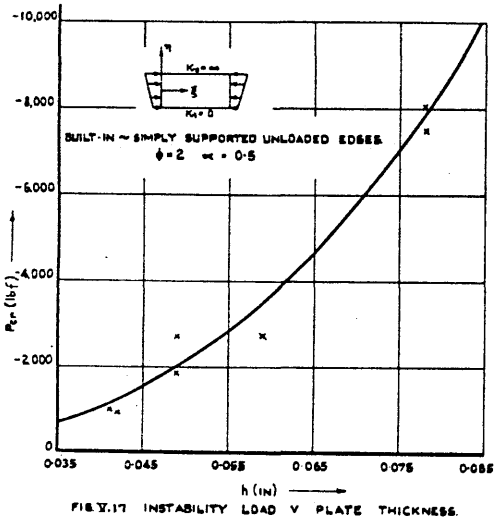

FIG V.17 INSTABILITY LOAD V PLATE THICKNESS.

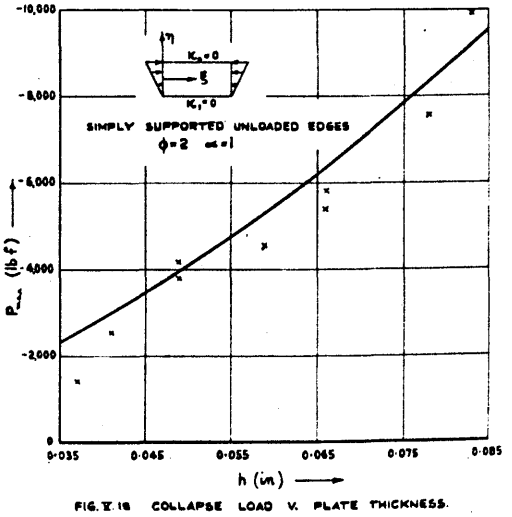

FIG. V.18 COLLAPSE LOAD V. PLATE THICKNESS.

these constraints at both unloaded edges, in all other results the scatter, caused by variations of Young's Modulus, thickness and the inherent approx-:imations of Southwell's method is, in general, evenly distributed about the theoretical curve.

It is demonstrated in Appendix III that a finite difference technique can be used to obtain the instability loads of plates loaded in eccentric edge compression. When specimen results from this method were compared to the corresponding values obtained using the Galerkin method developed elsewhere in this thesis it was seen that the agreement was usually within 1%. Thus although the experimental results were compared in this chapter to the predict-:ions of the Galerkin method the same conclusions could equally have been drawn if the results of the finite difference method had been used.

The conclusions therefore are that the Southwell Plot method gave consistent results for the instability loads of actual plates which were in good agreement with those predicted from flat plate considerations thus confirming the rationality of the theoretical approach.

V.4 Collapse Loads.

The use of a yield criterion as a theoretical basis of collapse of the plate leads to simple methods

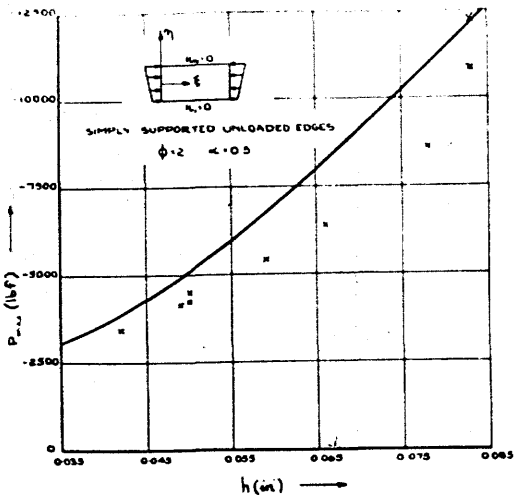

FIG V 19 COLLAPSE LOAD V PLATE THICKNESS

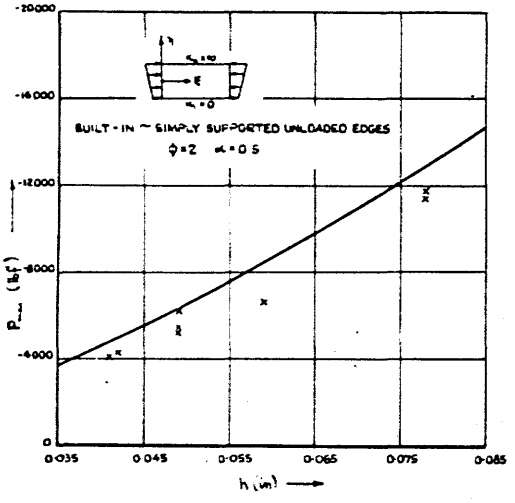

FIG V 20 COLLAPSE LOAD V PLATE THICKNESS

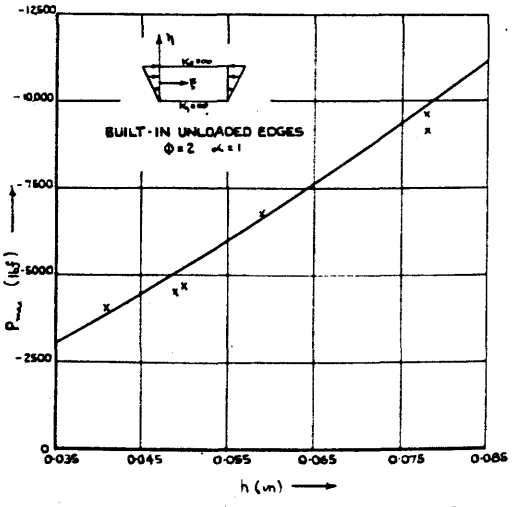

FIG V 21 COLLAPSE LOAD V PLATE THICKNESS

of collapse load calculation. It also allowed the use of purely elastic considerations in the mathemat-:ical analysis of the problem, again easing the task of solution. In the theory therefore it was assumed that the plate material was wholly in an elastic condition just prior to collapse and that this collapse was caused by yielding of a vital portion of the plate, usually the edges, which in turn affected the stress distribution to such an extent that collapse immediately followed. This theory could, of course, only be applicable to those materials which possessed a definite yield point and underwent large plastic flow at this load. Such materials are the cold worked mild steels used in light civil engineering and the titanium alloys now being used in high speed aircraft.

That the assumptions made in the theoretical analysis are rational is indicated by the similarity of the test collapse loads to the predicted curves shown in Figures V.18 - V.22. In these it is seen that the results of the plates subjected to triangular loading ($\alpha = 1$) show very good agreement while those of plates subjected to the other loading geometry studied ($\alpha = 0.5$), although still good, lie below the theoretical curves. The main reason for this was the imperfections in the plates. As the plate approached the collapse load the imperfections, whether they be variations of thick-:ness, material properties or damage to the plate, became more likely to cause stress concentrations. These of course would lead to premature collapse if

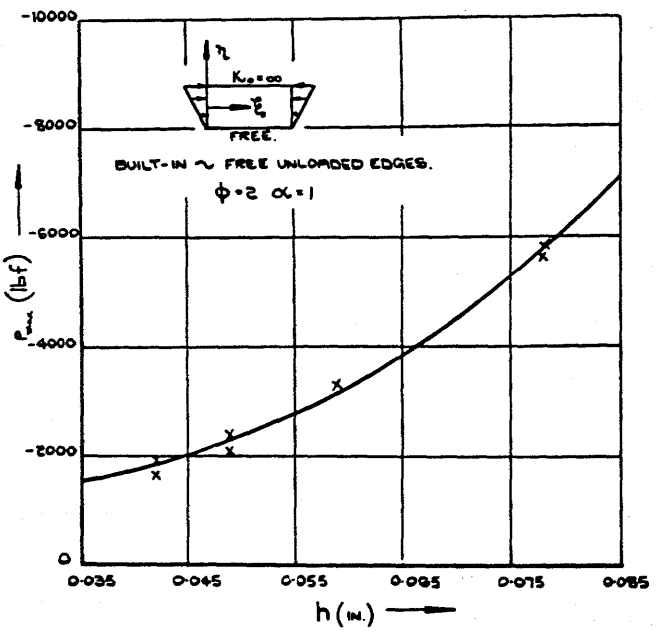

FIG. X.22 COLLAPSE LOAD V. PLATE THICKNESS.

they were located near the edge or near the crest of a buckle. Where the high stress regimes were more widespread throughout the plate, e.g. in the trapezoidal loaded plate rather than the triangularly loaded one, this effect would become more general since the material at the buckle crests was subjected to additional bending stresses.

In simply supported plates subjected to trapezoidal loading this condition was even more aggrevated by the initial deviations from flatness causing an increase in the deflections and so increasing the possibility of overstressing and the corresponding local yielding of the plate surface. These conditions are illustrated by the decreasing order of error from the theoretical in the Figures V.19, V.20, V.18, V.21 and V.22.

These defects were unfortunately unavoidable in actual plates so that the effects commented upon above would, in practice, be countered by coefficients to convert purely theoretical calculations to safe workable design values. That such an approach could be used here is shown by Figure V.19 where even in the worst case the trend is followed very closely.

Thus it may be concluded that the theoretical considerations have been amply substantiated by the test results and that the collapse loads for plates subjected to eccentric end compressive loading can be calculated using the Galerkin solution to the generalised elastic equations developed here together with the application

of a simple yield criterion.

V.5 Conclusions.

1. An approximate solution using Galerkin's method has been presented for the Von Karman equations and the appropriate boundary conditions with a degree of convergence sufficient for engineering purposes.

2. The solution gives the strain distributions accurately on the plate surface and although deflection values are given only approximately the deflected shape of the plate is predicted closely.

3. The introduction of a simple yield criterion leads to good engineering approximations for the collapse loads for plates loaded in eccentric edge compression.

4. The use of the Southwell Plot method to determine the elastic instability load from experimental results is shown to be acceptable for plates under eccentric compression.

C H A P T E R V I

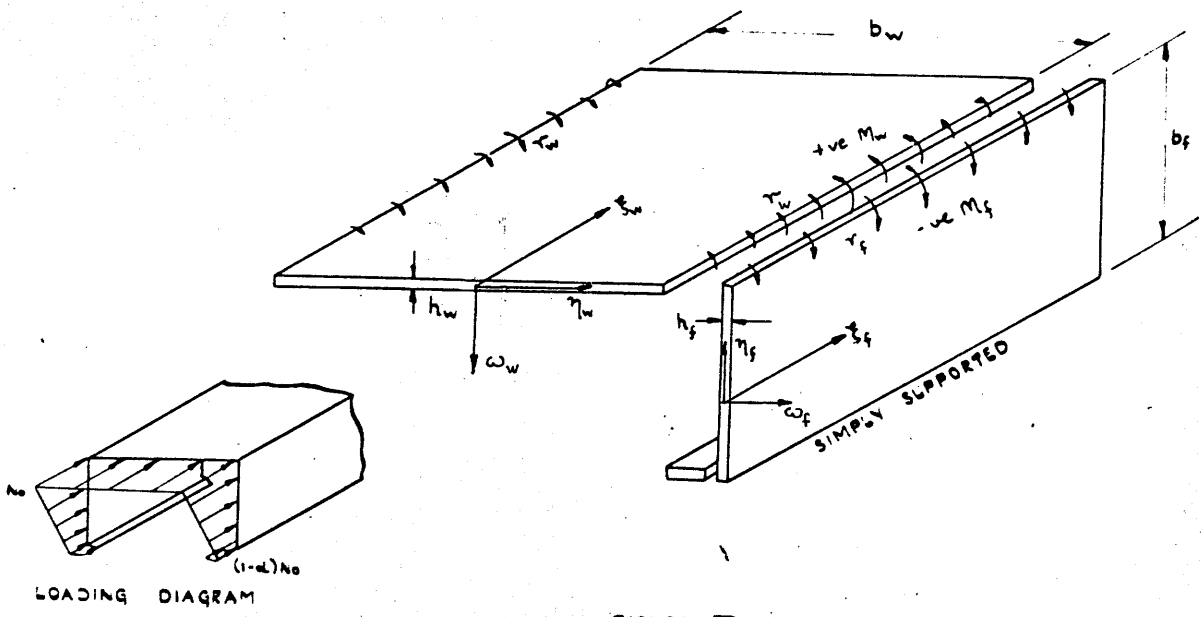
b_w
r_w
+ve M_w
r_w
ξ_w
r_f
-ve M_f
b_f
h_w
η_w
h_f
η_f
ξ_f
ω_w
ω_f
SIMPLY SUPPORTED
N_0
$(1-\alpha)N_0$
LOADING DIAGRAM

FIGURE VI 1.

CHAPTER VI.

DETERMINATION OF THE INSTABILITY AND COLLAPSE LOADS OF LIPPED AND PLAIN CHANNEL SECTIONS.

In this chapter the load bearing capabilities of certain structural shapes are considered. These structural sections when subjected to end compressive load actions may be thought of as being composed of compressed individual plates which have common boundary conditions at the adjoining unloaded edges. In this way the theoretical results obtained for plates may be combined to provide a mathematical prediction of the two particular loads which are to be studied here. These are (i) the initial instability load
and (ii) the maximum load which the section can sustain.

VI.1 Initial Elastic Instability Load.

a. Lipped channels.

Figure VI.1 shows how the section was subdivided into its constituent plates. The web was thus considered to be a uniformly loaded plate with equal amounts of rotational restraint along the unloaded edges with the flanges taken as eccentrically loaded

plates elastically restrained against rotation along the unloaded edge common to it and the web. The lip along the other unloaded edge could be thought of as providing a simple support type of condition. This assumption was shown by Chilver (1950) to provide values for the elastic instability loads of concentrically loaded channels which were very close to those obtained using the more rigorous approach, i.e. that the lip provided a flexural and torsional restraint dependant on its geometry. The other boundary conditions were as for the single plates previously considered, i.e. simply supported at the loaded edges, constrained against lateral movement along all the edges and free to allow "in plane" movement along the unloaded edges.

For any given combination of plates, i.e. for any section geometry $H (= b_f/b_w)$ the coefficient of restraint r along the adjoining edge was taken to be of equal magnitude but of opposite sign for the flange and web. Thus if, for example, r_w for the web was such as to oppose the increase of web deflection then r_f for the flange promoted the growth of flange deflection. The equality of magnitude arose from the assumption of equal moment reaction at the junction of the plate and also the maintenance of the original geometry.

Instability occurred in the section as a whole, that is, the individual plates had each to become

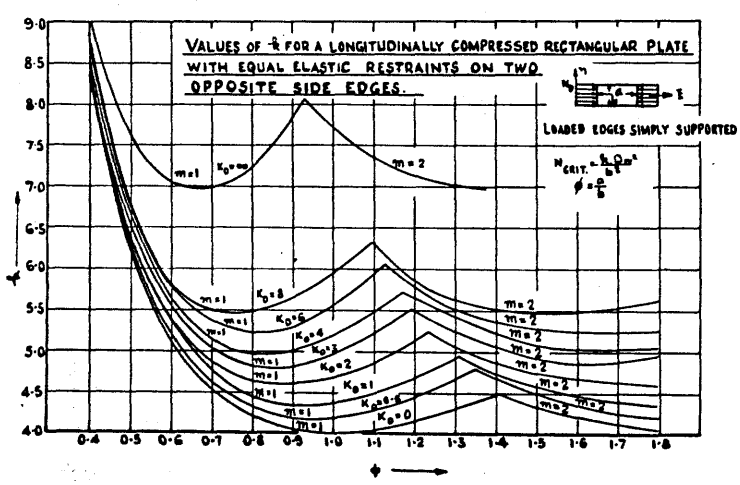

FIG. VI.2 BUCKLING CONSTANT v. ASPECT RATIO

unstable simultaneously at the particular load considered and for the relevant mutual boundary conditions. Thus by using an approximate geometrical procedure the flange plates could be matched to a given web plate so that the load at which the assembly became unstable as a unit was obtained. An example of this process is now given.

Figure VI.2 shows the plot of the buckling constant against aspect ratio for the web plate. By choosing a particular value of the aspect ratio and wavelength (in this case unity and plate length respectively) it was then possible to determine the value of the buckling constant for a chosen value of the restraint coefficient K_w.
Now

$$K_w = -\frac{b_w r_w}{D_w} \quad \text{and} \quad K_f = -\frac{b_f r_f}{D_f}$$

but $r_f = -r_w$ and $D_w = D_f$ thus with $H = b_f/b_w$

it is seen that $K_f = \frac{b_w r_w}{D_w} \cdot b_f/b_w = -H K_w$

Similarly $\phi_f = \phi_w \cdot \frac{1}{H}$ and $k_f = H^2 k_w$
Hence for any specific web value of ϕ_w and K_w it was possible, by using the above relationships and the Galerkin procedure described in Section 1 of Chapter III, to construct a plot of k_f/H^2 vs. H.

Since the constituent plates were required to

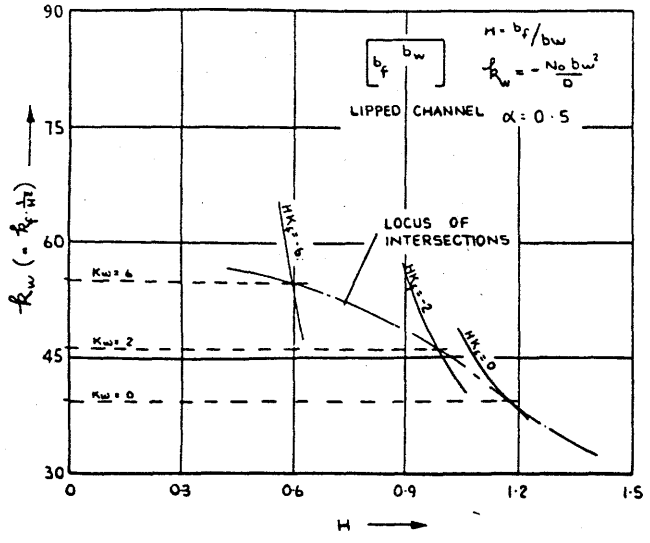

FIG. VI·3 BUCKLING CONSTANT vs. SHAPE FACTOR.

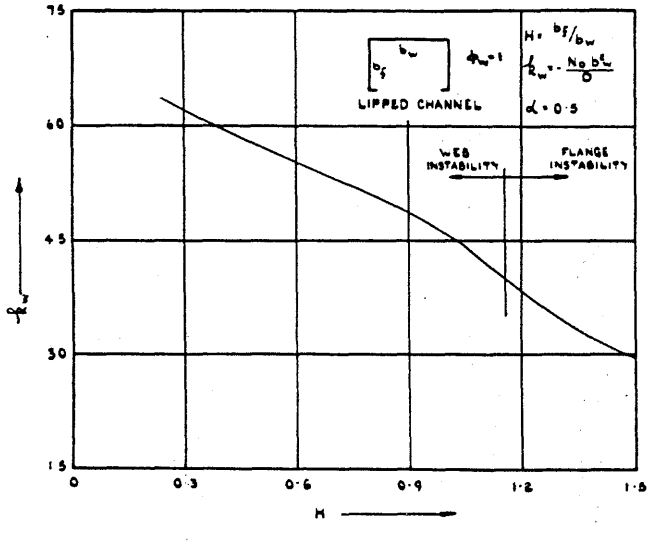

FIG. VI 4 BUCKLING CONSTANT Vs SHAPE FACTOR

be simultaneously unstable the only valid value of H was that which gives the same value of $-k_f/u^2$ for the flange as $-k_w$ for the web. This is shown geometrically in Figure VI.3 and by choosing other values of H a locus of such intersections was obtained. By this manner the curves in Figures VI.4 and VI.5 were constructed; the value of ϕ_w was taken as unity for both these figures and the web and flanges were assumed to have deflected in one half wave shape.

It should be noted here that there were two ranges for K_w , i.e. $0 \leq K_w \leq +\infty$ and $-\infty \leq K_w \leq 0$. These corresponded to the web initiating instability and the flange initiating instability respectively. In the above example of the method the former range was used, however both of the ranges were investigated for the study of the total spread of the section geometry.

b. Plain channels.

The process here was identical to that described above for the lipped channels in every respect except one. This was that the unconnected longitudinal boundary of the flange plates was considered to be free, as shown in Figure VI.6. Figures VI.7 and VI.8 show the results of the calculations where again the values of ϕ_w was unity and the section was con-:sidered to have deflected into a single half wave.

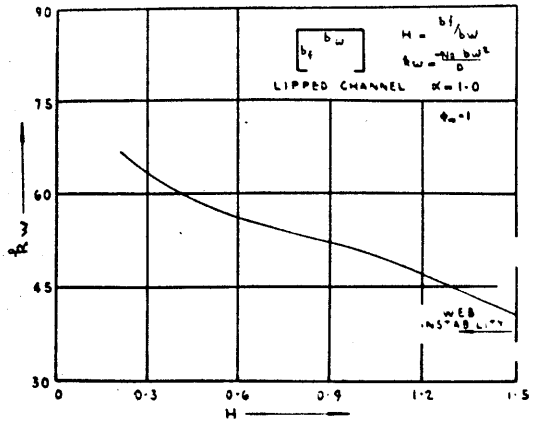

FIG VI 5 BUCKLING CONSTANT VS SHAPE FACTOR

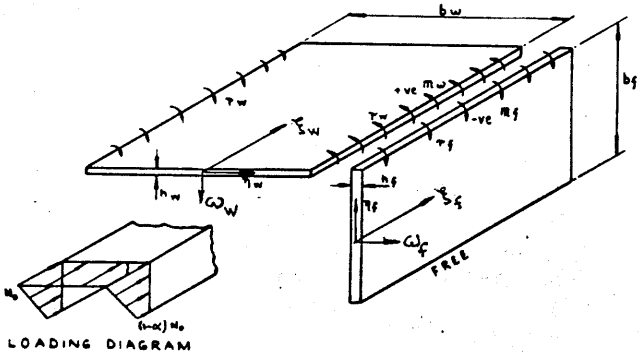

FIG VI 6

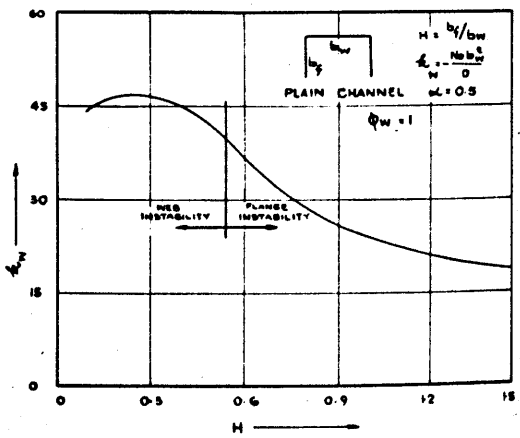

FIG VI 7 BUCKLING CONSTANT Vs SHAPE FACTOR

VI.2 Maximum Load Carrying Capacity of Lipped and Plain Channels.

a. Lipped channels.

Once again the section was considered mathe-:matically to be composed of individual plates which were matched in boundary conditions along the adjoin-:ing longitudinal unloaded edges. This matching was required to fulfil the following conditions for these common edges: (i) the degree of edge restraint for the flange and web was equal but opposite in sign, i.e. moment reactions were equal and the original corner geometry was maintained,

(ii) the numerical value of τ was to be equal for the flange and web

(iii) the value and distribution of the longitudinal direct stress, and therefore the unit shortening, were to be the same for the flange and web.

The simultaneous application of these requirements resulted in a very complicated problem. This was simplified greatly by assuming the stress distribution to be defined to sufficient accuracy by taking only one term in the ξ direction in the series equation III.2.1.

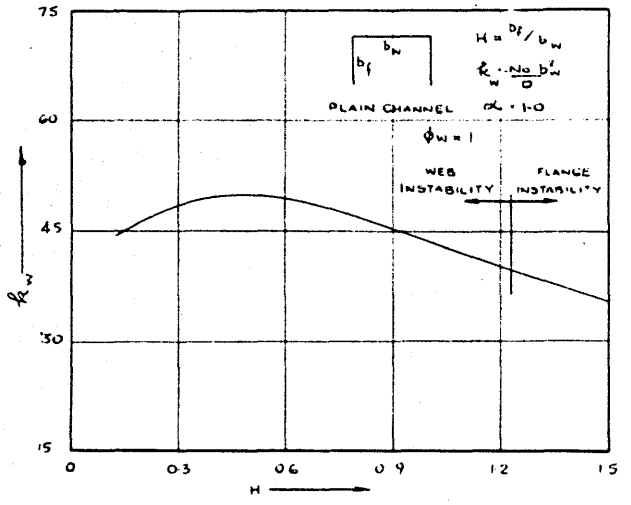

FIG VI 8 BUCKLING CONSTANT Vs SHAPE FACTOR

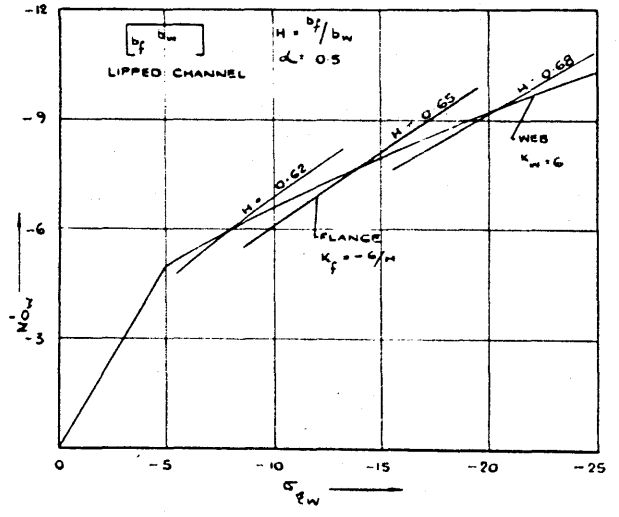

FIG VI 9 LONGITUDINAL STRESS AT $\eta = 0·5$ Vs LOAD

Thus the limit t was taken equal to unity for both the web and the flanges. By assuming a specific web geometry and using the procedure outlined in Section 2 of Chapter III a plot of non-dimensional edge stress vs. non-dimensional load parameter was obtained.

Similar plots were also obtained from the computer for flanges with the relevant rotational restraint coefficients and once more considering the lipped edges to be simply supported. These plots were for various values of H and by using

$$\sigma_{\varepsilon_w} = \frac{1}{H^2}\,\sigma_{\varepsilon_f} \qquad \text{and} \qquad N'_{o_w} = \frac{1}{H^2}\,N'_{o_f}$$

they were superimposed on to the web plot. An example of this is shown in Figure VI.9, - the intersections of these curves were valid geometries in that all the specified boundary conditions were fulfilled at the particular intersection load. These geometries were then considered to be sections at the point of collapse so that by using $\sigma_{\varepsilon_w} = \frac{\sigma_{x_w} a^2}{\phi_w^2 E h^2}$ and $\sigma_{x_w} = \sigma_{yield} = 35 \times 10^3$ lbf/in^2 the relevant material thicknesses were obtained. By limiting the range of thickness to be studied to 0".050 - 0".090 and introducing $\bar{\sigma} = \frac{\sigma_{max}}{\sigma_{yield}} \frac{b_w}{h}$ then a narrow band was described by this non-dimensional parameter when plotted against the form factor H. This is shown in the following example.

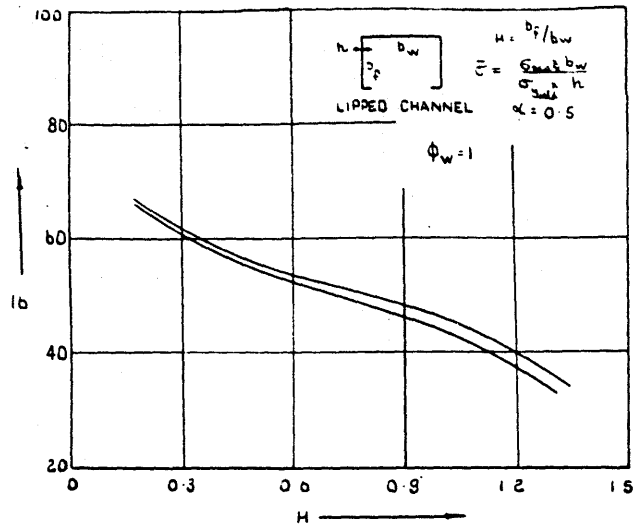

FIG VI 10 COLLAPSE STRESS Vs SHAPE FACTOR.

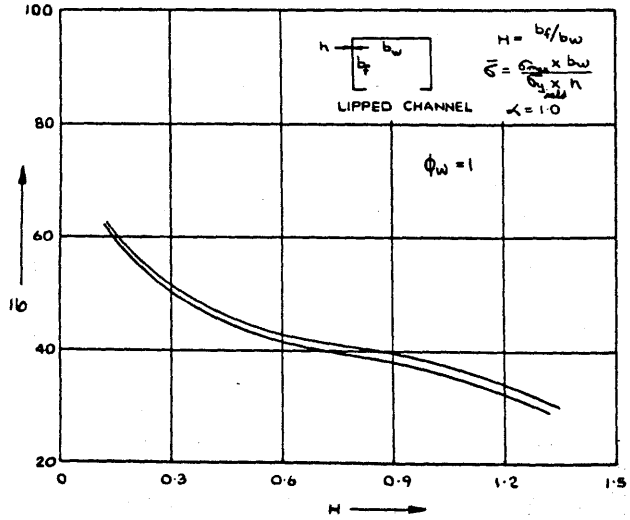

FIG VI 11 COLLAPSE STRESS Vs SHAPE FACTOR.

with $H = 0.62$ $\quad \sigma_{\xi_w} = -8.35$ $\quad N_o' = -6.02$

$$\therefore h^2 = \frac{\sigma_{xw} \times a^2}{\phi_w^2 \times E \times \sigma_{\xi w}} = \frac{-35\times10^3 \times 64}{1\times33\times10^6 \times -8.35} = 0.8132\times10^{-2}$$

$$\therefore h = 0''.0902$$

$$P_{max} = \frac{N_o' \times h^3 \times E \times b_w (1+1.5H+0.125)}{b_w^2} = 3.75\times10^3 \text{lbf.}$$

$$\bar{\sigma} = \frac{\sigma_{max}}{\sigma_{yield}} \times \frac{b_w}{h} = 52.9$$

Similarly

with $H = 0.65$ $\quad h = 0.0705$ $\quad \bar{\sigma} = 52.0$

and for $H = 0.68$ $\quad h = 0.0582$ $\quad \bar{\sigma} = 51.7$

In this way Figures VI.10 and VI.11 were constructed.

b. Plain channels.

The principle for this case differs from that followed in Case a only in that the related thickness for the material was found by use of the computer from the extreme stress in the ξ direction on the plate surface due to the bending of the flanges. The non-:dimensional parameter found suitable for use here was $\tilde{\sigma} = \frac{\sigma_{max}}{\sigma_{yield}} \cdot \left(\frac{b_w}{h}\right)^2$. The reason for the difference of this non-dimensional parameter from that used for the lipped channels was that in the latter theoretical failure was caused by material yielding at the corners due to direct stresses in the middle plane of the plate

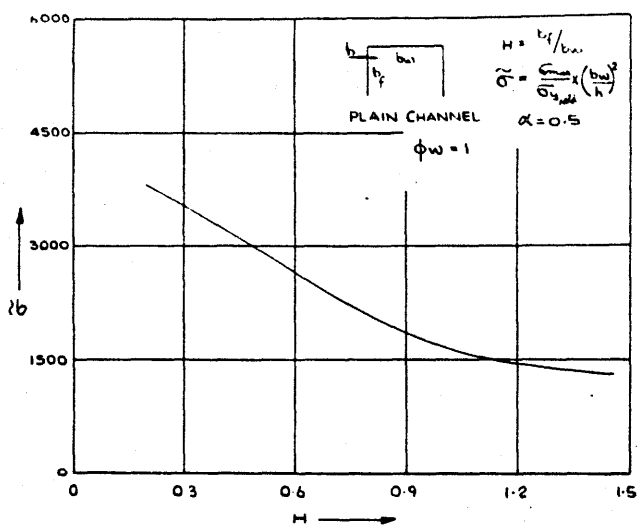

FIG VI 12 COLLAPSE STRESS Vs SHAPE FACTOR

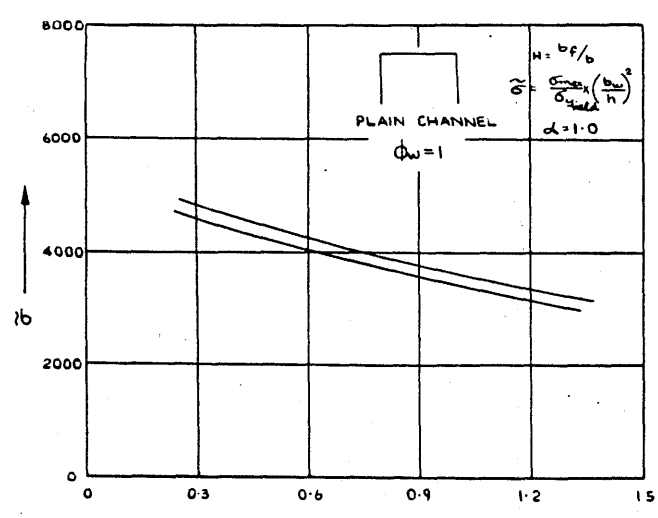

FIG VI 13 COLLAPSE STRESS Vs SHAPE FACTOR

whereas in the plain channels the material thickness was further involved in the calculations due to the assumption that failure was initiated by bending stresses in the flanges.

Figures VI.12 and VI.13 show the results of the calculations which were carried out with $\phi_w = 1$ and an assumed longitudinal deflected shape of one half wave.

C H A P T E R V I I

CHAPTER VII.

EXPERIMENTAL INVESTIGATION INTO THE LOAD BEARING BEHAVIOUR OF CERTAIN STRUCTURAL SHAPES.

In the previous chapter a mathematical approach was outlined which provided approximate forecasts of the instability and maximum, or collapse, loads for certain structural shapes. In this present chapter a description is given of an experimental programme designed to test the validity of these predictions.

The first section of the chapter deals with the general organisation of the test programmes, this being followed by a description of the special equip-:ment designed and built to carry out these tests. The chapter ends with a presentation of typical results obtained from this experimental investigation.

VII.1 Test Programmes.

As in the case of the individual plate investigation, the experimental programmes for the sections were carried out with two main aims in mind. The first was to provide evidence of the value of the theoretical approach. This involved some forty tests to collapse on lipped and plain channels of varying thicknesses and geometry,

loaded eccentrically with respect to the flanges. Two degrees of eccentricity, i.e. $\alpha = 0.5$ and $\alpha = 1.0$, were studied and the range of thicknesses was restricted to $0.050 \leq h \leq 0.080$ since below this considerable difficulties were experienced in machining the ends square, and above this the sections approached the plastic buckling range. The range of geometries studied was $0.25 \leq H \leq 1.25$ with five values in this range. Tensile test pieces were made from the various channels and the resulting material properties obtained are given in Appendix VI.

The second category of tests was designed to provide information on the more detailed aspects of the problem which could be obtained from a study of the strain distributions. For this several specimen lipped and plain channels were extensively strain gauged and loaded carefully in the loading rig described in the following section of this chapter.

VII.2 Special Loading Rig.

The general principle of loading used successfully in the plate testing equipment, and previously described in Chapter IV, was similarly applied to the equipment designed to test the short channel sections considered in this investigation. The analytical

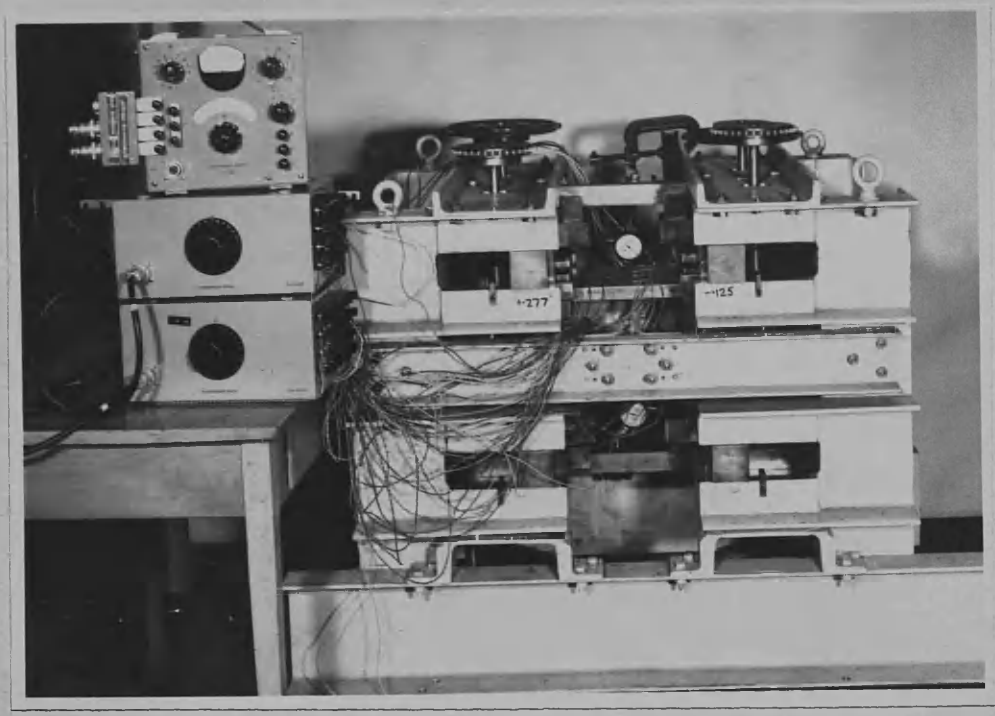

Fig. VII.1.

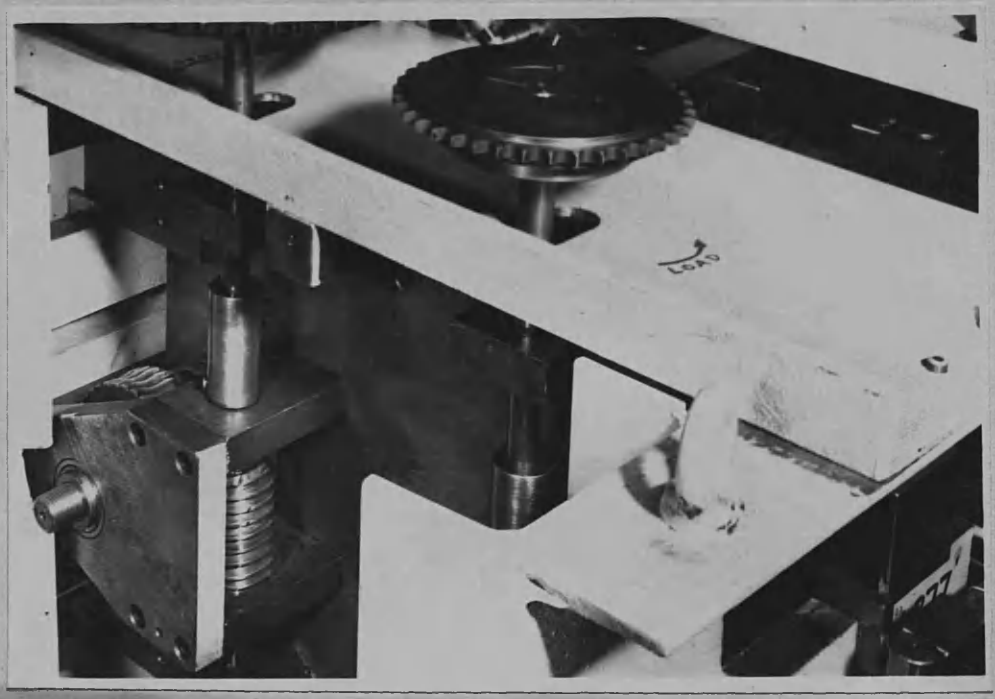

Fig. VII.2.

results were for lipped and plain channels which had square webs and in the practical cases dealt with here the web width and length was made 8".

The test rig is shown in Figure VII.1 with a strain gauged lipped channel section in position. Two relatively massive plattens opposed each other and were individually mounted on four arms for vertical restraint and on two trunnions for similar restraint horizontally. The bearings for the arms were provided by slots on the main frame which were accurately machined and hand finished after the frame had been welded and stress relieved. The trunnions fitted over two heavy steel bars, one above the plattens and one below, which ran the length of the frame and were firmly attached to it. The plattens were made to approach each other in a similar manner to the loading beams in the plate test rig. Once more the link bars were arranged as load measuring cells, in this case the cross-:section was more substantial so that the load was calibrated linearly at 37·9 tsf/μin/in within the calibrated range of 0-6 tonf.

The worm and wheel arrangement is shown in Figure VII.2 while Figure VII.3 shows clearly a detached link bar and pin and the trunnion arrange-:ment. The latter also shows the case hardened facing plate which was grooved to hold the sections.

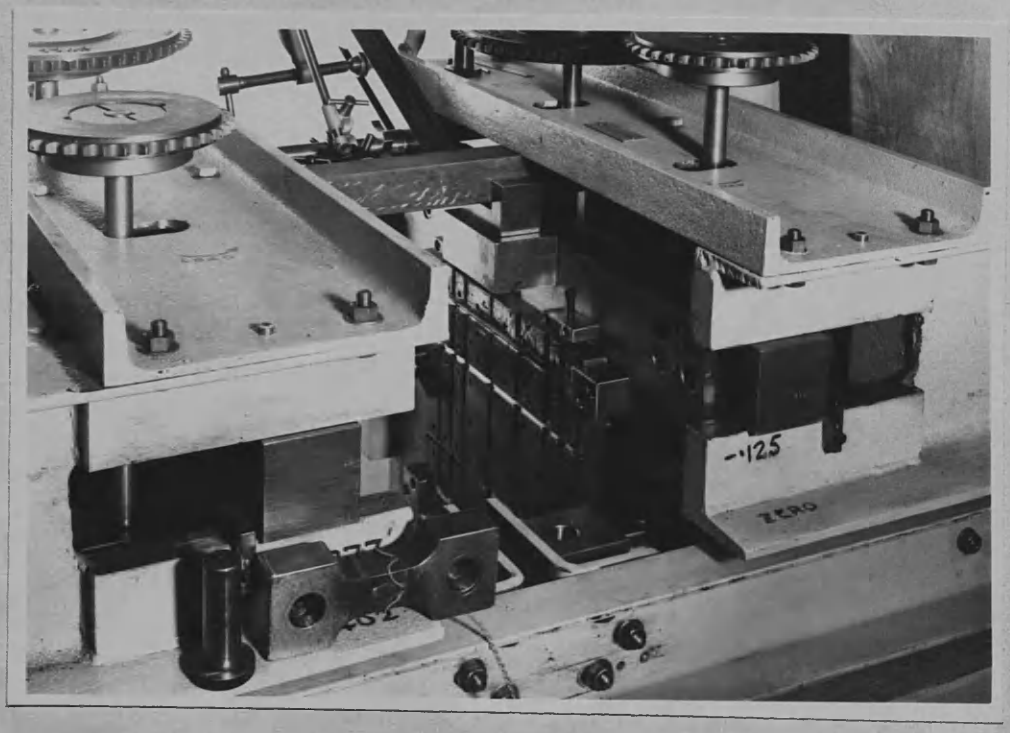

Fig. VII.3.

This plate was solidly keyed against horizontal movement relative to the platten and was restrained against vertical movement by setting screws. The vertical grooves which located the webs for the various channel sizes were semi-circular in shape whilst the others were carefully ground flat. The markings shown on the frame were reference sizes so that at any time the relative positions of the plattens could be determined by using a micrometer over the support arms and the setting block behind it.

The procedure used for a test was essentially as follows. The plattens were retracted to their maximum travel, the specimen channel was then placed so that the web fitted into the appropriate vertical slot in one of the hardened plates. The plattens were brought together and linked into place. Readings were taken using a micrometer at the before mentioned reference points and the plattens located parallel to each other and square to the run of the rig with a small load on the section. Clock gauges were then placed in position around the section and zero readings taken.

The load was induced by screwing one side into a position which produced a predetermined load with the other side similarly screwed into a corresponding position to give a calculated proportion of this load.

Readings were taken of the link bar strains on a Huggenberger strain bridge and the clock gauge readings noted. Collapse was indicated by a drop in the load for an inward movement of the plattens.

VII.3 Test Results.

(i) First series.

The instability loads for the channels were obtained using a method similar to that employed for the individual plates. Values of web and flange deflection were taken at each loading interval and after plotting it was seen that these deflections began to grow from the beginning of load application. It was found that if the method of Southwell was used for these plots then good straight lines were obtained which led to consistent results for instability loads. Figure VII.4 gives an example of the method for the flange of a lipped channel; this may be taken as typical and where the plots for the flange and web gave different values for the instability load an arithmetic average was taken.

The resulting instability loads for the channel geometries and loading eccentricities studied here

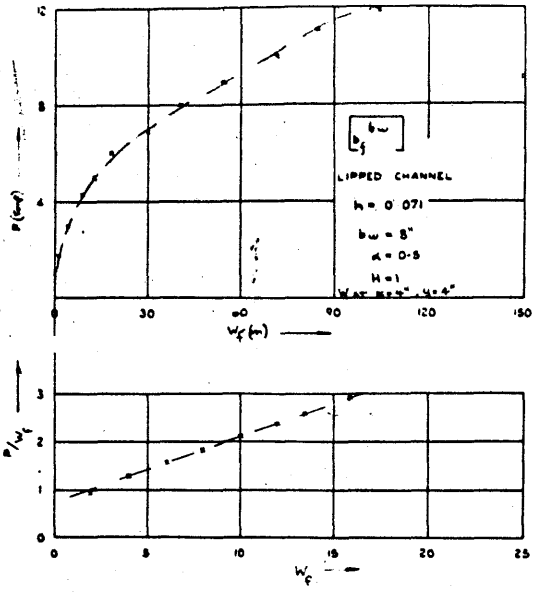

FIG VII.4 LOAD VS. DEFLECTION WITH ASSOCIATED SOUTHWELL PLOT

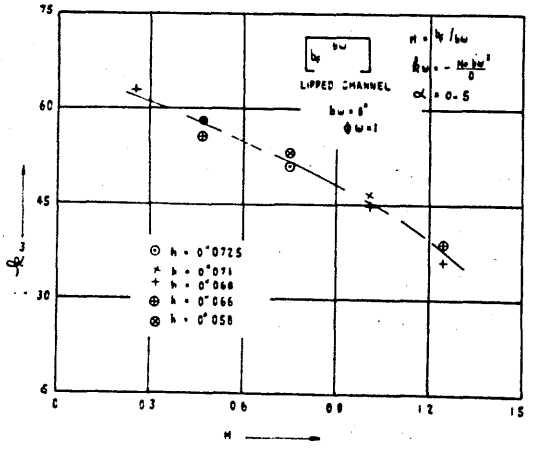

FIG VII.5 BUCKLING CONSTANT VS SHAPE FACTOR

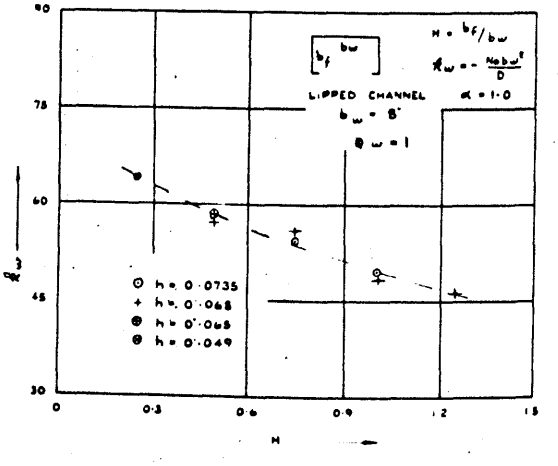

FIG VII.6 BUCKLING CONSTANT VS SHAPE FACTOR

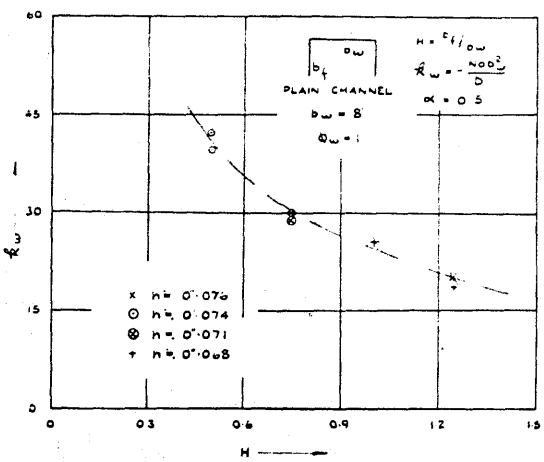

FIG VII.7 BUCKLING CONSTANT VS SHAPE FACTOR

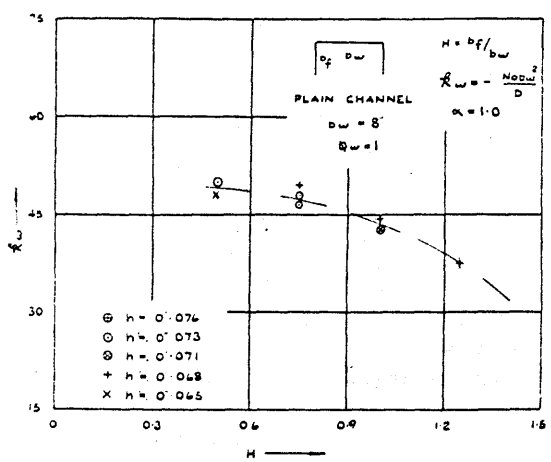

FIG VII.8 BUCKLING CONSTANT VS. SHAPE FACTOR

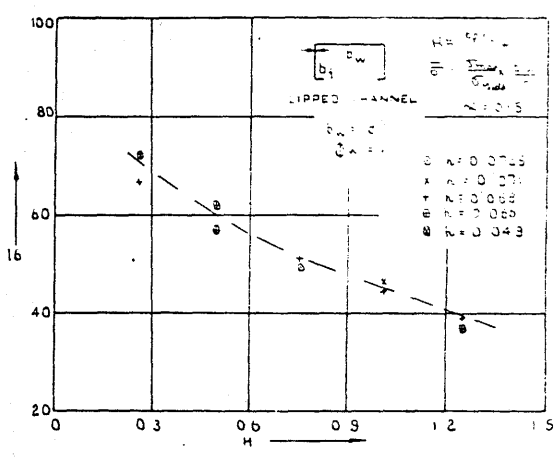

FIG VII.9 COLLAPSE STRESS VS SHAPE FACTOR

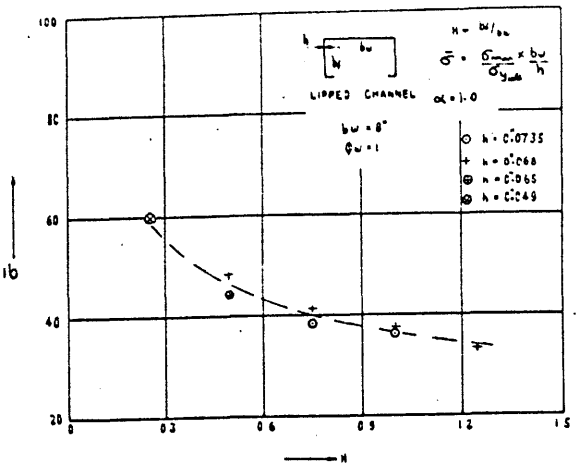

FIG VII.10 COLLAPSE STRESS VS. SHAPE FACTOR

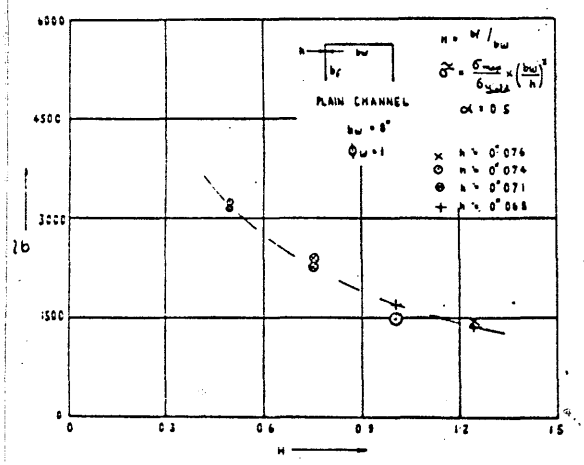

FIG VII.11 COLLAPSE STRESS VS SHAPE FACTOR

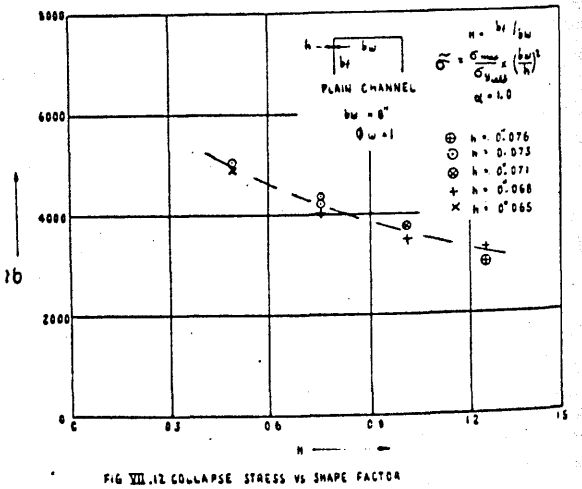

FIG VII.12 COLLAPSE STRESS VS SHAPE FACTOR

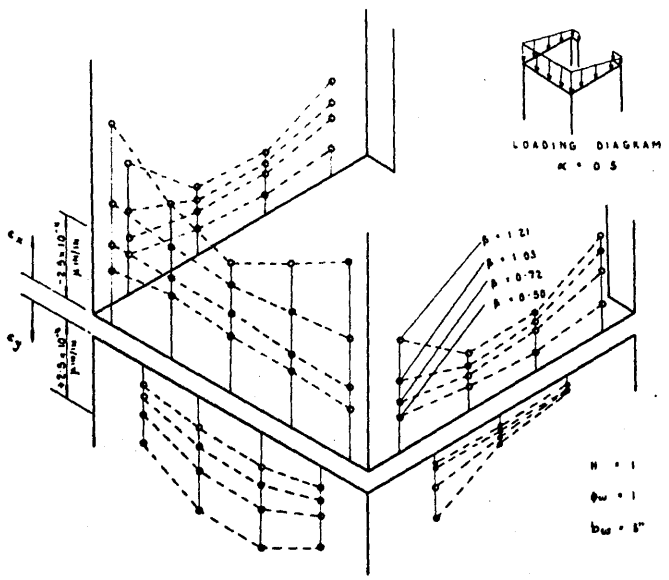

FIG. VIII 13 DISTRIBUTION OF ϵ_x AND ϵ_y ACROSS THE CENTRAL X SECTION OF A LIPPED CHANNEL. 0".071 THICK.

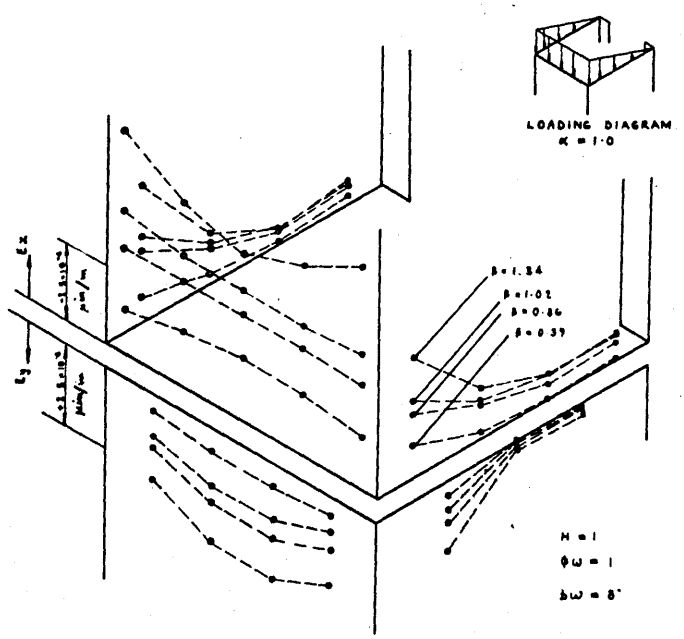

FIG VIII 14 DISTRIBUTION OF Ex AND Ey ACROSS THE CENTRAL X SECTION OF A LIPPED CHANNEL 0".1071 THICK

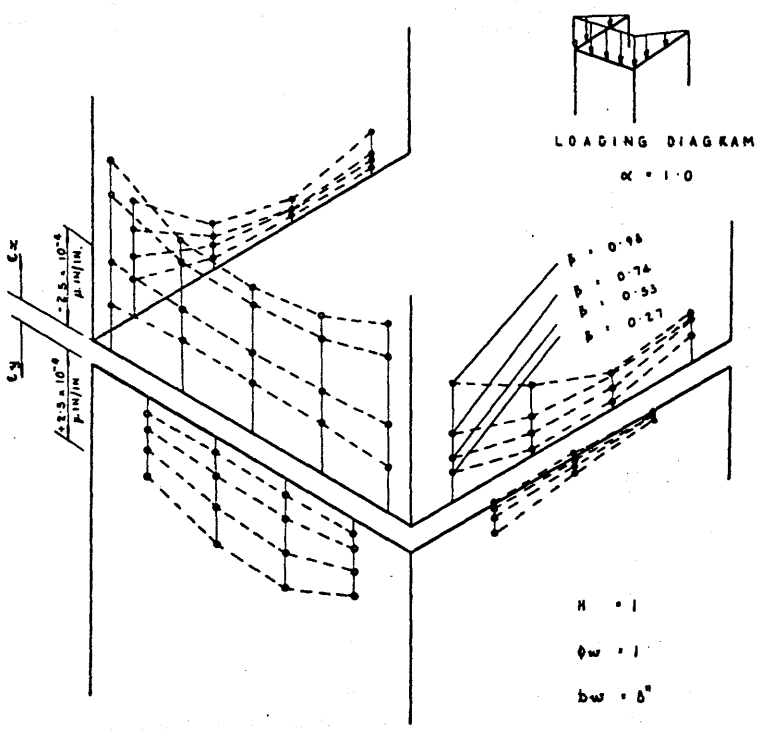

FIG. VIII.15 DISTRIBUTION OF ε_x AND ε_y ACROSS THE CENTRAL X SECTION OF A PLAIN CHANNEL. 0"·071 THICK.

are shown in Figures VII.5 - VII.8. The collapse loads corresponding to these test are shown in Figures VII.9 - VII.12.

(ii) Second series.

The strain distributions shown in Figures VII.13 - VII.15 were obtained from forty eight $\frac{1}{2}$" length 100 ohm electric resistance strain gauges bonded on to carefully prepared sections. The gauges were arranged in pairs, one exactly opposite the other on the two surfaces of the channel - in this way the middle surface strains could be obtained. The strain measuring equip-:ment was a Huggenberger strain bridge and switch boxes.

C H A P T E R V I I I

CHAPTER VIII.

COMPARISON OF THEORETICAL AND EXPERIMENTAL RESULTS FOR STRUCTURAL SHAPES.

In Chapter V the results of an experimental programme into the behaviour of single plates subjected to eccentric compressive loading were compared to the relevant theoretical values. The conclusions drawn from these comparisons were that the mathematical approach was rational and, within engineering require-:ments, gave good forecasts for the instability loads, post-buckling behaviour and collapse loads for such plates.

In this present chapter the results of an experi-:mental programme concerning tests on certain structural shapes are similarly compared to the relevant theoretical results. In the light of the conclusions of the plate investigation such comparisons are seen to be tests of the efficacy of the assumptions made, that these sections can be considered as being composed of individ-:ually compressed plates. They also test the further assumptions used in respect of the conditions thought to exist at the longitudinal edges of these individual plate components.

VIII.1 Instability Loads.

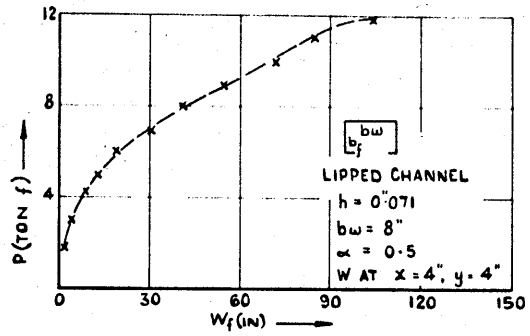

FIG VIII.1 LOAD Vs DEFLECTION

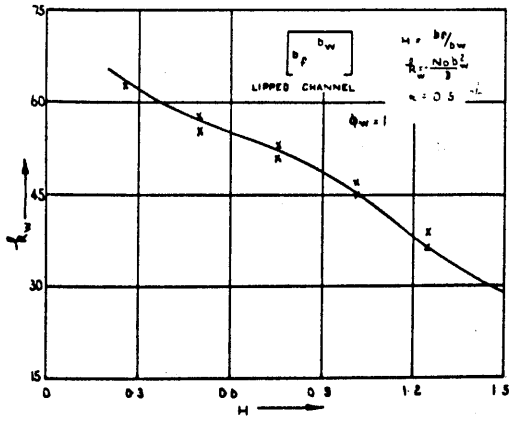

FIG VIII.2 BUCKLING CONSTANT Vs SHAPE FACTOR

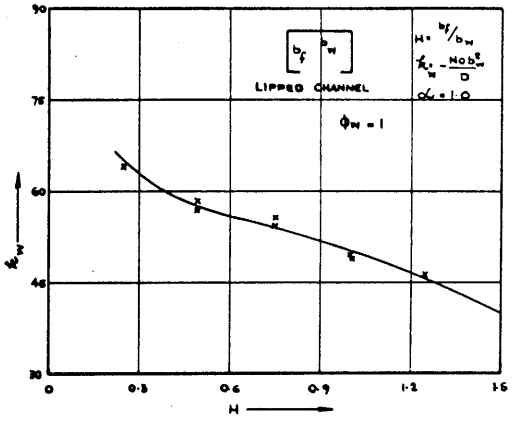

FIG VIII.3 BUCKLING CONSTANT Vs SHAPE FACTOR

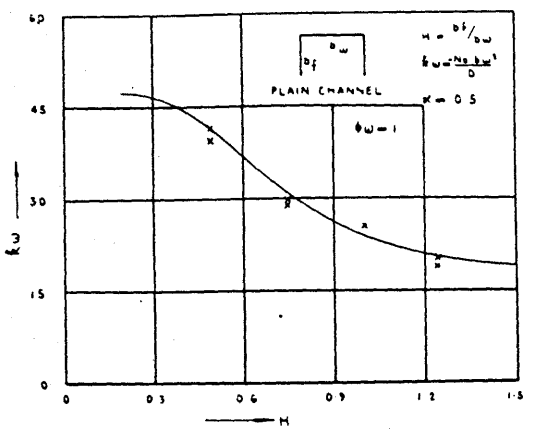

FIG VIII.4 BUCKLING CONSTANT VS SHAPE FACTOR.

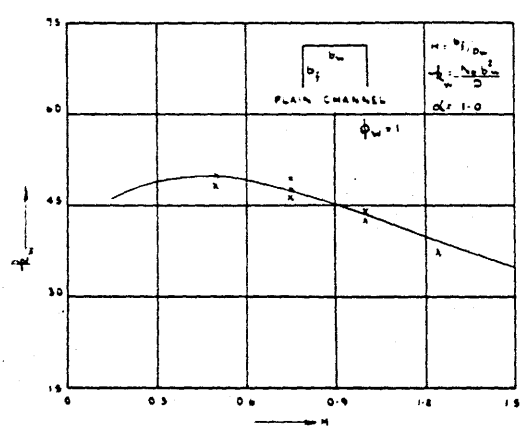

FIG VIII.5 BUCKLING CONSTANT Vs SHAPE FACTOR

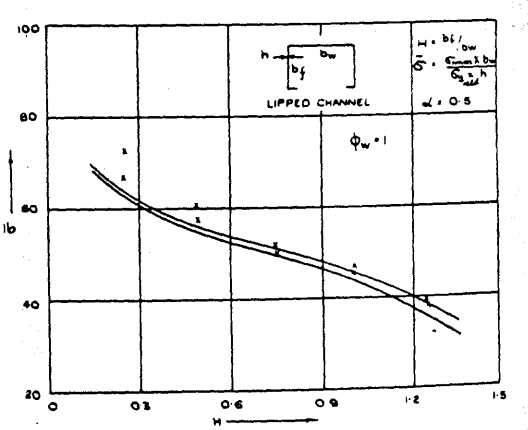

FIG VIII.6 COLLAPSE STRESS Vs SHAPE FACTOR

The first condition studied is instability. As in the case of the plates it was found in tests on sections that deflections began to grow almost immediately on the application of loading. This is shown clearly in Figure VIII.1 which may be taken as typical of this type of plot. It was therefore necessary to resort to an approximate method of deducing the actual load which was equivalent to the instability load in a perfectly formed section.

Chilver (1950) showed in a theoretical consider-:ation of the elastic stability of uniformly compressed open channel sections that a plot similar to that suggested by Southwell for individual elements could be employed to advantage. In a later section of his study Chilver indicated that if low deflection values were used then the straight lines in the plot predicted by the theory were in fact obtained experimentally. When this technique was applied to the eccentrically loaded section results of this present investigation it was found that straight lines were obtained and that the inverse slope of these gave good approximations to the theoretical "flat plate" section instability loads. These inferred values are shown compared to the corres-:ponding theoretical curves in Figures VIII.2 - VIII.5. In these, as in all the figures in this chapter, the full lines were obtained from analytical considerations and the points shown were obtained experimentally.

In Figures VIII.2 and VIII.3, which show the non-:dimensional buckling constant plotted against shape

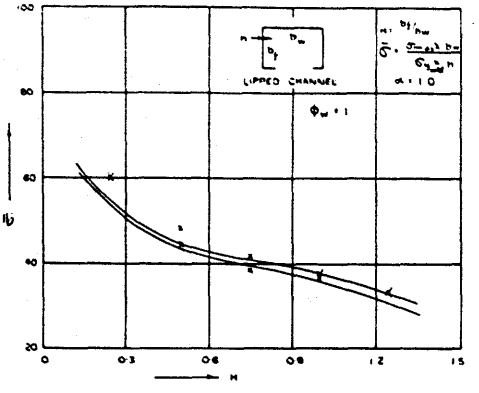

FIG VIII.7 COLLAPSE STRESS CONSTANT V_3 SHAPE FACTOR

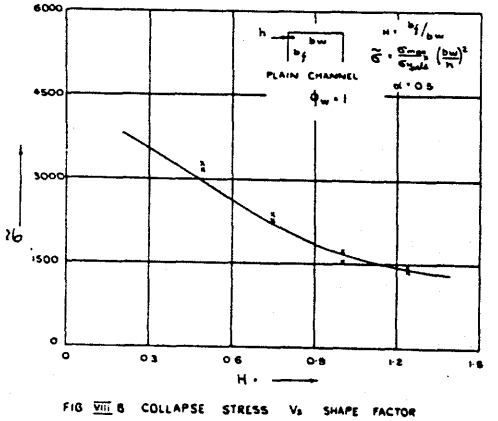

FIG VIII.8 COLLAPSE STRESS V_3 SHAPE FACTOR

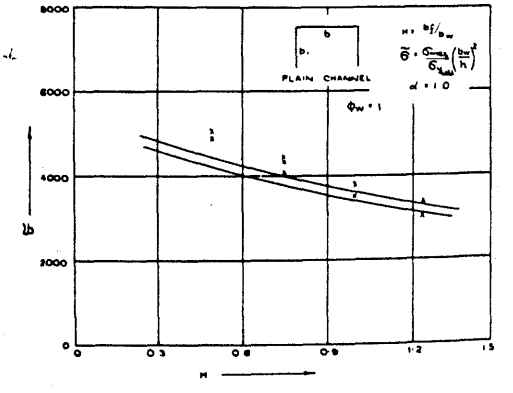

FIG VIII.9 COLLAPSE STRESS CONSTANT V_3 SHAPE FACTOR

factor for lipped channels subjected to two conditions of loading eccentricity, the experimental values are seen to lie close to the corresponding theoretical values. The scatter, caused by the unavoidable variations of the material constants in the section, is evenly distributed about the theoret-:ical curve.

The same comments may be made about the agreement shown in Figures VIII.4 and VIII.5 which give the buckling constant values for plain channels. From these four figures it may be concluded that the analy-:sis based on plate instability outlined in Chapter VI was rational and that the method derived by Chilver for concentrically loaded sections was also applicable to eccentrically loaded sections. The results also confirm the simplification that the lipped longitudinal edge for the range investigated could be considered as simply supported.

VIII.2 Collapse Loads.

The comparison of theoretical and experimental collapse loads for lipped and plain channels for various thicknesses and geometries is shown in Figures VIII.6 - VIII.9.

For the lipped channels, shown in Figures VIII.6 and VIII.7, the agreement is seen to be good, thus

indicating the rationality of the method used in the matching of the web and flange plates and also of the non-dimensional parameter employed. The reason for the slight deviation at the lower values of the shape factor was considered to be mainly due to the theoretical treatment of the lipped edges. This is to say that as the flange width was reduced, the lip, because of its increasing relative width, no longer could be regarded as merely providing simple support along this unloaded edge at high values of flange deflection. Instead, the torsional stiffness of the lip would have to be considered; this, however, would complicate the problem to such an extent that, since the method used already provided conservative results, it was doubtful if proportionally more valuable results would have ensued from such a correction.

It will be noted in Figure VIII.8 for plain channels that the theoretical collapse load for varying section geometry and thickness was defined by a single curve and not a narrow band as in the previous two figures. This was because the theoretical collapse load was found to be coincident with the initial instability load for this loading geometry. Such a prediction was, of course, conservative in nature due probably to the necessary restrictions in the size of the mathematical series solution for the collapse load. However, as the agreement with the experimental test results shows, these theoretical results are still of considerable practical value because of the effect of the deviations

from flatness in the unloaded sections. These caused the deflections in the region of the instability loads to be much larger than those predicted from flat plate considerations, thus producing higher bending stresses earlier collapse and hence closer correspondence to theoretically predicted values.

The comparison of theoretical and experimental results for plain channels subjected to loading of eccentricity $\alpha = 1$ is given in Figure VIII.9. The slight deviation at the lower values of shape factor was attributed to the theoretical results becoming more conservative due to the relatively very large deflections experienced by the narrow flanges.

The general good agreement observed in this and the preceding three figures allows the conclusion to be made that the method developed in Section 2 of Chapter VI provided rational and conservative engineering estimates to the collapse loads of eccentrically loaded lipped and plain channels.

VIII.3 Strain Distribution.

Examples of the distributions of the middle plane strains are given in Figures VII.13 - VII.15. In these it is seen that the shape of the various distributions in the flanges and webs were similar to those

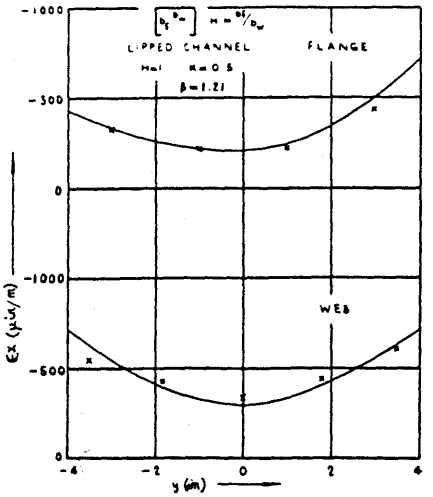

FIG. VIII.10 MIDDLE SURFACE STRAIN ACROSS SECTION AT CENTRAL X POSITION.

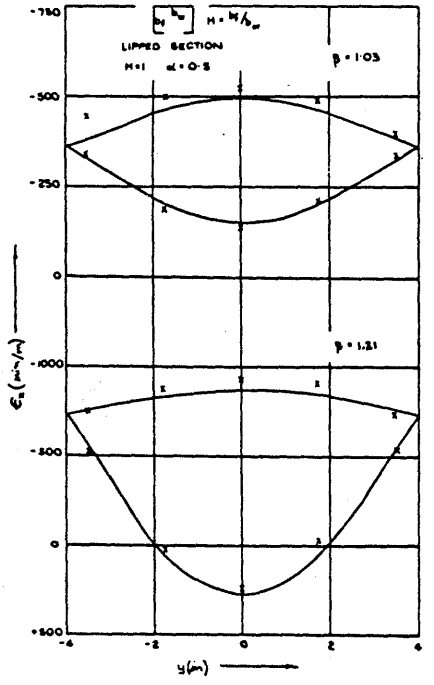

FIG VIII 11 SURFACE STRAIN ACROSS SECTION AT CENTRAL x POSITION

predicted for the individual plates considered earlier in this investigation. Because of the essentially trial and error nature of the analytical method of matching the flanges and webs of the sections it was very tedious to obtain many values of the strain distribution in a particular channel section at a specific load in the post-buckled region. However, some specimen distributions are given in Figures VIII.10 and VIII.11, for a lipped channel with a loading eccentricity $\alpha = 0.5$, compared to the corresponding experimental values. It is seen that agreement was good which further substantiates the conclusion that such sections may be treated theoretically as being composed of individually compressed plates.

VIII.4 Conclusions.

1. Approximate analytical methods have been developed which combine the theoretical plate characteristics to provide good estimates for the instability and collapse loads of eccentrically loaded channel structural sections.

2. The theoretical approach also allows the middle strain values to be closely determined.

3. The method suggested by Chilver for inferring

instability loads from experimental results is applicable to eccentrically loaded sections and gives values which are in good agreement with those obtained theoretically.

G E N E R A L S U M M A R Y

GENERAL SUMMARY.

The first part of this investigation was an analytical and experimental approach to the problem of eccentrically loaded thin plates with a variety of boundary conditions.

The theoretical instability loads were obtained from the solution of the biharmonic equation using the Galerkin method and also a finite difference technique. The results from these two approaches were found to be very close and in good agreement with the relevant values inferred from the experimental results using "Southwell's Plot".

The power of the Galerkin method was enhanced by using a digital computer to carry out the great deal of arithmetic work involved in the solution of the elastic large deflection equations. In this way sufficient terms could be included in the assumed series to obtain satisfactory convergence.

The collapse condition was also studied and here it was shown that the use of a simple material yield criterion leads to accurate, and easily obtained, engineering forecasts for the maximum load carrying capacities of such plates.

The experimental results mentioned before were obtained with the use of specially designed equipment, part of which was for a photogrammetric technique for

determining the plate deflected shapes. This technique proved very effective in providing information on the efficacy of the loading rig as well as the theoretical approach confirming that the deflected shape was given closely by the analytical solution.

The second part of the investigation was concerned with combining these plate results to provide reliable estimates for the instability and collapse loads of channel sections loaded eccentrically with respect to the flanges.

The experimental programme dealt with lipped and plain channel sections and it was shown that the instability and collapse loads from tests were in good agreement with the respect-:ive analytically predicted counterparts.

Thus it may be concluded that the results obtained and the techniques developed in this investigation go some way towards filling a presently existing gap in the information avail-:able to designers of thin plate structures.

A C K N O W L E D G E M E N T S

ACKNOWLEDGEMENTS.

I wish to express my respectful gratitude to Professor A. S. T. Thomson, Head of the Division of Mechanical, Civil and Chemical Engineering at the Royal College of Science and Technology, for the laboratory and workshop facilities placed at my disposal.

My very sincere gratitude is also due to Professor R. M. Kenedi, Research Professor in Bio-Engineering at the Royal College of Science and Technology, for his continued interest and encouragement during the period of this invest-:igation.

My thanks are given to the staffs of the Laboratories and Drawing Office.

Finally, I wish to record my indebtedness to the Institution of Mechanical Engineers whose granting of a Clayton Fellowship made it possible for me to undertake this work.

Alastair Walker.

Alastair Walker.

D I A G R A M S

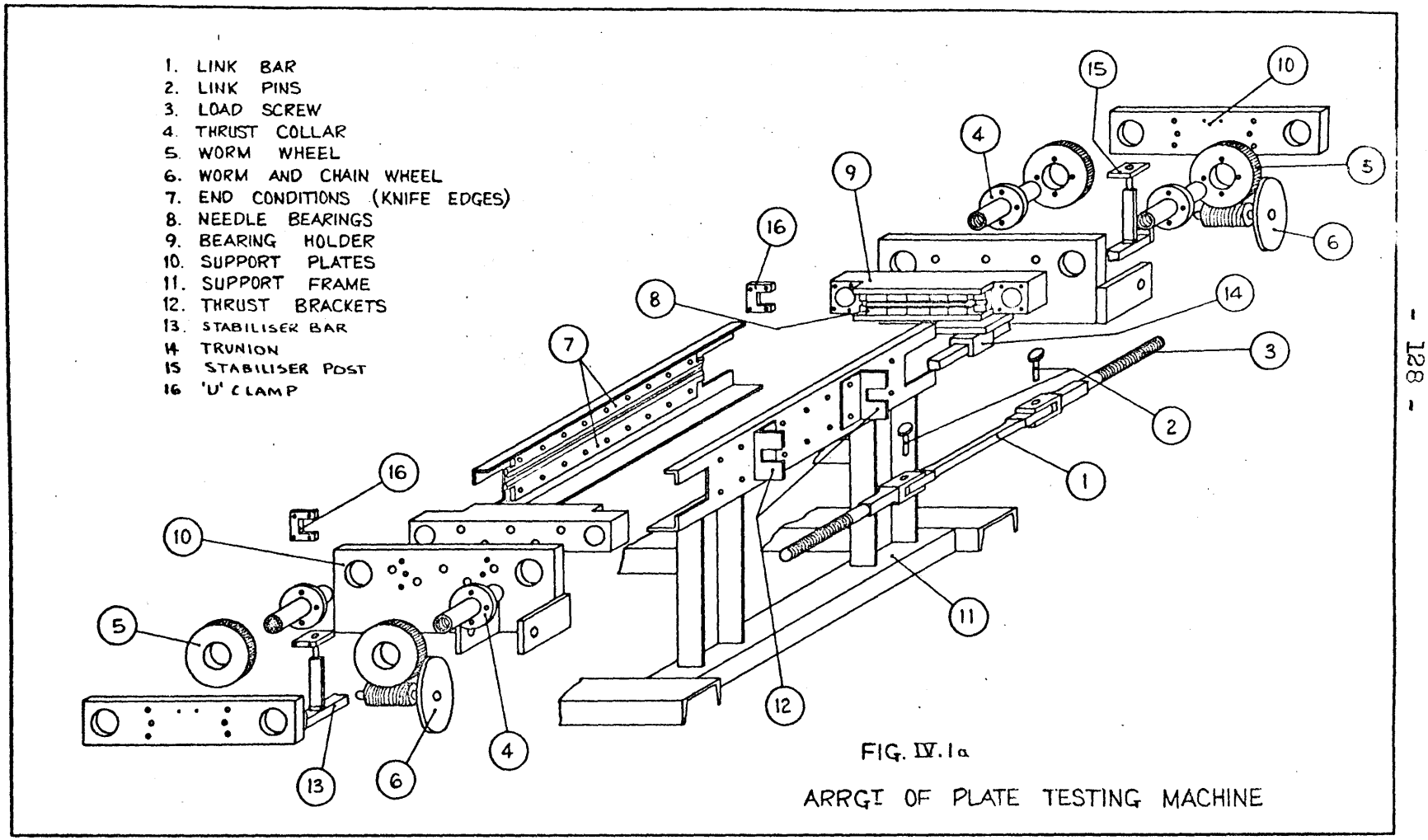

FIG. IV.1a

ARRGT OF PLATE TESTING MACHINE

13 STABILISER BAR
14 TRUNION
15 STABILISER POST

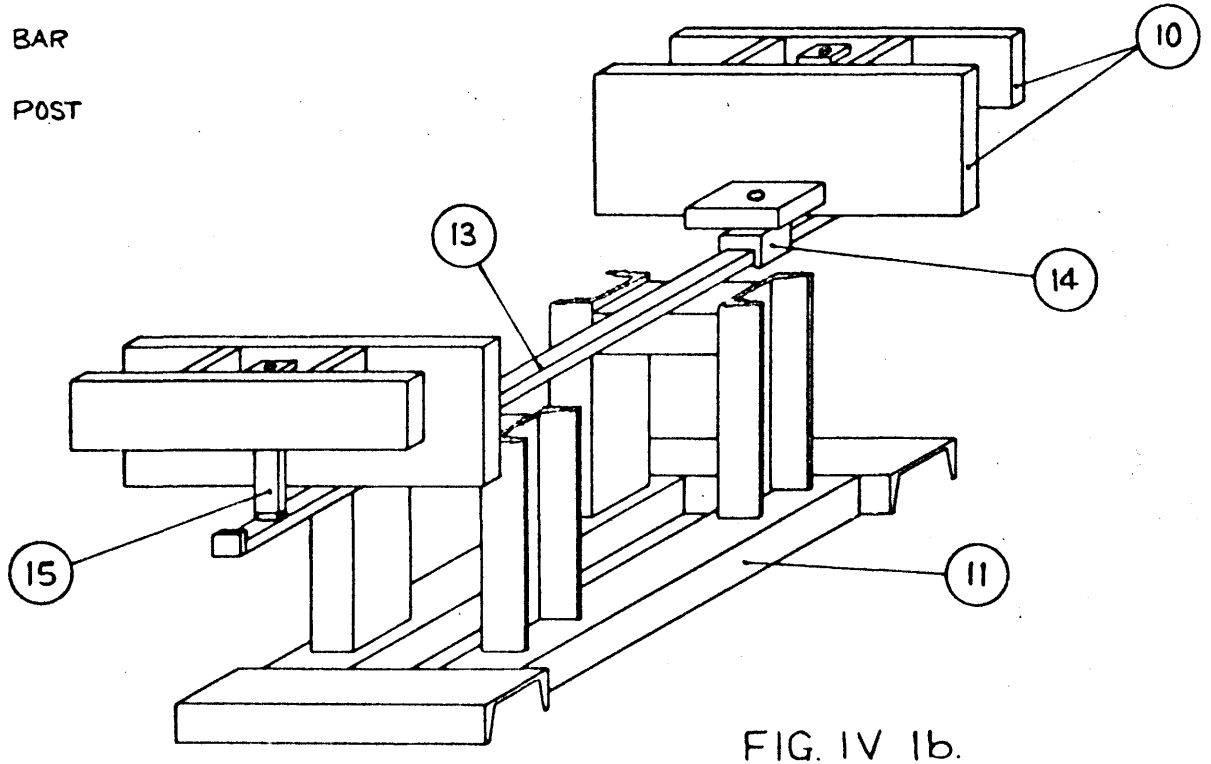

FIG. IV 1b.

PART ARRGI SHOWiiNG STABILISER GEAR

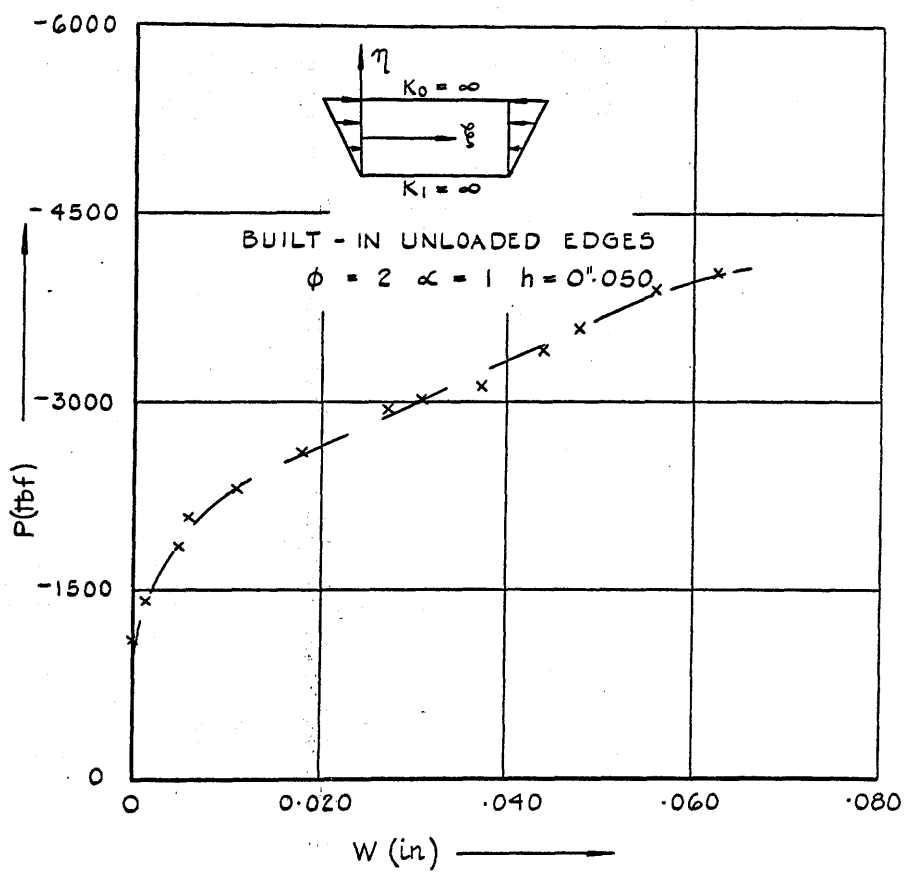

FIG. IV.7 LOAD Vs. DEFLECTION.

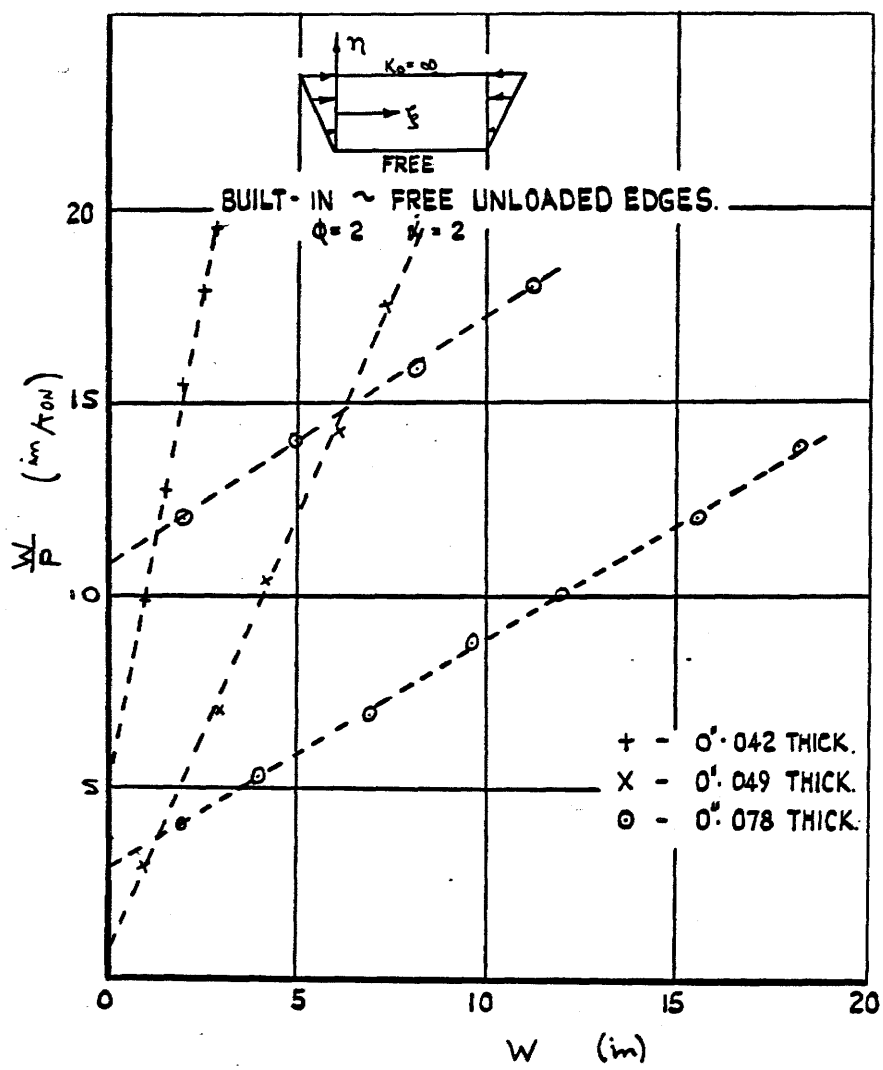

FIG. IV.8 EXAMPLE SOUTHWELL PLOTS.

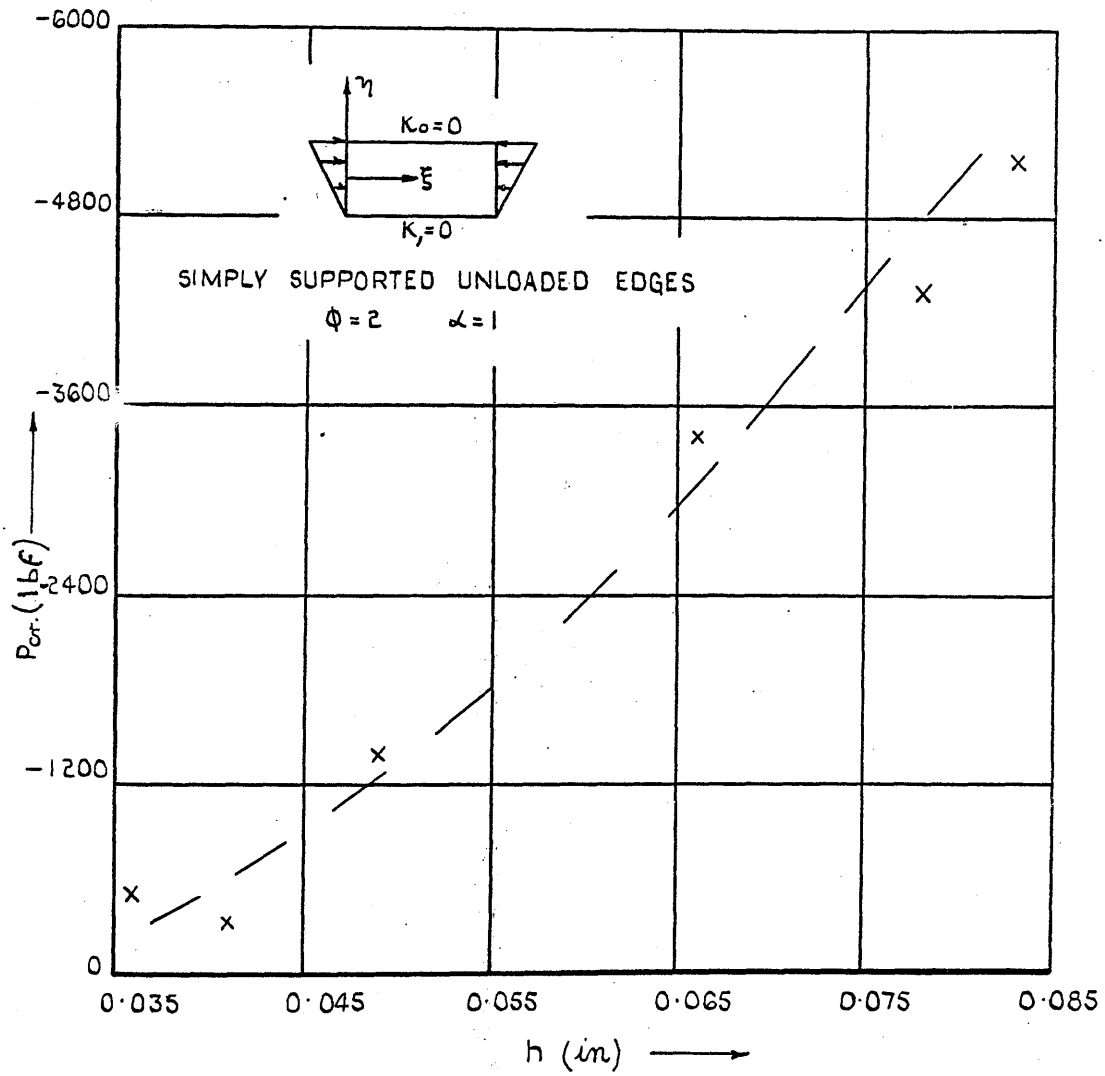

FIG. IV.9 INSTABILITY LOAD V. PLATE THICKNESS

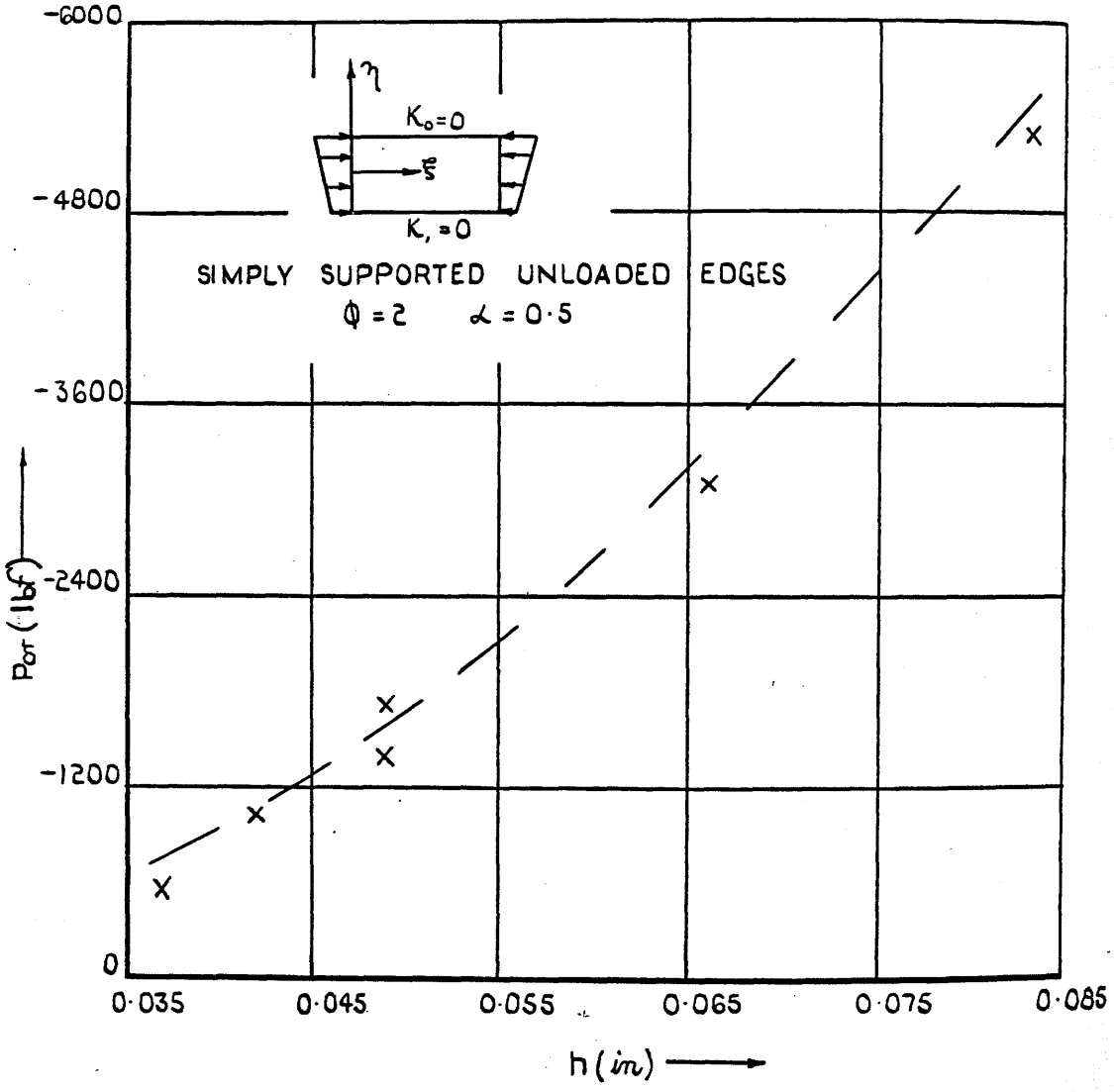

FIG. IV.10 INSTABILITY LOAD V. PLATE THICKNESS

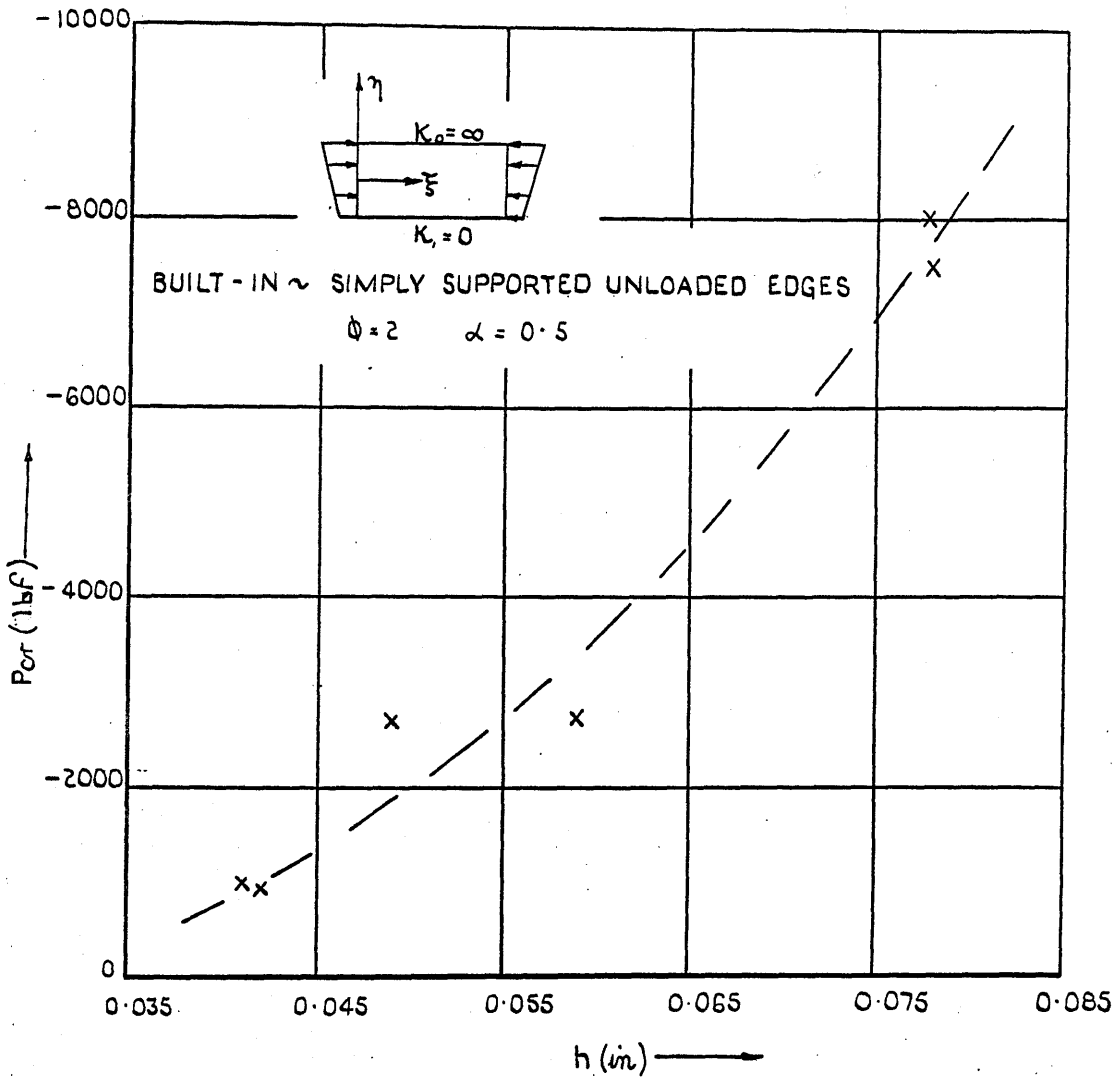

FIG. IV.11 INSTABILITY LOAD V. PLATE THICKNESS

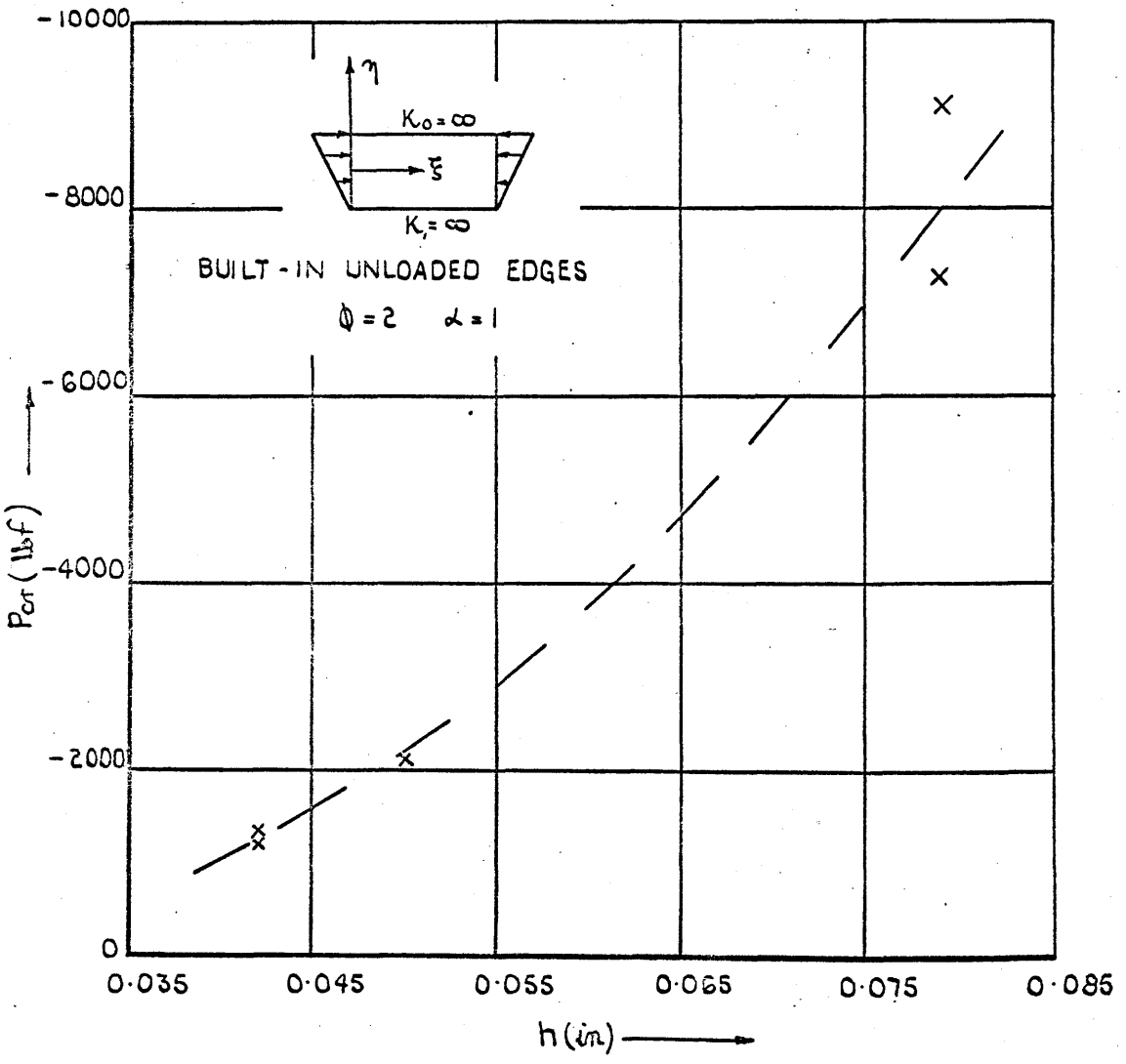

FIG. IV.12 INSTABILITY LOAD V. PLATE THICKNESS

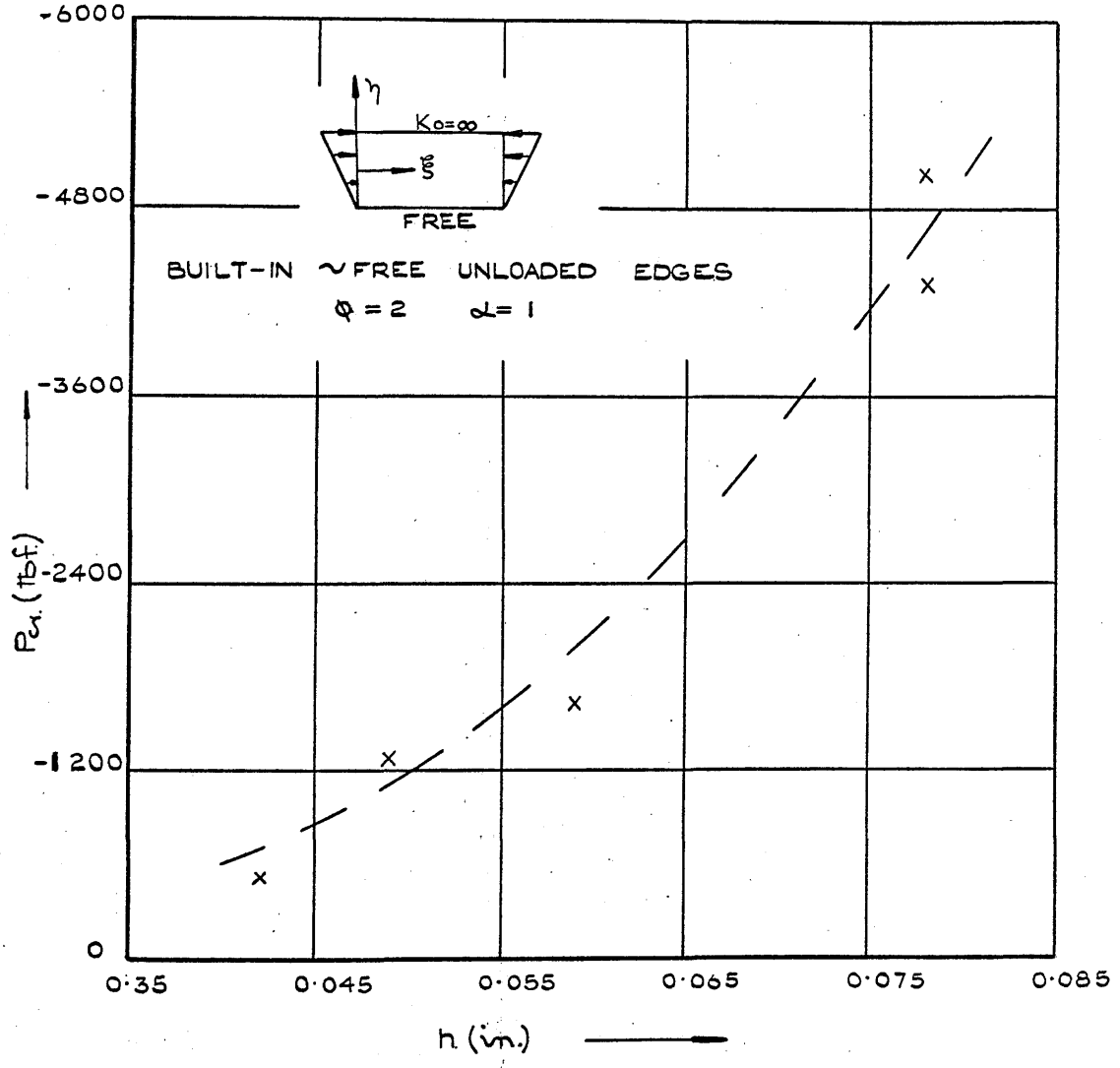

FIG.IV.13 INSTABILITY LOAD V. PLATE THICKNESS

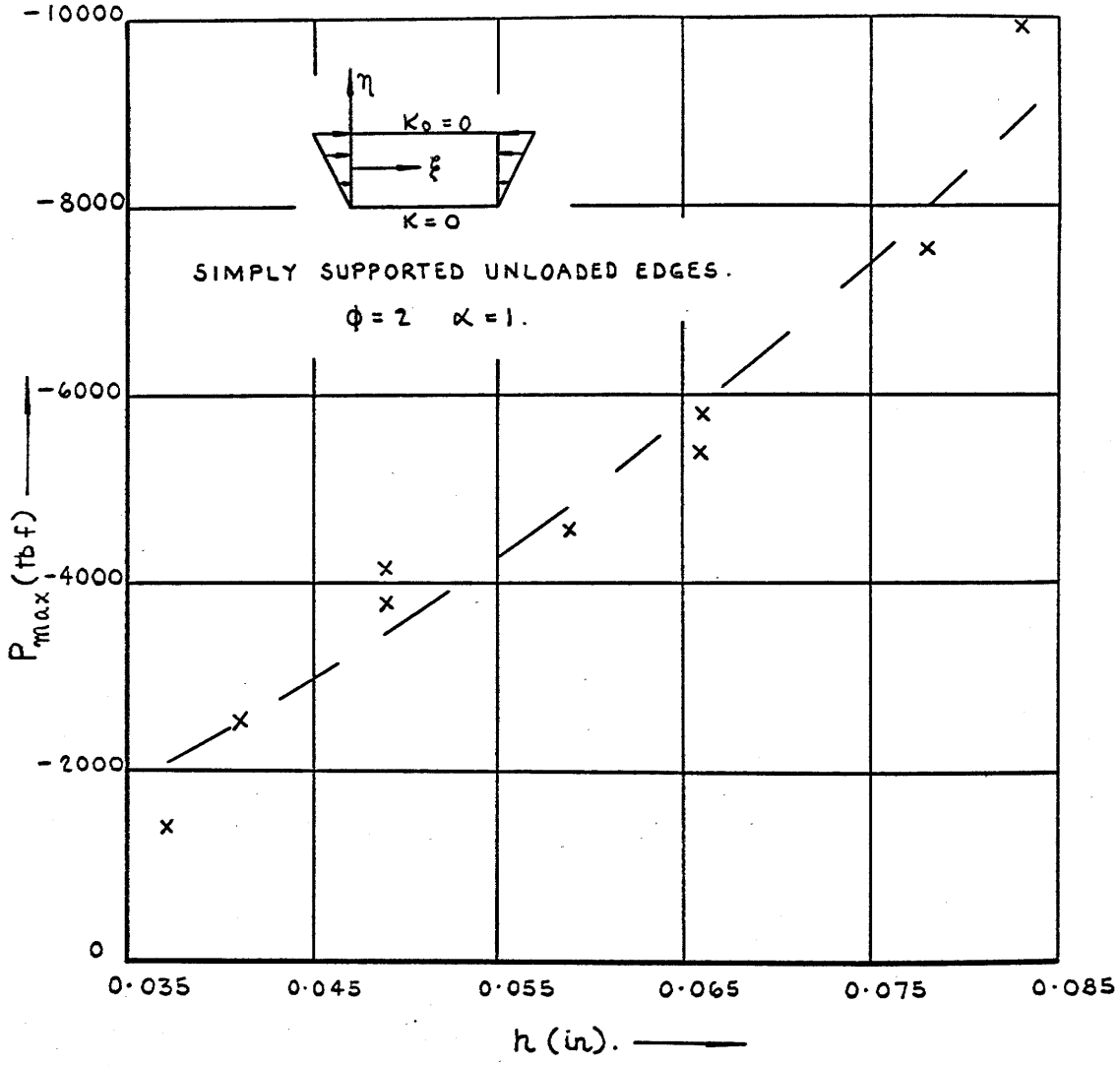

FIG.IV.14 COLLAPSE LOAD V. PLATE THICKNESS.

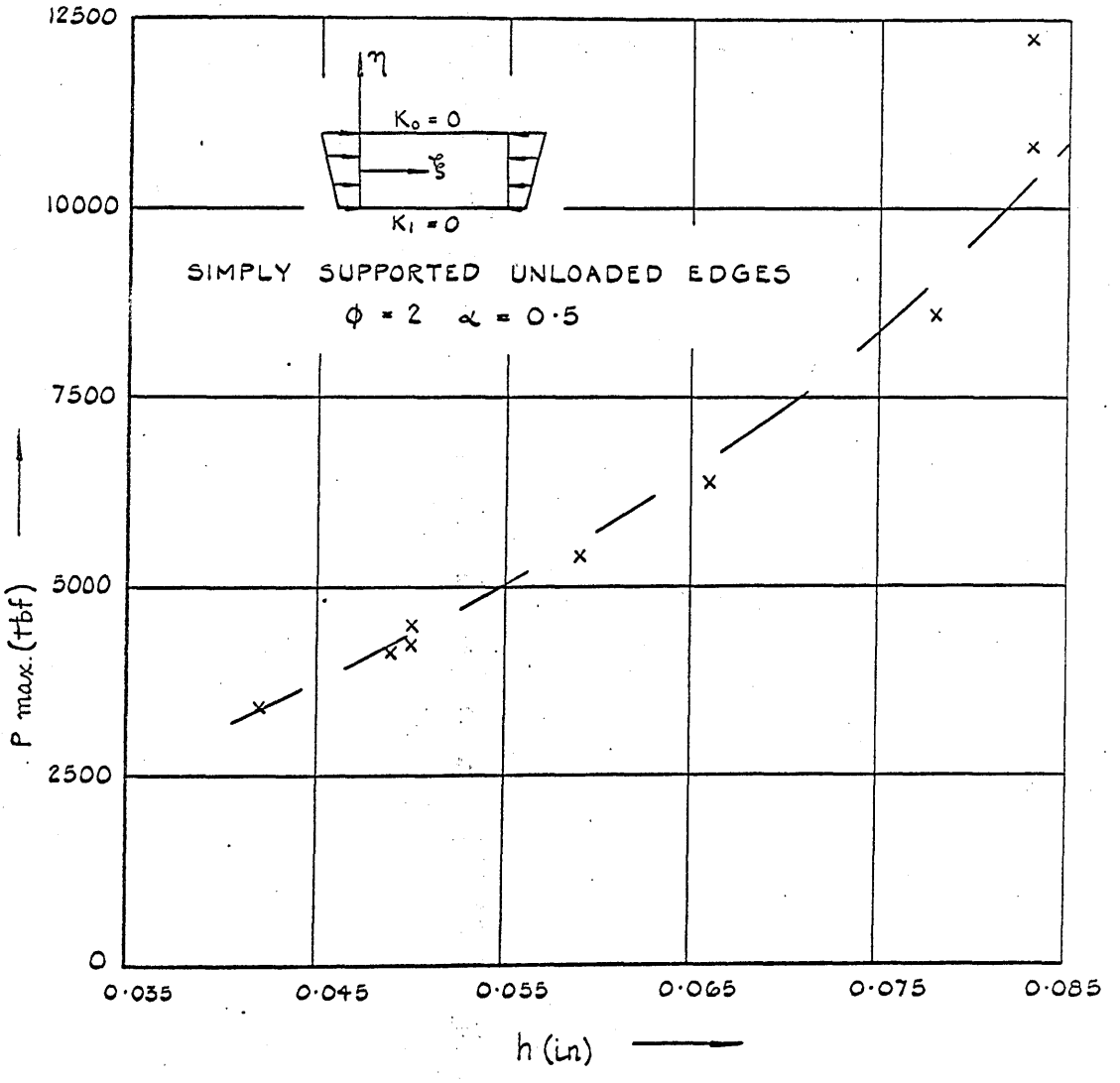

FIG. IV.15 COLLAPSE LOAD V. PLATE THICKNESS.

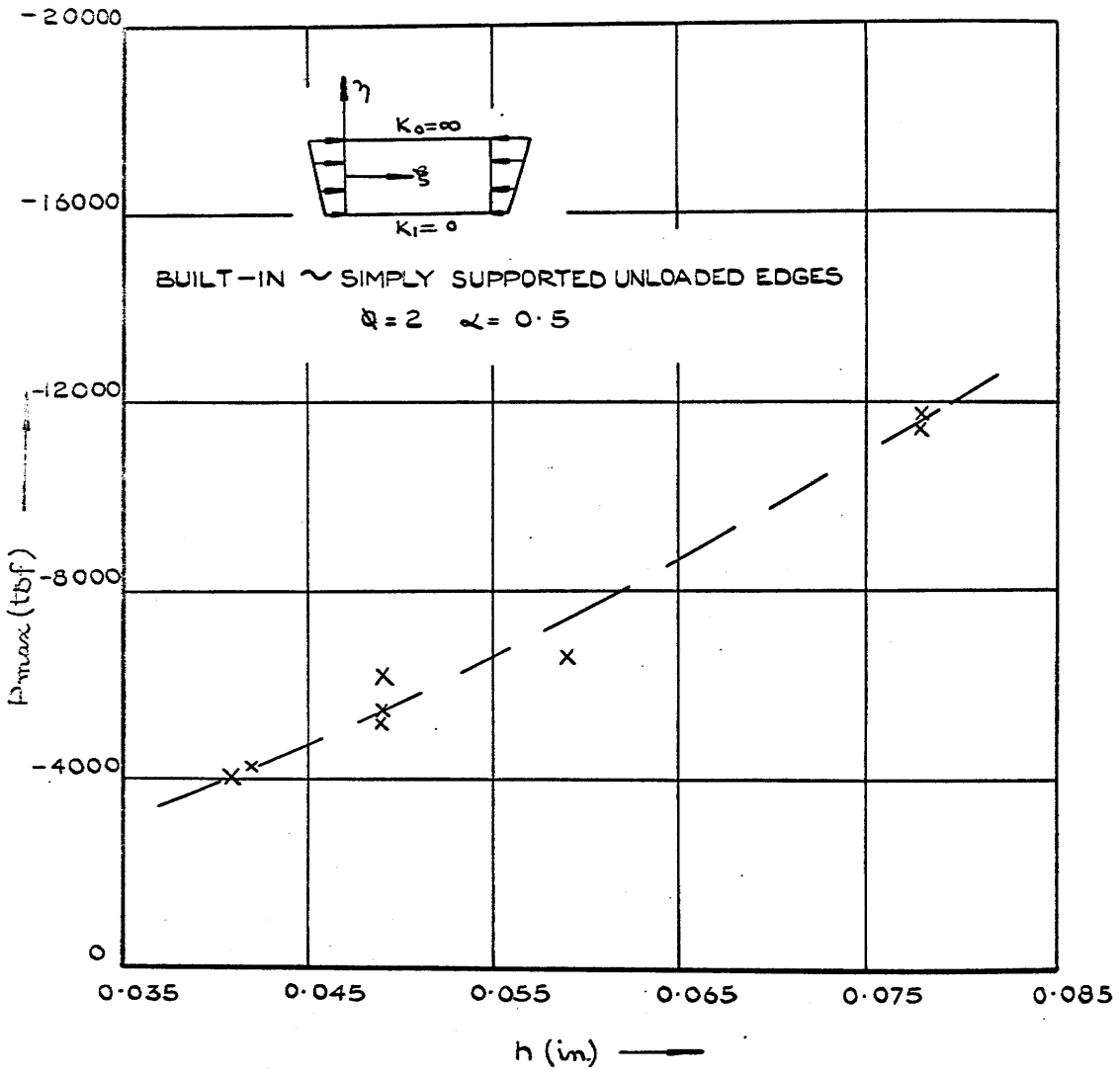

FIG. IV. 16 COLLAPSE LOAD v. PLATE THICKNESS

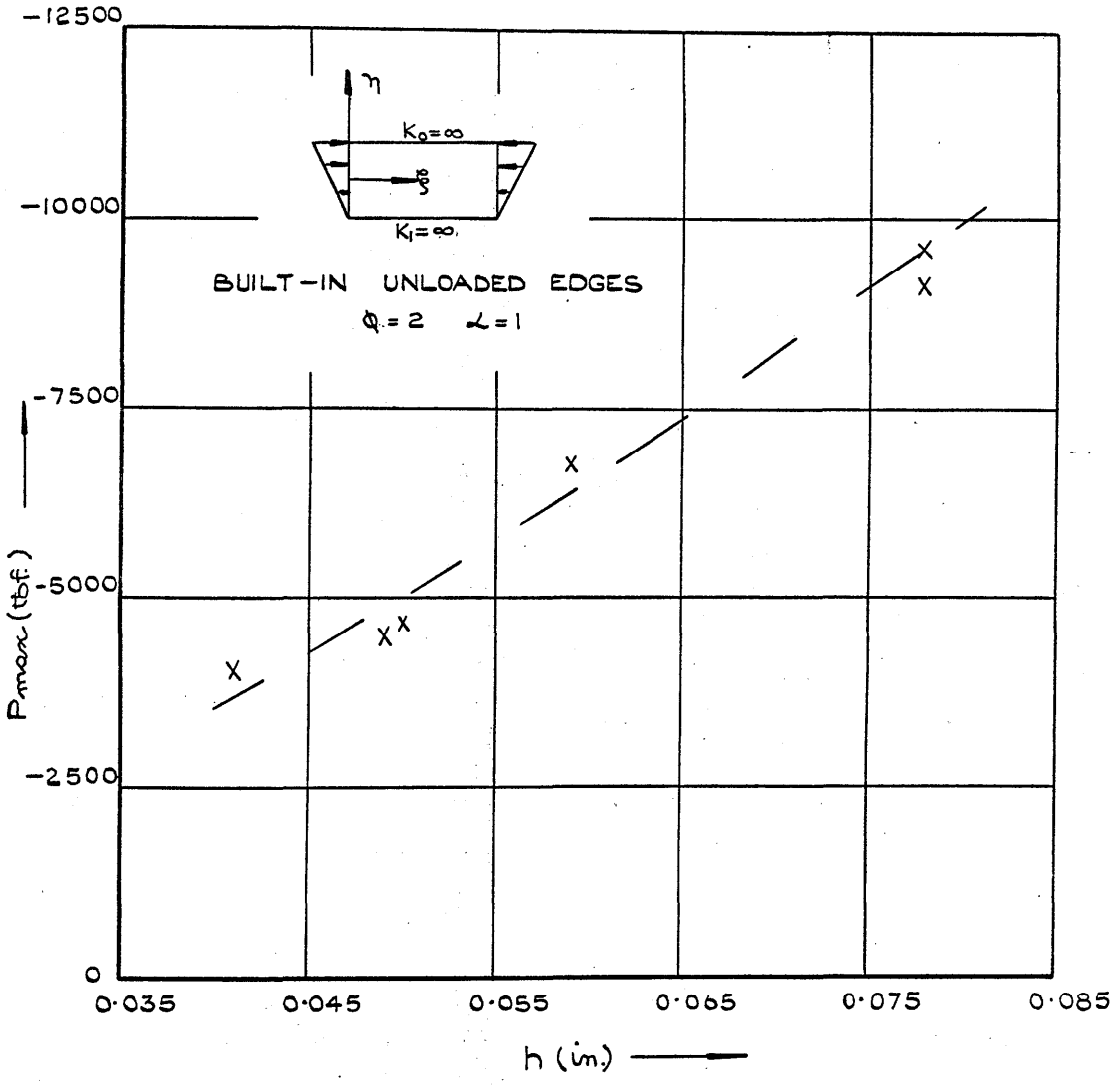

FIG. IV.17 COLLAPSE LOAD v. PLATE THICKNESS.

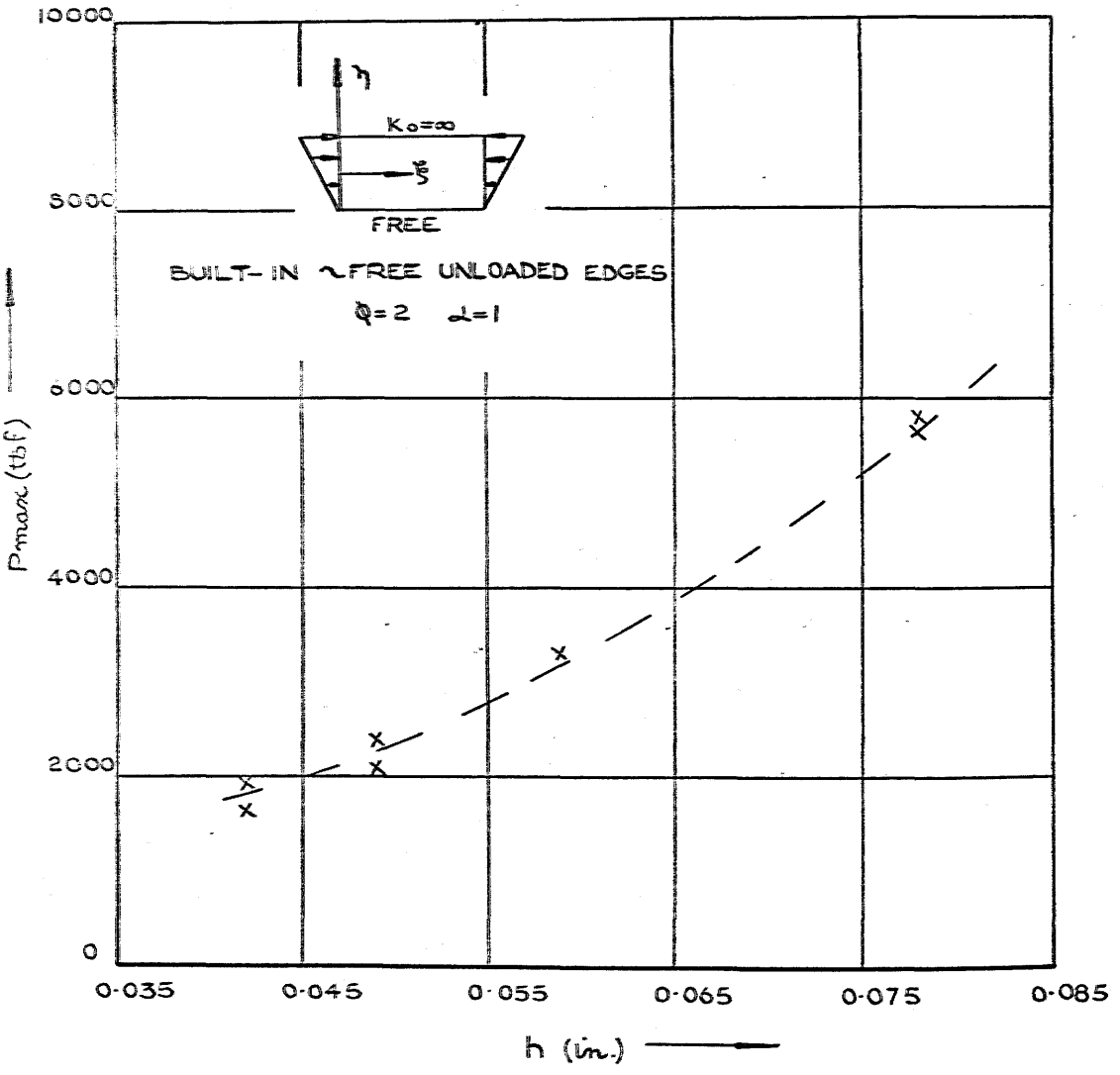

FIG. IV. 18 COLLAPSE LOAD v. PLATE THICKNESS

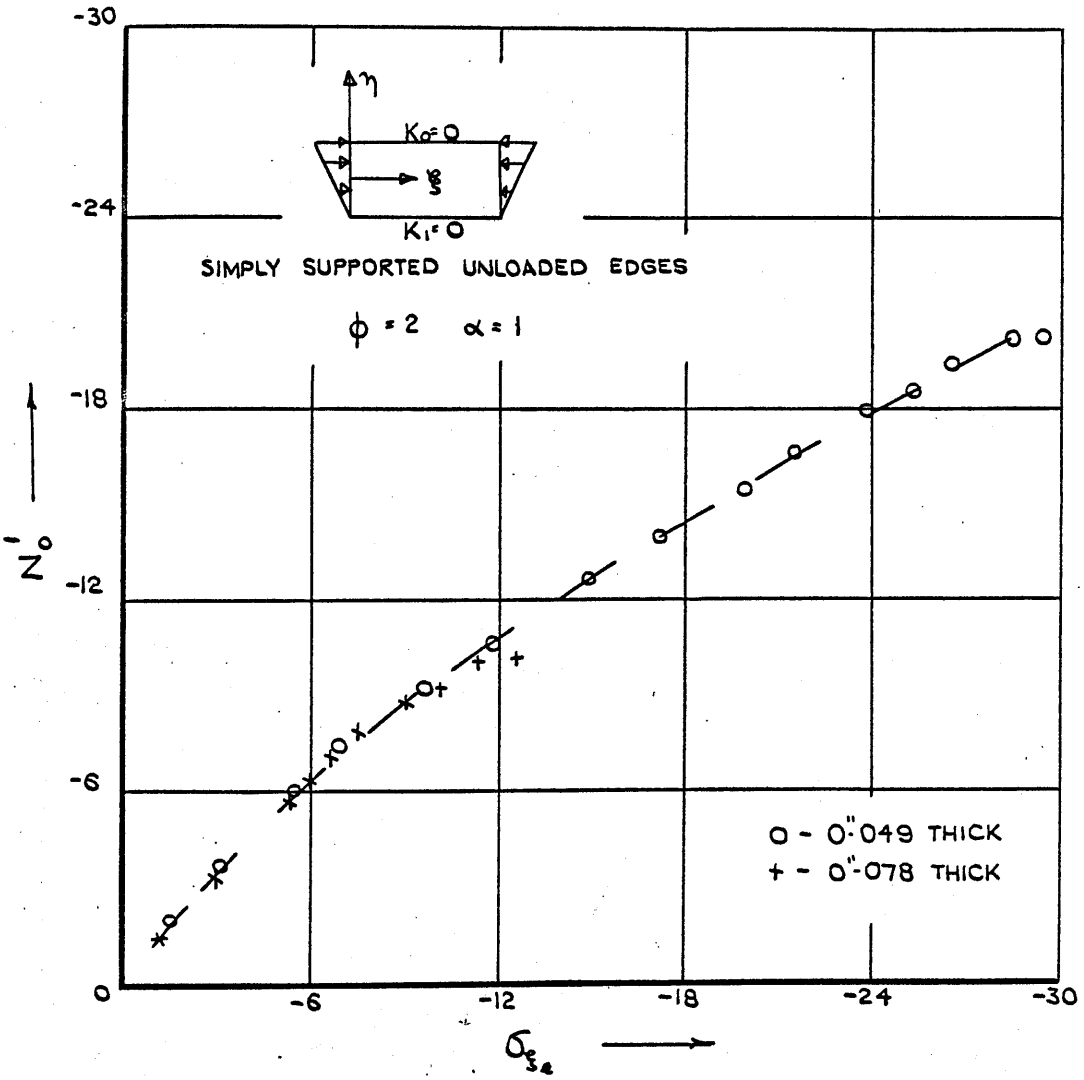

FIG. IV.19 LOAD V. EDGE STRESS.

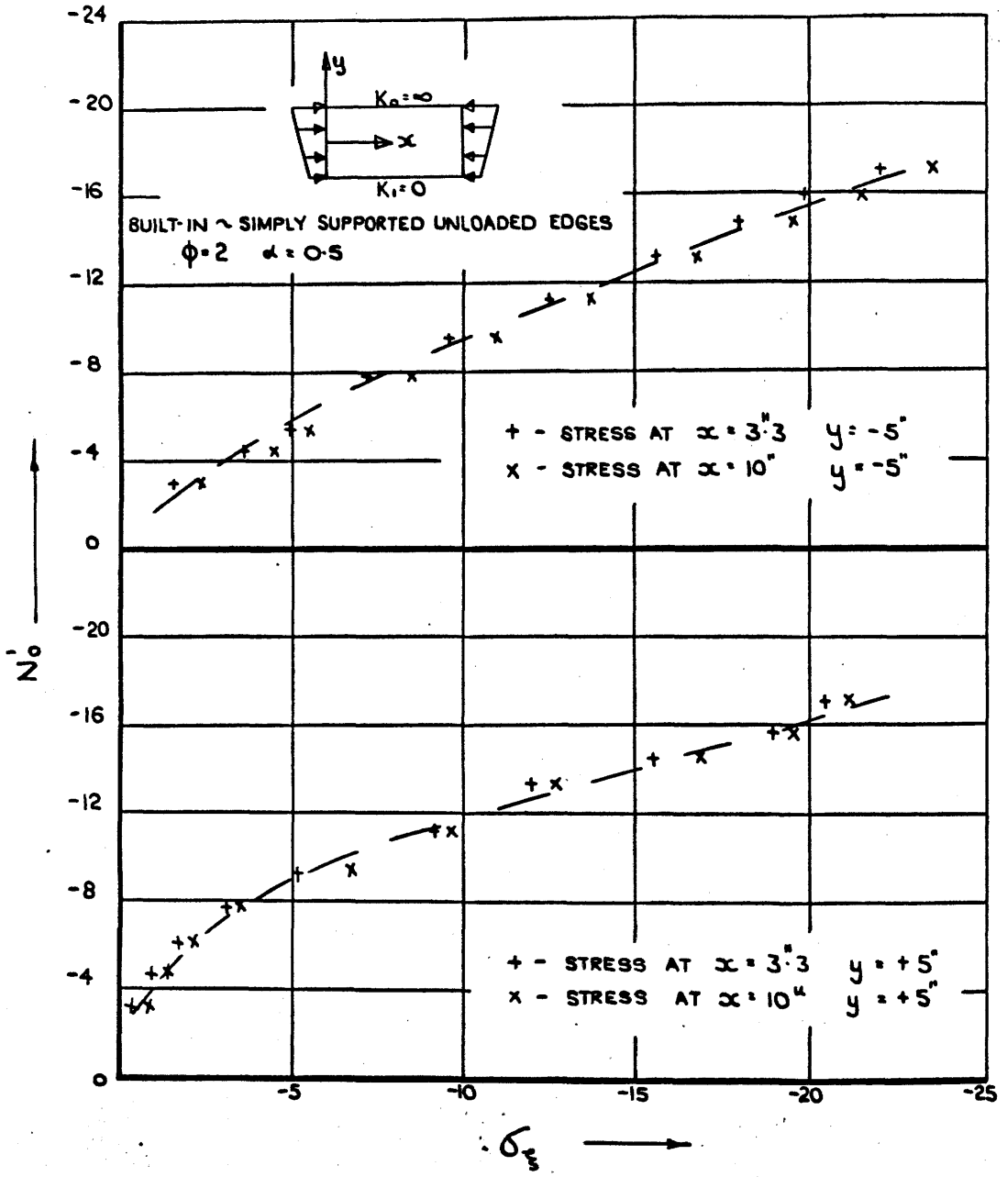

FIG. IV.20 LOAD V. EDGE STRESS

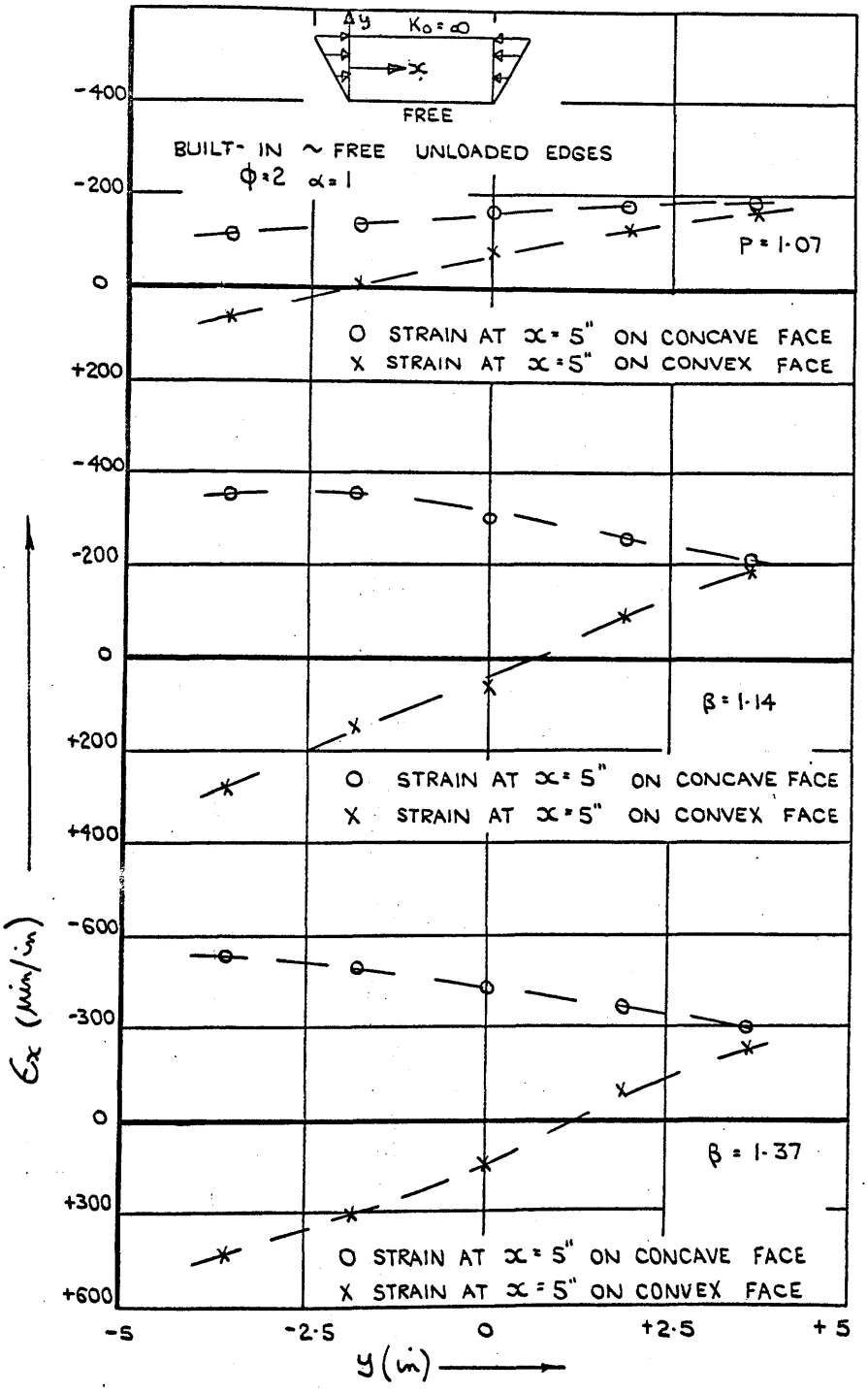

FIG. IV.21 PLATE SURFACE STRAIN V. PLATE WIDTH.

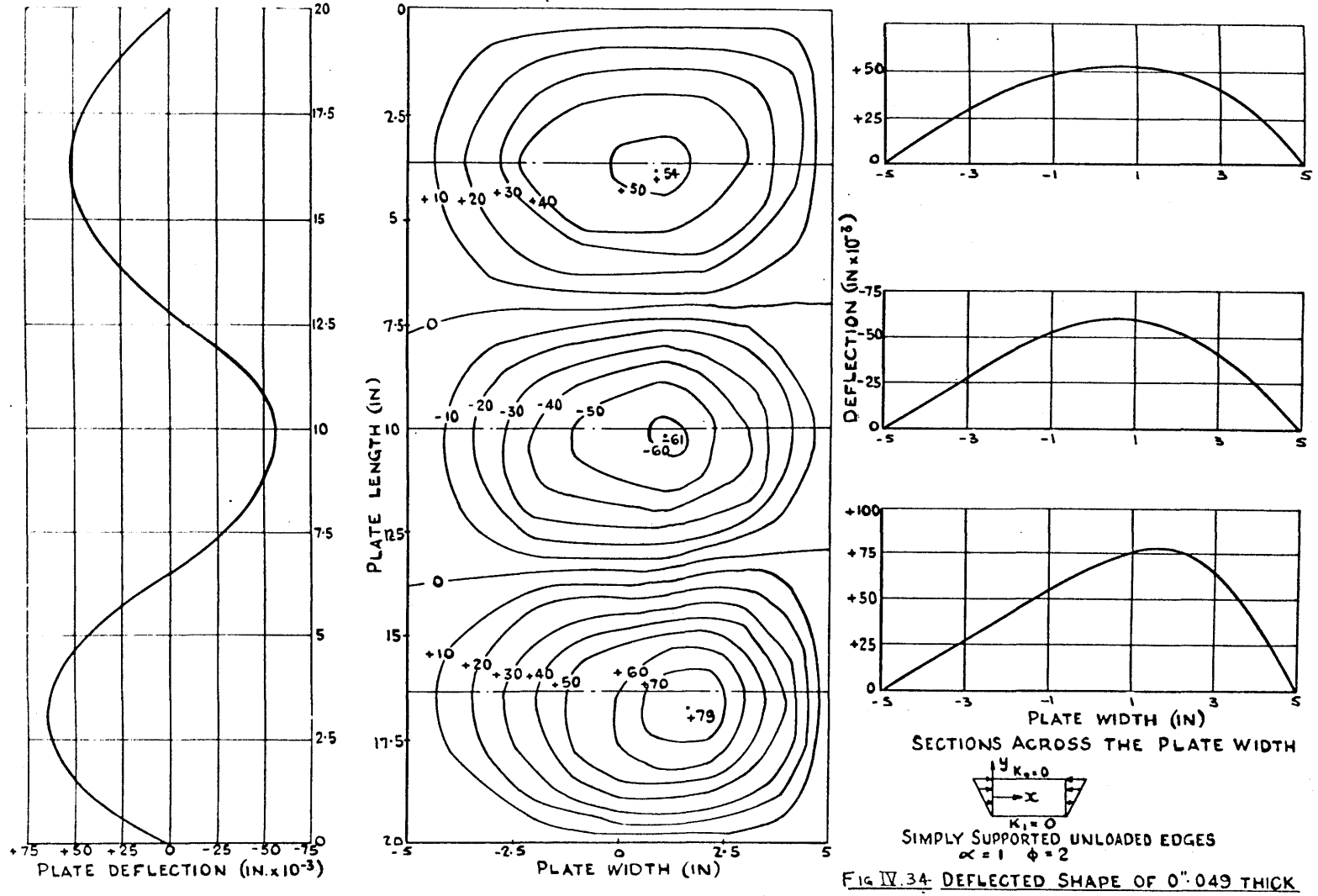

LONGITUDINAL SECTION THROUGH PLATE AT $y=0$"

FIG IV.34 DEFLECTED SHAPE OF 0".049 THICK PLATE AT A LOAD OF 2520 lb f.

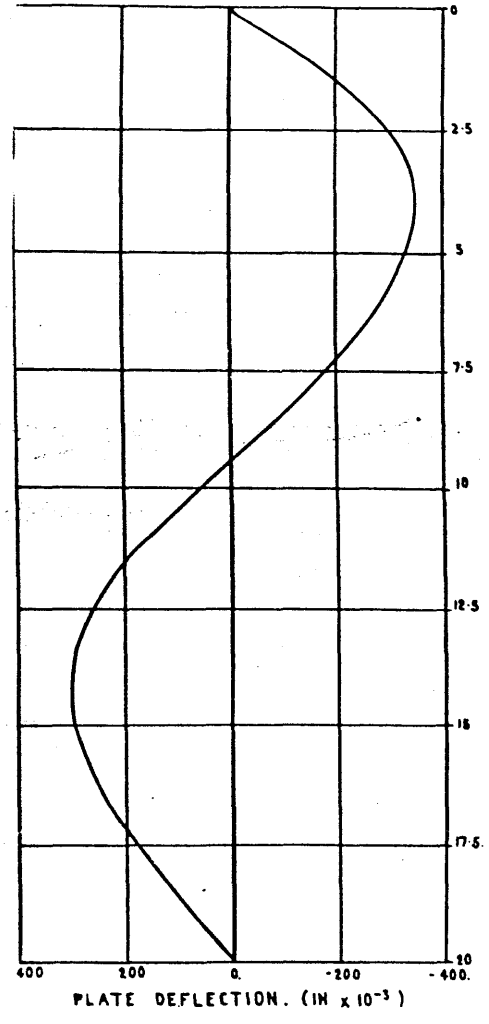

LONGITUDINAL SECTION THROUGH PLATE AT $y = -5"$

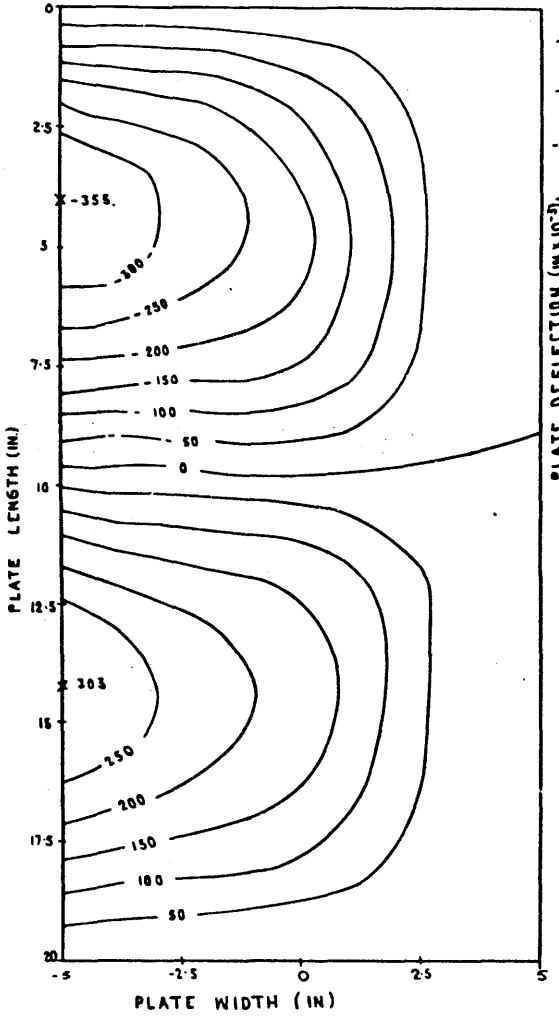

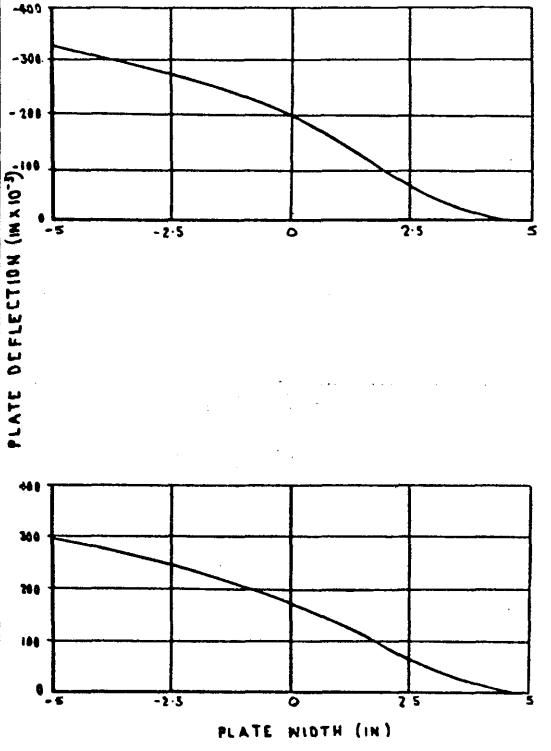

SECTIONS ACCROSS THE PLATE WIDTH.

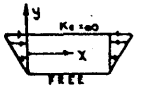

BUILT-IN ~ FREE UNLOADED EDGES.
$\alpha = 1 \quad \beta = 2$

FIG. IV.35a

DEFLECTED SHAPE OF 0".049 THICK PLATE AT A LOAD OF 2180 LB f.

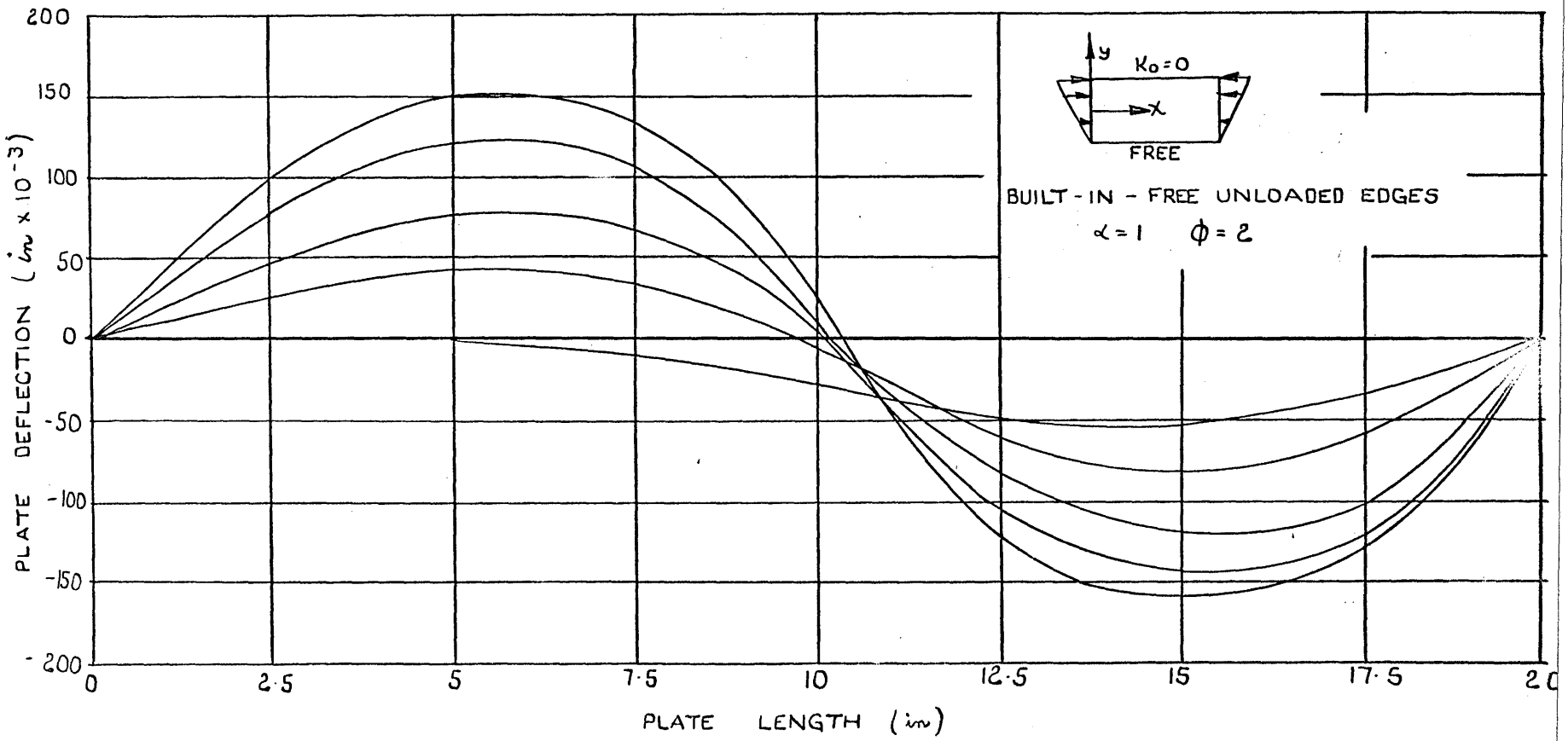

FIG. IV.35b SECTION THROUGH A 0"049 THICK PLATE AT VARIOUS LOADS.

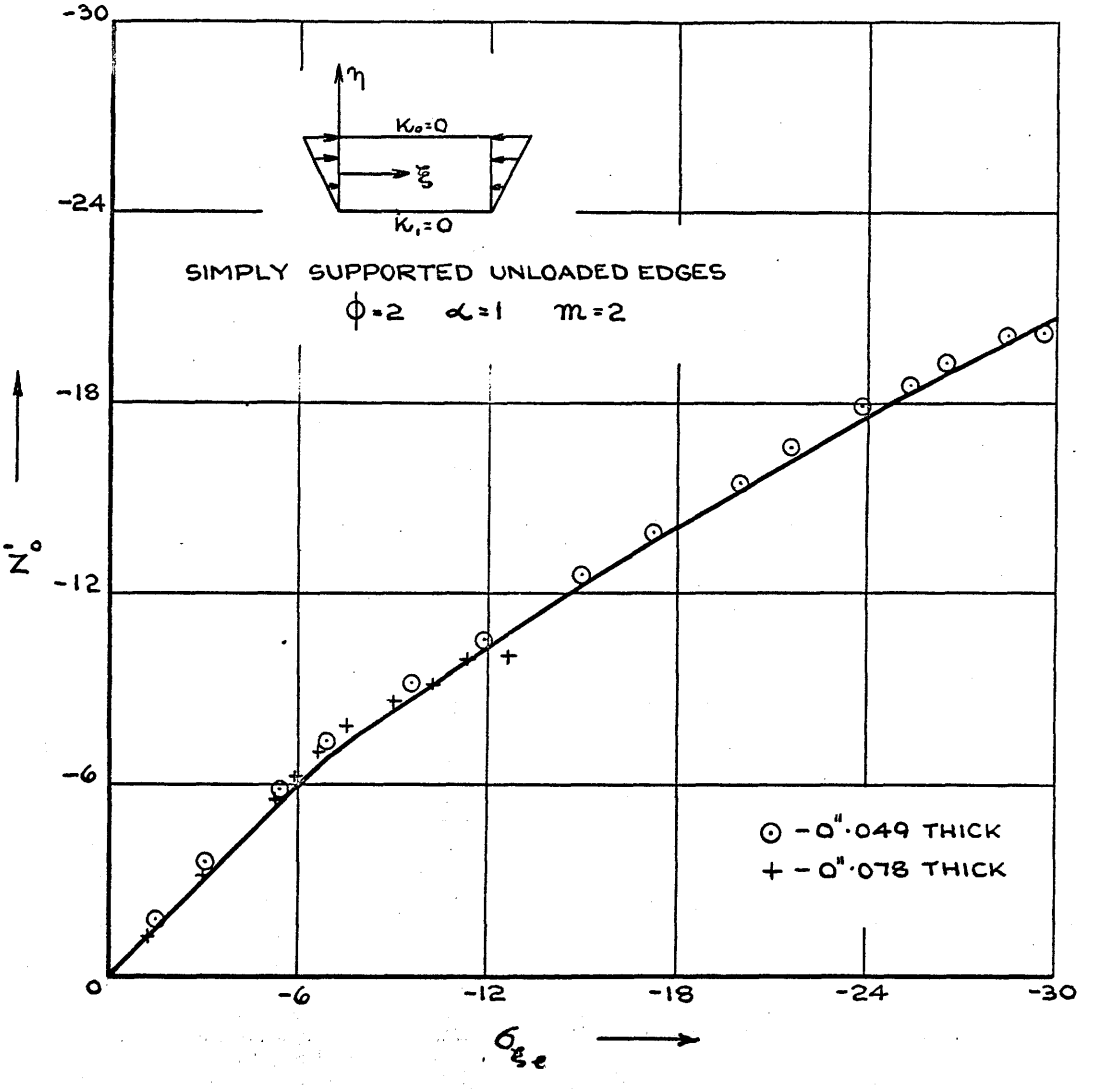

FIG. V.1 LOAD V. EDGE STRESS

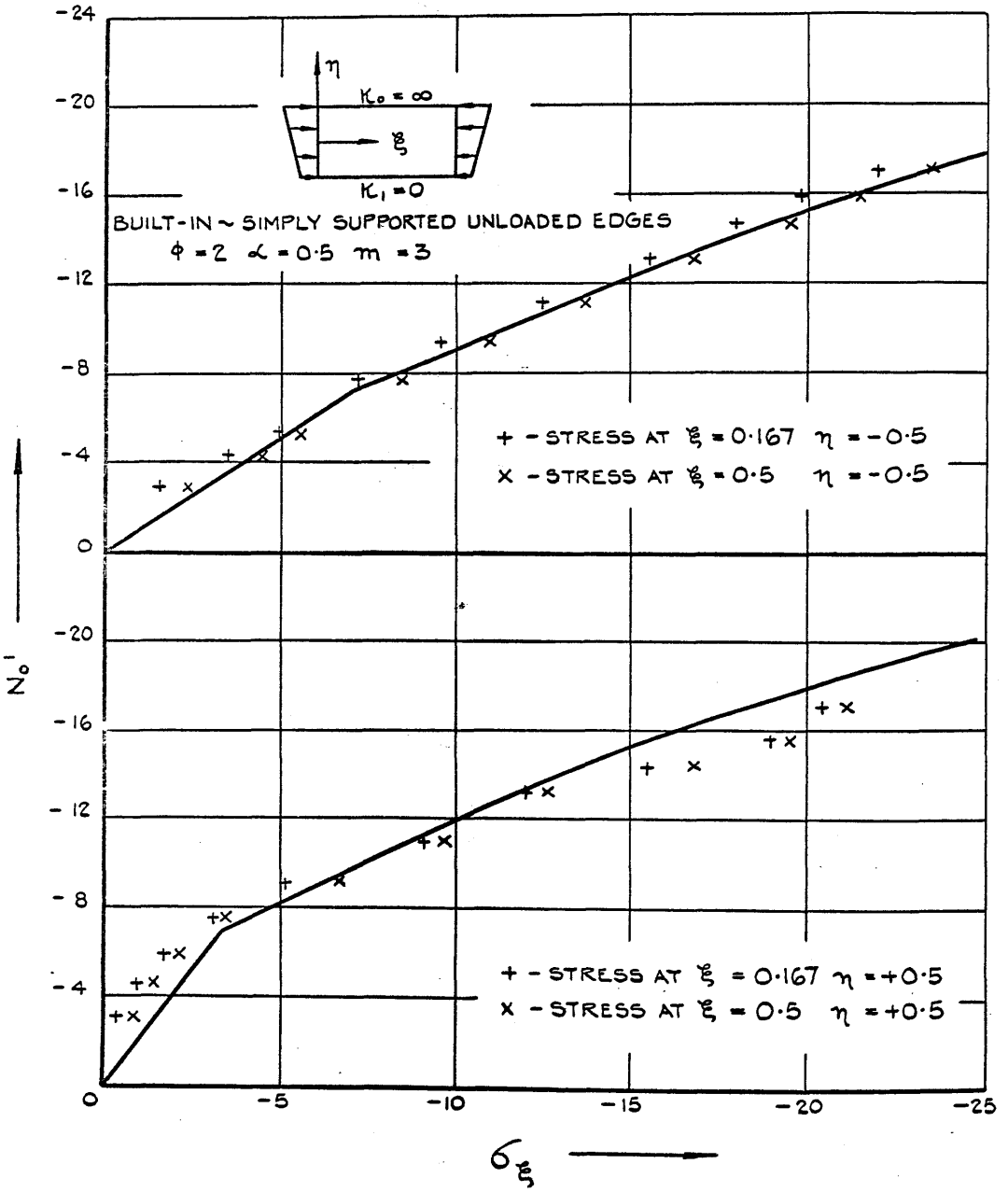

FIG. V.2 LOAD V. EDGE STRESS.

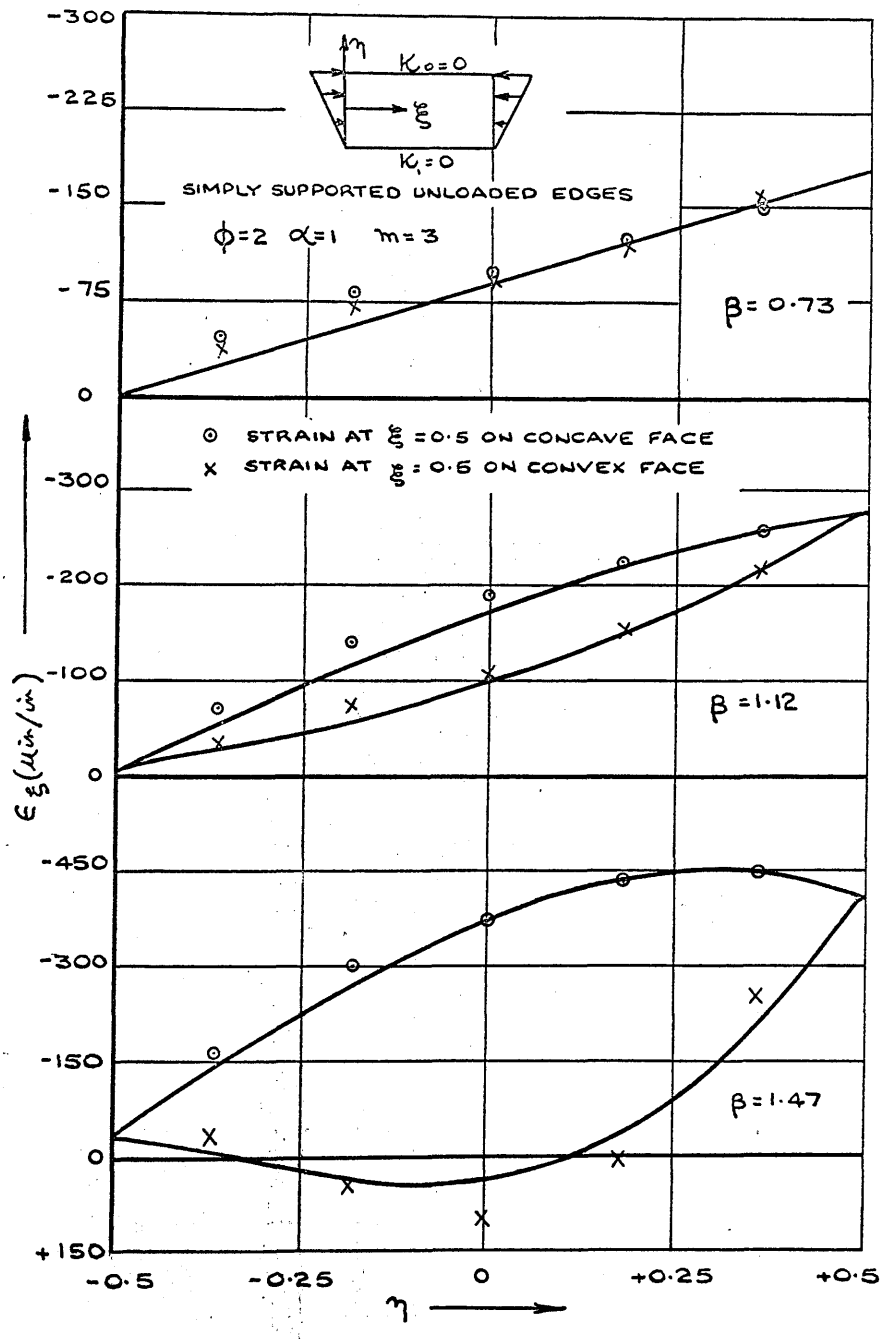

FIG. V.3 PLATE SURFACE STRAIN V. PLATE WIDTH

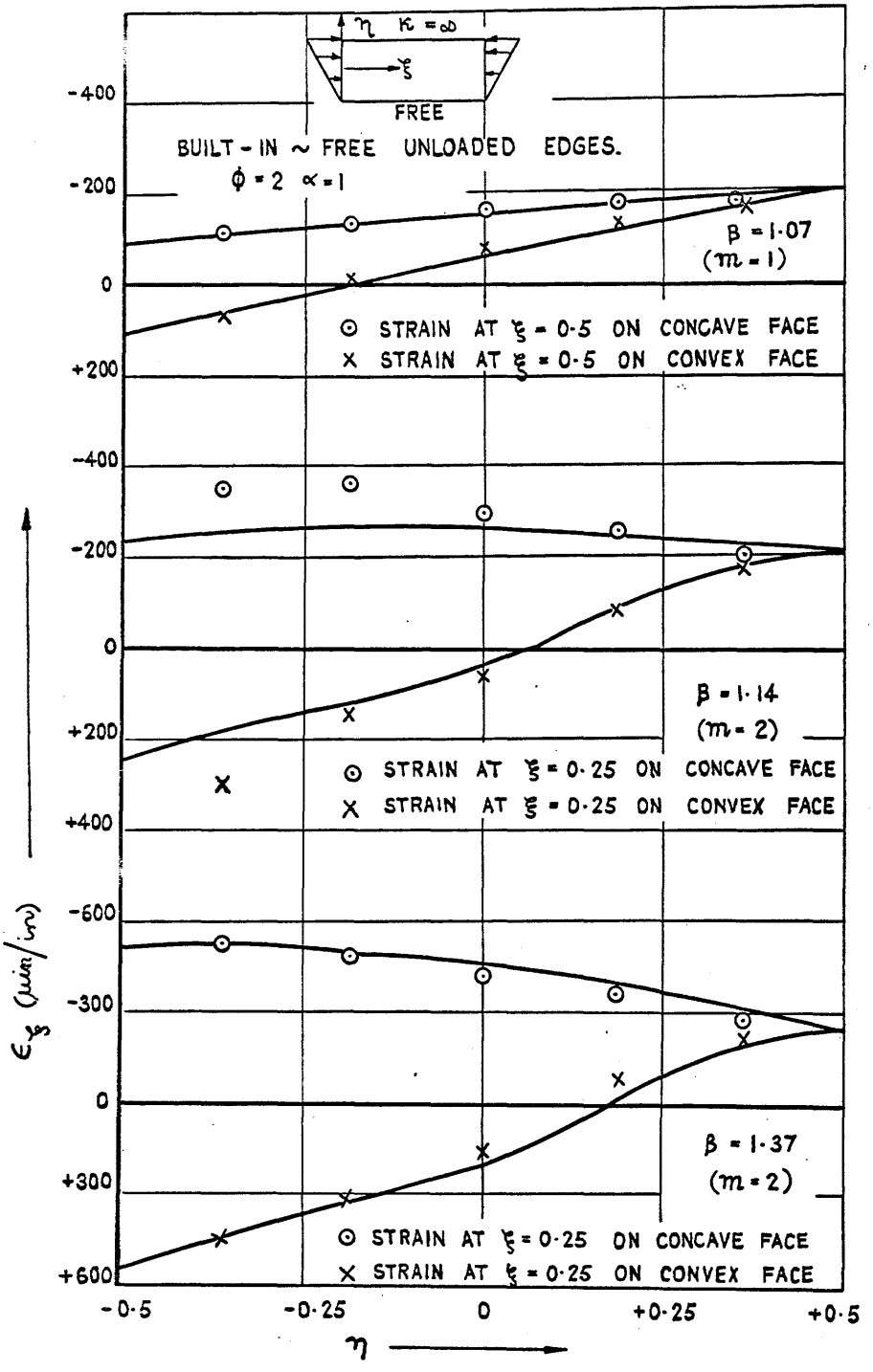

FIG. V.4- PLATE SURFACE STRAIN V. PLATE WIDTH.

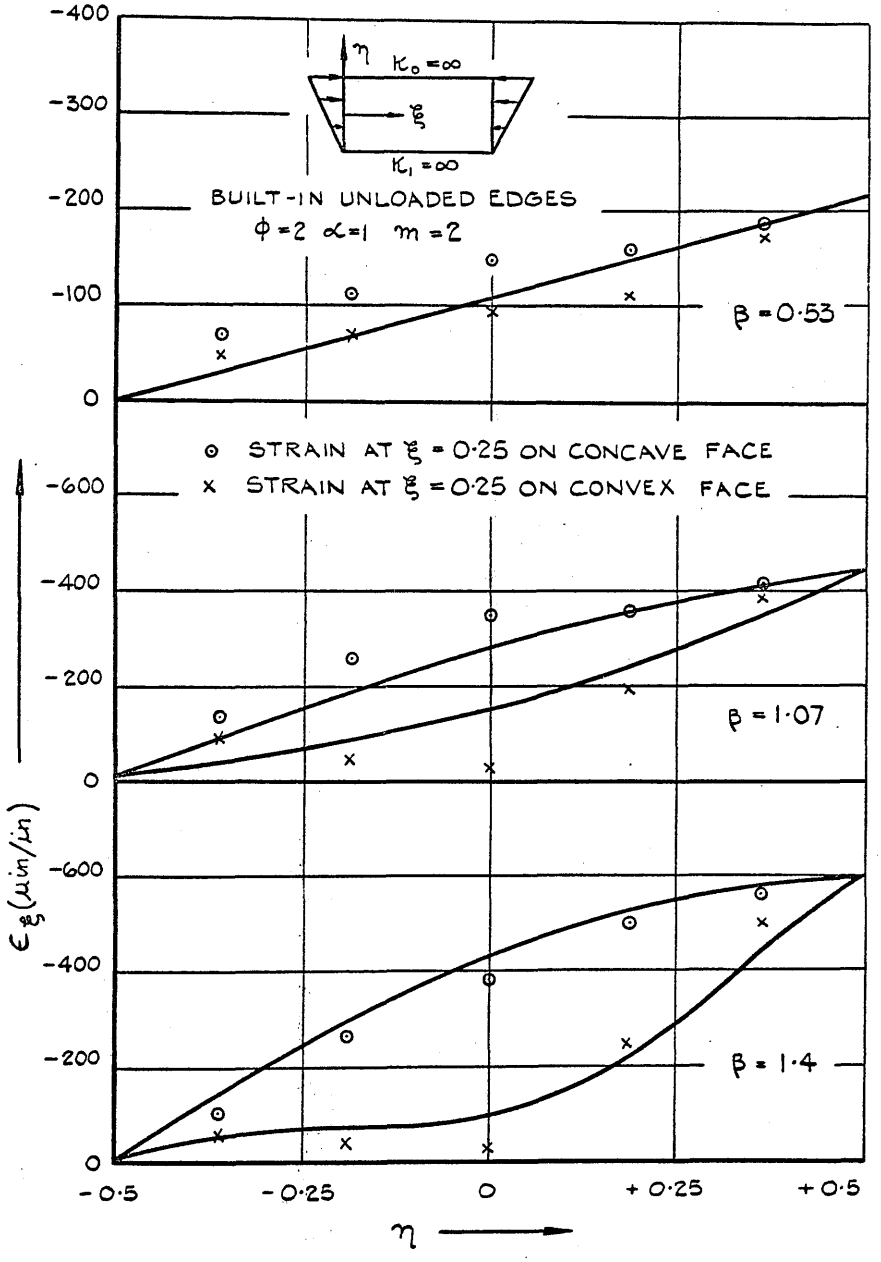

FIG. V.5 PLATE SURFACE STRAIN V. PLATE WIDTH.

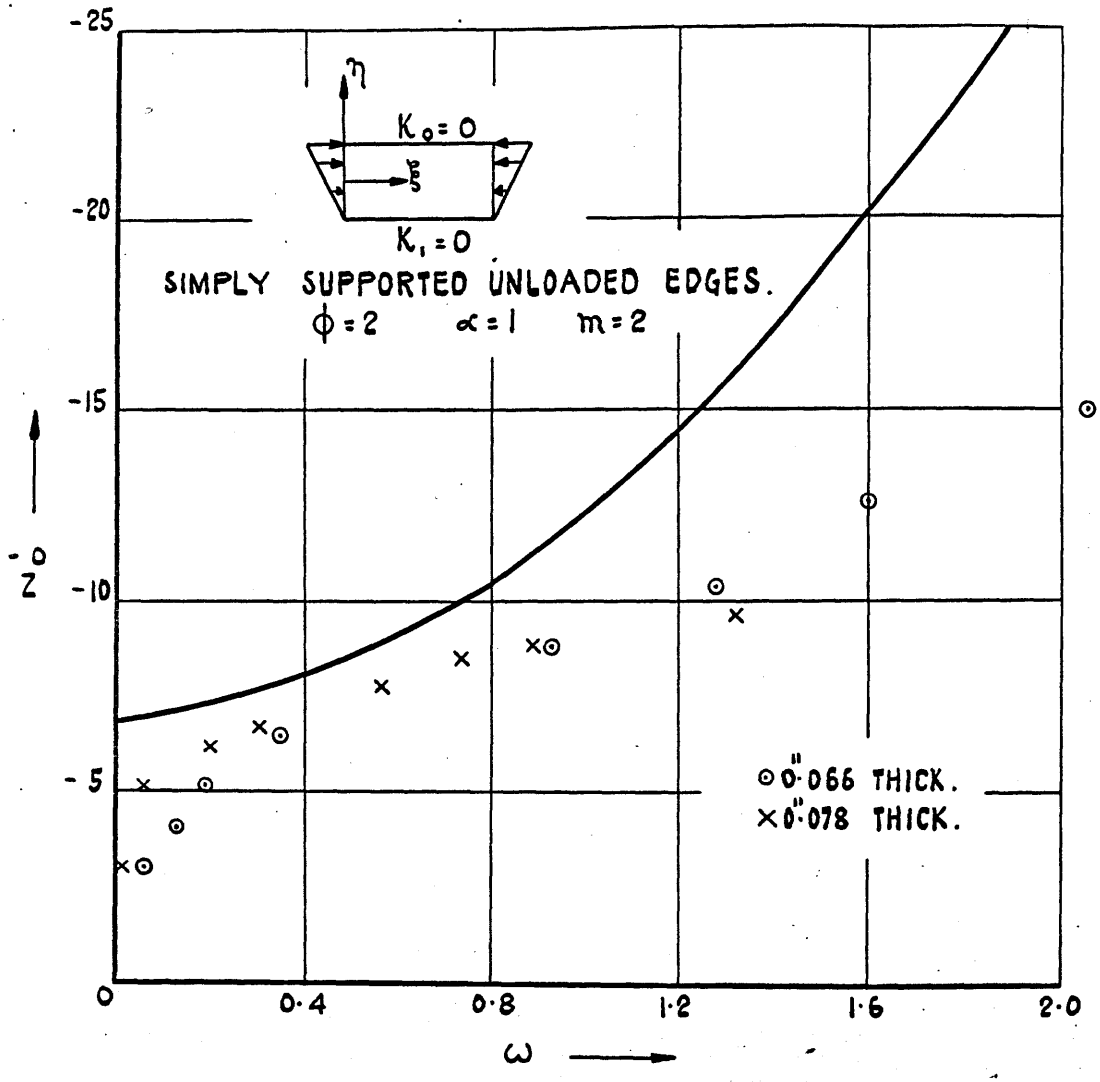

FIG. V.6 LOAD V. DEFLECTION.

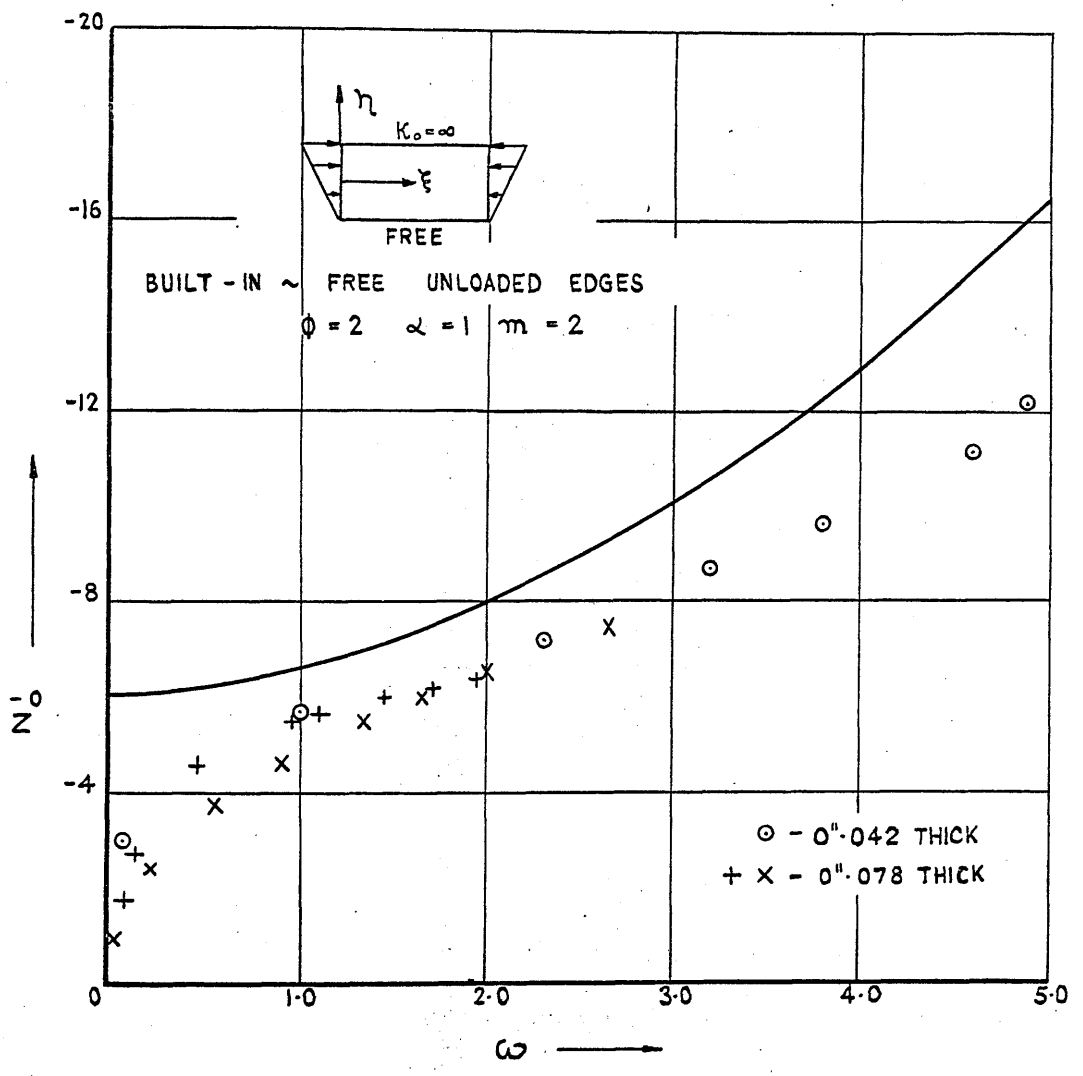

FIG.V.7 LOAD V. DEFLECTION.

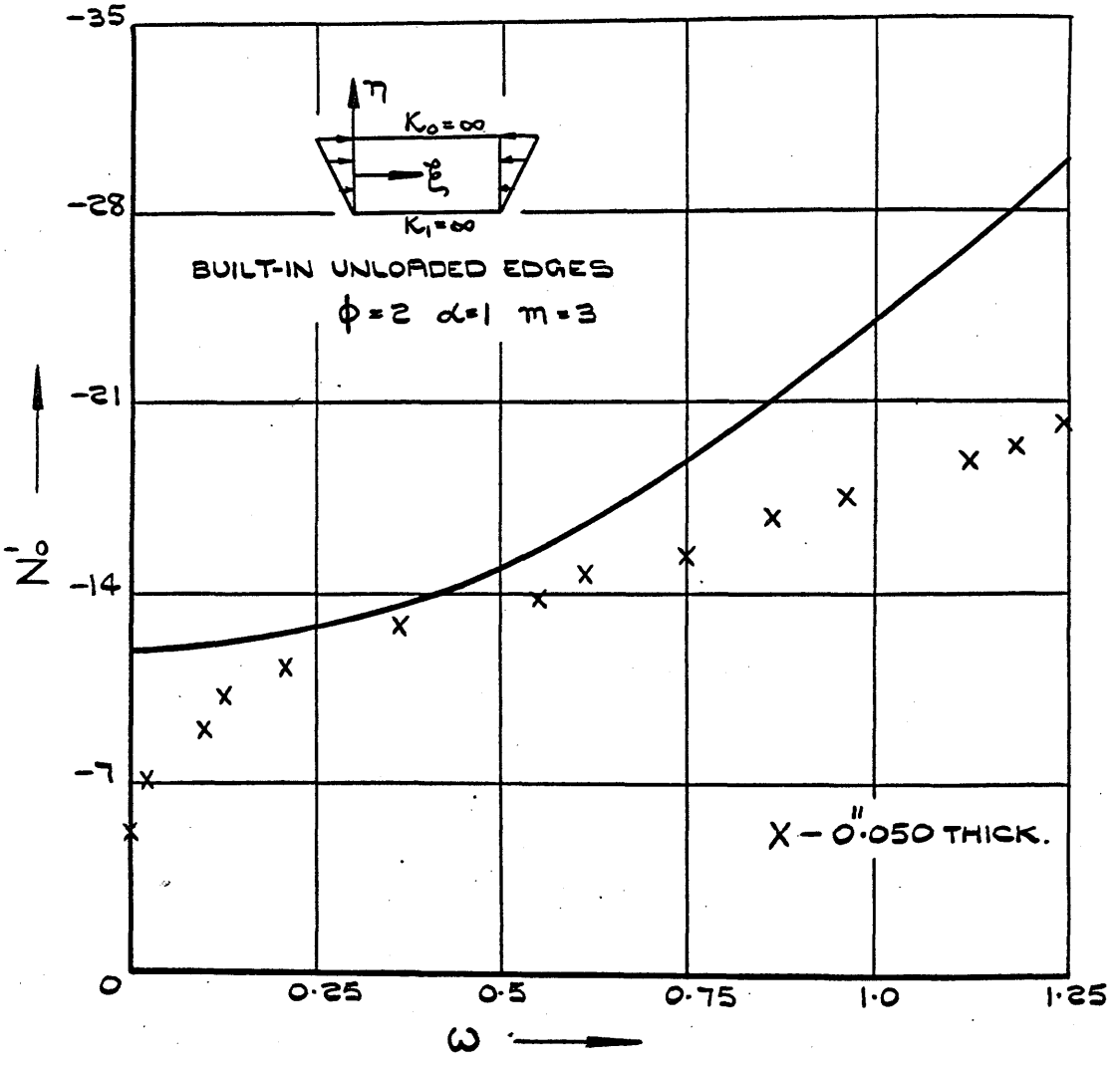

FIG. V.8 LOAD V. DEFLECTION.

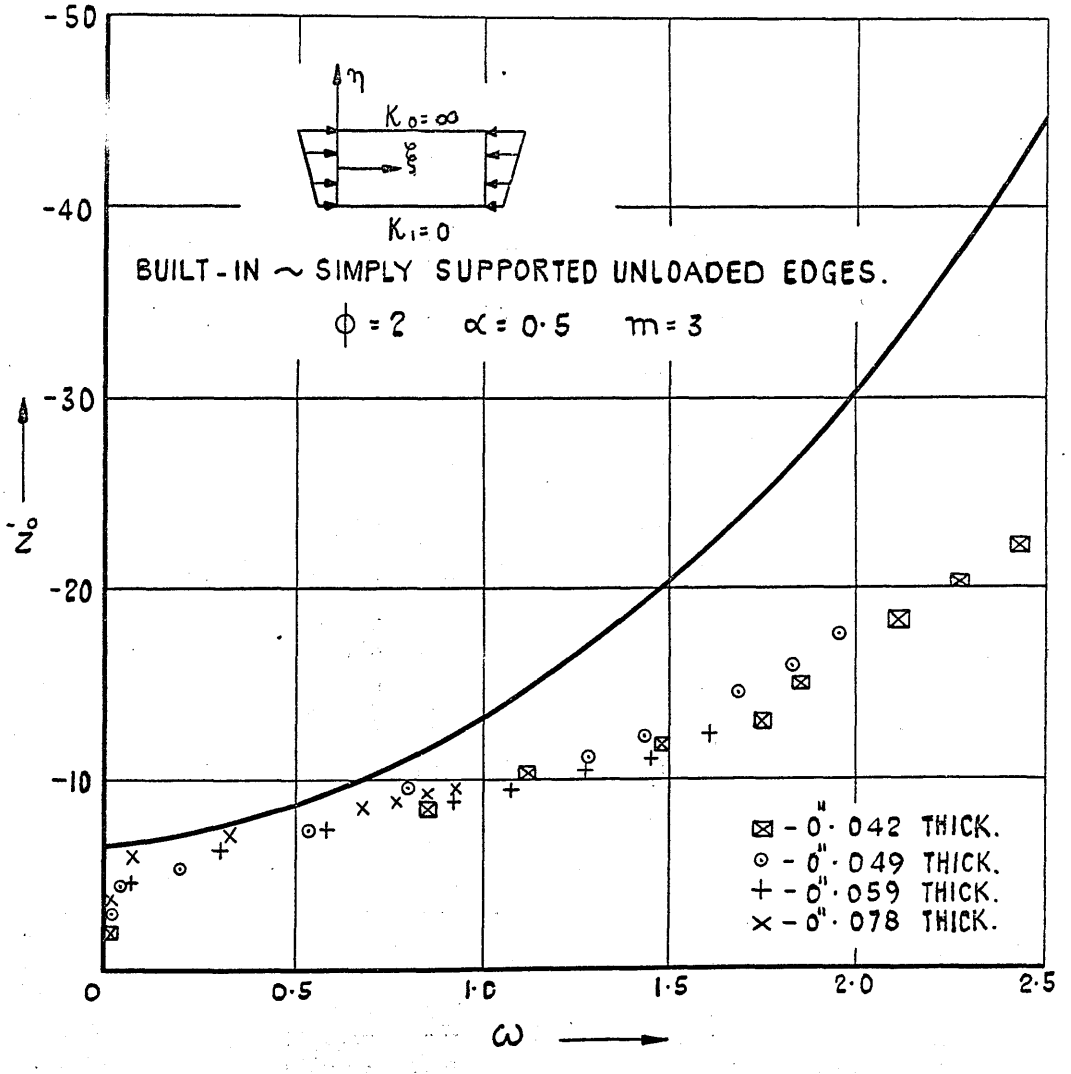

FIG. V.9 LOAD V. DEFLECTION.

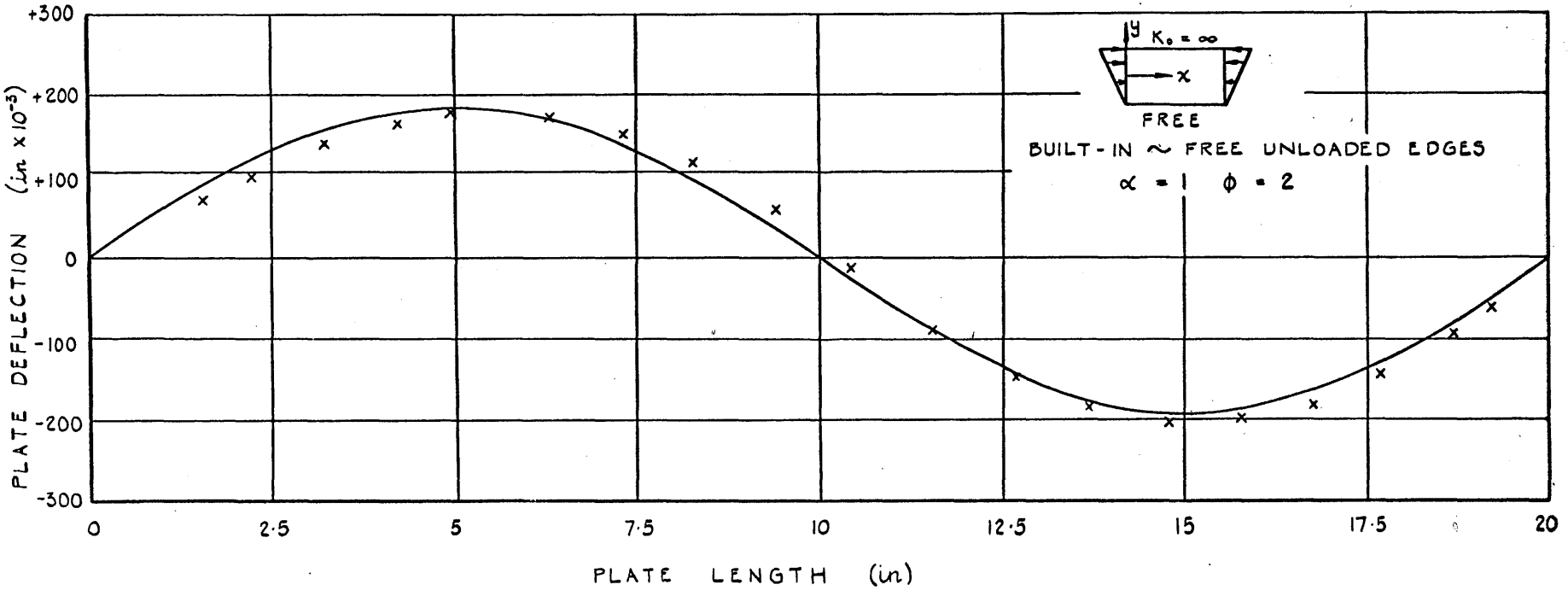

FIG. V.10 SECTION THROUGH 0"·049 THICK PLATE AT y = 0.

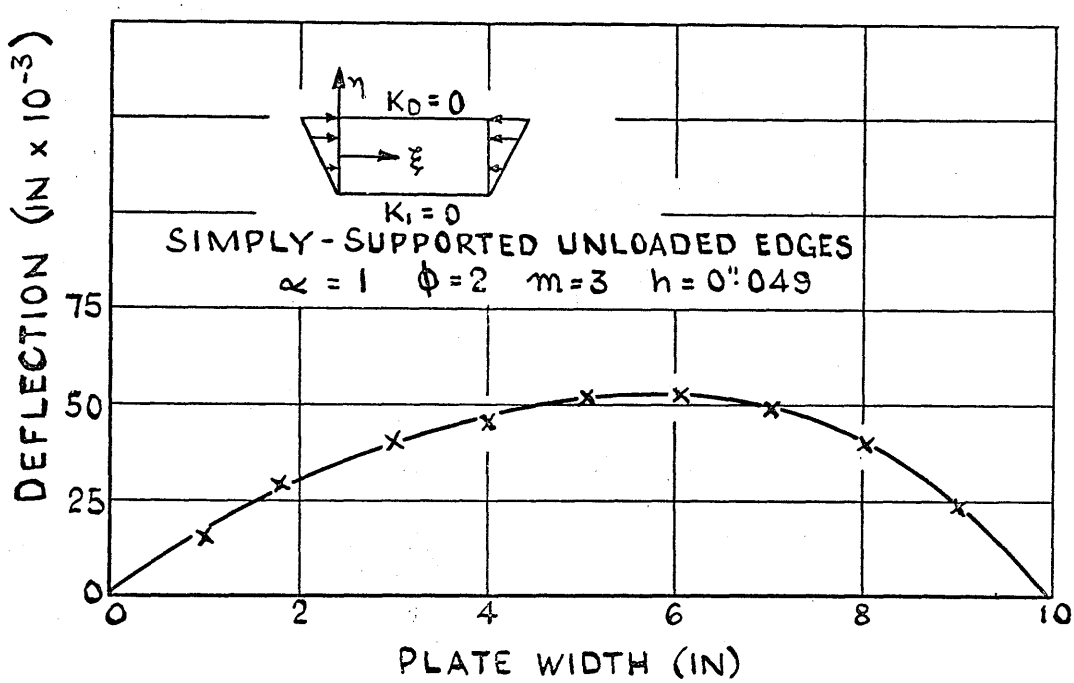

FIG. V.11 DEFLECTED SHAPE ACROSS THE PLATE AT THE CREST OF A BUCKLE.

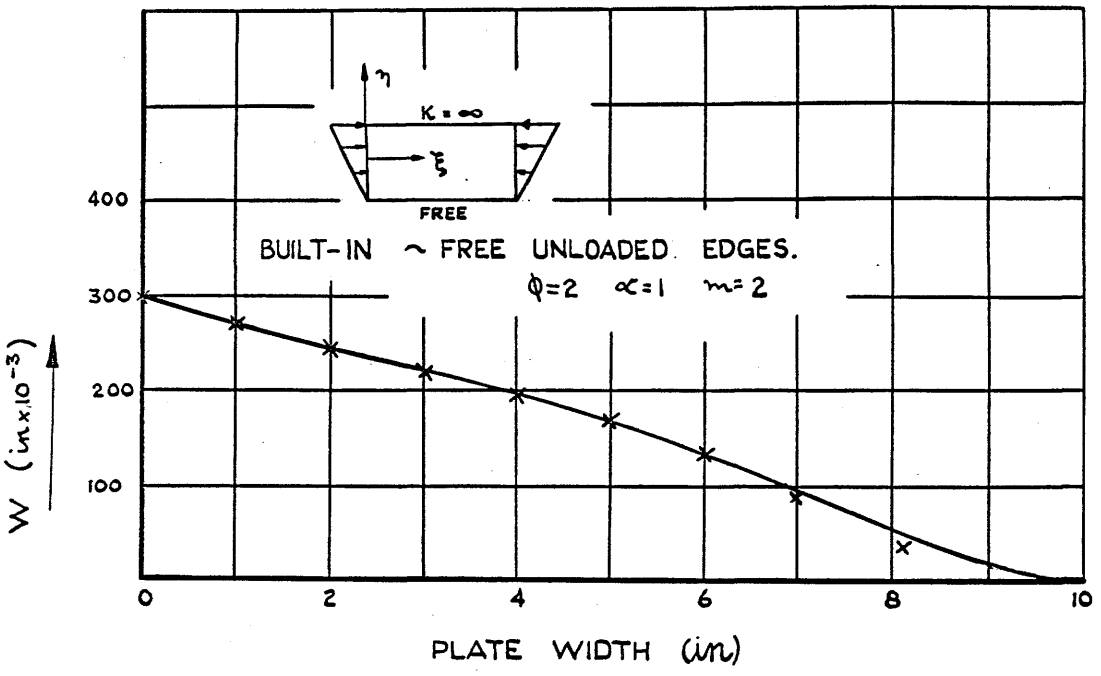

FIG. V.12 COMPARISON OF THEORETICAL AND EXPERIMENTAL DEFLECTION DISTRIBUTION ACROSS THE PLATE AT THE CREST OF A BUCKLE.

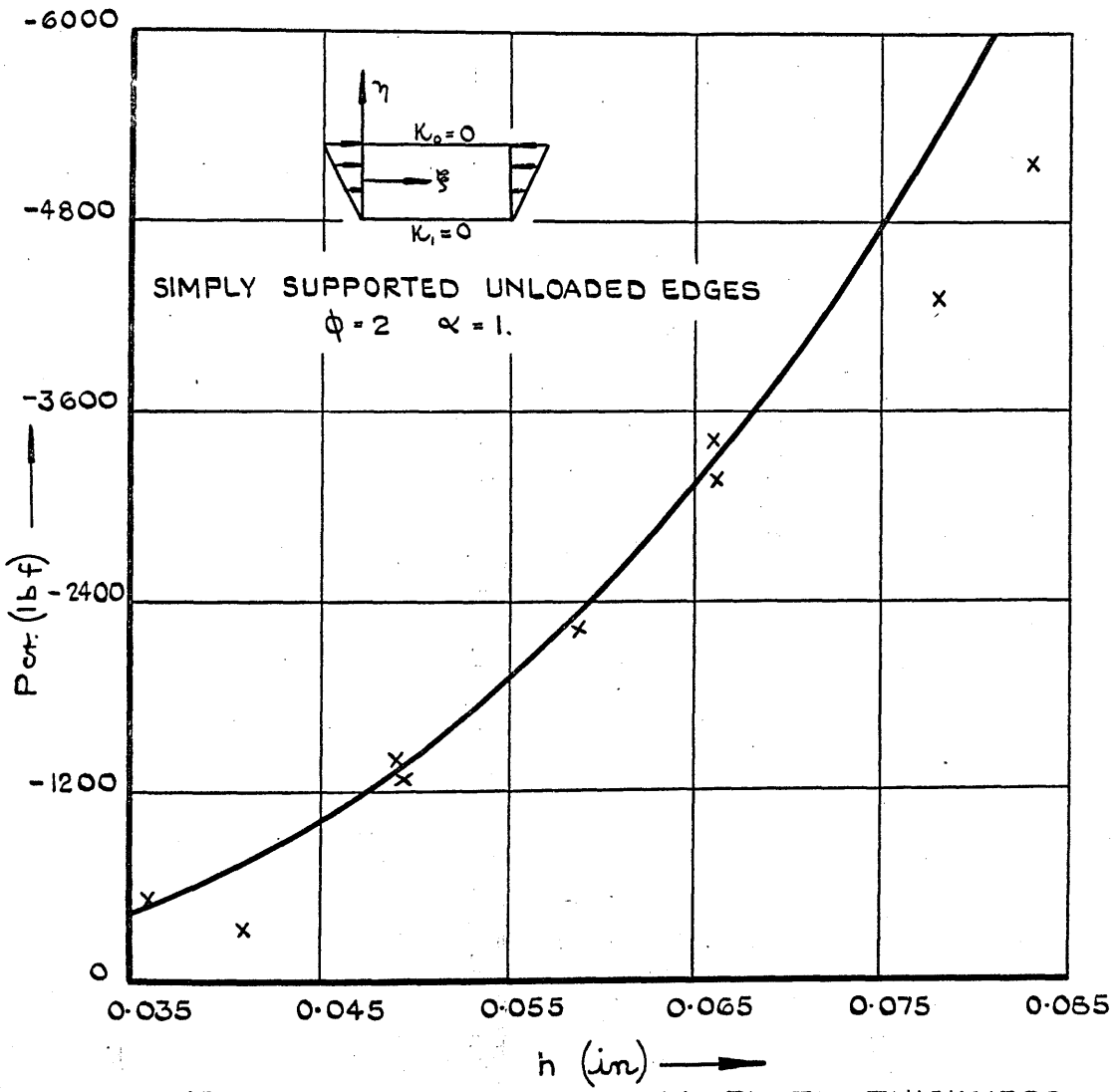

FIG. V.13 INSTABILITY LOAD V. PLATE THICKNESS.

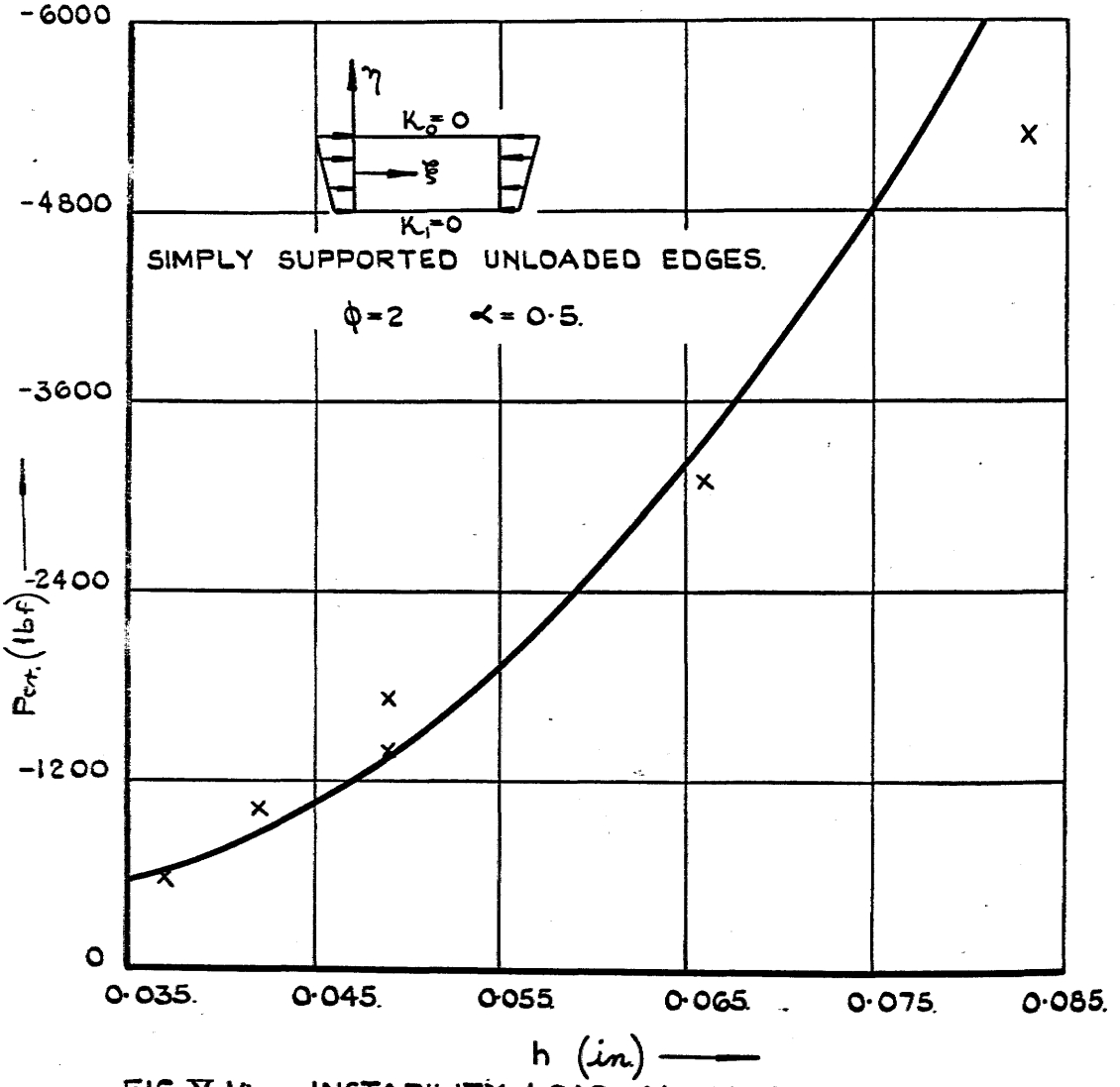

FIG. V.14 INSTABILITY LOAD V PLATE THICKNESS.

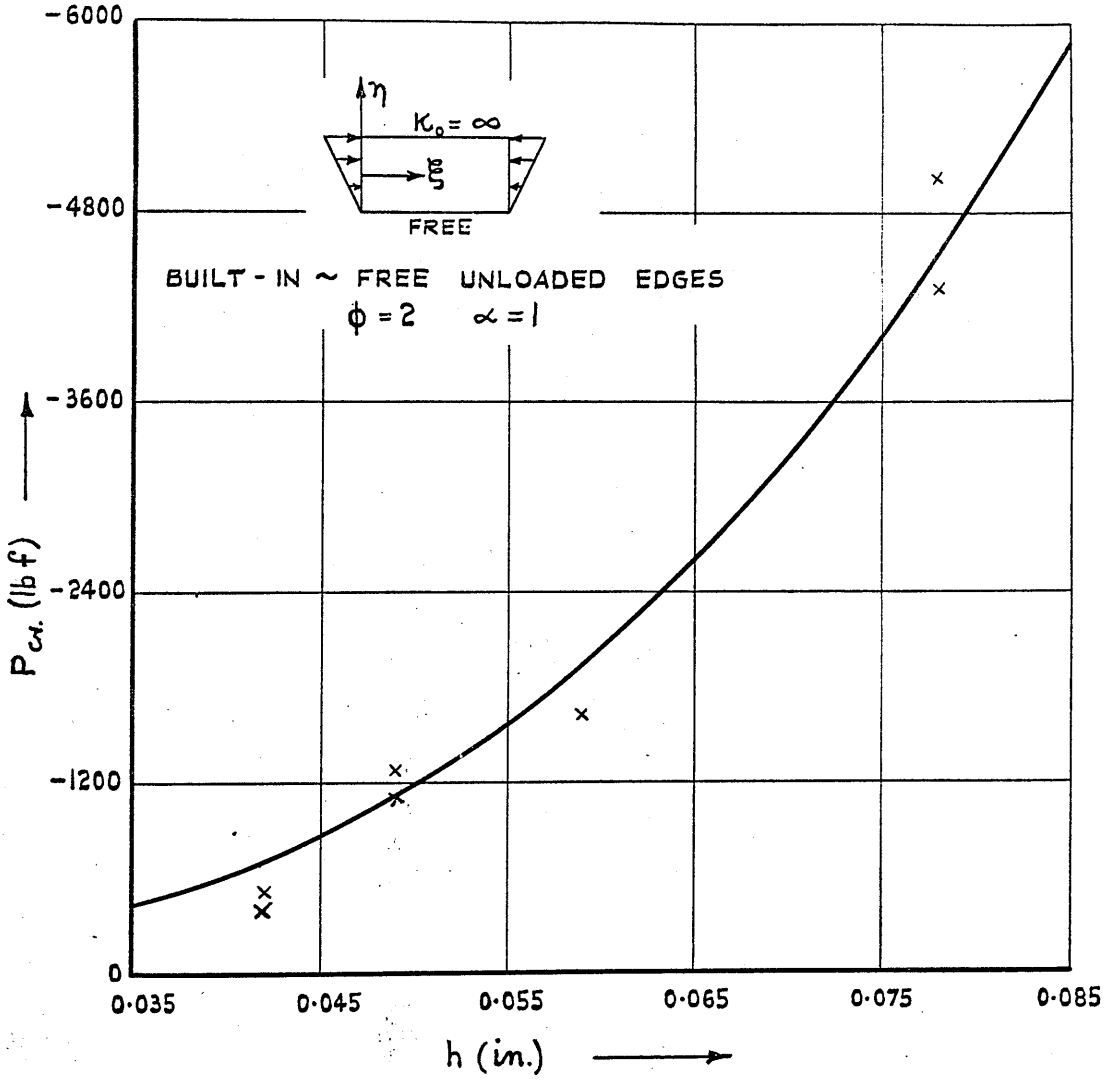

FIG. V. 15 INSTABILITY LOAD V. PLATE THICKNESS.

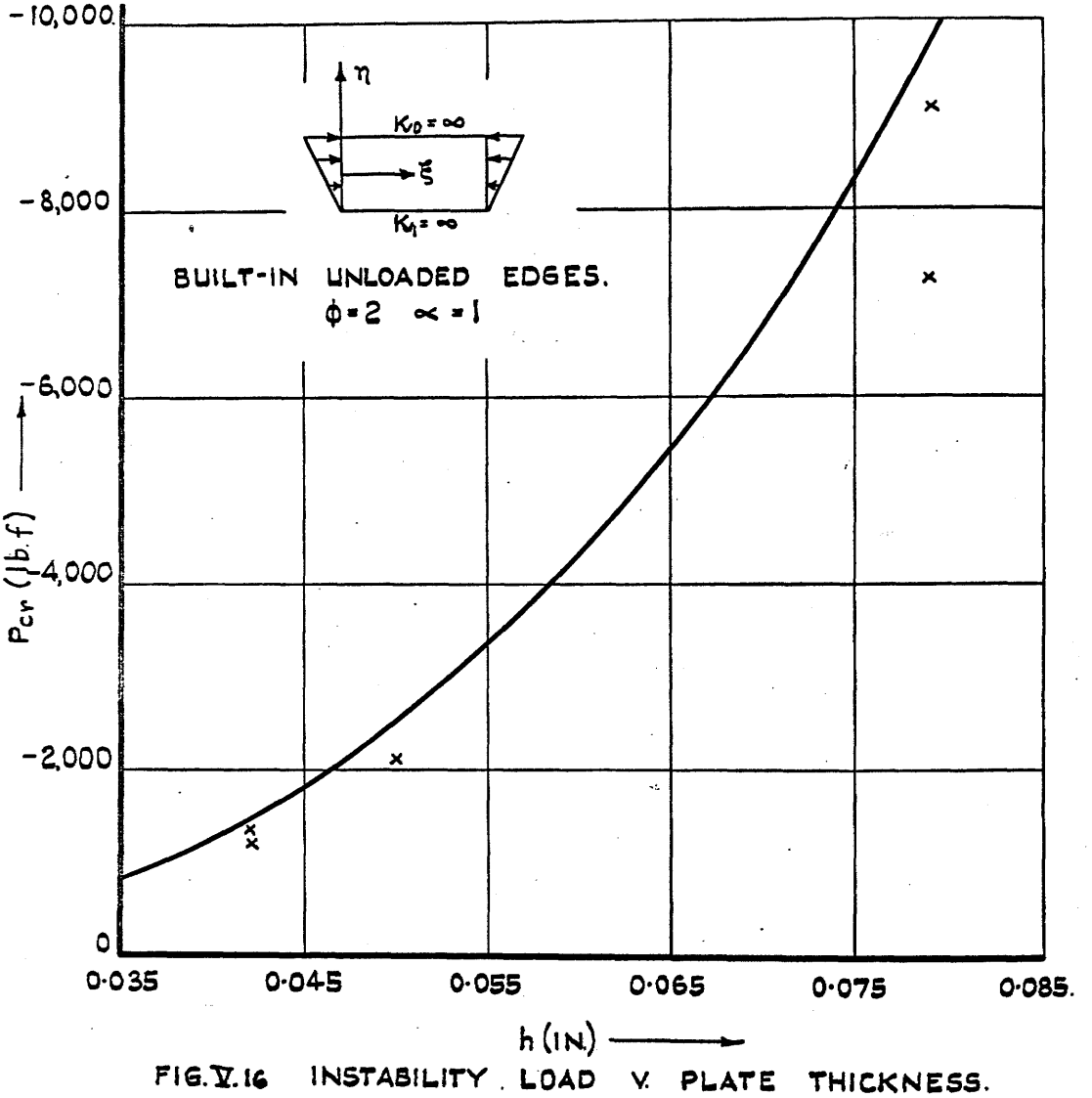

FIG. V. 16 INSTABILITY LOAD V. PLATE THICKNESS.

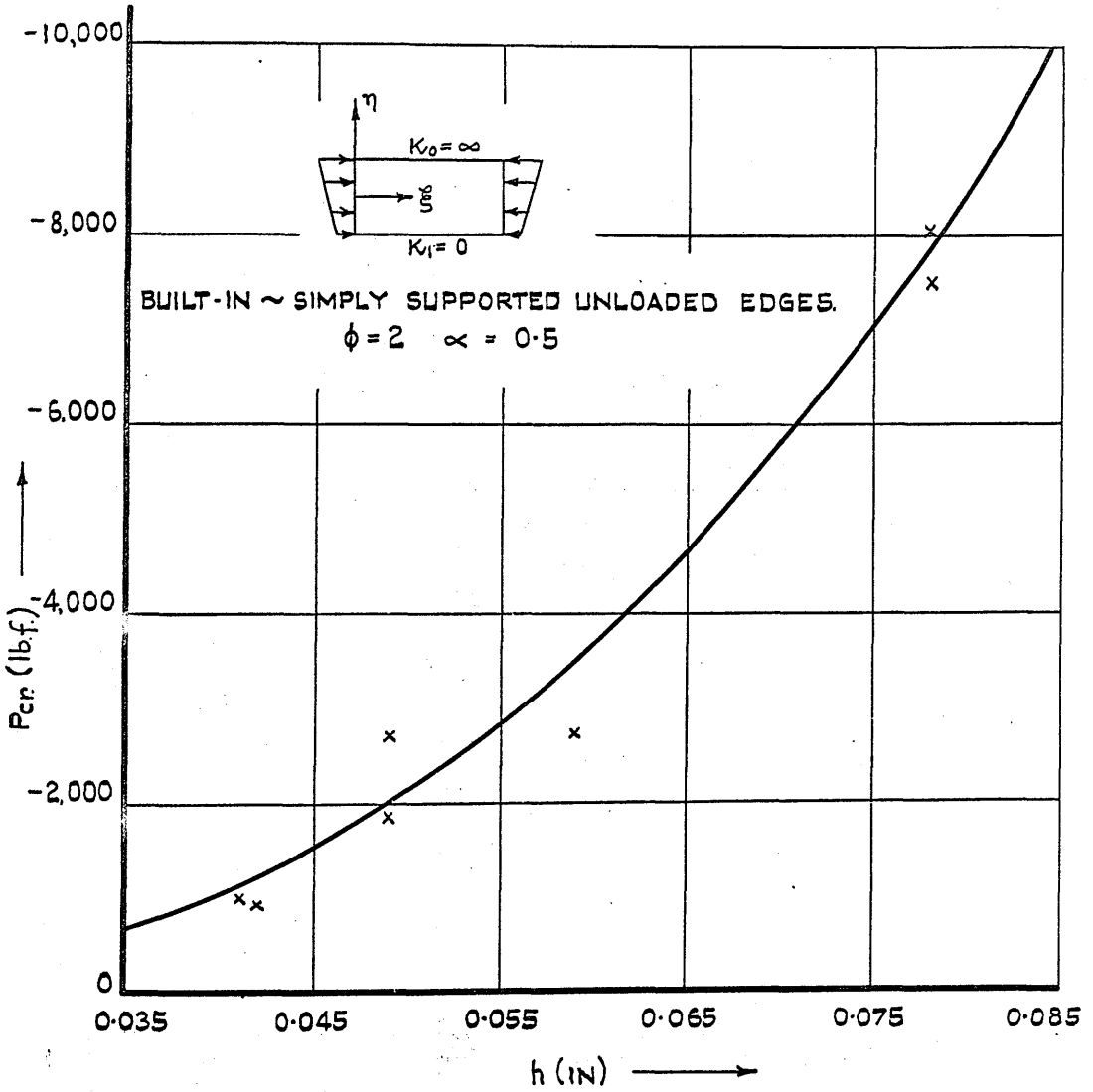

FIG. V.17 INSTABILITY LOAD V. PLATE THICKNESS.

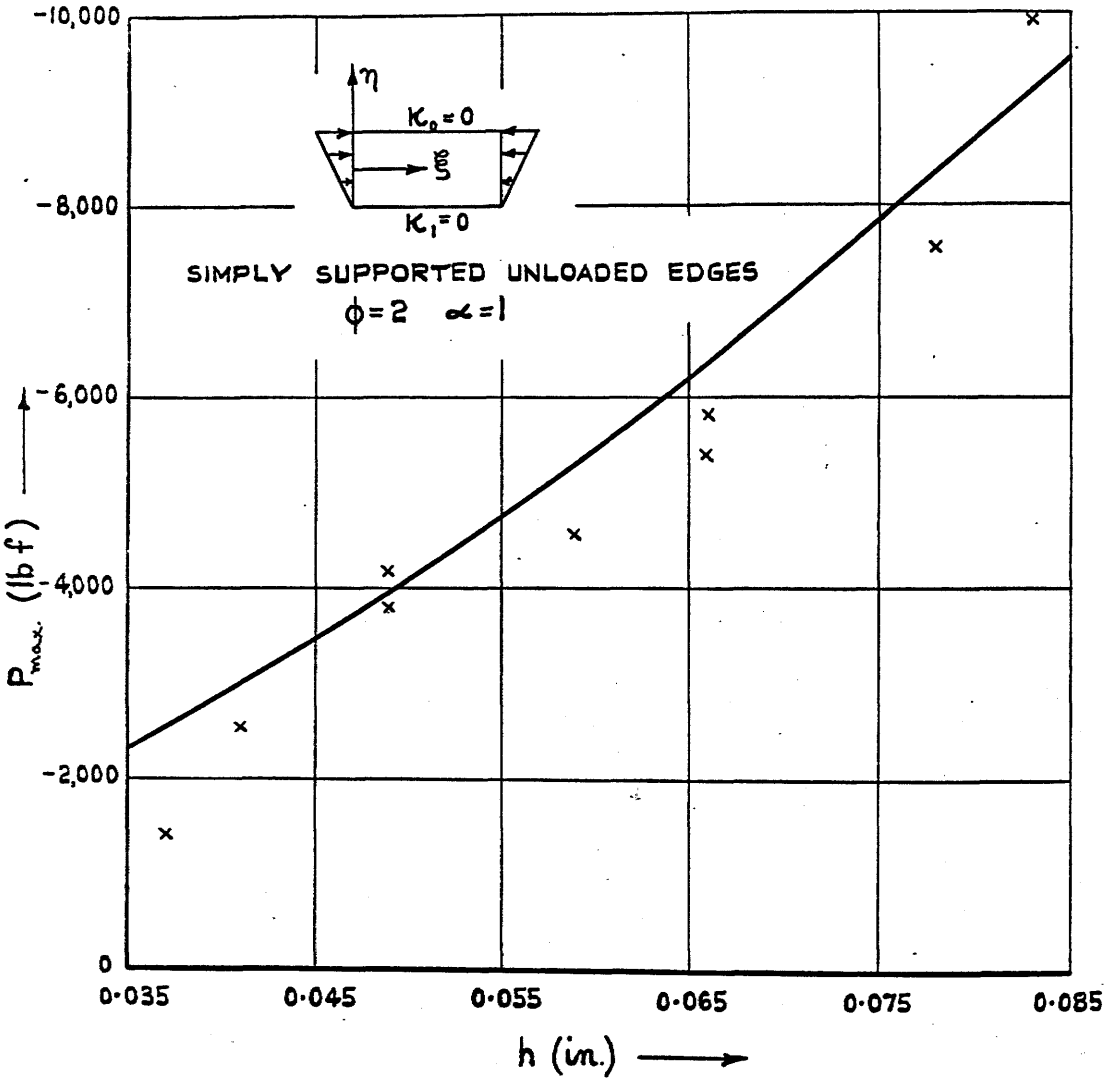

FIG. V. 18 COLLAPSE LOAD V. PLATE THICKNESS.

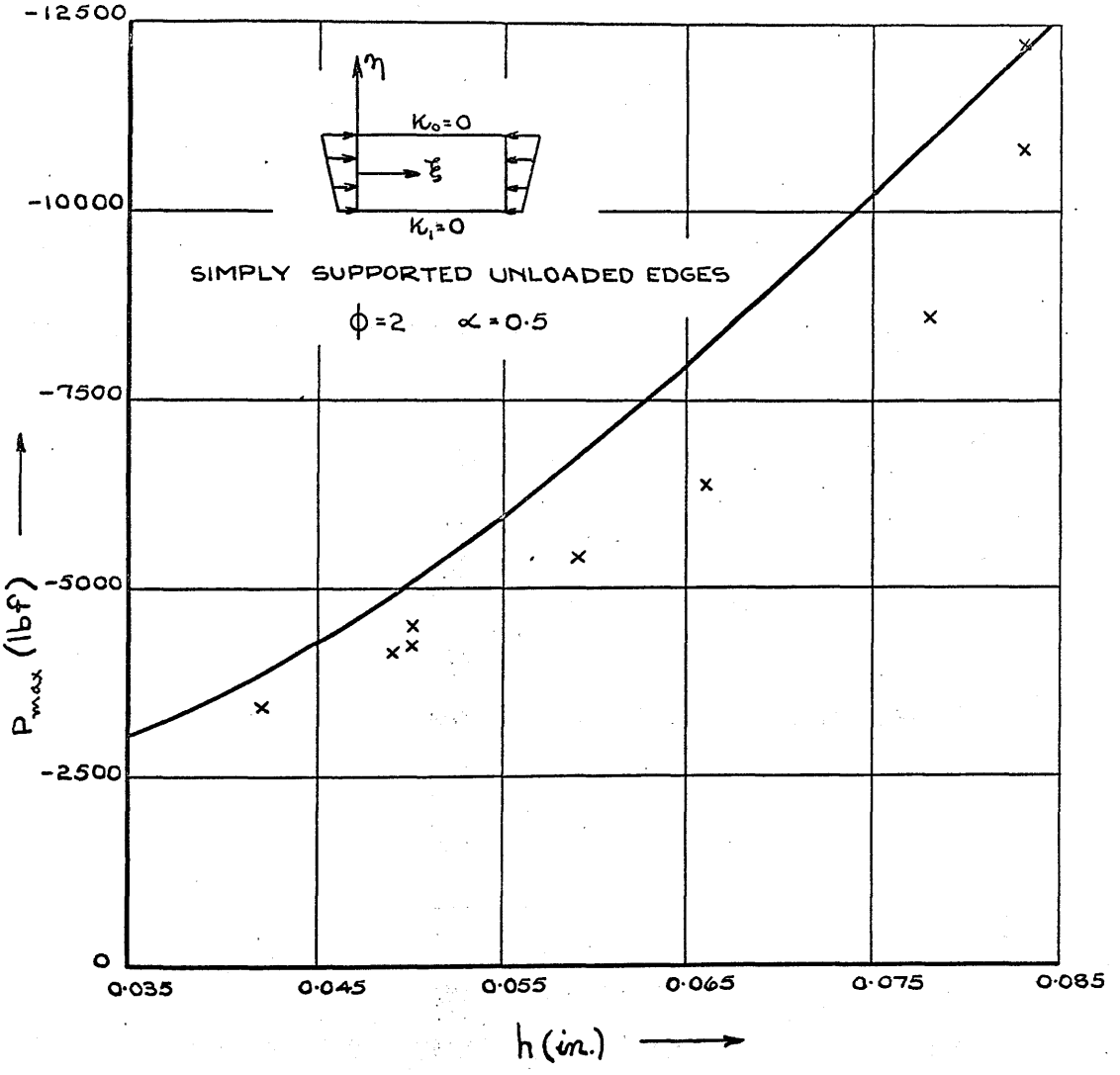

FIG. V.19 COLLAPSE LOAD V. PLATE THICKNESS.

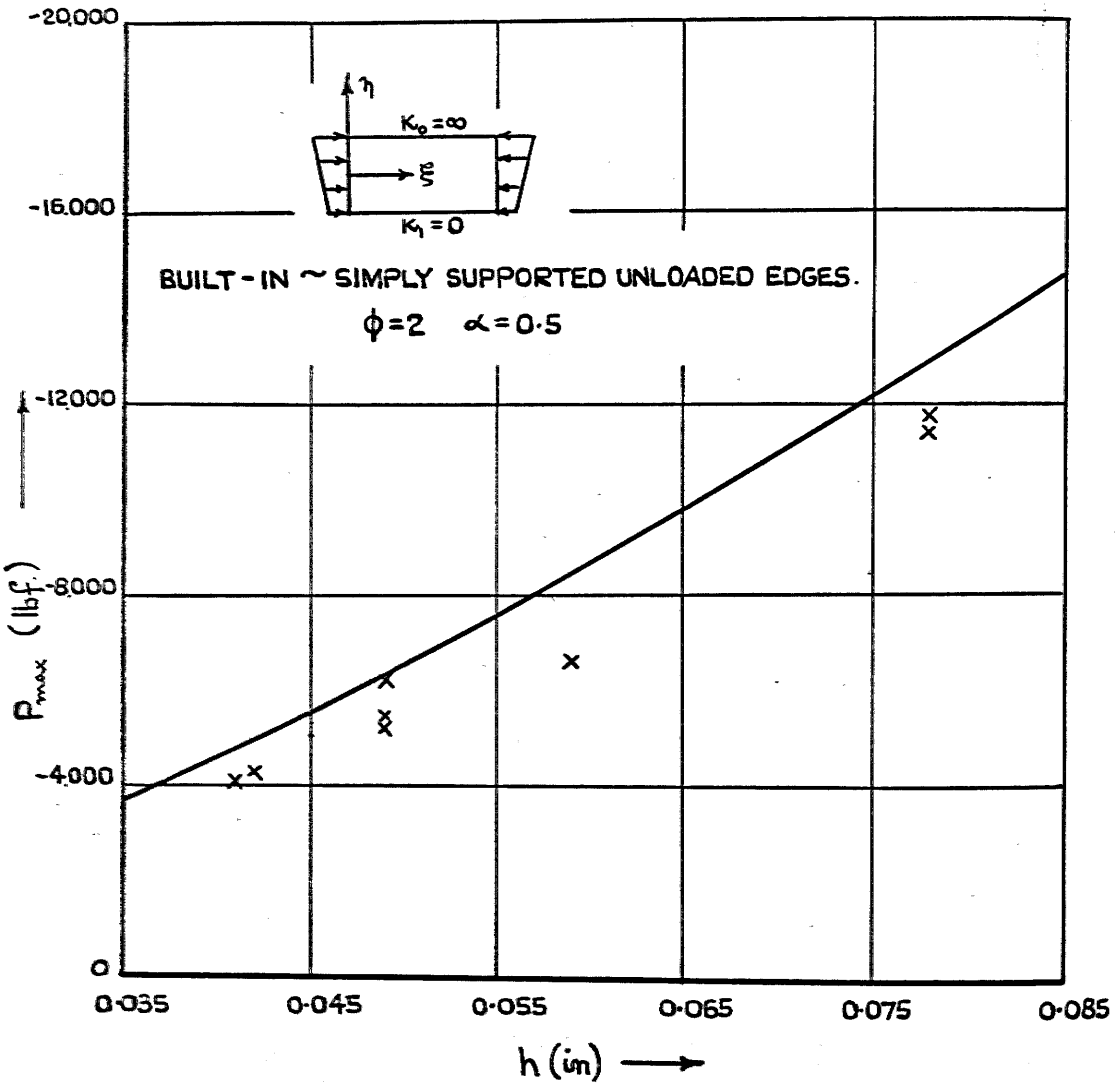

FIG. V.20 COLLAPSE LOAD V PLATE THICKNESS.

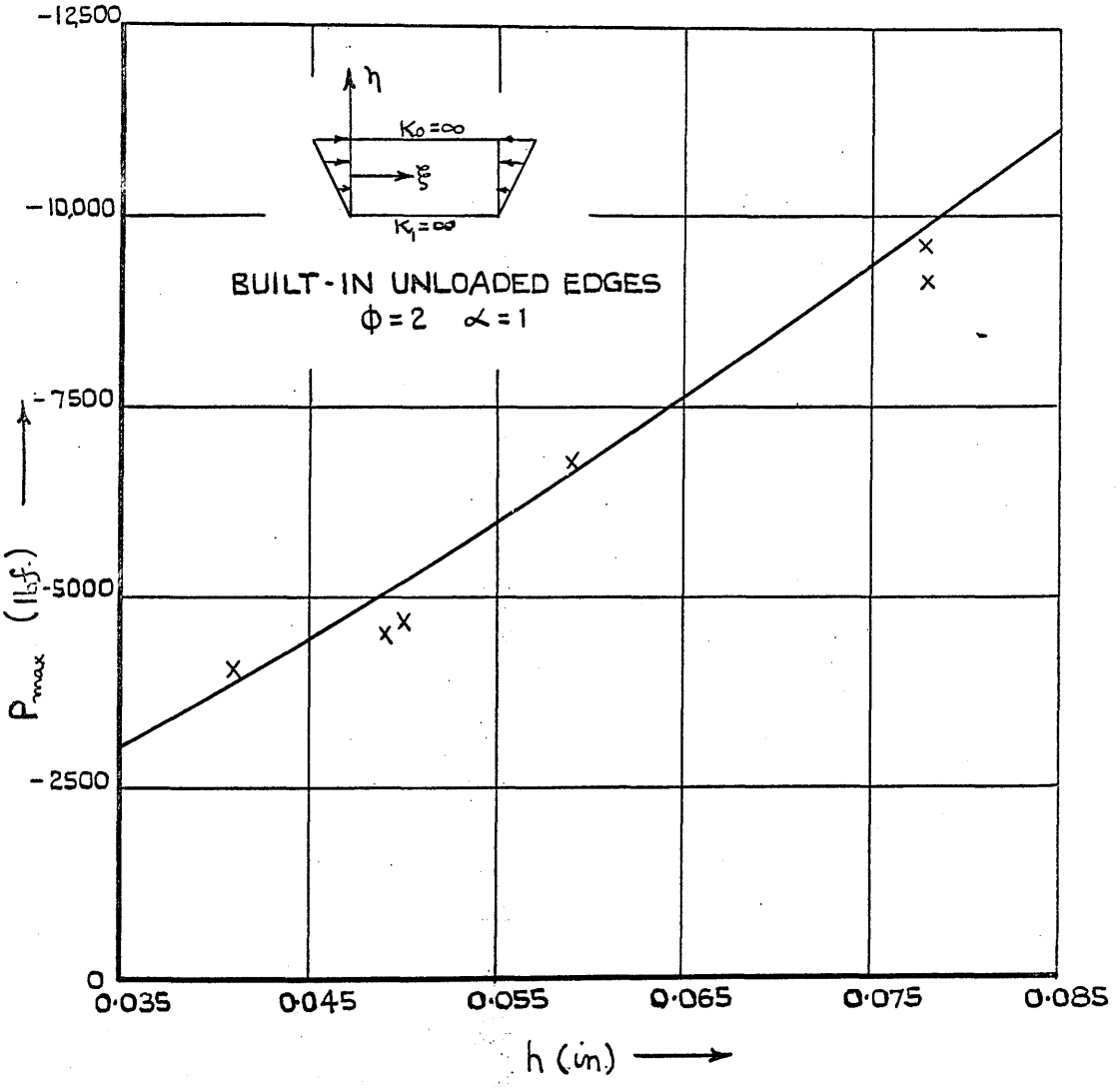

FIG. V.21 COLLAPSE LOAD V. PLATE THICKNESS.

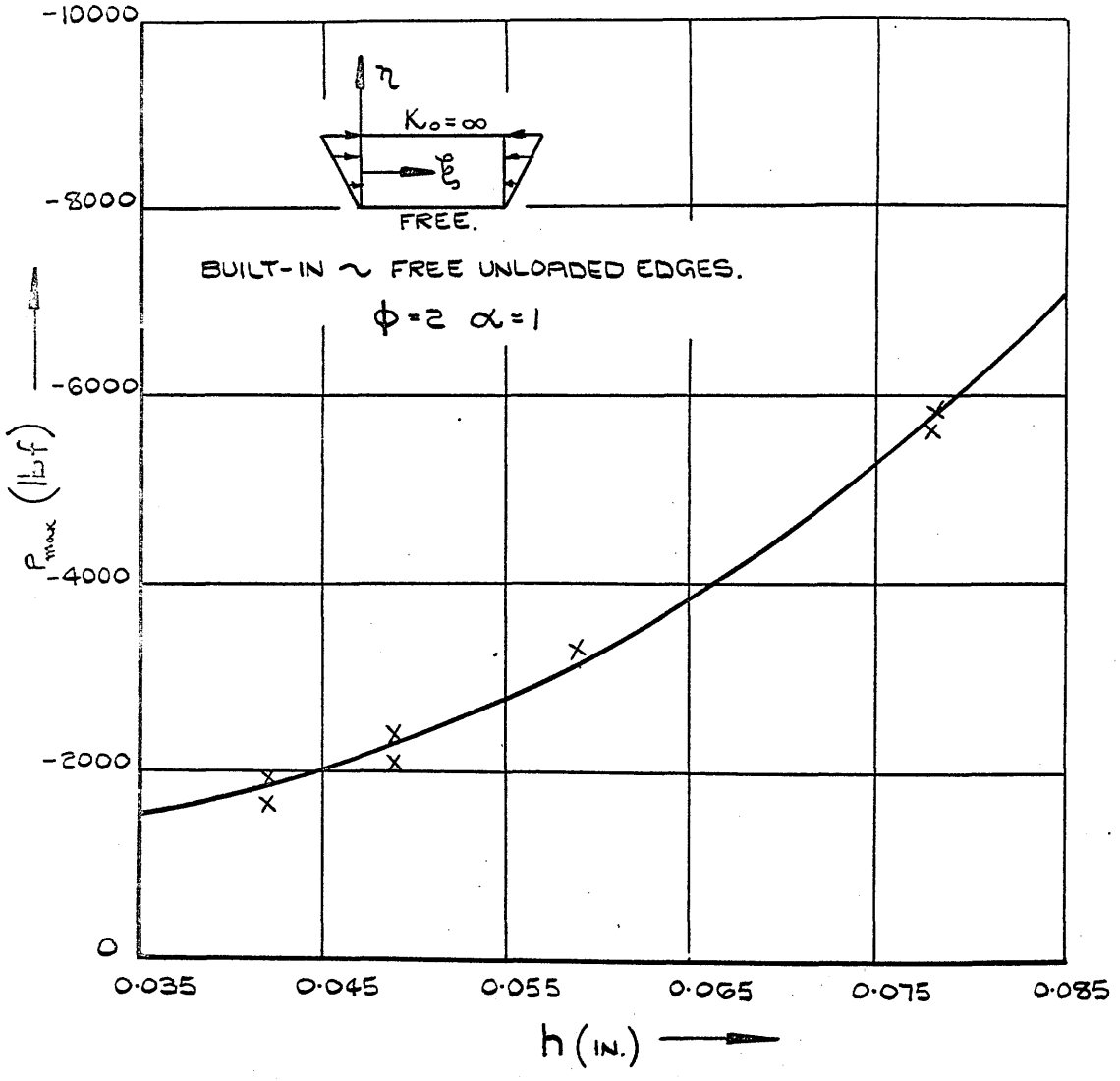

FIG. V.22 COLLAPSE LOAD V. PLATE THICKNESS.

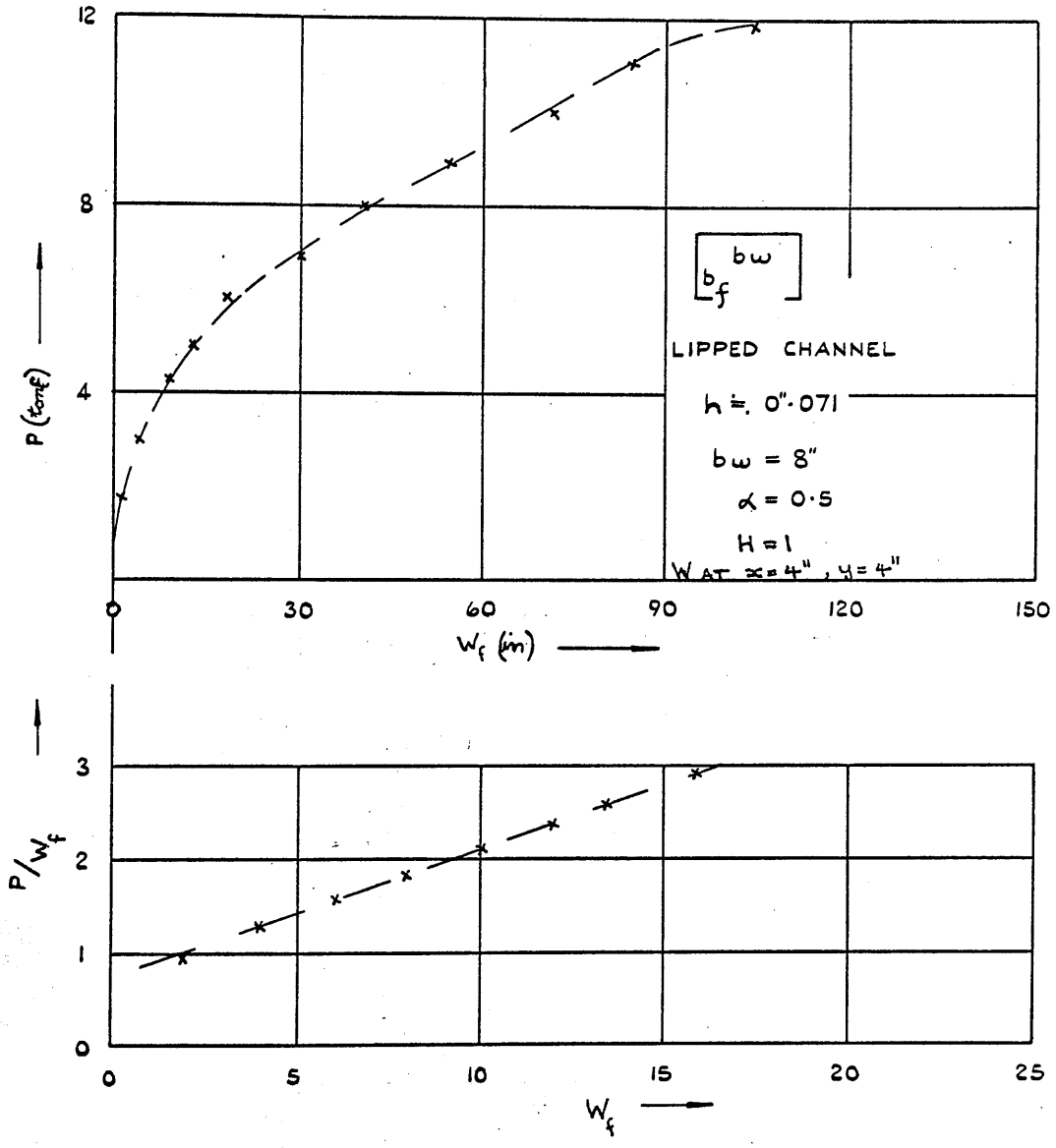

FIG. VII.4 LOAD VS. DEFLECTION WITH ASSOCIATED. SOUTHWELL PLOT.

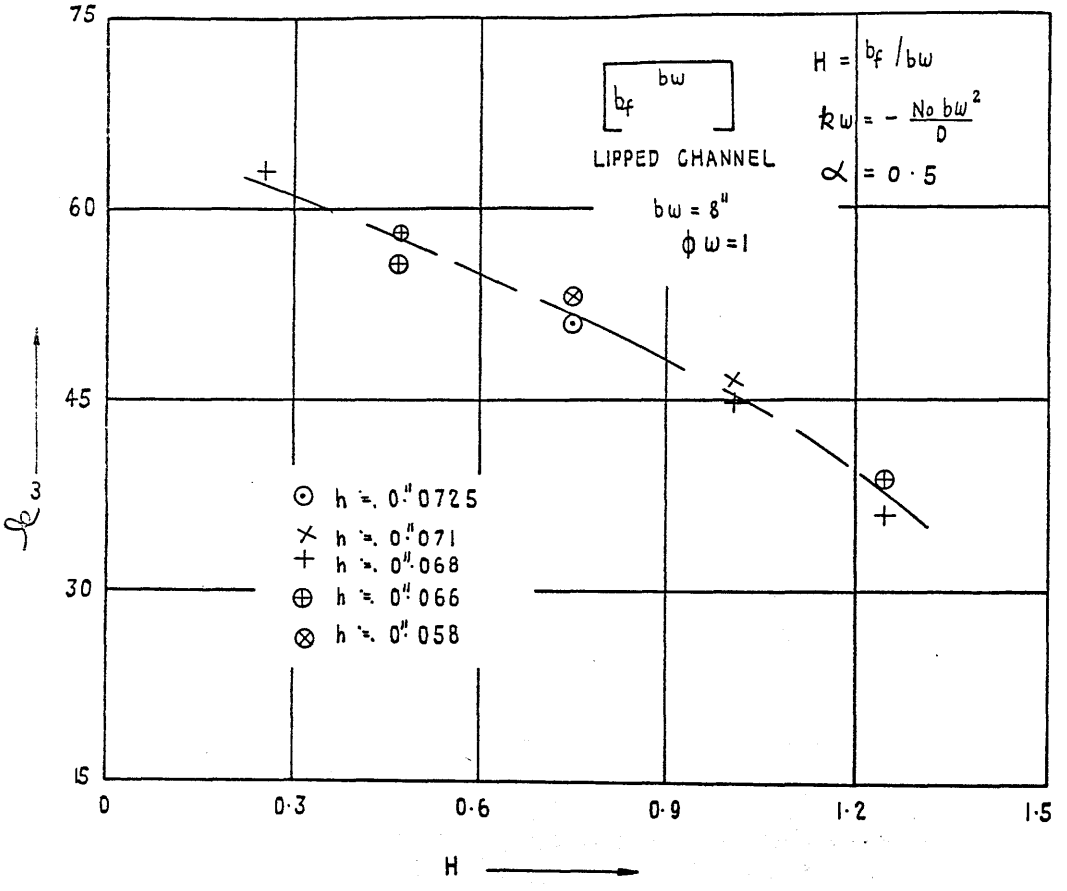

FIG. VII.5 BUCKLING CONSTANT VS. SHAPE FACTOR

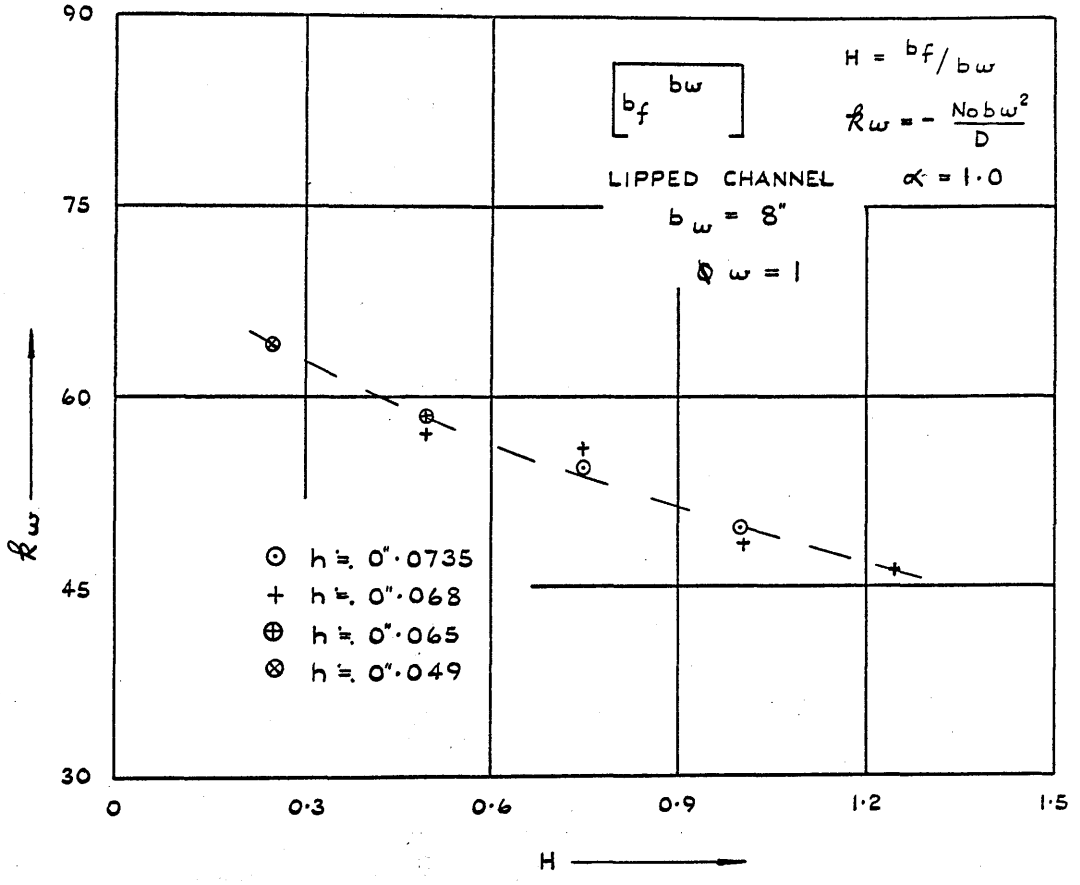

FIG. VII.6 BUCKLING CONSTANT VS. SHAPE FACTOR.

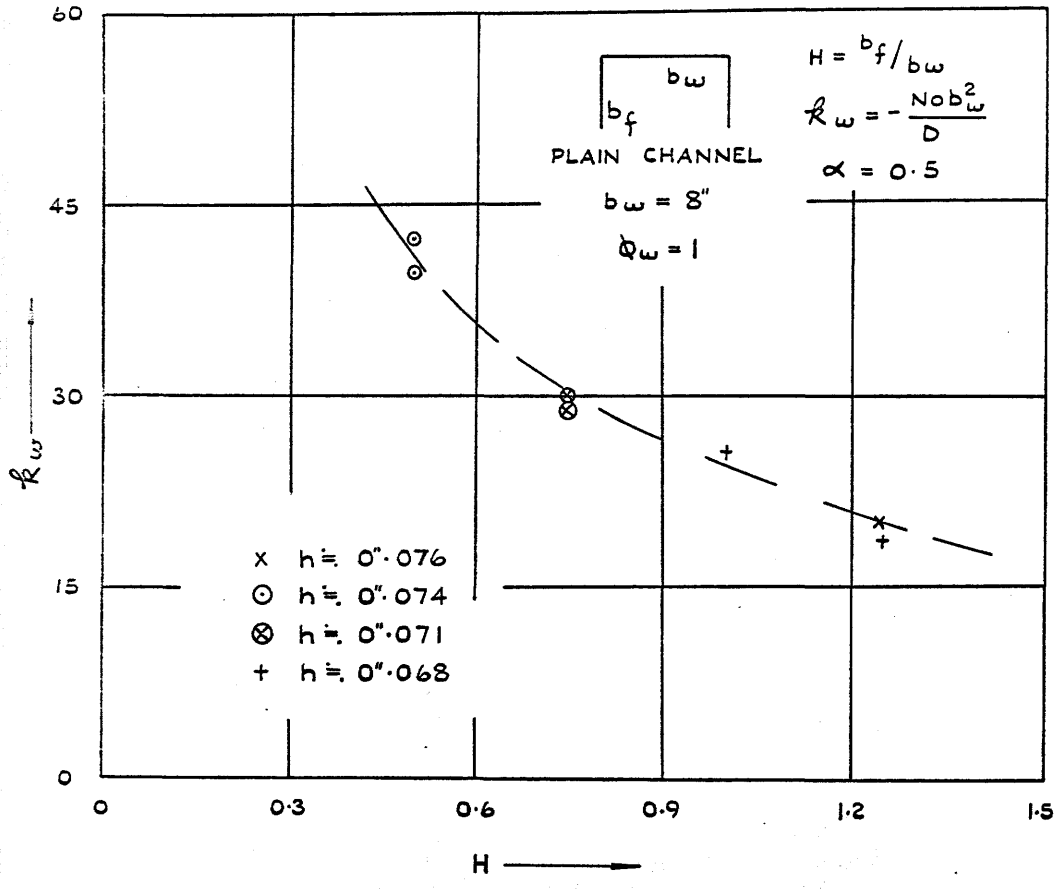

FIG. VII.7 BUCKLING CONSTANT VS. SHAPE FACTOR.

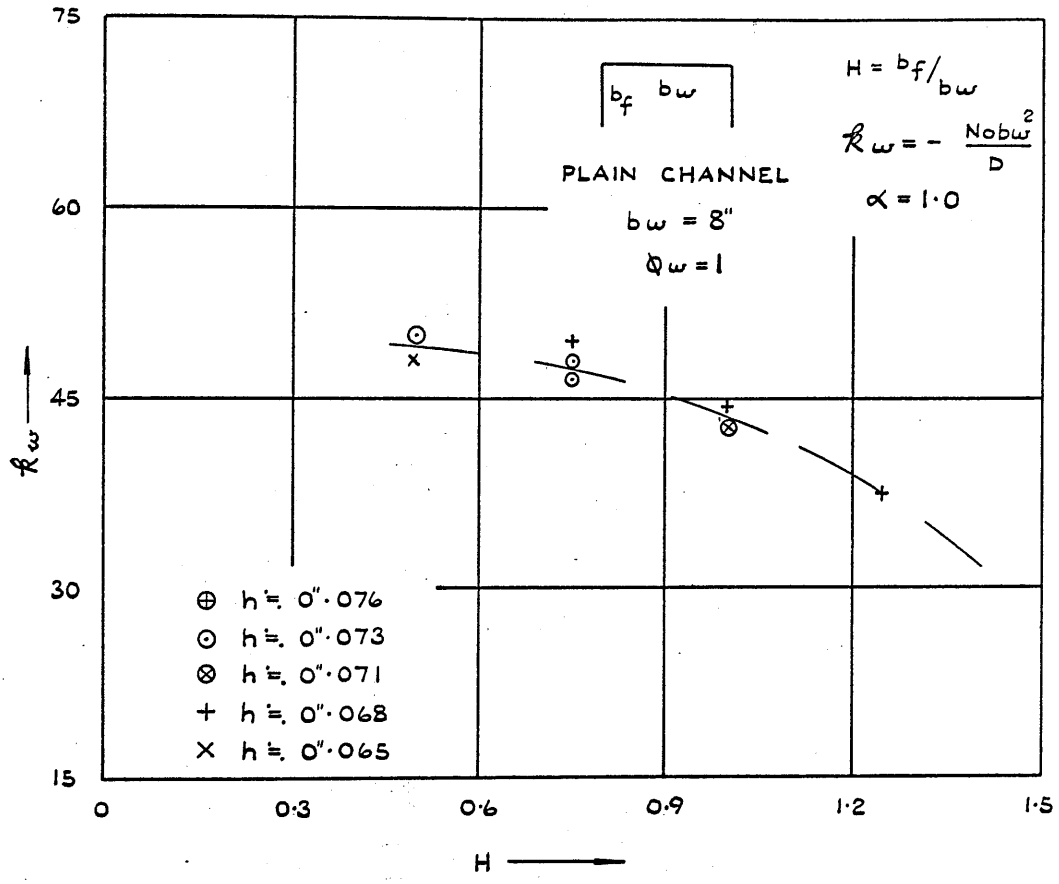

FIG. VII.8 BUCKLING CONSTANT VS. SHAPE FACTOR.

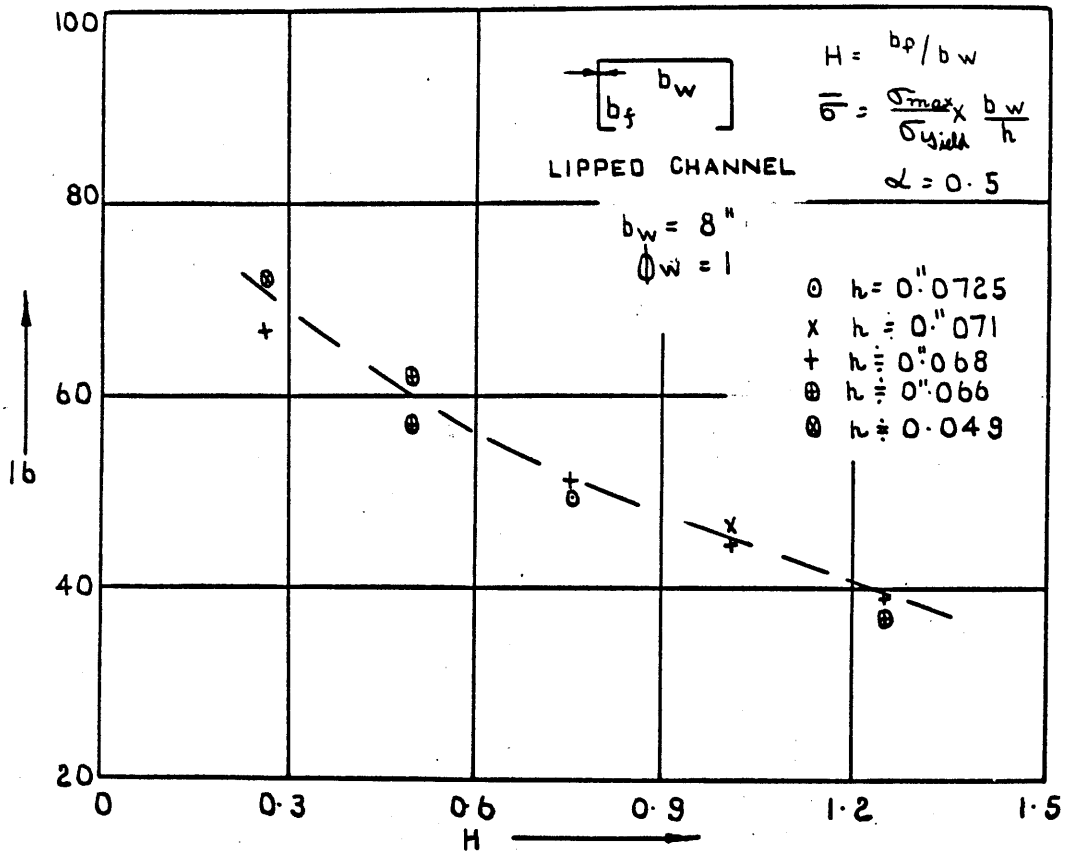

FIG. VII. 9 COLLAPSE STRESS Vs SHAPE FACTOR

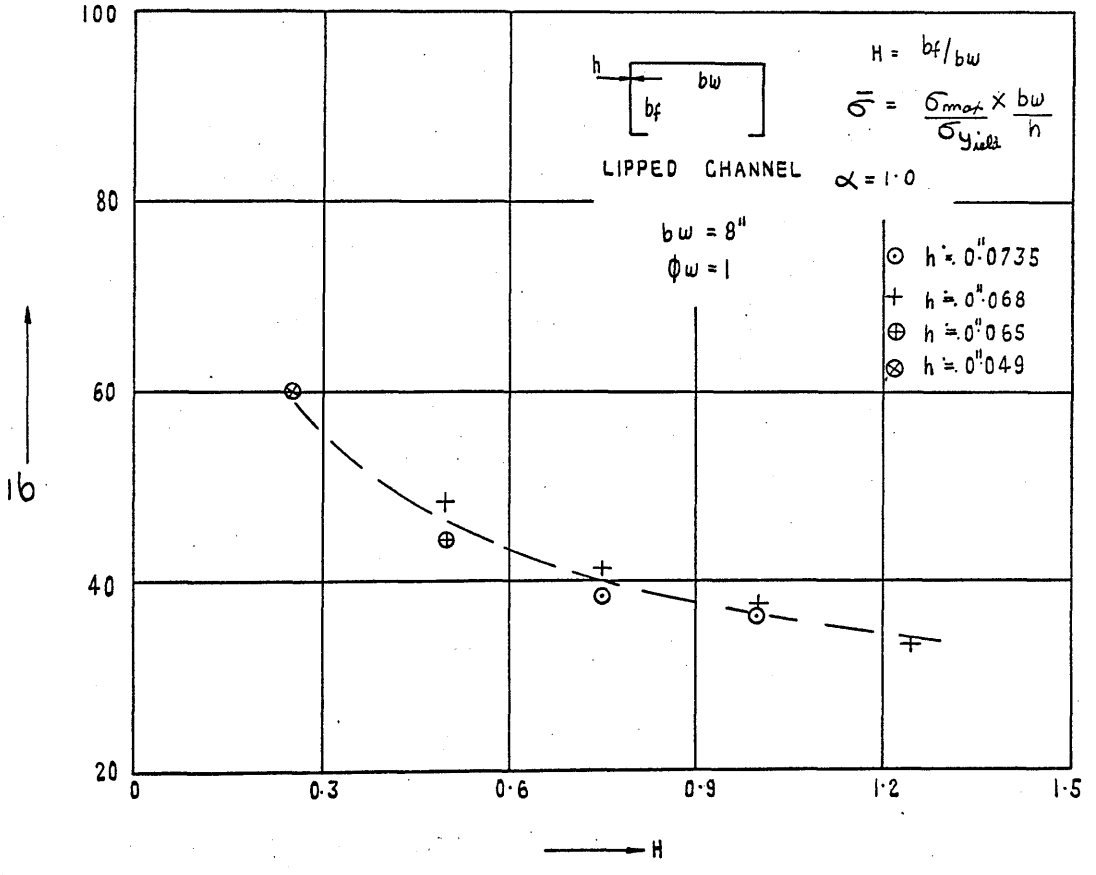

FIG. VII.10 COLLAPSE STRESS VS. SHAPE FACTOR

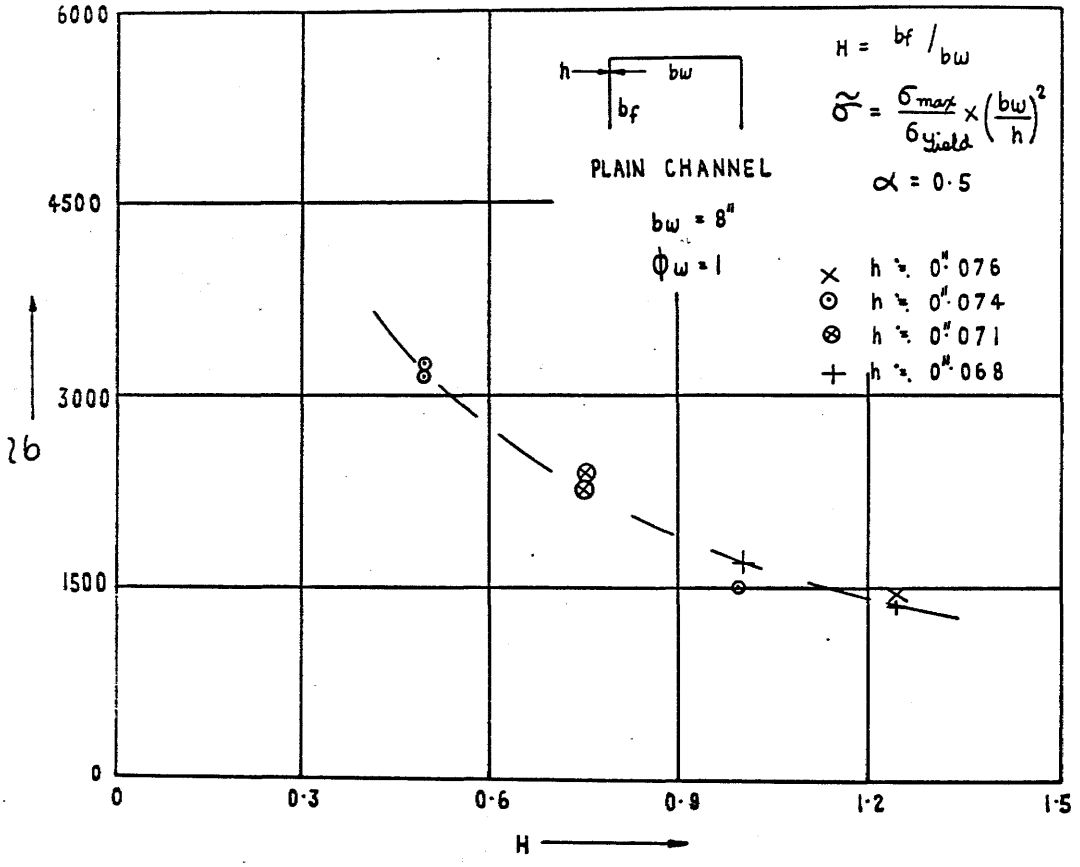

FIG. VII.11 COLLAPSE STRESS Vs. SHAPE FACTOR

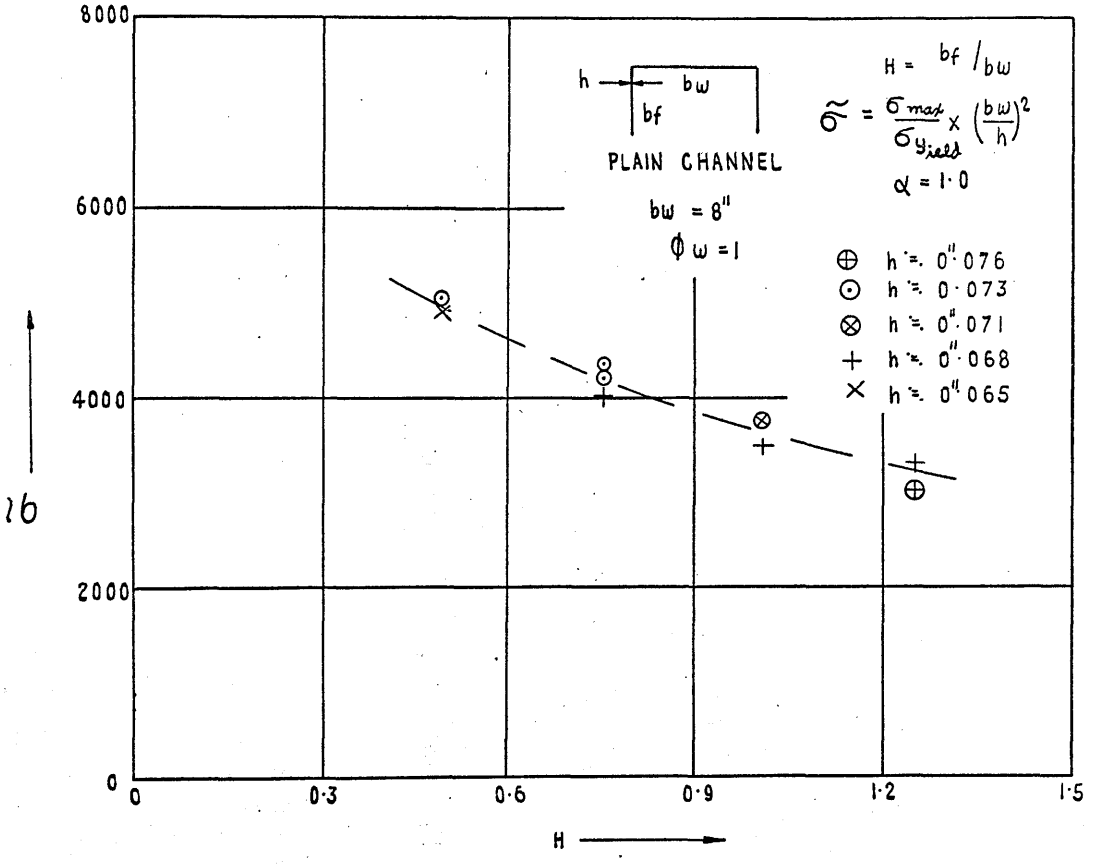

FIG VII.12 COLLAPSE STRESS Vs. SHAPE FACTOR

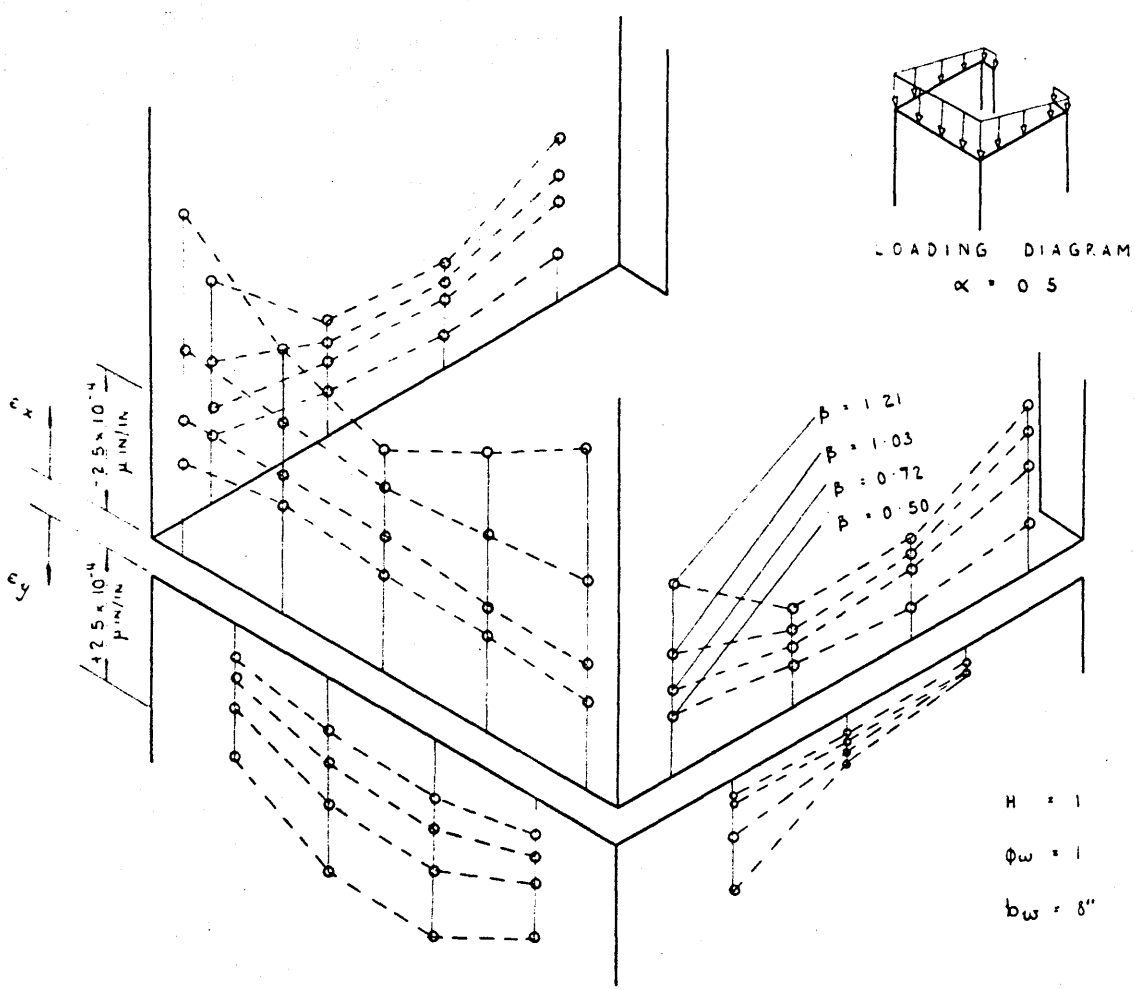

FIG. VII 13 DISTRIBUTION OF ϵx AND ϵy ACROSS - THE CENTRAL X SECTION OF A LIPPED CHANNEL. 0" · 071 THICK.

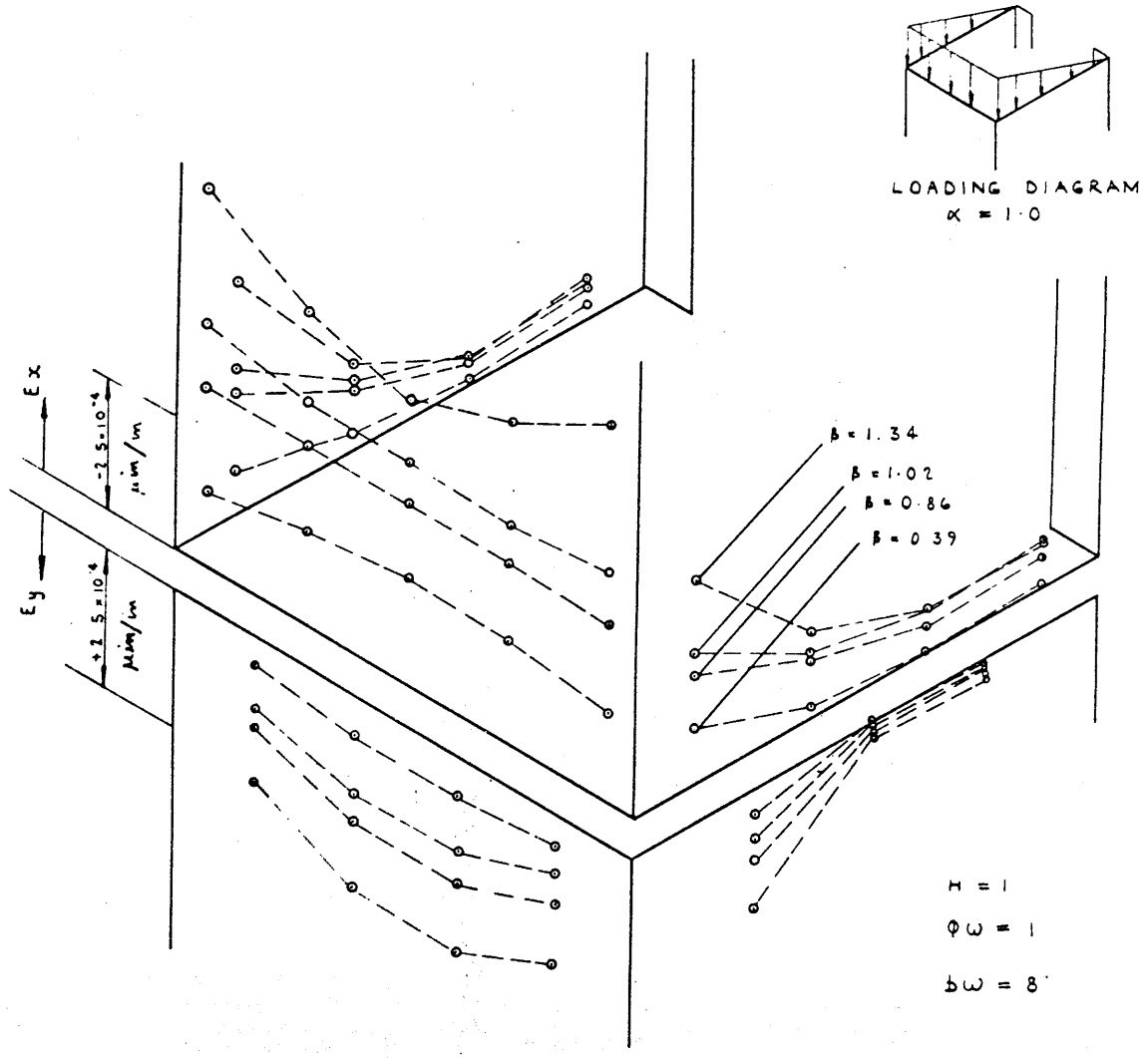

FIG VII 14 DISTRIBUTION OF Ex AND Ey ACROSS THE CENTRAL X SECTION OF A LIPPED CHANNEL 0·1071 THICK

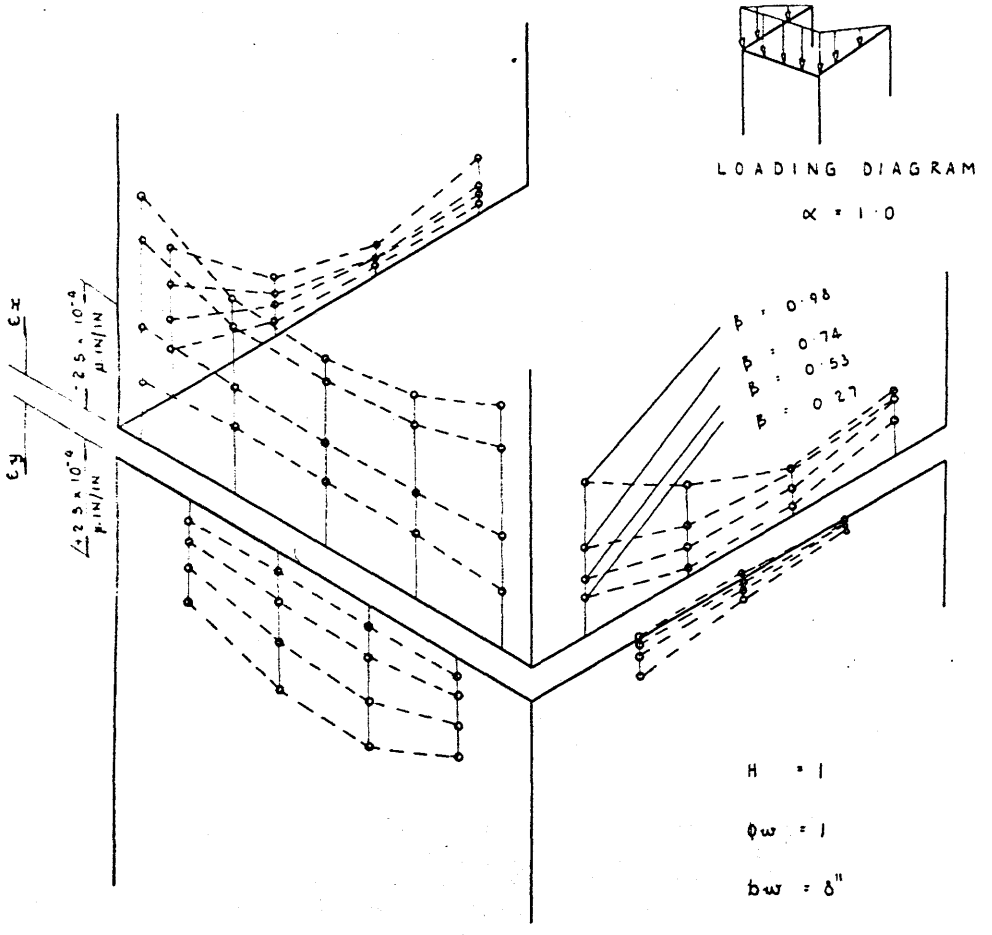

FIG. VIII. IS DISTRIBUTION OF ϵx AND ϵy ACROSS THE CENTRAL α SECTION OF A PLAIN CHANNEL. 0"·071 THICK

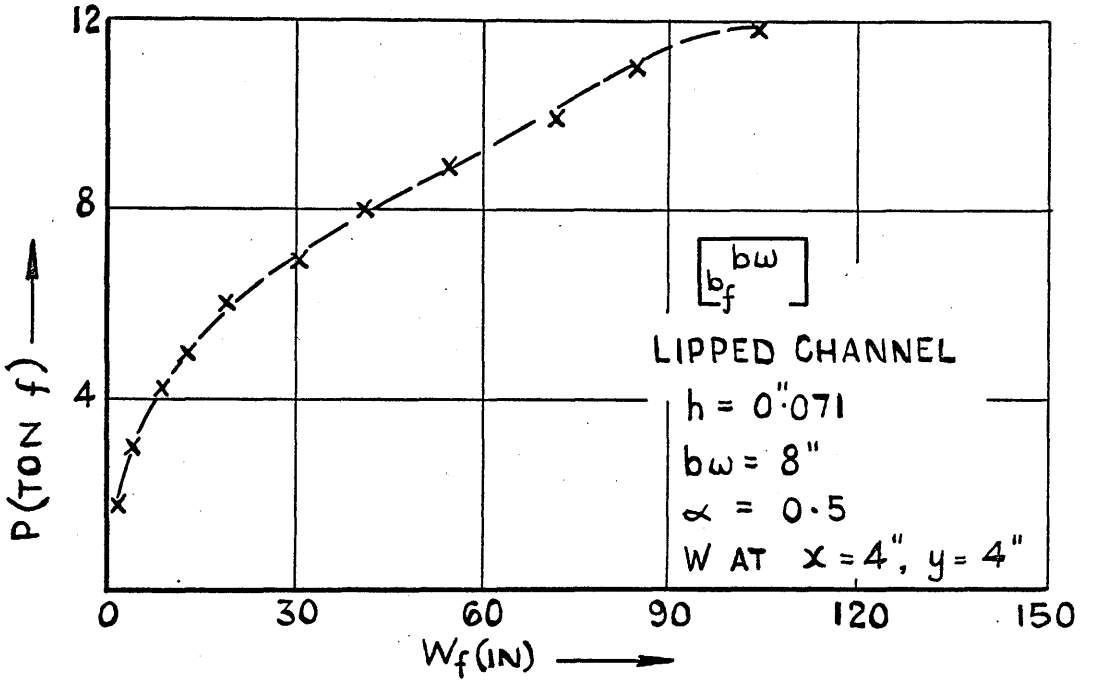

FIG: VIII. 1 LOAD Vs. DEFLECTION.

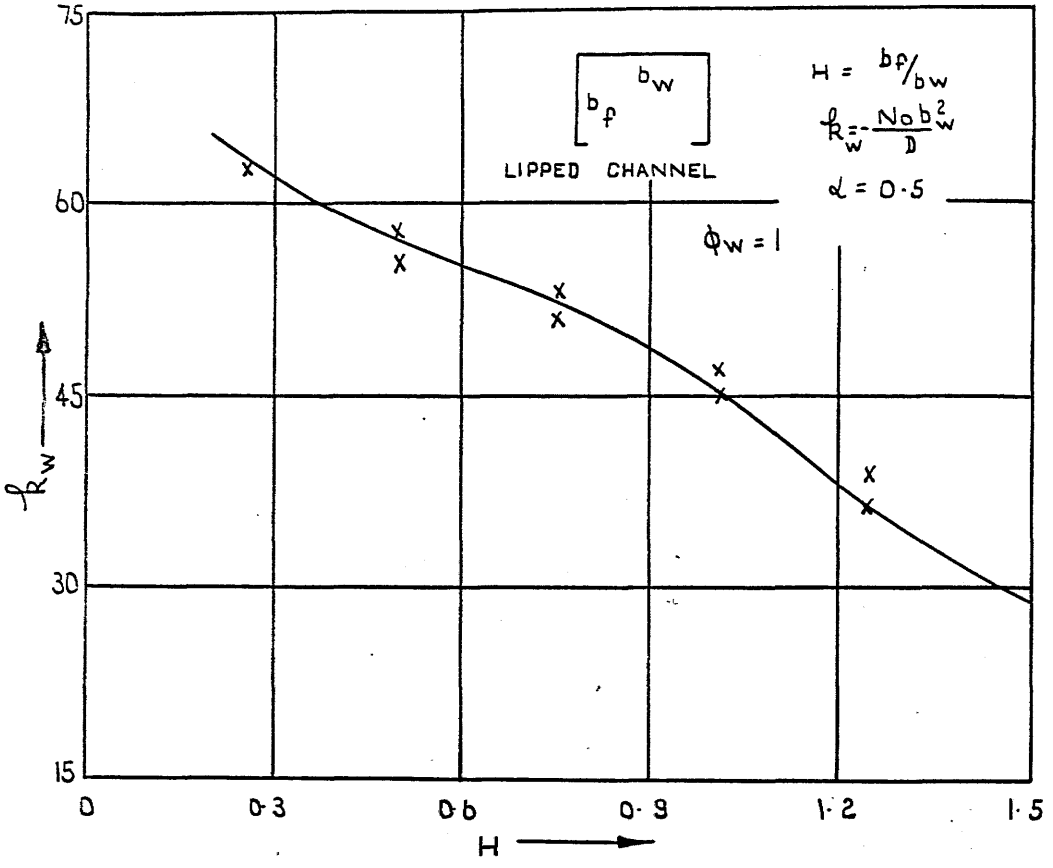

FIG VIII.2 BUCKLING CONSTANT Vc. SHAPE FACTOR

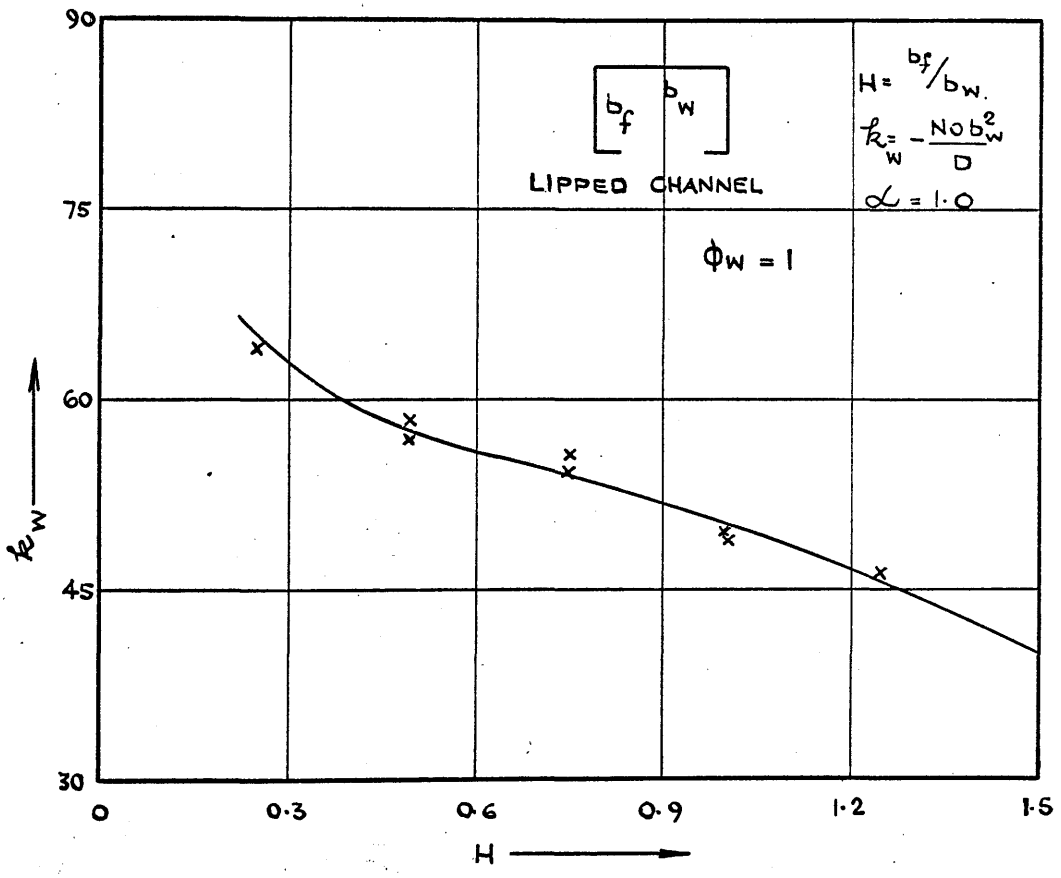

FIG VIII.3 BUCKLING CONSTANT Vs SHAPE FACTOR

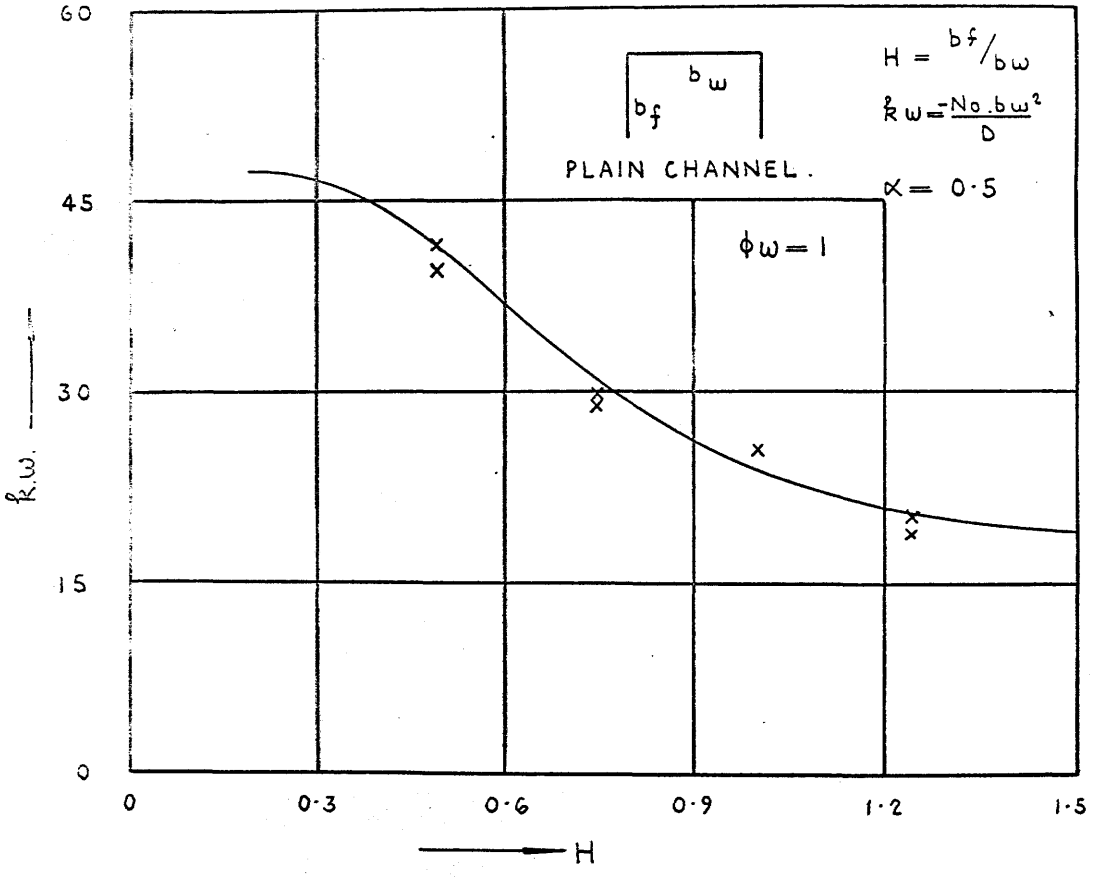

FIG. VIII.4 BUCKLING CONSTANT VS SHAPE FACTOR.

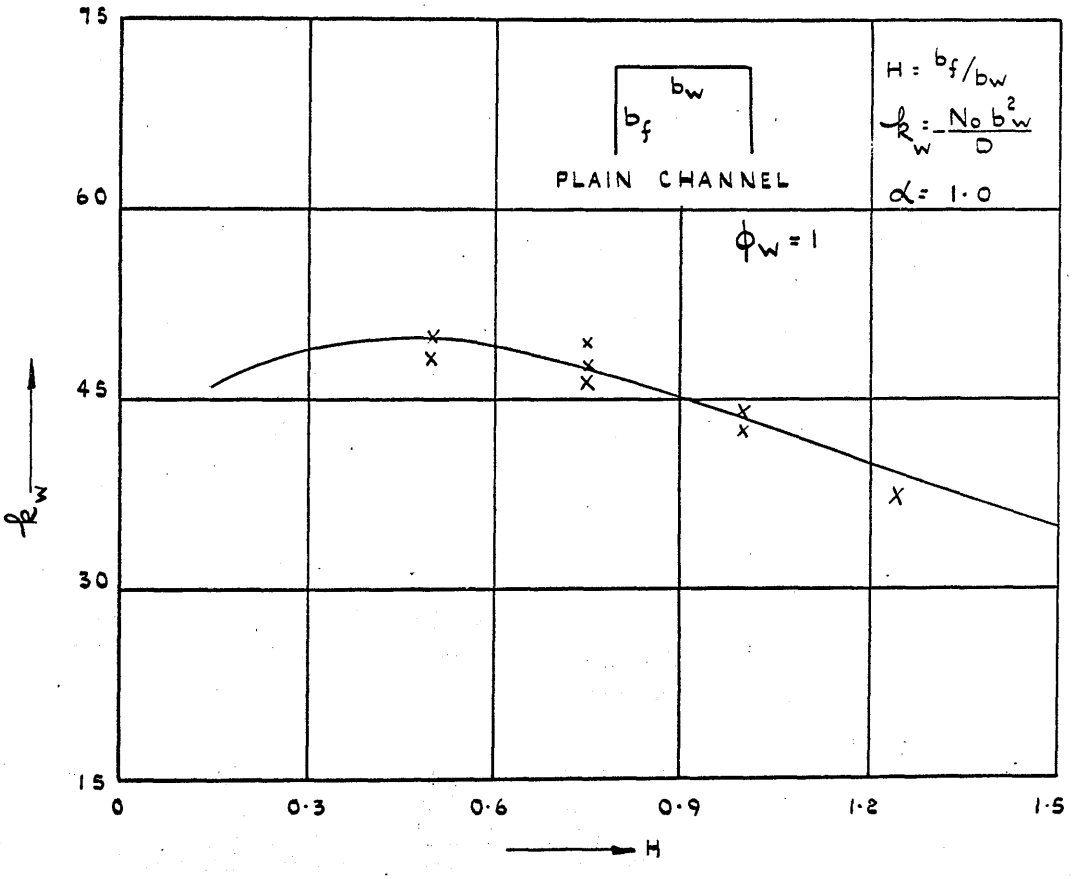

FIG. VIII.5 BUCKLING CONSTANT Vs. SHAPE FACTOR

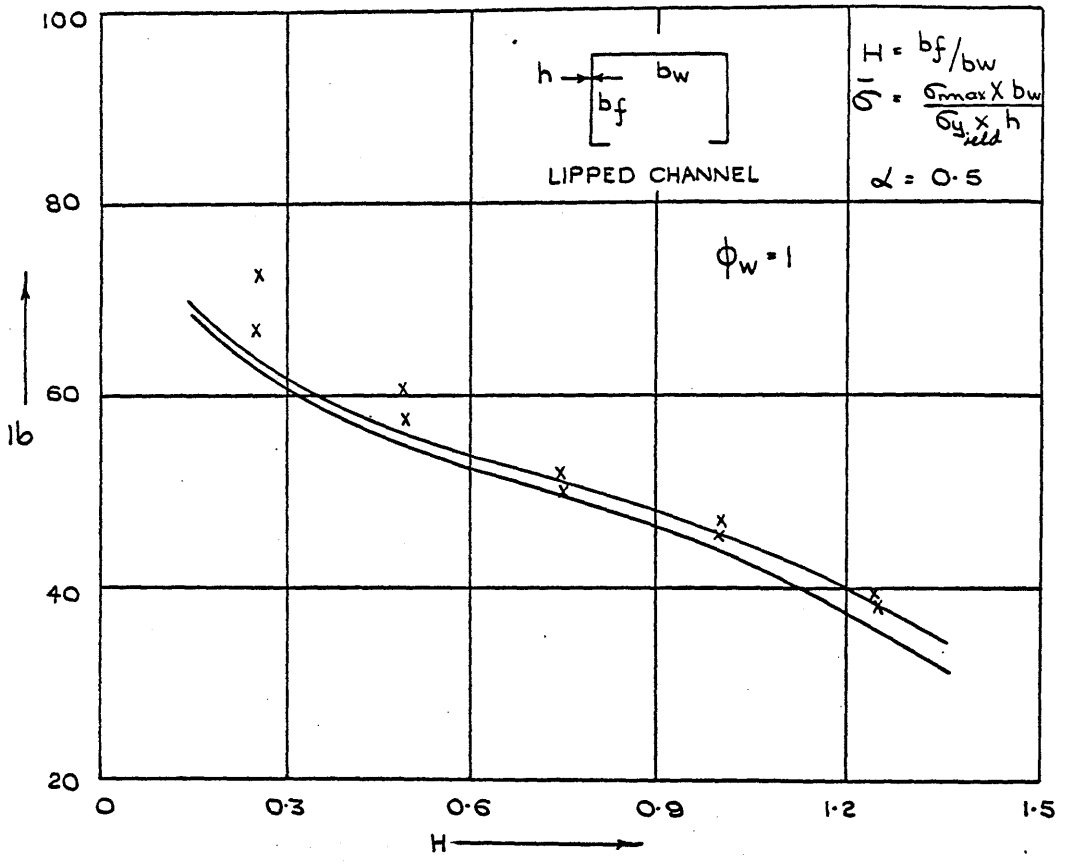

FIG. VIII. 6 COLLAPSE STRESS Vs SHAPE FACTOR.

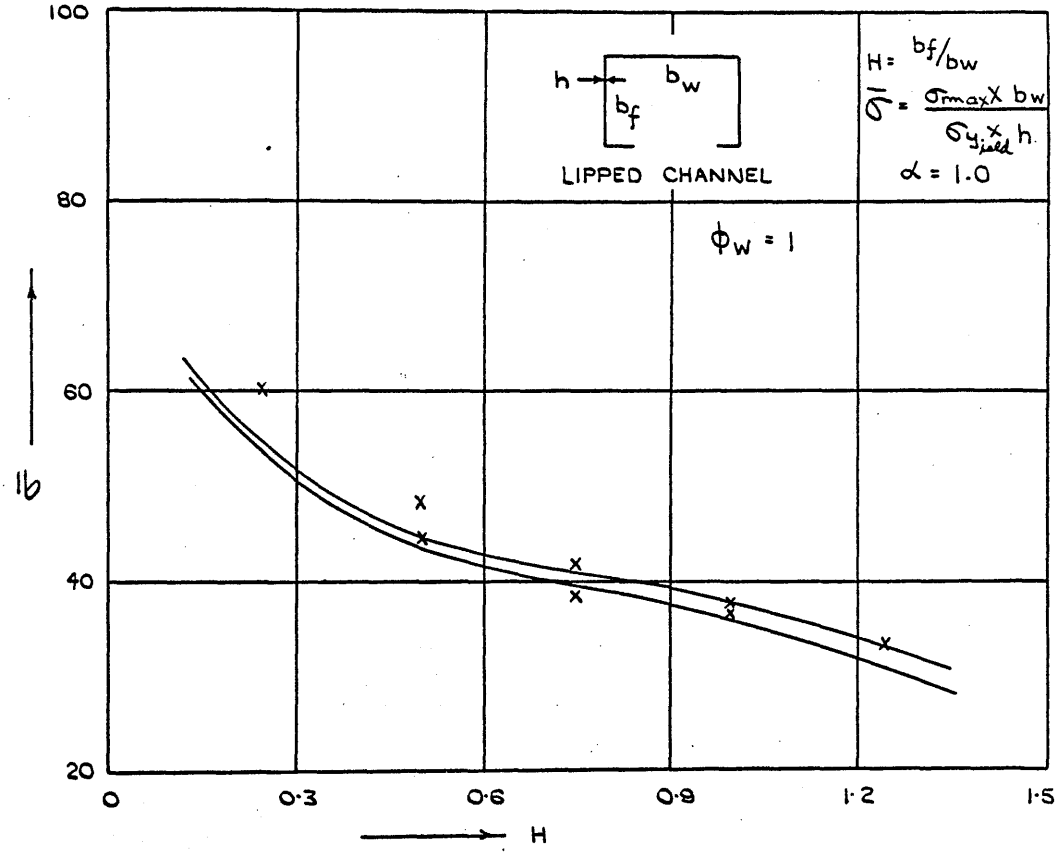

FIG. VIII.7 COLLAPSE STRESS CONSTANT Vs SHAPE FACTOR.

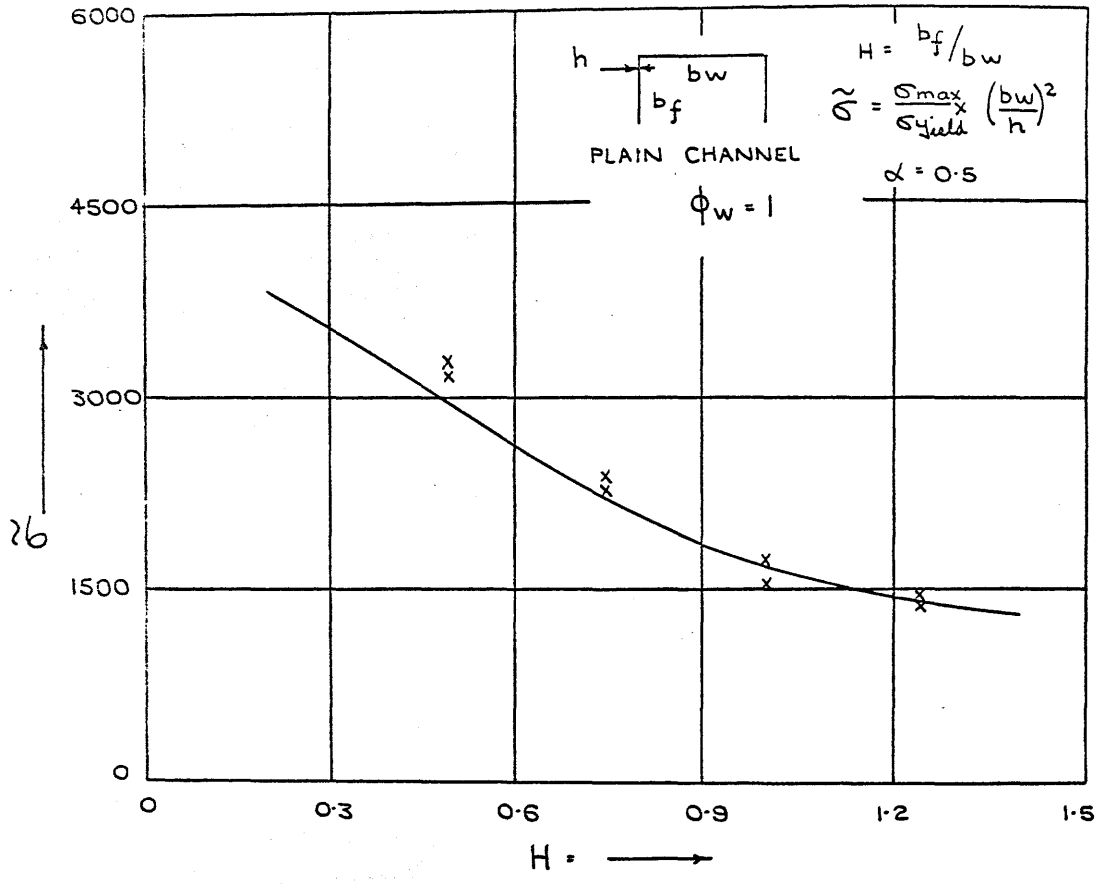

FIG. VIII. 8 COLLAPSE STRESS Vs SHAPE FACTOR.

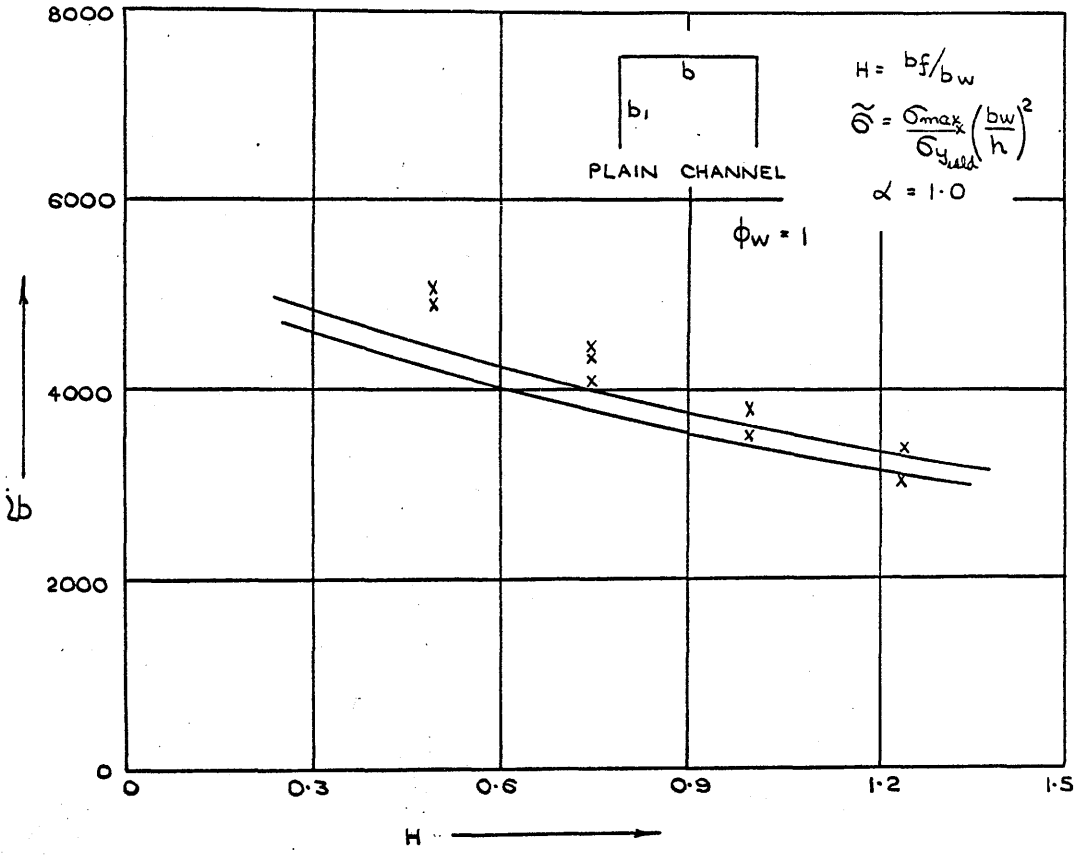

FIG. VIII.9 COLLAPSE STRESS CONSTANT V_6 SHAPE FACTOR.

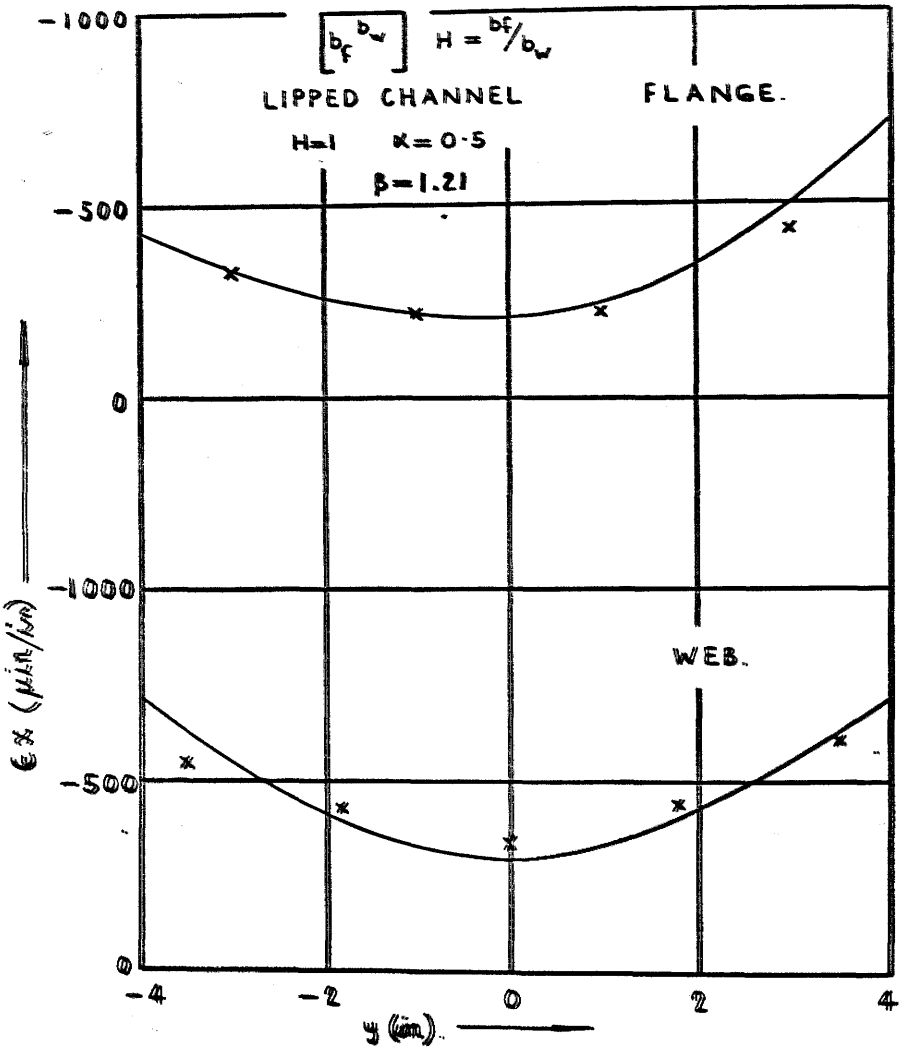

FIG. VIII.10 MIDDLE SURFACE STRAIN ACROSS SECTION AT CENTRAL X POSITION.

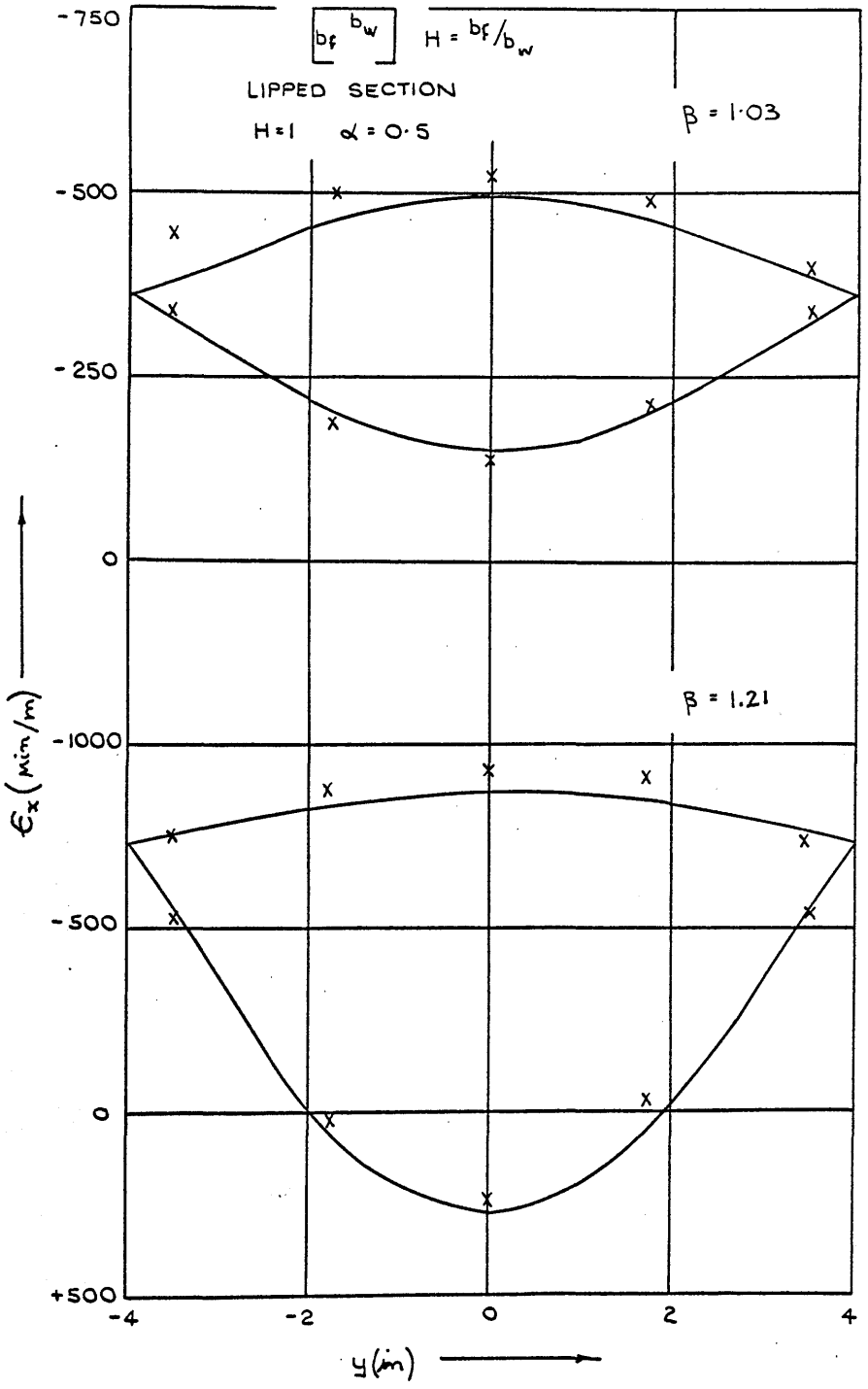

FIG. VIII.11 SURFACE STRAIN ACROSS SECTION AT CENTRAL x POSITION.

B I B L I O G R A P H Y

BIBLIOGRAPHY.

This bibliography consists of one section listing those publications reviewed and discussed in the text and a separate section giving a list of some of the more general publications consulted by the author in the course of this investigation.

Part 1.

BLEICH, F.

"Theorie und Berechnung der Eisernen Brucken". Julius Springer, Berlin 1924.

BOTMAN, M.

"The Experimental Determination of the Effective Width of Flat Plates in the Elastic and Plastic Range". Part II. Report S.414 Nat. Luchtvaartlaboratorium Amsterdam Jan. 1954.

BRYAN, G.H.

"On the Stability of a PlanePlate under Thrusts in its own Plane with Applications to the "Buckling" of the Sides of a Ship". Proc. London Math. Soc. Vol. 22 p. 54, 1891.

CHILVER, A.H.
"Thin-Walled Structural Members".
Ph.D. Dissertation.
University of Bristol, Oct. 1950.

CHILVER, A.H.
"Thin-Walled Structural Members in Compression".
Engineering: p.281, 1951.

CHILVER, A.H.
"The Maximum Strength of the Thin-Walled Strut".
Civil Engineering, Vol. 48, p.1143, 1953.

COAN, J.M.
"Large-Deflection Theory for Plates with Small Initial Curvature Loaded in Edge Compression".
Trans. A.S.M.E. Vol. 73, p.143, 1951.

DUNCAN, J.P. and BROWN, C.J.E.
"Slope Contours in Flexed Elastic Plates by Salet-Ikeda Technique".
Experimental Mechanics, pp.149-175.
Pergamon Press, 1963.

DUNCAN, W.J.

"Galerkin's Method in Mechanics and Differential Equations".
A.R.C. Tech. Rep.
R. & M. No. 1798, 1937.

FOX, L.

"The Numberical Solution of Two-Point Boundary Problems in Ordinary Differential Equations".
Oxford Univ. Press, 1957.

GERARD, G.

Handbook of Structural Stability Part IV.
"Failure of Plates and Composite Elements".
N.A.C.A. Tech. Note No. 3784, 1957.

HARVEY, J.M.

"Strength of Thin-Walled Channel Sections".
Engineering, March 1953.

HEIMERL, G.J.

"Determination of Plate Compressive Strengths".
N.A.C.A. Tech. Note No. 1480, 1947.

HEIMERL, G.J. and WOODS, W.

"Effect of Brake Forming on the Strength of 24S-T Aluminium Alloy Sheet".

N.A.C.A. Tech. Note No. 1072, May 1946.

HU, P.C., LUNDQUIST, E.E. and BATDORF, S.B.

"Effect of Small Deviations from Flatness on Effective Width and Buckling of Plates in Compression".

N.A.C.A. Tech. Note No. 1124, 1946.

IKEDA, K.

"Soap Film Techniques for Solving Torsion Problems".

Proc. First Japan Nat. Congress. for Applied Mech. 1 No. 38 pp.219-224, 1951.

JACKSON, K.E. and HALL, A.H.

"Curved Plates in Compression".

N.R.C. Canada.

Aero. Rep. Ar - 1, 1947.

JOHNSON, J.H. (Jr.) and NOEL, R.G.

"Critical Bending Stress for Flat Rectangular Plate Supported Along All Edges and Elastically Restrained Against Rotation Along the Unloaded Compression Edge".

Jour. Aero. Sciences. Vol. 20 p.535, 1953.

KENEDI, R.M., SHEARER SMITH and FAHMY, F.O.

"Light Structures - Research and its Application to Economic Design".
Trans. Inst. of Engineers and Shipbuilders of Scotland. Vol. 99, Part 4, p.207, 1955.

KROLL, W.D.

"Tables of Stiffness and Carry-Over Factor for Flat Rectangular Plates under Compression".
N.A.C.A. Arr No. 3K27, 1943.

LEVY, S.

"Bending of Rectangular Plates with Large Deflections".
N.A.C.A. Rep. No. 737, 1942.

LIGTENBERG, F.K.

"The Moiré Method - A New Experimental Method for the Determination of Moments in Small Slab Models".
Proc. Soc. Exp. Stress Analysis.
Vol. 12, No. 2 pp.83-98, 1955.

LUNDQUIST, E.E., STOWELL, E.Z. and SCHUETTE, E.H.
"Principles of Moment Distribution Applied to Stability of Structures Composed of Bars or Plates".
N.A.C.A. Rep. No. 809, 1943.

LUNDQUIST, E.E. and STOWELL, E.Z.
"Critical Compressive Stress for Flat Rectangular Plates Supported Along All Edges and Elastically Restrained Against Rotation Along the Unloaded Edges".
N.A.C.A. Rep. No. 733, 1942.

MARGUERRE, K.
"The Apparent Width of Plates in Compression".
N.A.C.A. Tech. Mem. No. 833, 1942.

MAYERS, J. and BUDIANSKY, B.
"Analysis of the Behaviour of Simply Supported Flat Plates Compressed Beyond the Buckling Load into the Plastic Range".
N.A.C.A. Tech. Note No. 3368, 1955.

NEEDHAM, R.A.
"The Ultimate Strength of Aluminium Alloy Formed Structural Shapes in Compression".
Jour. of Aero. Sciences Vol. 21, No. 4, pp.217-229 April, 1954.

PALMER, P.J.

"The Bending Stresses in Cantilever Plates by Moiré Fringes".

Aircraft Engineering Vol. 29, pp.377-380 Dec. 1957.

SALET, G.

"Nouvelle Methode de Mise en Oevre de L'Analogue de la Membrane pour L'Etude de la Torsion des Poutres Cylindriques".

Tech. Maritime et Aeronautique 43, pp.107-119, 1950.

SCHUETTE, E.H.

"Observations of the Maximum Average Stress of Flat Plates Buckled in Edge Compression".

N.A.C.A. Tech. Note No. 1625, 1949.

SECHLER, E.E.

"The Ultimate Strength of Thin Flat Sheet in Compression".

Publication No. 27, Guggenheim Aeronautics Laboratory, Calif. Inst. of Tech., Pasadena, 1933.

SECHLER, E.E. and DUNN, I.G.

"Airplane Structural Analysis and Design". John Wiley and Sons, Inc., New York, 1942.

SOUTHWELL, R.V.

"On the Analysis of Experimental Observations in Problems of Elastic Stability". Proc. Roy. Soc. A. Vol. 135, p.601, 1932.

STEIN, M.

"The Phenomenon of Change in Buckle Pattern in Elastic Structures". N.A.S.A. Tech. Rep. No. R-39. 1959.

STEIN, M.

"Loads and Deformation in Buckled Rectangular Plates". N.A.S.A. Tech. Rep. R-40. 1959.

STOWELL, E.Z.

"Compressive Strength of Flanges". N.A.C.A. Rep. No. 1029, 1951.

ST. VENANT.

"Theorie de L'Elasticite des Corps Solides". Clebsch p.704, 1883.

TIMOSHENKO, S.P. and GERE, J.M.
"Theory of Elastic Stability".
2nd Edition.
McGraw Hill Book Co. Inc. 1961.

VON KARMAN, T.
"Encyklopadie der Mathematischen Wissenshaften".
Vol. IV, p.349, 1910.

VON KARMAN, T., SECHLER, E.E. and DONNEL, L.H.
"Strength of Thin Plates in Compression".
Trans. A.S.M.E. Vol. 54, p.53, 1932.

WAGNER, H.
"Torsion and Buckling of Open Sections".
N.A.C.A. Tech. Mem. No. 807, 1936.

WINTER, G.
"Strength of Thin Steel Compression Flanges".
Proc. of the Amer. Soc. of Civil Eng.
Vol. LXXll, pp.199-226, 1946.

YAMAKI, N.
"Post-Buckling Behaviour of Rectangular Plates with Small Initial Curvature Loaded in Edge Compression".
Jour. of Appl. Mech. Vol. 26, pp.407-414, 1959.

Part 2.

ANDERSON, R.A., ANDERSON, M.S.

"Correllation of Crippling Strength of Plate Structures with Material Properties".
N.A.C.A. Tech. Note No. 3600, 1956.

BERGER, H.M.

"A New Approach to the Analysis of the Large Deflection of Plates".
Jour. of App. Mech. Vol. 22, p.465, 1955.

BIJLAARD, P.P.

"Theory of Plastic Buckling of Plates and Application to Simply Supported to Bending or Eccentric Compression in Their Plane".
Jour. of App. Mech. Vol. 23, pp.27-34, 1956.

BLEICH, F.

"Buckling Strength of Metal Structures".
McGraw Hill Book Co., 1952.

BOTMAN, M. and BESSELING, J.F.

"The Effective Width in the Plastic Range of Flat Plates under Compression".
Nationall Luchtvaartbaboratorium
Rep. S.445, Amsterdam, 1954.

COX, H.L.
"The Distortion of a Flat Rectangular Plate in its Own Plane".
A.R.C. Tech. Rep. R. & M. No. 2200, 1948.

COX, H.L.
"Buckling of Thin Plates in Compression".
A.R.C. Tech. Rep. R. & M. No. 1554, 1933.

COX, H.L., THURSTON, F.R. and COLEMAN, E.P.
"Compression Tests on Seven Panels of Monocoque Construction".
A.R.C. Tech. Rep. R. & M. No. 2042, 1945.

CRANDALL, S.H.
"Engineering Analysis".
McGraw Hill Book Co., 1956.

DUNCAN, J.P.
"Interferometry Applied to the Study of Elastic Flexure".
Proc. Inst. Mech. Engrs. Vol. 176, No. 16 pp.379-389, 1962.

DUNCAN, J.P. and MICHEJDA, O.

"Gridwork Rigidity Determined by Interferometry".

Proc. Inst. Mech. Engrs. Vol. 176, No. 16, pp.390-403, 1962.

DUNCAN, W.J.

"The Principles of Galerkin's Method".

A.R.C. Tech. Rep. R. & M. No. 1848, 1937.

FARRAR, D.J.

"Investigation of Skin Buckling".

A.R.C. Tech. Rep. R. & M. No. 2652, 1953.

FISHER, H.R.

"An Extension of Southwell's Method of Analysing Experimental Observations in Problem of Elastic Stability".

Proc. Roy. Soc. A. Vol. 144, p.625, 1934.

FRAZER, R.A., JONES, W.P. and SKAN, S.W.
"Approximations to Functions and to the Solutions of Differential Equations".
A.R.C. Tech. Rep. R. & M. No. 1799, 1937.

FRIEDRICHS, K.D. and STOKER, J.J.
"The Non-Linear Boundary Problem of the Buckled Plate".
Proc. of the Nat. Acad. of Sciences. Vol. 25, pp.535-540, 1939.

HARVEY, J.M.
"Studies on the Interaction of Plate Components of Structural Sections under Selected Load Conditions".
Ph.D. Dissertation Univ. of Glasgow, 1952.

HOFF, J.M., BOLEY, B.A. and COAN, J.M.
"The Development of a Technique for Testing Stiff Panels in Edgewise Compression".
Proc. Soc. Exp. Stress Analysis. Vol. V, No. II, pp.14-24, 1948.

HOUBOLT, J.C. and STOWELL, E.Z.
"Critical Stress of Plate Columns".
N.A.C.A. Rep. No. 2163.

HU, P.C. and McCULLOCH, J.C.
"The Local Buckling Strength of Lipped Z Columns with Small Lip Width".
N.A.C.A. Tech. Note No. 1335, 1947.

LEVY, S.
"Square Plates with Clamped Edges Under Normal Pressure Producing Large Deflections".
N.A.C.A. Rep. No. 740, 1942.

LUNDQUIST, E.E.
"Local Instability of Symmetrical Rectangular Tubes Under Axial Compression".
N.A.C.A. Tech. Note No. 686, 1939.

LUNDQUIST, E.E. and FLIGG, C.M.
"A Theory of Primary Failure of Straight Centrally Loaded Columns".
N.A.C.A. Tech. Note No. 582, 1937.

OSGOOD, W.R. and HOLT, M.
"The Column Strength of Two Extruded Aluminium Alloy H Sections".
N.A.C.A. Rep. No. 656, 1939.

REINITSHUBER, F.
"Calculation of Centrally Loaded Thin-Walled Columns above the Buckling Limit".
N.A.C.A. Tech. Mem. No. 1077, 1942.

SCHUETTE, E.H.
"Observations on the Maximum Average Stress of Flat Plates Buckled in Edge Compression".
N.A.C.A. Tech. Note No. 1625, 1949.

SHULESKO, P.
"Buckling of Rectangular Plates with Two Unsupported Edges".
Jour. of App. Mech. p.573, 1957.

SOKOLNIKOFF, I.S.
"Mathematical Theory of Elasticity".
McGraw Hill Book Co., 1946.

TODHUNTER and PEARSON.
"History of the Theory of Elasticity".
Vol. 1, 1886.

VAN DE VOOREN.
"Post Buckling Behaviour of Simply Supported Flat Panels that Change in Thickness Discontinuously in Cases Where Two Different Buckling Modes are Possible".
N.L.R. T.N. W17, 1961.

WANG, CHI-TEH.
"Non-Linear Large Deflection Boundary Value Problems of Rectangular Plates".
N.A.C.A. Tech. Note No. 1425, 1948.

WANG, CHI-TEH.
"Bending of Rectangular Plates with Large Deflections".
N.A.C.A. Tech. Note No. 1462, 1948.

WAY, S.
"Uniformly Loaded, Clamped, Rectangular Plates with Large Deflections".
Fifth Int. Congress. of App. Mech.
p.123, 1938.

WAY, S.

"Bending of Circular Plates with Large Deflections".

Trans. A.S.M.E. Vol. 56, p.627, 1934.

WITTRICK, W.H.

"Some Observations on the Compressive Buckling of Rectangular Plates".

Aero. Quart. Vol. XIV. Part 1, Feb. 1963.

ZIZICAS, G.A.

"Stability of Thin Elastic Plates Covering an Arbitrary Simply Connected Region and Subject to Any Admissable Boundary Conditions".

Jour. of App. Mech. Vol. 20, p.33, 1953.

A P P E N D I X I

APPENDIX I.

NOTES ON VARIOUS DIGITAL COMPUTING TECHNIQUES.

The services of the digital computer permitted the scope of the theoretical analysis in the plate investigation to cover the range investigated and was the means which rendered possible the prediction of the structural section collapse loads. In this appendix a description of the particular machine used is given together with some notes on the techniques used by the author to prepare programmes for it.

The machine used was a Ferranti "Sirius" which was housed in the Department of Mathematics at the Royal College of Science and Technology at Glasgow. This was a small and rather slow machine which had been designed for teaching purposes as well as for use on small commercial and scientific problems. The storage space was limited to 4000 words in the particular model at Glasgow and the storage medium was nickel delay lines. The speed of some 30 operations per second compared unfavour-:ably with the 750 - 1000 operations per second of the latest generation of computers. Input and output was effected by means of five hole punched paper tape, two input channels were provided but only one output channel.

There were two main programming "languages", i.e. Basic Code and Autocode. The latter was the one generally used since it automatically compiled and ranked the variables and also included all the more widely used subroutines such as the common algebraic and trigonometric functions. It had the awkward feature, however, that it occupied two thousand words of the store, that is to say, half the storage space was used before the programme was even entered into the machine. Of the remain-:ing half a portion had to be allocated to working space, i.e. the positions in which the active values were located. Thus it can be seen that when autocode was used, although a certain facility was obtained in designing the programme, the size of it was consider-:ably restricted. The way in which this was overcome in this investigation was to construct the programmes in autocode form in self-contained portions, develop these, compile, edit and reconstruct them.

Developing was the process whereby the mistakes in the programme were located and removed. This was often a complicated business since as the programmes included many loops and cycles then several conditions of the original algebraic equations had to be calcul-:ated by hand to check that the loops were performed in the correct sequence and with no carry-over. Com-:piling was carried out on the machine with the aid of a special programme, thus the machine read in autocode

instructions and printed out, on tape, the related basic language equivalents. The resulting basic code programme then probably had many redundant orders. The most common example of these was the continual allocation of values to a particular store. In the autocode form this could not be avoided but in the basic form much space and computing time could be saved by retaining that particular store in the working section of the machine.

When orders were deleted, however, the programme had been shortened and the loop loca-:tions had to be re-organised as also had several of the initial instructions. This process was known as editing and was completed by redeveloping the programme to check that no errors had been made in the compiling and editing as could easily happen. The space required by the individual programmes was then considerably reduced and so several could now be joined appropriately to form the complete programme. This was then put into "Primary Input" form, the reason for this being that in the basic language form it did not include the necessary sub-routines and these had to be entered in the machine separately every time the programme was used. The time spent on the con-:version to Primary Input form, a process carried out by the machine with the use of a special

programme, was amply repaid by the saving in time and trouble when the programme was being used.

Even after the procedures outlined above it was found that the expansion of the Galerkin equations (see Appendix IV) had to be computed in four parts. This required the printing out of intermediary results and, since it was impossible to ascertain before hand the magnitudes of these numbers, it was decided to print them as machine numbers so that no loss of accuracy would result. This required the construction of a special sub-:routine and the result was that the numbers were printed out as they were held in the machine, i.e. a block of ten figures, the first eight of which were the actual number and the remaining two being a measure of the position of the decimal point.

Similarly a new subroutine was necessary to read these numbers into the machine for the programme used in the next section of the problem which was the solution of the system of simultaneous equations. As indicated in Chapter II matrix algebra was used to reduce the system of equations to a set of simultaneous cubic equations the solution to which had to be obtained, in general, by employing approximate methods. This procedure is now outlined for the example case where there are three cubic equations.

In order to give the iterative process a good start selected values of the equation coefficients were solved exactly to give two of the three deflection series coefficients. These were then substituted into the first full cubic equation which was then solved to give the third coefficient. Taking this coefficient together with one of the approximate coefficients the second cubic was then solved to give a more accurate approximation to the other series co-:efficient. The third coefficient was obtained in a similar manner to get the first approximation to the deflection series. The cubics were solved using Horner's method and since this loop was used many times in the course of a solution it was made very efficient by careful design and editing.

The first approximations were then substituted into the first cubic and this solved, if the second approximation was the same as the first then this cubic had been exactly satisfied by the first approx-:imation and the solution for this series coefficient had been obtained. Since this was not generally the case the iterative cycling procedure was continued until an approximation was sufficiently close to the preceding one. The procedure was found to be rapid and stable.

This programme printed out the coefficients of the stress and deflection series. Further programmes designed and developed by the author enabled these results to be converted to stress, strain and deflection distributions over the plate surface.

A P P E N D I X I I

APPENDIX II.

ALTERNATIVE ASSUMED FORM OF THE STRESS FUNCTION IN THE GALERKIN SOLUTION.

One of the attributes of the Galerkin method is that it is convergent to the exact analytical solution no matter what form of terms are chosen for the series provided that they exactly satisfy the prescribed boundary conditions.

As an example of this property an alternative form was chosen for the terms in the stress function series in the ξ direction. Whereas in the main body of the thesis the terms were trig-:onometric in nature the ones derived in this appendix were polynomial. Examples of comparisons of the results obtained using each form are given at the end of the appendix and are discussed in Chapter V of this thesis.

The boundary conditions for the stress function in the ξ direction were found in Chapter II to be

$$\left[\frac{df_r(\xi)}{d\xi}\right]_{\xi=0,1} = 0 \quad \ldots\ldots \text{AII.1a.}$$

$$\left[f_r(\xi)\right]_{\xi=0,1} = 0 \quad \ldots\ldots \text{AII.1b.}$$

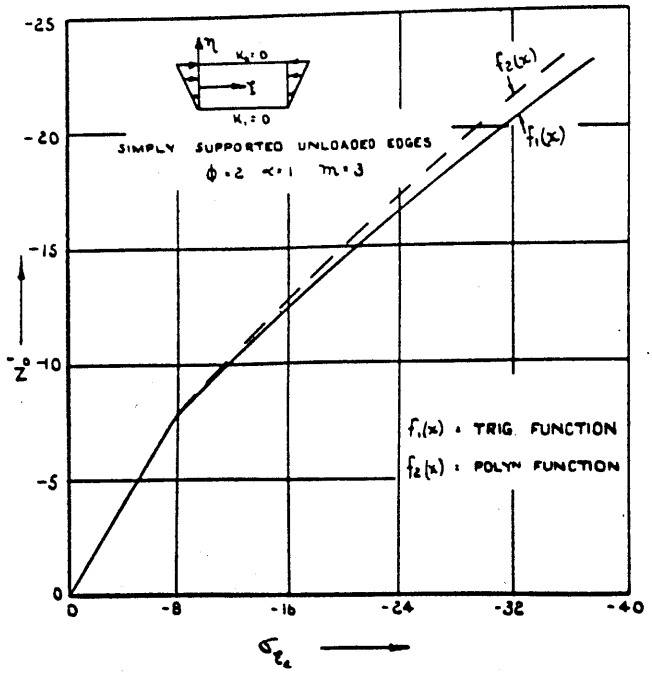

FIG. AII.1 LOAD Vs. EDGE STRESS

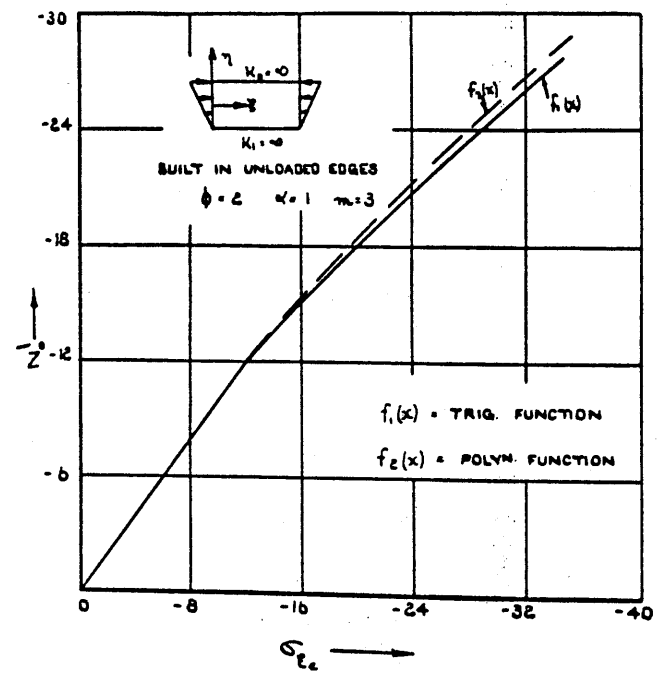

FIG. AII.2 LOAD Vs EDGE STRESS

For the $f_r(\xi)$ part of the series equation

$$F' = \frac{N'_0}{2}\left[\left(1-\frac{\alpha}{2}\right) + \frac{\alpha}{2}\eta\right]\eta^2 + \sum_r \sum_s b_{rs} f_r(\xi) g_s(\eta)$$

a polynomial was chosen, viz.,

$$f_r(\xi) = \xi^{r+4} + A_r \xi^{r+3} + B_r \xi^{r+2} + C_r \xi^{r+1} + D_r \xi^r \quad \ldots \text{ AII.2.}$$

where $r = 0, 1, 2,$ etc.

Application of conditions AII.1 to equation AII.2 gives

$$\left[(r+4)\xi^{r+3} + (r+3)A_r \xi^{r+2} + (r+2)B_r \xi^{r+1} + (r+1)C_r \xi^r + r D_r \xi^{r-1}\right]_{\xi=0,1} = 0$$

and

$$\left[\xi^{r+4} + A_r \xi^{r+3} + B_r \xi^{r+2} + C_r \xi^{r+1} + D_r \xi^r\right]_{\xi=0,1} = 0$$

which results in

$$C_r = D_r = 0 \qquad \text{and} \qquad A_r = -2 \;\; ; \;\; B_r = 1$$

Hence now the $f_r(\xi)$ is given by

$$f_r(\xi) = \left(\xi^{r+4} - 2\xi^{r+3} + \xi^{r+2}\right)$$

and the equivalent to equation II.4.4 is

$$F' = \frac{N'_0}{2}\left[\left(1-\frac{\alpha}{2}\right) + \frac{\alpha}{2}\eta\right]\eta^2 + \sum_{r=0,1,} \sum_{s=0,1,} b_{rs}\left(\xi^{r+4} - 2\xi^{r+3} + \xi^{r+2}\right)\left(\eta^{s+4} - \tfrac{1}{2}\eta^{s+2} + \tfrac{1}{16}\eta^s\right)$$

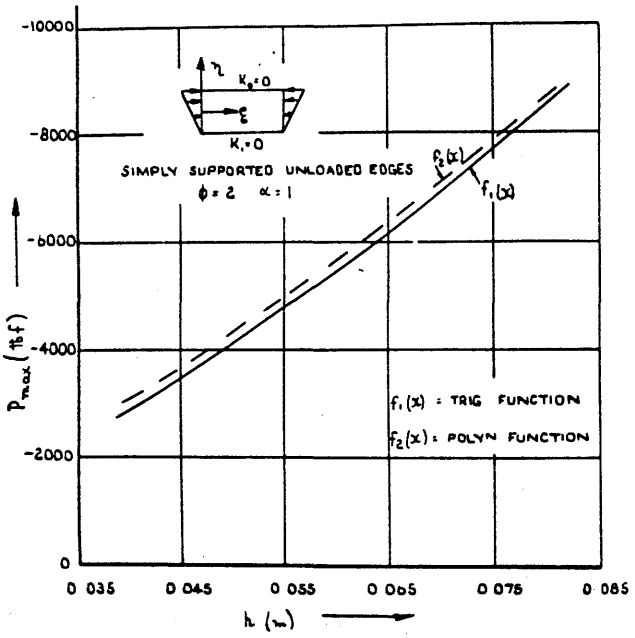

FIG. AII.2 COLLAPSE LOAD Vs PLATE THICKNESS

Figures AII.1 - AII.3 show example results obtained from this equation compared to those obtained using equation II.4.4.

A P P E N D I X I I I

APPENDIX III.

AN ALTERNATIVE METHOD OF SOLUTION OF THE BIHARMONIC EQUATION.

This appendix presents an alternative method for solving the biharmonic equation to determine the initial elastic instability loads of plates with various unloaded boundary conditions. In Chapter III a method of solution of this equation using Galerkin's method was given. It was seen from this that although the accuracy of the solution could be increased merely by increasing the number of terms included in the series the corresponding amount of arithmetic work involved was multiplied enormously. Thus it was almost imperative that the procedure be programmed for a digital computer even though only one plate geometry was being studied.

To provide a method of obtaining the instab-:ility loads of eccentrically loaded plates using only a desk calculator the solution now presented was developed. The principle of the method is to replace the infinitesimal elements of the differential equation by finite, but small, inter-:vals and thus reduce the problem to one of algebra.

It was shown in Chapter III that when instab-:ility was being studied then the general elastic

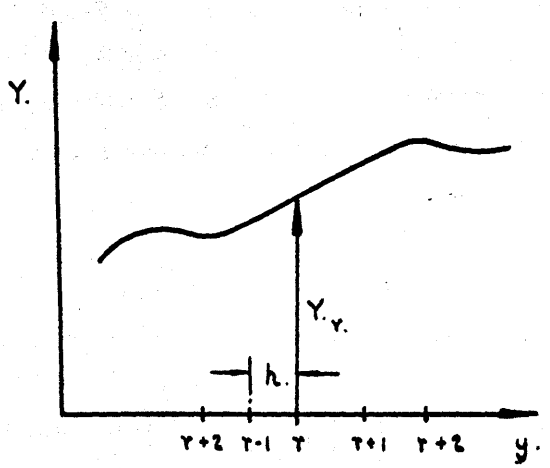

FIG. AIII.1

equations could be reduced to the biharmonic equation

$$\frac{1}{\phi^4}\frac{\partial^4\omega}{\partial\xi^4} + 2\frac{\partial^4\omega}{\partial\xi^2\partial\eta^2} + \phi^2\frac{\partial^4\omega}{\partial\eta^4} = \frac{N_o b^2}{D\phi^2}\left[(1-\tfrac{\alpha}{2}) + \alpha\eta\right]\frac{\partial^2\omega}{\partial\xi^2} \quad \text{AIII.1.}$$

Also it was shown that if the solution for a plate with simply supported loaded edges was taken in the form

$$\omega = \sin m\pi\xi \cdot Y \quad \text{AIII.2.}$$

where $Y = f(\eta)$ only and $m = 1, 2, 3,$ etc.

then equation AIII.1 could be further reduced to

$$\frac{d^4Y}{d\eta^4} - 2\frac{m^2\pi^2}{\phi^2}\cdot\frac{d^2Y}{d\eta^2} + \frac{m^4\pi^4}{\phi^4}Y = -k\cdot\frac{m^2\pi^2}{\phi^2}\left[(1-\tfrac{\alpha}{2}) + \alpha\eta\right]Y \quad \text{AIII.3.}$$

where $-k = -\frac{N_o b}{D}$ and $N_o \equiv N_{crit.}$

For simplicity of presentation equation AIII.2 is now written as

$$Y'' - 2GY'' + G^2Y = -kG\left[(1-\tfrac{\alpha}{2}) + \alpha\eta\right]Y \quad \text{AIII.4a.}$$

where

$$Y'' = \frac{d^4Y}{d\eta^4}\ ;\ Y'' = \frac{d^2Y}{d\eta^2}\ ;\ Y = f(\eta)\ ;\ G = \frac{m^2\pi^2}{\phi^2} \quad \text{AIII.4b.}$$

From the theory of finite differences (Fox, 1957) it can be shown that if h is the distance between consecutive pivotal points (see Figure AIII.1), r is any general point and ignoring sixth

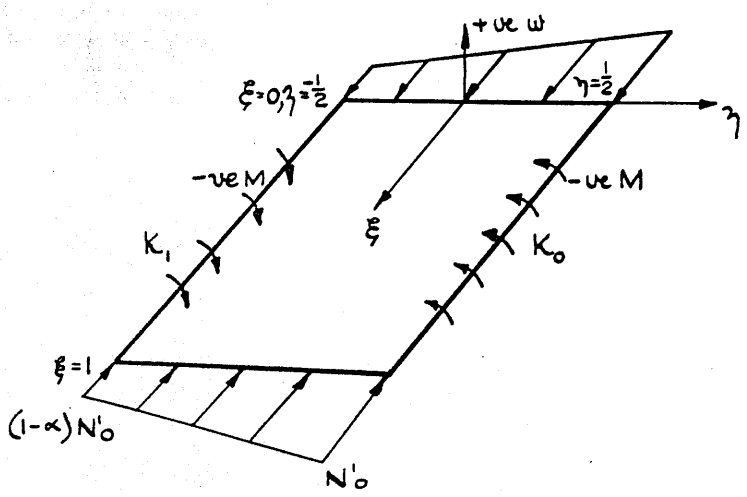

FIG. A III .2

and higher differences then

$$h^4 Y_r^{IV} = Y_{r+2h} - 4Y_{r+h} + 6Y_r - 4Y_{r-h} + Y_{r-2h} \quad \text{AIII.5a.}$$

$$h^2 Y_r'' = Y_{r+h} - 2Y_r + Y_{r-h} - \frac{1}{12}\left[Y_{r+2h} - 4Y_{r+h} + 6Y_r - 4Y_{r-h} + Y_{r-2h}\right] \quad \text{AIII.5b.}$$

Substituting equations AIII.4a and AIII.4b into equation AIII.3 and rearranging it is seen that

$$AY_{r-2h} + BY_{r-h} + CY_r + DY_{r+h} + EY_{r+2h} = 0 \quad \text{AIII.6.}$$

where

$$A = E = \left(1 + \frac{1}{6}h^2 G\right)$$

$$B = D = -\left(4 + \frac{8}{3}h^2 G\right)$$

$$C = \left\{6 + 5h^2 G + h^4 G^2 - \frac{1}{2} G h^4 \left[\left(1 - \frac{\alpha}{2}\right) + \alpha\eta\right]\right\}$$

Two conditions of plate unloaded edge boundary conditions will now be considered.

Case a Initially flat rectangular plate compressed by a linearly varying load action along two simply supported opposite edges and having equal or unequal rotational restraint along the other two edges (Figure AIII.2).

For the unloaded boundaries these conditions can be formulated as

$$\left[W\right]_{y=-\frac{b}{2},\frac{b}{2}} = 0$$

$$\left[M_y - r_1 \phi\right]_{y=-\frac{b}{2}} = 0$$

$$\left[M_y + r_0 \phi\right]_{y=\frac{b}{2}} = 0$$

where r_1, r_0 are the degrees of rotational restraint and ϕ is the slope of the plate middle plane in the y direction.

Transposing to non-dimensional terms the above conditions become

$$\left[\omega\right]_{\eta=-\frac{1}{2},\frac{1}{2}} = 0 \qquad \text{AIII.7a.}$$

$$\left[\frac{\partial^2\omega}{\partial\eta^2} + \frac{\nu}{\beta^2}\frac{\partial^2\omega}{\partial\xi^2}\right]_{\eta=-\frac{1}{2}} = K_1\left[\frac{\partial\omega}{\partial\eta}\right]_{\eta=-\frac{1}{2}} \qquad \text{AIII.7b.}$$

$$\left[\frac{\partial^2\omega}{\partial\eta^2} + \frac{\nu}{\beta^2}\frac{\partial^2\omega}{\partial\xi^2}\right]_{\eta=\frac{1}{2}} = -K_0\left[\frac{\partial\omega}{\partial\eta}\right]_{\eta=\frac{1}{2}} \qquad \text{AIII.7c.}$$

By taking equation AIII.2 into account and expressing in the terms defined in equations AIII.4b, equations AIII.7a and AIII.7c can be written as

$$Y_{\eta=\frac{1}{2}} = 0$$

$$(Y'' + K_0 Y')_{\eta=\frac{1}{2}} = 0$$

By using the finite difference approximations

$$h^2 Y_r'' = Y_{r+h} - 2Y_r + Y_{r-h} \quad \ldots\ldots \text{AIII.8a.}$$

$$h Y_r' = \tfrac{1}{2}(Y_{r+h} - Y_{r-h}) \quad \ldots\ldots \text{AIII.8b.}$$

where r is any typical pivotal point in the range it can be shown that the pivotal values around the boundary at $\eta = \frac{1}{2}$ are given by

$$Y_{\frac{1}{2}} = 0 \quad \ldots\ldots\ldots\ldots \text{AIII.9a.}$$

$$Y_{\frac{1}{2}+h} = \left[\frac{\frac{hK_0}{2} - 1}{\frac{hK_0}{2} + 1}\right] Y_{\frac{1}{2}-h} \quad \ldots\ldots \text{AIII.9b.}$$

It is a common feature in eigenvalue problems such as this one that the precise value of the dependant variable, in this case deflection, is indeterminable. For this reason the finite difference solution must be given "size", this is achieved by specifying a value for $Y_{\frac{1}{2}-h}$. From equation AIII.9b the corresponding value of $Y_{\frac{1}{2}+h}$ is obtained. If now values of $\frac{1}{k}$ and $Y_{\frac{1}{2}-2h}$ are

chosen arbitrarily it is possible by making use of equation AIII.6 to progressively integrate across the region and thus obtain the pivotal values around the boundary $\eta = -\frac{1}{2}$.

From equations AIII.7a and AIII.7b and using equation AIII.2 the specified conditions at this boundary can be written as

$$Y_{\eta=-\frac{1}{2}} = 0 \quad \ldots\ldots\ldots \text{AIII.10a.}$$

$$\left[Y'' - K_1 Y'\right]_{\eta=-\frac{1}{2}} = 0 \quad \ldots\ldots\ldots \text{AIII.10b.}$$

If after the integration process indicated above the conditions given by equations AIII.10 are fulfilled exactly this would mean that the correct values of k and $Y_{\frac{1}{2}-2h}$ had been chosen and the problem is solved. It would be a most fortunate circumstance, however, if in every instance these conditions were satisfied and since, in general, this is not the case some system of correction must be set up.

The values of $Y_{\eta=-\frac{1}{2}}$ and $(Y''-K_1Y')_{\eta=-\frac{1}{2}}$ are clearly functions of both k and $Y_{\frac{1}{2}-2h}$. If $Y_{\frac{1}{2}-2h}$ is denoted by p, $\frac{\partial Y}{\partial p}$ by q, $\frac{\partial Y}{\partial k}$ by z and $(Y''-K_1Y')_{\eta=-\frac{1}{2}}$, in finite difference terms, by E then the required correction can be obtained from a pair of simultaneous equations by using Newton's

iterative procedure, viz.,

$$Y_{-\frac{1}{2}} + \frac{\partial Y_{-\frac{1}{2}}}{\partial p}\,\delta p + \frac{\partial Y_{-\frac{1}{2}}}{\partial k}\,\delta k = 0 \quad . \quad . \quad . \quad . \text{AIII.11a.}$$

$$E + \frac{\partial E}{\partial p}\,\delta p + \frac{\partial E}{\partial k}\,\delta k = 0 \quad . \quad . \quad . \quad . \text{AIII.11b.}$$

Thus for the next cycle the values for the assumed parameters are given by $(k+\delta k)$ and $(p+\delta p)$.

In equation AIII.11b E is given by $(Y'' + K_1 Y')_{-\frac{1}{2}}$ hence

$$\frac{\partial E}{\partial p} = (q'' - K_1 q')_{-\frac{1}{2}}$$

and

$$\frac{\partial E}{\partial k} = (z'' - K z')_{-\frac{1}{2}}$$

i.e. equations AIII.11 can be expanded to the form

$$Y_{-\frac{1}{2}} + q_{-\frac{1}{2}}\,\delta p + z_{-\frac{1}{2}}\,\delta k = 0$$

$$\left[Y'' - K_1 Y'\right]_{-\frac{1}{2}} + \left[q'' - K_1 q'\right]_{-\frac{1}{2}}\delta p + \left[z'' - K_1 z'\right]_{-\frac{1}{2}}\delta k = 0$$

Thus in order to evaluate δp and δk the values of $q''_{-\frac{1}{2}}$, $q'_{-\frac{1}{2}}$, $q_{-\frac{1}{2}}$, $z''_{-\frac{1}{2}}$, $z'_{-\frac{1}{2}}$ and $z_{-\frac{1}{2}}$ must first be

evaluated.

Differentiating equation AIII.3 with respect to β the result is

$$q^{iv} - 2G\,q'' + G^2 q = -kG\left[(1-\tfrac{\alpha}{2}) + \alpha\eta\right]q \quad \ldots \text{AIII.12.}$$

which may be written in an analogous form to equation AIII.6 as

$$A\,q_{r-2h} + B\,q_{r-h} + C\,q_r + D\,q_{r+h} + E\,q_{r+2h} = 0$$

with the related boundary conditions as

$$q_{\frac{1}{2}+h} = 0 \qquad q_{\frac{1}{2}} = 0 \qquad q_{\frac{1}{2}-h} = 0 \qquad q_{\frac{1}{2}-2h} = 1$$

Since all four conditions are known at the outset it is an easy matter to integrate across the range and obtain, in finite difference terms, the required values of $q'_{-\frac{1}{2}}$, $q'_{-\frac{1}{2}}$ and $q_{-\frac{1}{2}}$.

Similarly for z; if equation AIII.3 is differ-:entiated with respect to k the result is

$$z^{iv} - 2Gz'' + G^2 z = -kG\left[(1-\tfrac{\alpha}{2}) + \alpha\eta\right]z + G\left[(1-\tfrac{\alpha}{2}) + \alpha\eta\right]Y$$

which may be formulated in finite difference terms as

$$A\,z_{r-2h} + B\,z_{r-h} + C\,z_r + D\,z_{r+h} + E\,z_{r+2} + F\,Y_r = 0$$

where A, B, C, D and E have the same values as in

equation AIII.6 and

$$F = -G\left[(1-\tfrac{\alpha}{2}) + \alpha\eta\right]$$

The relevant boundary conditions are

$$z_{\frac{1}{2}+h} = 0 \qquad z_{\frac{1}{2}} = 0 \qquad z_{\frac{1}{2}-h} = 0 \qquad z_{\frac{1}{2}-2h} = 0$$

Hence in a like manner to q the required values of $z''_{-\frac{1}{2}}$, $z'_{-\frac{1}{2}}$ and $z_{-\frac{1}{2}}$ are obtained in finite difference terms and from these using equation AIII.11 the values $\delta\phi$ and δk can now be obtained.

This cycling process is continued until $\delta\phi$ and δk became acceptably close to zero. To allow of the investigation of its convergence characteristics for various geometric boundary and loading conditions the iterative procedure outlined above was for the sake of convenience programmed by the author for the "Sirius" digital computer.

It was found that due to the power of Newton's method the convergence was rapid for all the con-:ditions investigated and with up to twenty five intervals in the range of integration. It may be seen, therefore, that the method also lends itself very well to a method of tabulation and calculation

using a desk calculator.

Given below are comparisons of the results of this method of solution with those obtained by previous workers.

k values obtained by the author using the method outlined above.

k' values obtained by the author using the Galerkin method (see Chapter III).

k^* values given by Lundquist and Stowell (1942)

k'' values given by Timoshenko (1961, Chap. 8)

Table 1 Comparison of values of k for a uniformly compressed plate simply supported along both unloaded edges. $K_1 = K_2 = 0 \quad \alpha = 0$

ϕ	0.4	0.8	1.1
k	82.984	41.461	39.791
k^*	83.003	41.468	39.834
k'	83.003	41.477	39.838

Table 2 Comparison of values of k for a uniformly compressed plate, elastically restrained equally along both unloaded edges.

$K_1 = K_2 = 4 \quad \alpha = 0$

ϕ	0.4	1.0	1.2
k	85.094	51.297	57.680
k^*	85.107	51.355	57.704
k'	85.056	51.365	57.791

Table 3 Comparison of values for k for a uniformly compressed plate, built-in along one unloaded edge and simply supported along the other. $K_1 = \infty \quad K_2 = 0 \quad \alpha = 0$

ϕ	0.6	0.8	1.0
k	58.249	53.179	56.379
k'	59.800	53.333	56.742
k''	58.405	53.393	56.653

Table 4 Comparison of values of k for eccentrically compressed plate, simply supported along both unloaded edges.

$K_1 = K_2 = 0 \quad \alpha = 1$

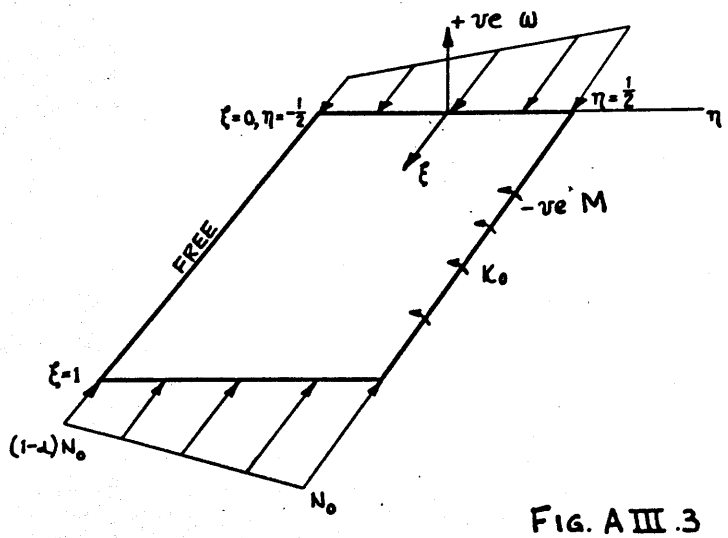

FIG. A III .3

ϕ	0.4	0.6	0.8	1.0
k	149.471	96.104	80.197	77.030
k''	149.030	95.735	79.944	76.938
k'	149.536	96.164	80.255	77.101

Case b Initially flat rectangular plate compressed by a linearly varying load action along two simply supported opposite edges and having one unloaded edge rotationally restrained and the other free (Figure AIII.3).

The solution for this type of plate is identical in every respect to that in Case a except that the boundary conditions at the free edge lead to slightly more complicated expressions.

It was shown in Chapter II that the conditions at the free edge may be formulated in non-dimensional terms as

$$\left[\frac{\partial^3\omega}{\partial\eta^3} + \frac{(2-\nu)}{\phi^2}\frac{\partial^3\omega}{\partial\eta\,\partial\xi^2}\right]_{\eta=-\frac{1}{2}} = 0$$

$$\left[\frac{\partial^2\omega}{\partial\eta^2} + \frac{\nu}{\phi^2}\frac{\partial^2\omega}{\partial\xi^2}\right]_{\eta=-\frac{1}{2}} = 0$$

which in the terms defined in equations AIII.4b may

be written as

$$\left[Y''' - G(2-\nu) Y' \right]_{\eta=-\frac{1}{2}} = 0$$

$$\left[Y'' - \nu G Y \right]_{\eta=-\frac{1}{2}} = 0$$

If these are now approximated to by the finite difference equations

$$h^3 Y_r''' = \tfrac{1}{2}\left[Y_{r+2h} - 2Y_{r+h} + 2Y_{r+h} - Y_{r-2h} \right]$$

$$h^2 Y_r' = Y_{r+h} - 2Y_r + Y_{r-h}$$

$$h Y_r' = \tfrac{1}{2}\left[Y_{r+h} - Y_{r-h} \right]$$

and redesignated M and N respectively then, analogous to equation AIII.11, the corrections to the assumed values of k and $Y_{\frac{1}{2}-2h}$ can be obtained from

$$M + \frac{\partial M}{\partial p}\delta p + \frac{\partial M}{\partial k}\delta k = 0 \quad \ldots\ldots \text{AIII.13a.}$$

$$N + \frac{\partial N}{\partial p}\delta p + \frac{\partial N}{\partial k}\delta k = 0 \quad \ldots\ldots \text{AIII.13b.}$$

From previous definition it is possible to write

$$\frac{\partial M}{\partial p} = q'''_{-\frac{1}{2}} - G(2-\nu) q'_{-\frac{1}{2}} \quad ; \quad \frac{\partial M}{\partial k} = z'''_{-\frac{1}{2}} - G(2-\nu) z'_{-\frac{1}{2}}$$

$$\frac{\partial N}{\partial p} = q''_{-\frac{1}{2}} - G\nu q_{-\frac{1}{2}} \quad ; \quad \frac{\partial N}{\partial k} = z''_{-\frac{1}{2}} - G\nu z_{-\frac{1}{2}}$$

Substituting these in equations AIII.13 the result is

$$\left[q''' - G(2-\nu)q'\right]_{-\frac{1}{2}} \delta p + \left[z''' - G(2-\nu)z'\right]_{-\frac{1}{2}} \delta k + \left[Y''' - G(2-\nu)Y'\right]_{-\frac{1}{2}} = 0$$

$$\left[q'' - G\nu q\right]_{-\frac{1}{2}} \delta p + \left[z'' - G\nu z\right]_{-\frac{1}{2}} \delta k + \left[Y'' - G\nu Y\right]_{-\frac{1}{2}} = 0$$

The required values of $z'''_{-\frac{1}{2}}$, $z'_{-\frac{1}{2}}$, $q'_{-\frac{1}{2}}$, etc. are found in finite difference terms as indicated previously for plate in Case a; the corrections δp and δk follow from equations AIII.14.

Again this iterative process was programmed for the digital computer and it was found to be rapidly convergent for the range of load geometries and boundary conditions investigated.

In tables 5, 6, 7 and 8 comparisons are made for sample values of k obtained by this method with the corresponding values found by previous workers.

k values obtained by the author using the method outlined above.

k' values obtained by the author using the Galerkin method (see Chapter III).

k'' values given by Timoshenko (1961, Chap. 8)

Table 5 Comparison of values of k for a uniformly compressed plate, simply supported along one unloaded edge, free along the other. $K_0 = 0 \quad \alpha = 0$

ϕ	1.0	1.4	1.5	2.0
k	14.144	9.404	8.737	6.962
k''	14.222	9.396	8.751	6.889
k'	14.154	9.400	8.764	6.888

Table 6 Comparison of values of k for a uniformly compressed plate, rotationally restrained along one unloaded edge and free along the other. $K_0 = 8 \quad \alpha = 0$

ϕ	1.0	1.5	2.0
k	15.530	11.392	11.087
k''	15.596	11.448	11.054
k'	15.573	11.411	11.099

Table 7 Comparison of values of k for an eccentrically loaded plate, built-in along one unloaded edge and free along the other. $K_0 = \infty \quad \alpha = 0.5$

ϕ	1.0	1.5	1.75	2.0
k	27.238	21.813	21.819	22.623
k'	27.316	21.793	21.807	22.690

Table 8 Comparison of values of k for an eccentrically loaded plate, elastically restrained along one unloaded edge and free along the other. $K_o = 4$ $\alpha = 1.0$

ϕ	1.0	1.5	1.75	2.0
k	54.286	42.326	41.080	41.313
k'	54.262	42.235	40.973	41.255

A P P E N D I X I V

EXPANSION OF THE GALERKIN INTEGRALS FOR PLATE INSTABILITY

TAKING $Y_m = q_m\left[\eta^{m+4} + A_m\eta^{m+3} + B_m\eta^{m+2} + C_m\eta^{m+1} + D_m\eta^m\right]$

AND $Y_i = q_i\left[\eta^{i+4} + A_i\eta^{i+3} + B_i\eta^{i+2} + C_i\eta^{i+1} + D_i\eta^i\right]$ AS TYPICAL TERMS OF THE GALERKIN SERIES FOR DEFLECTION THEN IT IS POSSIBLE TO WRITE THE EQUATION FOR INSTABILITY AS

$$\sum_{m=0,1}^{m=M}\int_{-\frac{1}{2}}^{\frac{1}{2}}\left\{\frac{d^4Y_m}{d\eta^4} - 2\frac{m^2\pi^2}{\phi^2}\frac{d^2Y_m}{d\eta^2} + \frac{m^4\pi^4}{\phi^4}Y_m - \frac{N_0b^2}{D}\cdot\frac{m^2\pi^2}{\phi^2}\left[(1-\alpha_2) + \alpha\eta\right]Y_m\right\}\frac{dY}{dq_i}d\eta = 0.$$

EXPANDING THIS EXPRESSION TERM BY TERM GIVES

$$\int_{-\frac{1}{2}}^{\frac{1}{2}} Y_m\frac{dY}{dq_i}d\eta = \int_{-\frac{1}{2}}^{\frac{1}{2}} q_m\left[\eta^{m+4} + A_m\eta^{m+3} + B_m\eta^{m+2} + C_m\eta^{m+1} + D_m\eta^m\right]\left[\eta^{i+4} + A_i\eta^{i+3} + B_i\eta^{i+2} + C_i\eta^{i+1} + D_i\eta^i\right]$$

$$= q_m\eta^{m+i}\left[\eta^8 + (A_m+A_i)\eta^7 + (B_m+A_mA_i+B_i)\eta^6 + (C_m+B_mA_i+A_mB_i+C_i)\eta^5 +\right.$$

$$+ (D_m+C_mA_i+B_mB_i+A_mC_i+D_i)\eta^4 + (D_mA_i+C_mB_i+B_mC_i+A_mD_i)\eta^3 + (D_mB_i+C_mC_i+B_mD_i)\eta^2 +$$

$$\left. + (D_mC_i+C_mD_i)\eta + D_mD_i\right]d\eta$$

TWO CONDITIONS MUST BE CONSIDERED WHEN INTEGRATING THE ABOVE EXPRESSION i.e. (i) WHEN $(m+i)$ IS EVEN ; (ii) WHEN $(m+i)$ IS ODD

(i) $K^1(=i+m)$ IS EVEN

$$\int_{-\frac{1}{2}}^{\frac{1}{2}} Y_m\frac{dY}{dq_i}d\eta = q_m\frac{1}{2^{K+8}}\left[\frac{1}{K+9} + \frac{4}{K+7}(B_i+A_mA_i+B_m) + \frac{16}{K+5}(D_m+C_mA_i+B_mB_i+A_mC_i+D_i) +\right.$$

$$\left. + \frac{64}{K+3}(D_mB_i+C_mC_i+B_mD_i) + \frac{256}{K+1}D_mD_i\right]$$

(ii) $K^1(=i+m)$ IS ODD

$$\int_{-\frac{1}{2}}^{\frac{1}{2}} Y_m\frac{dY}{dq_i}d\eta = q_m\frac{1}{2^{K+7}}\left[\frac{1}{K+8}(A_m+A_i) + \frac{4}{K+6}(C_m+B_mA_i+A_mB_i+C_i) + \frac{16}{K+4}(D_mA_i+C_mB_i+B_mC_i+A_mD_i) +\right.$$

$$+ \frac{64}{K'+2}(D_n C_i + C_n D_i)\Big]$$

SIMILARLY IT CAN BE SHOWN THAT :

(i) $K'(=n+i)$ IS EVEN

$$\int_{-\frac{1}{2}}^{\frac{1}{2}} \frac{d^2 Y_n}{d\eta^2}\frac{dY}{dq_i}\,d\eta = q_n \frac{1}{2^{K'+6}}\left\{\frac{1}{K'+7}(n+4)(n+3) + \frac{4}{K'+5}\left[(n+4)(n+3)B_i + (n+3)(n+2)A_i A_n + (n+1)(n+2)B_n\right] + \right.$$

$$+ \frac{16}{K'+3}\left[(n+4)(n+3)D_i + (n+3)(n+2)A_n C_i + (n+2)(n+1)B_n B_i + (n+1)n\,C_n A_i + n(n-1)D_n\right] + \frac{64}{K'+1}\left[(n+2)(n+1)B_n D_i + \right.$$

$$\left.\left. + (n+1)n\,C_n C_i + n(n-1)D_n B_i\right] + \frac{256}{K'-1}\,n(n-1)D_n D_i\right\}.$$

$$\int_{-\frac{1}{2}}^{\frac{1}{2}} \frac{d^3 Y_n}{d\eta^3}\cdot\frac{dY}{dq_i}\,d\eta = q_n \frac{1}{2^{K'+6}}\left\{\frac{1}{K'+5}(n+4)(n+3)(n+2)(n+1) + \frac{4}{K'+3}\left[(n+4)(n+3)(n+2)(n+1)B_i + (i+3)(i+2)(i+1)i\,A_n A_i + \right.\right.$$

$$+ (n+2)(n+1)n(n-1)B_n\Big] + \frac{16}{K'+1}\Big[(n+4)(n+3)(n+2)(n+1)D_i + (n+3)(n+2)(n+1)n\cdot A_n C_i + (n+2)(n+1)n(n-1)B_n B_i +$$

$$+ (i+1)n(n-1)(n-2)C_n A_i + n(n-1)(n-2)(n-3)D_n\Big] + \frac{64}{K'-1}\Big[(n+2)(n+1)n(n-1)B_n D_i + (n+1)n(n-1)(n-2)C_n C_i + n(n-1)(n-2)(n-3)D_n B_i\Big] +$$

$$\left. + \frac{256}{K'-3}\,n(n-1)(n-2)(n-3)D_n D_i\right\}.$$

$$\int_{-\frac{1}{2}}^{\frac{1}{2}} \eta\, Y_n \frac{dY}{dq_i}\,d\eta = q_n \frac{1}{2^{K'+8}}\left[\frac{1}{K'+9}(A_i + A_n) + \frac{4}{K'+7}(C_i + B_i A_n + A_i B_n + C_n) + \frac{16}{K'+5}(D_i A_n + C_i B_n + \right.$$

$$\left. + B_i C_n + A_n D_i) + \frac{64}{K'+3}(D_i C_n + C_i D_n)\right]$$

(ii) $K'(=n+i)$ IS ODD

$$\int_{-\frac{1}{2}}^{\frac{1}{2}} \frac{d^2 Y_n}{d\eta^2}\cdot\frac{dY}{dq_i}\,d\eta = q_n \frac{1}{2^{K'+5}}\left\{\frac{1}{K'+6}\left[(n+4)(n+3)A_i + (n+2)(n+2)A_n\right] + \frac{4}{K'+4}\left[(n+4)(n+3)C_i + (n+3)(n+2)A_n B_i + \right.\right.$$

$$(n+2)(n+1)B_n A_i + (n+1)n\,C_n\Big] + \frac{16}{K'+2}\Big[(n+2)(n+2)A_n D_i + (n+1)(n+1)B_n C_i + (n+1)n\,C_n B_i + n(n-1)D_n A_i\Big] +$$

$$\left. + \frac{64}{K'}\left[(n+1)n\,C_n D_i + n(n-1)D_n C_i\right]\right\}.$$

$$\int_{-\frac{1}{2}}^{\frac{1}{2}} \frac{d^n Y_n}{d\eta^n} \cdot \frac{dY}{dq_i}\, d\eta = q_n \frac{1}{2^{2n+2}} \left\{ \frac{1}{k^{1+4}} \left[(n+3)(n+2)(n+1)(n) A_n + (n+2)(n+1)(n) A_i \right] + \frac{4}{k^{1+2}} \left[(n+3)(n+2)(n+1)(n) C_i + \right.\right.$$

$$+ (n+2)(n+1)(n) A_n B_i + (n+1)(n)(n-1) B_n A_i + (n)(n-1)(n-2) C_n \Big] + \frac{16}{k^1} \Big[(n+2)(n+1)(n) A_n D_i +$$

$$\left.\left. + (n+1)(n)(n-1) B_n C_i + (n)(n-1)(n-2) C_n B_i + (n-1)(n-2)(n-3) D_n A_i \right] + \frac{64}{k^{1-2}} \left[(n)(n-1)(n-2) C_n D_i + (n-1)(n-2)(n-3) D_n C_i \right] \right\}$$

$$\int_{-\frac{1}{2}}^{\frac{1}{2}} \eta Y_n \frac{dY}{dq_i}\, d\eta = q_n \frac{1}{2^{2n+4}} \left[\frac{1}{k^{1+10}} + \frac{4}{k^{1+8}} (B_i + A_n A_i + B_n) + \frac{16}{k^{1+6}} (D_i + C_n A_i + B_i B_n + A_n C_i + D_n) \right.$$

$$\left. + \frac{64}{k^{1+4}} (D_i B_n + C_i C_n + B_i D_n) + \frac{256}{k^{1+2}} D_i D_n \right]$$

EXPANSION OF THE GALERKIN INTEGRALS FOR GENERAL ELASTIC EQUATIONS.

TAKING $F'_{rs} = b_{rs} \sin^2 r\pi\xi \left[\eta^{s+4} - \frac{1}{2}\eta^{s+2} + \frac{1}{16}\eta^s \right]$

$F'_{pq} = b_{pq} \sin^2 r\pi\xi \left[\eta^{s+4} - \frac{1}{2}\eta^{s+2} + \frac{1}{16}\eta^s \right]$

$\omega_{mn} = q_{mn} \sin m\pi\xi \left[\eta^{n+4} + A_n \eta^{n+3} + B_n \eta^{n+2} + C_n \eta^{n+1} + D_n \eta^n \right]$

$\omega_{mi} = q_{mi} \sin m\pi\xi \left[\eta^{i+4} + A_i \eta^{i+3} + B_i \eta^{i+2} + C_i \eta^{i+1} + D_i \eta^i \right]$

AS TYPICAL TERMS OF THE SERIES PARTS OF

$$F' = \frac{N'_0}{2}\left[(1 - \tfrac{\alpha}{2}) + \tfrac{\alpha}{3}\eta \right]\eta^2 + \sum_{r=1,2,}^{r=\xi} \sum_{s=0,1,}^{s=4} b_{rs} \sin r\pi\xi \left[\eta^{s+4} - \tfrac{1}{2}\eta^{s+2} + \tfrac{1}{16}\eta^s \right]$$

$$\omega = \sin m\pi\xi \sum_{n=0,1,}^{n=\ell} q_{mn} \left[\eta^{n+4} + A_n \eta^{n+3} + B_n \eta^{n+2} + C_n \eta^{n+1} + D_n \eta^n \right]$$

THEN THE LARGE DEFLECTION EQUATIONS MAY BE WRITTEN AS

$$\sum_{m=0,1,}^{m=\ell} \sum_{r=1,2,}^{r=\xi} \sum_{s=0,1,}^{s=4} \int_0^1 \int_{-\frac{1}{2}}^{\frac{1}{2}} \left[\frac{1}{\phi^4} \frac{\partial^8 F'_{rs}}{\partial \xi^8} + 2 \frac{\partial^6 F'_{rs}}{\partial \xi^4 \partial \eta^2} + \phi^4 \frac{\partial^4 F'_{rs}}{\partial \eta^4} - \left(\frac{\partial^2 \omega_{mn}}{\partial \xi \partial \eta} \right)^2 - \frac{\partial^2 \omega_{mn}}{\partial \xi^2} \cdot \frac{\partial^2 \omega_{mn}}{\partial \eta^2} \right] \frac{dF'}{db_{pq}} \, d\eta \, d\xi = 0$$

$$\sum_{m=0,1,}^{m=\ell} \sum_{r=1,2,}^{r=\xi} \sum_{s=0,1,}^{s=4} \int_0^1 \int_{-\frac{1}{2}}^{\frac{1}{2}} \left[\frac{1}{\phi^4} \frac{\partial^8 \omega_{mn}}{\partial \xi^8} + 2 \frac{\partial^6 \omega_{mn}}{\partial \xi^4 \partial \eta^2} + \phi^4 \frac{\partial^4 \omega_{mn}}{\partial \eta^4} - 12(1-\nu^2) \left(\frac{\partial^2 F'_{rs}}{\partial \eta^2} \cdot \frac{\partial^2 \omega_{mn}}{\partial \xi^2} + \right. \right.$$

$$\left. \left. + \frac{\partial^2 F'_{rs}}{\partial \eta^2} \cdot \frac{\partial^2 \omega_{mn}}{\partial \xi^2} + \frac{\partial^2 F'_{rs}}{\partial \xi^2} \cdot \frac{\partial^2 \omega_{mn}}{\partial \eta^2} - 2 \frac{\partial^2 F'_{rs}}{\partial \xi \partial \eta} \cdot \frac{\partial^2 \omega_{mn}}{\partial \xi \partial \eta} \right) \right] \frac{d\omega}{dq_{mi}} \, d\eta \, d\xi = 0$$

WHERE $F'_s = \frac{N'_0}{2}\left[(1 - \frac{\alpha}{2}) + \frac{\alpha}{3}\eta \right]\eta^2$

BY TAKING THE ABOVE DIFFERENTIAL EQUATIONS TERM BY TERM, EXPANDING AND INTEGRATING THEM, THE FOLLOWING EXPRESSIONS WERE OBTAINED.

$$\int_0^1\int_{-\frac{1}{2}}^{\frac{1}{2}} \frac{\partial^r F_{rs}'}{\partial \xi^r} \frac{dF'}{db_{pq}}\, d\eta\, d\xi = b_{rs}\, f_1(\xi)\, g_1(\eta)$$

WHERE $f_1(\xi) = \begin{cases} 2\pi^{r+1} & \text{IF } r = p \\ 0 & \text{IF } r \neq p \end{cases}$

AND IF $K=(s+q)$ IS ODD $g_1(\eta) = 0$

AND IF $K=(s+q)$ IS EVEN $g_1(\eta) = \frac{1}{2^{K+10}}\left[\frac{4}{K+9} - \frac{16}{K+7} + \frac{24}{K+5} - \frac{16}{K+3} + \frac{4}{K+1}\right]$

$$\int_0^1\int_{-\frac{1}{2}}^{\frac{1}{2}} \frac{\partial^r F_{rs}'}{\partial \xi^r \partial \eta^s} \frac{dF'}{db_{pq}}\, d\eta\, d\xi = b_{rs}\, f_2(\xi)\, g_1(\eta)$$

WHERE $f_2(\xi) = \begin{cases} -\frac{r^2\pi}{2} & \text{IF } r = p \\ 0 & \text{IF } r \neq p \end{cases}$

AND IF $K (= s+q)$ IS ODD THEN $g_2(\eta) = 0$

AND IF $K (= s+q)$ IS EVEN THEN $g_2(\eta) = \frac{1}{2^{K+6}}\left[\frac{1}{K+7}(s+4)(s+3) - \frac{2}{K+5}\left[(s+2)(s+1) + (s+4)(s+3)\right] + \frac{1}{K+3}\left[s(s-1) + \right.\right.$

$\left.\left. + 4(s+2)(s+1) + (s+4)(s+3)\right] - \frac{2}{K+1}\left[s(s-1) + (s+2)(s+1)\right] + \frac{1}{K-1}\, s(s-1)\right]$

$$\int_0^1\int_{-\frac{1}{2}}^{\frac{1}{2}} \frac{\partial^s F_{rs}'}{\partial \eta^s} \frac{dF'}{db_{pq}}\, d\eta\, d\xi = b_{rs}\, f_3(\xi)\, g_2(\eta)$$

WHERE $f_3(\xi) = \begin{cases} 3/8 & \text{IF } r = p \\ 1/4 & \text{IF } r = p \end{cases}$

AND IF $K(=s+q)$ IS ODD THEN $g_2(\eta) = 0$

AND IF $K (= s+q)$ IS EVEN THEN $g_2(\eta) = \frac{1}{2^{K+4}}\left[\frac{1}{K+5}(s+4)(s+3)(s+2)(s+1) - \frac{2}{K+3}\left[(s+4)(s+3)(s+2)(s+1) + \right.\right.$

$\left.\left. + (s+2)(s+1)s(s-1)\right] + \frac{1}{K+1}\left[(s-1)(s-2)(s-3) + 2(s+2)(s+1)s(s-1) + (s+4)(s+2)(s+2)(s+1)\right] - \frac{2}{K-1}\left[s(s-1)(s-2)(s-3) + (s+2)(s+1)s(s-1)\right] + \right.$

$\left. + \frac{1}{K-3}\, s(s-1)(s-2)(s-3)\right]$

$$\int_0^1\int_{-\frac{1}{2}}^{\frac{1}{2}} \frac{\partial^2 \omega_{mn}}{\partial \xi\, \partial \eta}\, \frac{dF'}{db_{pq}}\, d\eta\, d\xi = q_{mn} q_{ni}\, f_4(\xi)\, g_4(\eta)$$

WHERE $f_4(\xi) = \frac{m^2\pi^2}{6}$ IF $m=p$

$\frac{m^2\pi^2}{4}$ IF $m \neq p$

AND IF $K''\,(=n+i+q)$ IS ODD THEN $g_4(\eta) = \frac{1}{2^{K''+9}}\left\{\frac{1}{K''+10}\left[(n+3)(i+4)A_n + (n+4)(i+3)A_i\right] + \right.$

$+\frac{1}{K''+8}\left[4\left[(n+1)(i+4)C_n + (n+2)(i+3)B_nA_i + (n+3)(i+2)A_nB_i + (n+4)(i+1)C_i\right] - 2\left[(n+3)(i+4)A_n + (n+4)(i+3)A_i\right]\right] +$

$+\frac{1}{K''+6}\left[16\left[n(i+4)D_n + (n+1)(i+3)C_nA_i + (n+2)(i+2)B_nB_i + (n+3)(i+1)A_nC_i + (n+4)iD_i\right] - 8\left[(n+1)(i+4)C_i + \right.\right.$

$\left.\left.+(n+2)(i+3)B_nA_i + (n+3)(i+2)A_nB_i + (n+4)(i+1)C_i\right] + \left[(n+3)(i+4)A_n + (n+4)(i+3)A_i\right]\right] + \frac{1}{K''+4}\left[64\left[n(i+1)D_nC_i + \right.\right.$

$\left.\left.+(n+1)iC_nD_i\right] - 32\left[n(i+3)D_nA_i + (n+1)(i+2)C_nB_i + (n+2)(i+3)B_nC_i + (n+3)iA_nD_i\right] + 4\left[(n+1)(i+4)C_n + \right.$

$\left.+(n+2)(i+3)B_nA_i + (n+3)(i+2)A_nB_i + (n+4)(i+1)C_i\right]\right] - \frac{1}{K''+2}\left[128\left[n(i+1)D_nC_i + (n+1)iC_nD_i\right] - 32\left[n(i+3)D_nA_i + \right.\right.$

$\left.\left.+(n+1)(i+2)C_nB_i + (n+2)(i+1)B_nC_i + (n+3)iA_nD_i\right]\right] + \frac{1}{K''}\left[64\left[n(i+1)D_nC_i + (n+1)iC_nD_i\right]\right]\Bigg\}$

AND IF $K''\,(=n+i+q)$ IS EVEN THEN $g_4(\eta) = \frac{1}{2^{K''+10}}\left\{\frac{1}{K''+11}\left[(n+4)(i+4)\right] + \frac{1}{K''+9}\left[4\left[(n+2)(i+4)B_n + \right.\right.\right.$

$\left.\left.\left.+(n+3)(i+3)A_nA_i + (n+4)(i+2)B_i\right] - 2(n+4)(i+4)\right] + \frac{1}{K''+7}\left[16\left[n(i+4)D_n + (n+1)(n+3)C_nA_i + (n+2)(i+2)B_nB_i + \right.\right.$

$\left.\left.+(n+3)(i+1)A_nC_i + (n+4)iD_i\right] - 8\left[(n+2)(i+4)B_n + (n+3)(i+3)A_nA_i + (n+4)(i+2)B_i\right] + (n+4)(i+4)\right] + \frac{1}{K''+5}\left[64\left[n(i+2)D_nB_i + \right.\right.$

$\left.\left.+(n+1)(i+1)C_nC_i + (n+2)iB_nD_i\right] - 32\left[n(i+4)D_n + (n+1)(i+3)C_nA_i + (n+2)(i+2)B_nB_i + (n+3)(i+1)A_nC_i + \right.\right.$

$\left.\left.+(n+4)iD_i\right] + 4\left[(n+2)(i+4)B_n + (n+3)(i+3)A_nA_i + (n+4)(i+2)B_i\right]\right] + \frac{1}{K''+3}\left[256\,ni\,D_nD_i - 128\left[n(i+2)D_nB_i + \right.\right.$

$\left.\left.+(n+1)(i+1)C_nC_i + (n+2)iB_nD_i\right] + 16\left[n(i+4)D_n + (n+1)(i+3)C_nA_i + (n+2)(i+2)B_nB_i + (n+3)(i+1)A_nC_i + \right.\right.$

$$+ (n+4)\lambda\, D_\lambda \Big]\Big] - \frac{1}{K^{11}+1}\Big[512\, n\lambda\, D_n D_\lambda - 64\Big[n(\lambda+2)\, D_n B_\lambda + (n+1)(\lambda+1) A_n A_\lambda + (n+2)\lambda\, B_n D_\lambda\Big]\Big] + \frac{256}{K^{11}-1}\, n\lambda\, D_n D_\lambda\Big\}$$

$$\int_0^1 \int_{-\frac{1}{2}}^{\frac{1}{2}} \frac{\partial^2 \omega_{mn}}{\partial \xi^2} \cdot \frac{\partial^2 \omega_{m\lambda}}{\partial \eta^2} \cdot \frac{dF'}{db_{pq}}\, d\eta\, d\xi = q_{mn}\, q_{m\lambda}\, f_s(\xi)\, g_s(\eta)$$

$$\text{WHERE} \quad f_s(\xi) = \begin{cases} -\frac{3m^2\pi^2}{8} & \text{IF } m = p \\ -\frac{m^2\pi^2}{4} & \text{IF } m \neq p \end{cases}$$

AND IF K'' $(= n+\lambda+q)$ IS ODD THEN $g_s(\eta) = \frac{1}{2^{K''+9}}\Big\{\frac{1}{K''+10}\Big[(\lambda+4)(\lambda+3)A_n + (\lambda+2)(\lambda+2)A_\lambda\Big] +$

$$+ \frac{1}{K''+8}\Big[4\Big[(\lambda+4)(\lambda+3)C_n + (\lambda+3)(\lambda+2)B_n A_\lambda + (\lambda+2)(\lambda+1)A_n B_\lambda + (\lambda+1)\lambda\, C_\lambda\Big] - 2\Big[(\lambda+4)(\lambda+3)A_n + (\lambda+3)(\lambda+2)A_\lambda\Big]\Big] +$$

$$+ \frac{1}{K''+6}\Big[16\Big[(\lambda+3)(\lambda+2)D_n A_\lambda + (\lambda+2)(\lambda+1)C_n B_\lambda + (\lambda+1)\lambda\, B_n C_\lambda + \lambda(\lambda-1)A_n D_\lambda\Big] - 8\Big[(\lambda+4)(\lambda+3)C_n + (\lambda+3)(\lambda+2)B_n A_\lambda + (\lambda+2)(\lambda+1)A_n B_\lambda +$$

$$+ (\lambda+1)\lambda\, C_\lambda\Big] + \Big[(\lambda+4)(\lambda+3)A_n + (\lambda+3)(\lambda+2)A_\lambda\Big]\Big] + \frac{1}{K''+4}\Big[64\Big[(\lambda+1)\lambda\, D_n C_\lambda + \lambda(\lambda-1)\, C_n D_\lambda\Big] - 32\Big[(\lambda+3)(\lambda+2)D_n A_\lambda +$$

$$+ (\lambda+2)(\lambda+1)C_n B_\lambda + (\lambda+1)\lambda\, B_n C_\lambda + \lambda(\lambda-1)A_n D_\lambda\Big] + 4\Big[(\lambda+4)(\lambda+3)C_\lambda + (\lambda+3)(\lambda+2)B_n A_\lambda + (\lambda+2)(\lambda+1)A_n B_\lambda + (\lambda+1)\lambda\, C_\lambda\Big] -$$

$$- \frac{1}{K''+2}\Big[128\Big[(\lambda+1)\lambda\, D_n C_\lambda + \lambda(\lambda-1)\, C_n D_\lambda\Big] - 32\Big[(\lambda+3)(\lambda+2)D_n A_\lambda + (\lambda+2)(\lambda+1)C_n B_\lambda + (\lambda+1)\lambda\, B_n C_\lambda + \lambda(\lambda-1)A_n D_\lambda\Big]\Big] +$$

$$+ \frac{1}{K''}\Big[64\Big[(\lambda+1)\lambda\, D_n C_\lambda + \lambda(\lambda-1)\, C_n D_\lambda\Big]\Big]\Big\}$$

AND IF K'' $(= n+\lambda+q)$ IS EVEN THEN $g_s(\eta) = \frac{1}{2^{K''+10}}\Big\{\frac{1}{K''+11}\Big[(\lambda+4)(\lambda+3)\Big] + \frac{1}{K''+9}\Big[4\Big[(\lambda+4)(\lambda+3)\, B_n +$

$$+ (\lambda+3)(\lambda+2)\, A_n A_\lambda + (\lambda+2)(\lambda+1)B_\lambda\Big] - 2(\lambda+1)(\lambda+3)\Big] + \frac{1}{K''+7}\Big[16\Big[(\lambda+4)(\lambda+3)D_n + (\lambda+3)(\lambda+2)C_n A_\lambda + (\lambda+2)(\lambda+1)\, B_n B_\lambda +$$

$$+ (\lambda+1)\lambda\, A_n C_\lambda + \lambda(\lambda-1)\, D_\lambda\Big] - 8\Big[(\lambda+4)(\lambda+3)B_n + (\lambda+3)(\lambda+2)A_n A_\lambda + (\lambda+2)(\lambda+1)\, B_\lambda\Big]\Big] + \frac{1}{K''+5}\Big[64\Big[(\lambda+2)(\lambda+1)B_\lambda D_n +$$

$$+ (\lambda+1)\lambda\, C_n C_\lambda + \lambda(\lambda-1)\, B_n D_\lambda\Big] - 32\Big[(\lambda+4)(\lambda+3)D_n + (\lambda+3)(\lambda+2)C_n A_\lambda + (\lambda+2)(\lambda+1)B_n B_\lambda + (\lambda+1)\lambda\, A_n C_\lambda + \lambda(\lambda-1)D_\lambda\Big] +$$

$$+ 4\Big[(\lambda+4)(\lambda+3)\, B_n + (\lambda+3)(\lambda+2)\, A_n A_\lambda + (\lambda+2)(\lambda+1)\, B_\lambda\Big]\Big] + \frac{1}{K''+3}\Big[256\,\lambda(\lambda-1)D_n D_\lambda - 128\Big[(\lambda+2)(\lambda+1)D_n B_\lambda +$$

$$+(\lambda+1)\lambda\, C_m C_\lambda + \lambda(\lambda-1)\, B_m D_\lambda\Big] + 16\Big[(\lambda+4)(\lambda+3)D_m + (\lambda+3)(\lambda+2)C_m A_\lambda + (\lambda+2)(\lambda+1)B_m B_\lambda + (\lambda+1)\lambda\, A_m C_\lambda +$$

$$+\lambda(\lambda-1)\, D_\lambda\Big]\Big] - \frac{1}{K'+1}\Big[512\,\lambda(\lambda-1)\,D_m D_\lambda - 64\Big[(\lambda+2)(\lambda+1)D_m B_\lambda + (\lambda+1)\lambda\, A_m A_\lambda + \lambda(\lambda-1)B_m D_\lambda\Big] + \frac{256}{K'-1}\lambda(\lambda-1)D_m D_\lambda\Big\}$$

$$\int_0^{\xi}\int_{-\xi}^{\xi} \frac{\partial^n \omega_{mn}}{\partial \xi^n}\cdot\frac{d\omega}{dq_{m\lambda}}\, d\eta\, d\xi = q_{m_n} f_n(\xi)\, g_n(\eta) \qquad \text{WHERE} \quad f_n(\xi) = m_{\frac{n}{2}}\xi^n +$$

AND IF $K'=(n+\lambda)$ IS ODD THEN $g_6(\eta) = \frac{1}{2^{K'+7}}\Big[\frac{1}{K'+8}(A_m + A_\lambda) + \frac{4}{K'+6}(C_m + B_m A_\lambda + A_m B_\lambda + C_\lambda) +$

$$+\frac{16}{K'+4}(D_m A_\lambda + C_m B_\lambda + B_m C_\lambda + A_m D_\lambda) + \frac{64}{K'+2}(D_m C_\lambda + C_m D_\lambda)\Big]$$

AND IF $K'=(n+\lambda)$ IS EVEN THEN $g_6(\eta) = \frac{1}{2^{K'+8}}\Big[\frac{1}{K'+9} + \frac{4}{K'+7}(B_\lambda + A_m A_\lambda + B_m) + \frac{16}{K'+5}(D_m + C_m A_\lambda +$

$$+B_m B_\lambda + A_m C_\lambda + D_\lambda) + \frac{64}{K'+3}(D_m B_\lambda + C_m C_\lambda + B_m D_\lambda) + \frac{256}{K'+1} D_m D_\lambda\Big]$$

$$\int_0^{\eta}\int_{-\xi}^{\xi} \frac{\partial^n \omega_{mn}}{\partial \xi^2 \partial \eta^2}\,\frac{d\omega}{dq_{m\lambda}}\, d\eta\, d\xi = q_{m_n} f_7(\xi)\, g_7(\eta) \qquad \text{WHERE} \quad f_7(\xi) = -\frac{m_n \xi^2}{2}$$

AND IF $K'(=n+\lambda)$ IS ODD THEN $g_7(\eta) = \frac{1}{2^{K'+6}}\Big[\frac{1}{K'+6}\Big[(n+4)(n+3)A_\lambda + (n+3)(n+2)A_m\Big] + \frac{4}{K'+4}\Big[(n+4)(n+3)C_\lambda +$

$$+(n+3)(n+2)A_m B_\lambda + (n+2)(n+1)B_m A_\lambda + (n+1)n C_m\Big] + \frac{16}{K'+2}\Big[(n+3)(n+2)A_m D_\lambda + (n+2)(n+1)B_m C_\lambda + (n+1)n\, C_m B_\lambda +$$

$$+n(n-1)\, D_m A_\lambda\Big] + \frac{64}{K'}\Big[(n+1)n\, C_m D_\lambda + n(n-1)D_m C_\lambda\Big]\Big]$$

AND IF $K'(=n+\lambda)$ IS EVEN THEN $g_7(\eta) = \frac{1}{2^{K'+7}}\Big[\frac{1}{K'+7}(n+4)(n+3) + \frac{4}{K'+5}\Big[(n+4)(n+3)B_\lambda + (n+3)(n+2)A_\lambda A_m +$

$$+(n+1)(n+2)B_m\Big] + \frac{16}{K'+3}\Big[(n+4)(n+3)D_\lambda + (n+3)(n+2)A_m C_\lambda + (n+2)(n+1)B_m B_\lambda + (n+1)n\, C_m A_\lambda + n(n-1)D_m\Big] +$$

$$+\frac{64}{K'+1}\Big[(n+2)(n+1)B_m D_\lambda + (n+1)n\, C_m C_\lambda + n(n-1)D_m B_\lambda\Big] + \frac{256}{K'-1}\, n(n-1)\, D_m D_\lambda\Big]$$

$$\int_0^1 \int_{-\frac{1}{2}}^{\frac{1}{2}} \frac{\partial^4 \omega_{mn}}{\partial \eta^4} \frac{d^4 \omega}{dq_{mi}} \, d\eta \, d\xi = q_{mn} f_s(\xi) g_s(\eta) \quad \text{WHERE} \quad f_s(\xi) = \frac{1}{2}$$

AND IF $K'(=i+n)$ IS ODD THEN $g_s(\eta) = \frac{1}{2^{K'+3}} \Big[\frac{1}{K'+4} \big[(n+4)(n+3)(n+2)(n+1) A_n + (n+3)(n+2)(n+1) n A_i \big] +$

$+ \frac{4}{K'+2} \big[(n+4)(n+3)(n+2)(n+1) C_i + (n+3)(n+2)(n+1) n A_n B_i + (n+2)(n+1) n (n-1) B_n A_i + (n+1) n (n-1)(n-2) C_n \big] +$

$+ \frac{16}{K'} \big[(n+3)(n+2)(n+1) n A_n D_i + (n+2)(n+1) n (n-1) B_n C_i + (n+1) n (n-1)(n-2) C_n B_i + n (n-1)(n-2)(n-3) D_n A_i \big] +$

$+ \frac{64}{K'-2} \big[(n+1) n (n-1)(n-2) C_n D_i + n (n-1)(n-2)(n-3) D_n C_i \big] \Big]$

AND IF $K'(=i+n)$ IS EVEN THEN $g_s(\eta) = \frac{1}{2^{K'+4}} \Big[\frac{1}{K'+5} \big[(n+4)(n+3)(n+2)(n+1) \big] + \frac{4}{K'+3} \big[(n+4)(n+3)(n+2)(n+1) B_i +$

$+ (i+2)(i+2)(i+1) i A_n A_i + (n+2)(n+1) n (n-1) B_n \big] + \frac{16}{K'+1} \big[(n+4)(n+3)(n+2)(n+1) D_i + (n+3)(n+2)(n+1) n A_n C_i +$

$+ (n+2)(n+1) n (n-1) B_n B_i + (n+1) n (n-1)(n-2) C_n A_i + n (n-1)(n-2)(n-3) D_n \big] + \frac{64}{K'-1} \big[(n+2)(n+1) n (n-1) B_n D_i +$

$+ (n+1) n (n-1)(n-2) C_n C_i + n (n-1)(n-2)(n-3) D_n B_i \big] + \frac{256}{K'-3} n (n-1)(n-2)(n-3) D_n D_i \Big]$

$$\int_0^1 \int_{-\frac{1}{2}}^{\frac{1}{2}} \frac{\partial^2 F^*_{rs}}{\partial \eta^2} \cdot \frac{\partial^2 \omega_{mn}}{\partial \xi^2} \frac{d\omega}{dq_{mi}} \, d\eta \, d\xi = b_{rs} q_{mn} f_q(\xi) g_q(\eta)$$

$$\text{WHERE} \quad f_q(\xi) = \begin{cases} -\frac{3 m^2 n^2}{8} & \text{IF } m = r \\ -\frac{m^2 n^2}{4} & \text{IF } m \neq r \end{cases}$$

AND IF $K''(i+n+s)$ IS ODD THEN $g_q(\eta) = \frac{1}{2^{K''+9}} \Big[\frac{1}{K''+10} \big[(s+4)(s+3)(A_i + A_n) \big] +$

$+ \frac{1}{K''+8} \big[4 (s+4)(s+3)(C_n + C_i + A_n B_i + B_n A_i) - 2 (s+2)(s+1)(A_n + A_i) \big] + \frac{1}{K''+6} \big[s(s-1)(A_n + A_i) - 8 (s+2)(s+1)(C_n + C_i + A_i B_n + B_i A_n) +$

$+ 16 (s+4)(s+3)(B_n C_i + C_n B_i + A_n D_i + D_n A_i) \big] + \frac{1}{K''+4} \big[16 s(s-1)(C_n + C_i + B_n A_i + A_n B_i) - 128 (s+2)(s+1)(A_n D_i +$

$+ D_n A_i + B_n C_i + C_n B_i) + 256 (s+4)(s+3)(C_n D_i + D_n C_i) \big] + \frac{1}{K''+2} \big[64 s(s-1)(A_n D_i + D_n A_i + B_n C_i + C_n B_i) -$

$- 512 (s+2)(s+1)(C_n D_i + D_n C_i) \big] + \frac{1}{K''} \big[256 s(s-1)(C_n D_i + D_n C_i) \big] \Big]$

AND IF $K''(=\lambda+n+s)$ IS EVEN THEN $g_q(\eta) = \frac{1}{2^{K''+10}}\Big[\frac{1}{K''+11}(s+4)(s+3) +$

$+\frac{1}{K''+9}\Big[4(s+4)(s+3)(B_n+B_\lambda+A_nA_\lambda)-2(s+2)(s+1)\Big]+\frac{1}{K''+7}\Big[16(s+4)(s+3)(A_nC_\lambda+C_nA_\lambda+B_nB_\lambda+D_n+D_\lambda)\Big]-$

$-8(s+2)(s+1)(B_n+B_\lambda+A_nA_\lambda)+s(s-1)\Big]+\frac{1}{K''+5}\Big[64(s+4)(s+3)(B_nD_\lambda+D_nB_\lambda+C_nC_\lambda)-32(s+2)(s+1)(D_n+D_\lambda+$

$+A_nC_\lambda+C_nA_\lambda+B_nB_\lambda)+4s(s-1)(B_n+B_\lambda)\Big]+\frac{1}{K''+3}\Big[256(s+4)(s+3)D_nD_\lambda-128(s+2)(s+1)(B_nD_\lambda+D_nB_\lambda+$

$+C_nC_\lambda)+16s(s-1)(A_nC_\lambda+C_nA_\lambda+B_nB_\lambda+D_nD_\lambda)\Big]+\frac{1}{K''+1}\Big[64s(s-1)(B_nD_\lambda+D_nB_\lambda+C_nC_\lambda)-512(s+2)(s+1)D_nD_\lambda\Big]+$

$+\frac{1}{K''-1}\Big[256s(s-1)D_nD_\lambda\Big]\Big]$

$$\int_0^1\int_{-\frac{1}{2}}^{\frac{1}{2}}\frac{\partial^2F_c}{\partial\eta^2}\cdot\frac{\partial^2\omega_{mn}}{\partial\xi^2}\cdot\frac{d\omega}{dq_{m\lambda}}\,d\eta\,d\xi = q_{mn}\cdot N_0'\Big[(1-\tfrac{\alpha}{2})f_{10}(\xi)g_{10}(\eta)+\alpha f_{11}(\xi)g_{11}(\eta)\Big]$$

WHERE $f_{10}(\xi)=f_{11}(\xi)=-\frac{m^2\pi^2}{2}$ AND $g_{10}(\eta)=g_0(\eta)$

AND IF $K'(=\lambda+n)$ IS ODD THEN $g_n(\eta)=\frac{1}{2^{K'+9}}\Big[\frac{1}{K'+10}+\frac{4}{K'+8}(B_\lambda+A_n'A_\lambda+B_n)+$

$+\frac{16}{K'+6}(D_nA_\lambda+C_nB_\lambda+B_nC_\lambda+A_nD_\lambda)+\frac{64}{K'+4}(B_nD_\lambda+C_\lambda C_n+D_nB_\lambda)+\frac{256}{K'+2}D_\lambda D_n\Big]$

AND IF $K'(=\lambda+n)$ IS EVEN THEN $g_n(\eta)=\frac{1}{2^{K'+8}}\Big[\frac{1}{K'+9}(A_\lambda+A_m)+\frac{4}{K'+7}(C_\lambda+B_\lambda A_n+A_\lambda B_n+C_n)+$

$+\frac{16}{K'+5}(D_\lambda A_n+C_\lambda B_n+B_\lambda C_n+D_nA_\lambda)+\frac{64}{K'+3}(C_nD_\lambda+D_nC_\lambda)\Big]$

$$\int_0^1\int_{-\frac{1}{2}}^{\frac{1}{2}}\frac{\partial F_{12}'}{\partial\xi}\cdot\frac{\partial^2\omega_{mn}}{\partial\eta^2}\,\frac{d\omega}{dq_{m\lambda}}\,d\eta\,d\xi = b_{12}\cdot q_{mn}\cdot f_{12}(\xi)\,g_n(\eta)$$

WHERE $f_{12}(\xi)=\begin{cases}-\frac{\pi^2\pi^2}{2} & \text{IF } m=r\\ 0 & \text{IF } m\neq r\end{cases}$

AND IF $K''(=\lambda+n+s)$ IS ODD THEN $g_{12}(\eta)=\frac{1}{2^{K''+9}}\Big[\frac{1}{K''+10}\Big[(n+3)(n+2)A_n+(n+4)(n+3)A_\lambda\Big]+$

$$+\frac{1}{K^{n+8}}\Big[4\,n(n+1)C_n + 4(n+4)(n+3)C_\lambda + 4(n+2)(n+1)B_nA_\lambda + 4(n+3)(n+2)A_nB_\lambda - 2(n+3)(n+2)A_n - 2(n+4)(n+3)A_\lambda\Big] +$$

$$+\frac{1}{K^{n+6}}\Big[16(n+3)(n+2)A_nD_\lambda + 16\,n(n-1)D_nA_\lambda + 16(n+1)n\,C_nB_\lambda + 16(n+2)(n+1)B_nC_\lambda - 8(n+1)n\,C_n -$$

$$-8(n+4)(n+3)C_\lambda - 8(n+3)(n+2)A_nB_\lambda - 8(n+2)(n+1)B_nA_\lambda + (n+4)(n+3)A_\lambda + (n+3)(n+2)A_n\Big] +$$

$$+\frac{1}{K^{n+4}}\Big[64(n+1)n\,C_nD_\lambda + 64\,n(n-1)D_nC_\lambda - 32\,n(n-1)D_nA_\lambda - 32(n+3)(n+2)A_nD_\lambda - 32(n+1)n\,C_nB_\lambda -$$

$$-32(n+2)(n+1)B_nC_\lambda + 4(n+2)(n+1)B_nA_\lambda + 4(n+3)(n+2)A_nB_\lambda + 4(n+1)n\,C_n + 4(n+4)(n+3)C_\lambda\Big] +$$

$$+\frac{1}{K^{n+2}}\Big[16(n+3)(n+2)A_nD_\lambda + 16\,n(n-1)D_nA_\lambda + 16(n+2)(n+1)B_nC_\lambda + 16(n+1)n\,C_nB_\lambda - 128\,n(n-1)D_nC_\lambda -$$

$$-128(n+1)n\,C_nD_\lambda\Big] + \frac{64}{K^{n}}\Big[n(n-1)D_nC_\lambda + (n+1)n\,C_nD_\lambda\Big]\Big]$$

AND IF $K''(=\lambda+n+5)$ IS EVEN THEN $g_{12}(\gamma) = \frac{1}{2^{K''+10}}\Big[\frac{1}{K''+11}(n+4)(n+3) + \frac{1}{K''+9}\Big[4(n+2)(n+1)B_n +$

$$+4(n+4)(n+3)B_\lambda + 4(n+3)(n+2)A_nA_\lambda - 2(n+4)(n+3)\Big] + \frac{1}{K''+7}\Big[16(n+3)(n+2)A_nC_\lambda + 16(n+1)n\,C_nA_\lambda +$$

$$+16(n+2)(n+1)B_nB_\lambda + 16\,n(n-1)D_n + 16(n+4)(n+3)D_\lambda - 8(n+2)(n+1)B_n - 8(n+4)(n+3)B_\lambda -$$

$$-8(n+3)(n+2)A_nA_\lambda + (n+4)(n+3)\Big] + \frac{1}{K''+5}\Big[64(n+2)(n+1)B_nD_\lambda + 64\,n(n-1)D_nB_\lambda + 64(n+1)n\,C_nC_\lambda -$$

$$-32(n+3)(n+2)A_nC_\lambda - 32(n+1)n\,C_nA_\lambda - 32(n+2)(n+1)B_nB_\lambda - 32\,n(n-1)D_n - 32(n+4)(n+3)D_\lambda +$$

$$+4(n+3)(n+2)A_nA_\lambda + 4(n+2)(n+1)B_n + 4(n+4)(n+3)B_\lambda\Big] + \frac{1}{K''+3}\Big[256\,n(n-1)D_nD_\lambda - 128(n+2)(n+1)B_nD_\lambda -$$

$$-128\,n(n-1)D_nB_\lambda - 128\,n(n+1)C_nC_\lambda + 16(n+3)(n+2)A_nC_\lambda + 16(n+1)n\,C_nA_\lambda + 16\,n(n-1)D_n +$$

$$+16(n+4)(n+3)D_\lambda\Big] + \frac{1}{K''+1}\Big[64(n+2)(n+1)B_nD_\lambda + 64\,n(n-1)D_nB_\lambda + 64(n+1)n\,C_nC_\lambda - 512\,n(n-1)D_nD_\lambda\Big] +$$

$$+\frac{256}{K''-1}\,n(n-1)D_nD_\lambda\Big]$$

$$\int_0^1 \int_{-\frac{1}{2}}^{\frac{1}{2}} \frac{\partial^2 F_{rs}}{\partial \xi \partial \eta} \cdot \frac{\partial^2 \Omega_{mn}}{\partial \xi \partial \eta} \frac{d\omega}{dq_{mi}} d\eta d\xi = b_{ie}\, q_{mn}\, f_{ie}(\xi)\, g_{ie}(\eta)$$

WHERE $f_{ie}(\xi) = \begin{cases} \frac{m+n\pi^2}{2} & \text{IF } m=r \\ 0 & \text{IF } m \neq r \end{cases}$

AND IF $K''(=n+i+s)$ IS ODD THEN $g_{ie}(\eta) = \frac{1}{2^{K''+9}}\Big[\frac{1}{K''+10}\big[(s+4)(n+3)A_n + (s+4)(n+4)A_i\big] +$

$+ \frac{1}{K''+8}\big[4(s+4)(n+3)A_nB_i + 4(s+4)(n+2)B_nA_i + 4(s+4)(n+1)C_n + 4(s+4)(n+2)C_i - 2(s+2)(n+3)A_n -$

$- 2(s+2)(n+4)A_i\big] + \frac{1}{K''+6}\big[16(s+4)(n+3)A_nD_i + 16(s+4)n\,D_nA_i + 16(s+4)(n+2)B_nC_i + 16(s+4)(n+1)C_nB_i -$

$- 8(s+2)(n+3)A_nB_i - 8(s+2)(n+2)B_nA_i - 8(s+2)(n+1)C_n - 8(s+2)(n+4)C_i + 8(n+3)A_n +$

$+ 8(n+4)A_i\big] + \frac{1}{K''+4}\big[64(s+4)(n+1)C_nD_i + 64(s+4)n\,D_nC_i - 32(s+2)(n+3)A_nD_i - 32(s+2)n\,D_nA_i -$

$- 32(s+2)(n+2)B_nC_i - 32(s+2)(n+1)C_nB_i + 4s(n+3)A_nB_i + 4s(n+2)B_nA_i + 4s(n+1)C_n + 4s(n+4)C_i\big] +$

$+ \frac{1}{K''+2}\big[16s(n+3)A_nD_i + 16s.n.\,D_nA_i + 16s(n+2)B_nC_i + 16s(n+1)C_nB_i - 128(s+2)(n+1)C_nD_i -$

$- 128(s+2)n\,D_nC_i\big] + \frac{64}{K''}\big[s(n+1)C_nD_i + s.n.\,D_nC_i\big]\Big]$

AND IF $K''(=n+i+s)$ IS EVEN THEN $g_{ie}(\eta) = \frac{1}{2^{K''+10}}\Big[\frac{1}{K''+11}(s+4)(n+4) + \frac{1}{K''+9}\big[4(s+4)(n+3)A_nA_i +$

$+ 4(s+4)(n+2)B_n + 4(s+4)(n+4)B_i - 2(s+2)(n+4)\big] + \frac{1}{K''+7}\big[16(s+4)(n+3)A_nC_i + 16(s+4)(n+1)C_nA_i +$

$+ 16(s+4)(n+2)B_nB_i + 16(s+4)n\,D_n + 16(s+4)(n+4)D_i - 8(s+2)(n+2)A_nA_i - 8(s+2)(n+2)B_n - 8(s+2)(n+4)B_i +$

$+ 8(n+4)\big] + \frac{1}{K''+5}\big[64(s+4)(n+2)B_nD_i + 64(s+4)n\,D_nB_i + 64(s+4)(n+1)C_nC_i - 32(s+2)(n+3)A_nC_i -$

$- 32(s+2)(n+1)C_nA_i - 32(s+2)(n+2)B_nB_i - 32(s+2)n\,D_n - 32(s+2)(n+4)D_i + 4s(n+3)A_nA_i +$

$+ 4s(n+2)B_n + 4s(n+4)B_i\big] + \frac{1}{K''+3}\big[256(s+4)n\,D_nD_i - 128(s+2)(n+2)B_nD_i - 128(s+2)n\,D_nB_i -$

$$-128(s+2)(n+1)C_nC_\lambda + 16s(n+2)A_nC_\lambda + 16s(n+1)C_nA_\lambda + 16s(n+2)B_nB_\lambda + 16s.n\,D_n +$$

$$+16s(n+4)D_\lambda\Big] + \frac{1}{K^n+1}\Big[64s(n+2)B_nD_\lambda + 64s.n.D_nB_\lambda + 64s(n+1)C_nC_\lambda - 512(n+2)nD_nD_\lambda\Big] +$$

$$+\frac{256}{K^n-1}\,s.n.D_nD_\lambda\Big].$$

A P P E N D I X V

APPENDIX V.

PHOTOGRAMMETRIC METHOD OF DEFLECTION MEASUREMENT.

In order to assess the capabilities of the developed mathematical theory to predict accurately the deflected shape of a compressed plate it was necessary to determine the deflection distribution over the surface of sample test plates. Such distributions were also valuable for determining the accuracy with which the experimental boundary restraints reproduced the conditions for which they were designed. Since, in general, the more con-:ventional methods of deflection measurements, such as clock gauges, give values at separate widely spaced points it was necessary to construct special equipment embodying photogrammetric principles.

Photogrammetry is the science of measurement by means of photographic optical equipment. It has a very wide range of applications, from aiding the construction of maps by aerial stereoscopic photography to the study of very small deflections in flexed thick steel elastic plates. As high definition optical equipment becomes increasingly available more and more of these techniques are being developed for use in the various branches of engineering. These techniques of course all have their special advantages and corres-:ponding disadvantages; before proceeding to a descrip-

:tion of the equipment used in this investigation a brief resume of some examples of these engineering applications is now given.

In plates the force and moment resultants at any point may be expressed mathematically, for small deflections, in terms of the second derivatives of the deflection at that point. For complicated cases of plate geometry where an exact theoretical analysis is difficult, an experimental measure of deflection may facilitate the development of an accurate empirical approach. Duncan (1963) designed equipment for this task along the lines of that previously used by Salet (1939) and Ikeda (1951). In this the image of an illuminated target of spec-:ific design was projected on to the deflected model, a resulting image of the target was then reflected through a lens system and pinhole on to a photographic plate. By this method the lines recorded by the camera joined points of equal slope on the model, the direction and magnitude of the slope being specified by the target geometry.

A similar result to this was obtained by Ligtenberg (1955) and Palmer (1957) by using an application of the Moire fringe technique. In this method an image of a ruled target was reflected from the unloaded model through a pinhole on to a photographic plate. The model was then loaded and the resulting distorted target image again recorded photographically. The two photo-

:graphs when superimposed displayed a series of fringes which represented lines of equal change of slope; the magnitude and direction of which could be determined from the system geometry. These results were then either integrated geometri-:cally to give deflection or differentiated to give moments and forces. The disadvantages arise mainly from the lack of accuracy due to the diffi-:culty of determining the actual position of the fringes. They also suffer from the necessity of having a good reflecting model, a consideration which precludes the use of actual metal test plates, usually black perspex models are used.

A method which determines deflections directly and may also be used in experimental tests was that developed by Jackson & Hall (1947). This work dealt with the deformation of curved thin plates under axial loads. A vertical line-filament lamp used as a light source cast sharp shadows of grid wires on the surface of the specimen. The position of the lamp, wire grid, and the scale of the photographs were arranged in such a way that images of shadows were formed in straight lines and kept a constant distance, 0.5 mm, from the adjacent images of the wires. Under axial loading the plate deformed and the shadow of the curved grid would bend to the right if the vertical section of the specimen bent backwards. The photographs were measured over 0.5

Fig. AV.1.

inch centres and contours of the deflection were plotted.

This method has the disadvantages that expensive equipment is necessary to measure the photographs and also because of the inherent inaccuracies of the measuring process very small deflections cannot be determined precisely.

Description of Apparatus.

Since in this investigation it was necessary to use the actual test specimens and since large deflections were involved the obvious choice of technique to be used was the last one in the above section.

In this application the light sourse (Figure AV.1) was a 1 kw. line element lamp enclosed in a thin metal casing. The inside surface of this casing was carefully blacked out so that the only light emanating from the source was directly from the element, knife edged shutters were also fitted on the casing to allow adjustment to be made to the width of the beam and so minimising the amount of background illumination falling on to the specimen. Cooling was provided by blowing air through the casing and a variac was included in the light circuit thus extending the life of the lamp by using

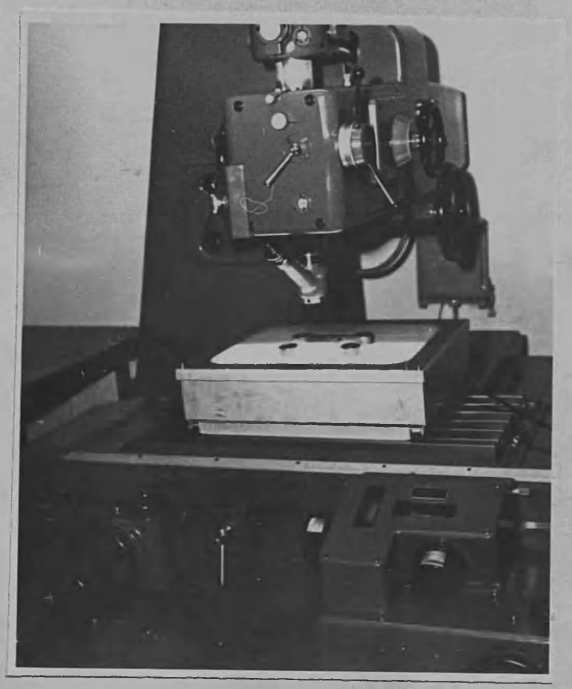

Fig. AV.2.

reduced power for setting up and full power only during an actual test.

Very fine shadows were obtained by using 0".005 diameter wire about 0".5 above the plate surface. The best results were obtained using ni-chrome which had a dull finish thus reflecting very little light on to the camera. The wire was arranged to form a grid with 0".5 between the lines by lacing it round pegs fitted in accurately machined metal strips which were screwed firmly on to each side of the loading rig.

The photographic recording equipment was a Micro-Technical camera with a Schneider-Kreuznach Symar lens of 150 mm focal length; Kodak P300 plates developed using Microdol-X were found to give a good image with little grain effect while maintaining a medium speed with a small aperture setting. The camera was mounted on a scaffolding at approximately 47" above the plate surface, the scaffolding also formed a framework over which black sheets were draped to exclude extraneous light.

The photographic records of the shadow horiz-:ontal movements on the test plates were measured on a Societe Genevoise Jig Borer (Figure AV.2). The plates were mounted and illuminated on the

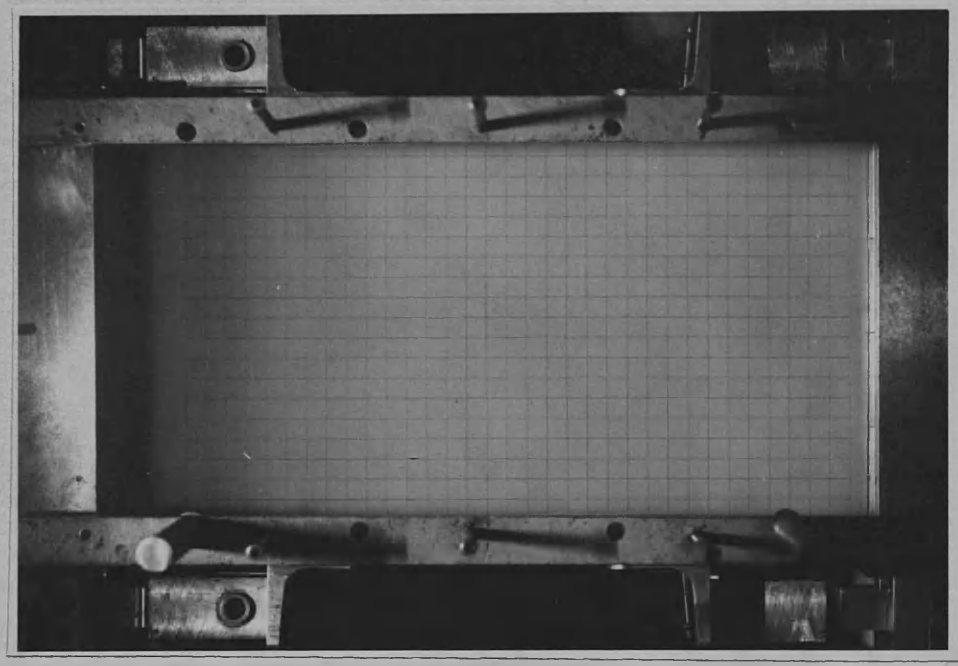

Fig. AV.3.

Direction of light. ⟶

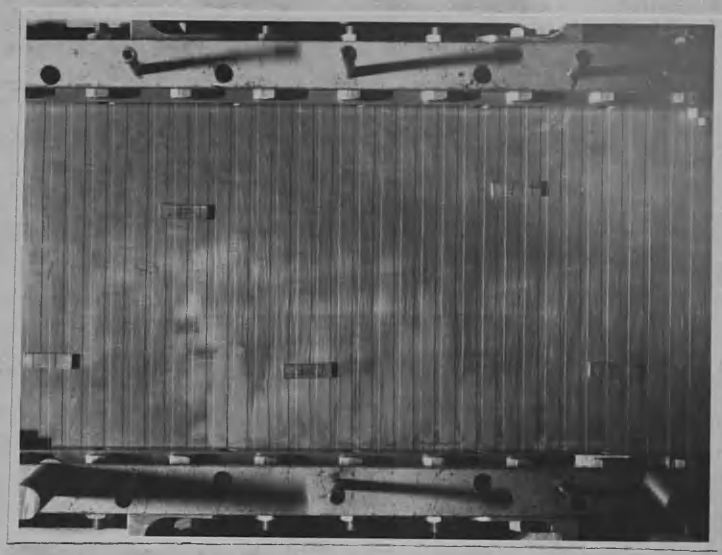

Fig. AV.4.

moveable machine table and viewed through the machine's standard graticuled microscope attach-:ment which gave a 12X magnification.

Calibration and Use of Equipment.

In order that the photographic measurements can be correlated to the test plate movements it was necessary to know the scale and, if any, distortion. In this equipment the calibration was performed as follows.

The camera was set up with the object glass perfectly level so that it was parallel to the previously levelled test rig. A perspex sheet which had a grid marked on it was placed in the rig instead of a specimen and photographed (Figure AV.3). The grid was of 0"5 pitch and had been engraved using a vernier stand, it was sub-:sequently measured on the jig borer. The photo-:graphic plate was then measured and the results compared to the actual sizes. It was found that the scale was 7.14 and that when a small aperture was used there was no discernable aberration across that portion of the lens. In order to reduce the error introduced by distortion of the photographic plates care was taken at all times that they were not subjected to temperatures outwith the range of 65-70^{o}F. It was also found that with care and

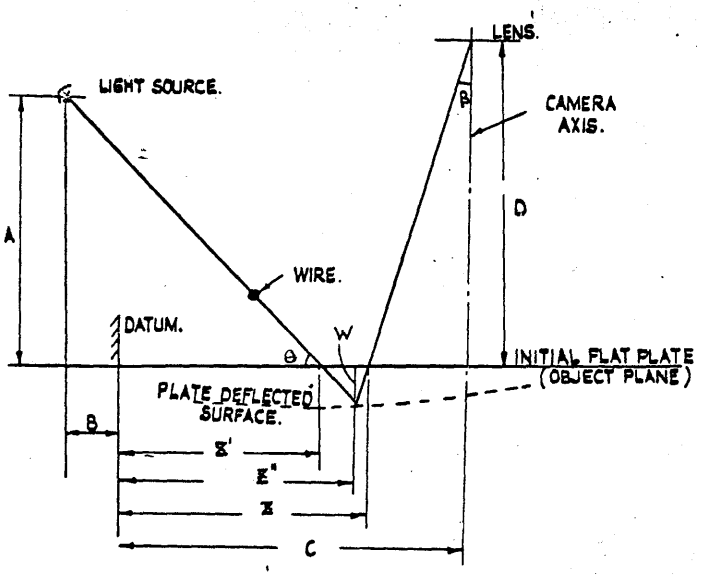

REQUIRED : W & Z'

MEASURED ON PHOTOGRAPHS: Z' & Z

CONSTANT DIMENSIONS : A (56'.25) ; B (47'.875); C (9'.4) ; D (18'.675); PHOTO. SCALE (7·14.)

FIG. AV.5 OPTICAL SYSTEM GEOMETRY.

practice it was possible to measure differences of 0".0002 on the photographic plate. A measure of the accuracy of the whole equipment was assessed using Johansson slip gauges of known size (0".145) on the surface of the test specimen and obtaining the deflection indicated by the shadows of the wires (Figure AV.4). The resulting variation of about ± 1% was taken as very satisfactory.

System Geometry.

Figure AV.5 shows the system geometry for a specimen wire. The convention is that if the wire is to the left of the camera axis then angle β is taken as positive, if it is to the right then β is negative, upwards deflections of the plate are taken as positive, downwards deflections are negative. It will be seen therefore that there are four com-:binations of systems which must be considered. It was found, however, that these may be calculated using

$$w' = \frac{\tan\theta \cdot Mod(z'-z)}{1 + \tan\beta \tan\theta}$$

with $w = -w'$ if $z' > z$

and $w = w'$ if $z' < z$

$$z'' = z + w \tan\beta .$$

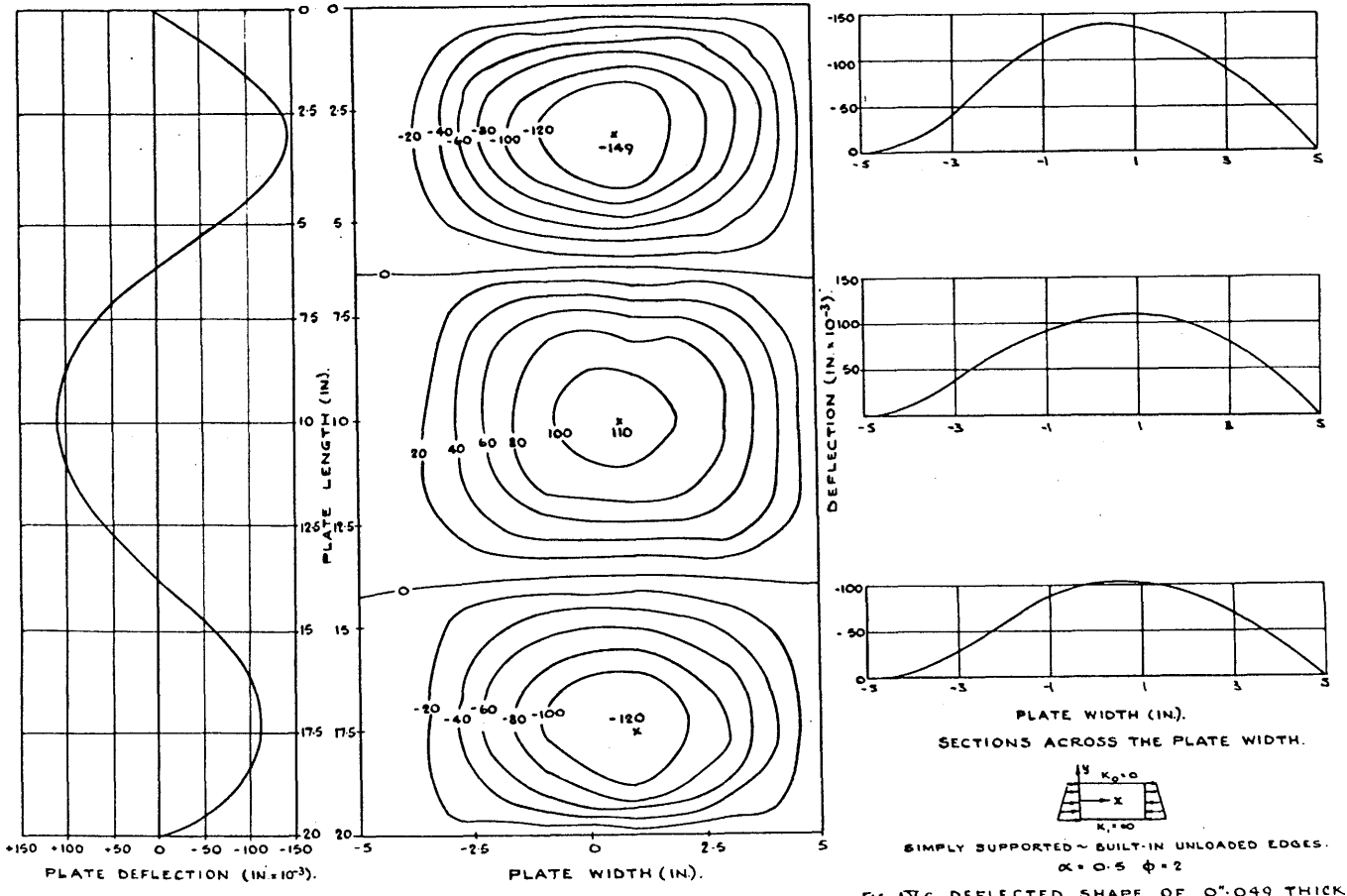

LONGITUDINAL SECTION THROUGH PLATE AT y = 0.

FIG. AV.6 DEFLECTED SHAPE OF 0".049 THICK PLATE AT A LOAD OF 5090 lb. f.

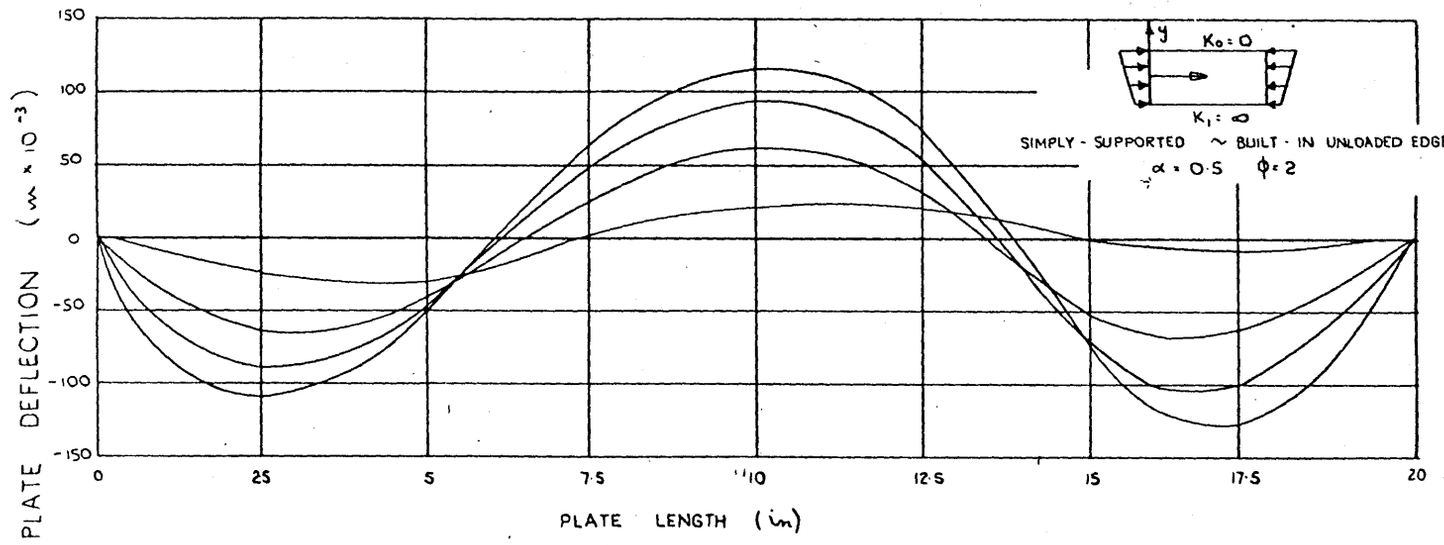

FIG. AV.7 SECTION THROUGH A 0".049 THICK PLATE AT VARIOUS LOADS

Direction of light.

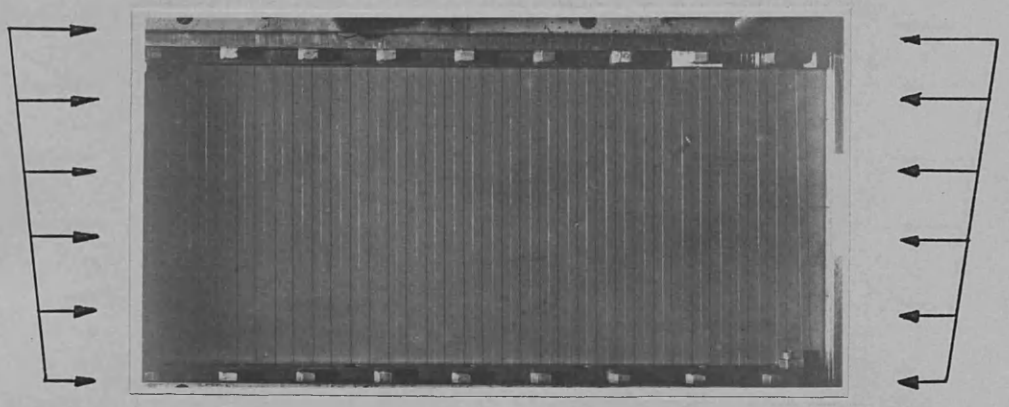

Fig. AV.8 Load = 0 lbf.

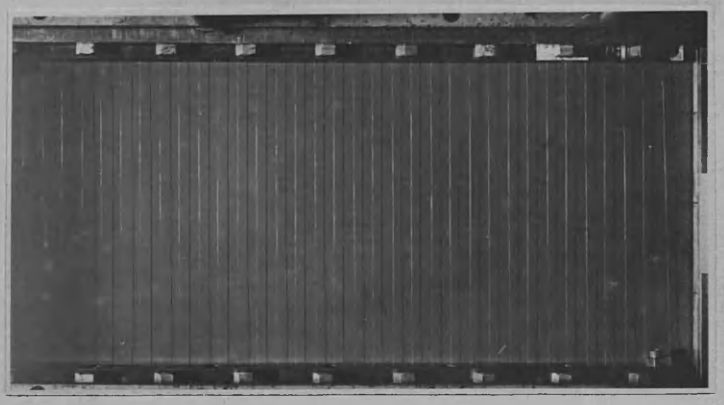

Fig. AV.9 Load = 1865 lbf.

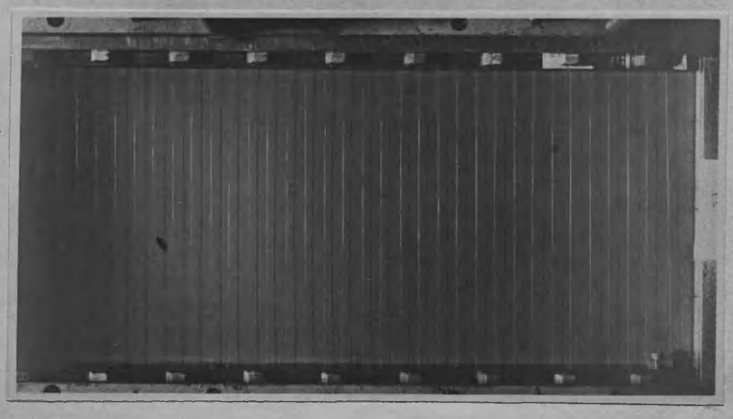

Fig. AV.10 Load = 2940 lbf.

Direction of light.

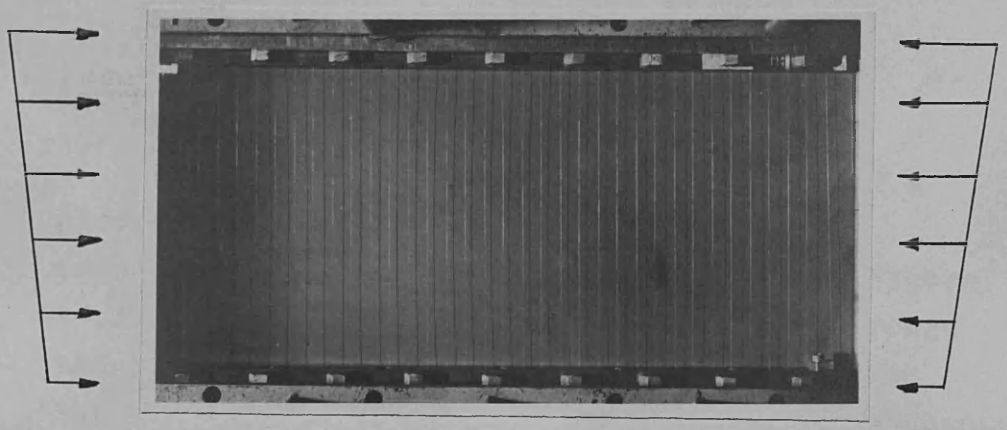

Fig. AV.11 Load = 4150lbf.

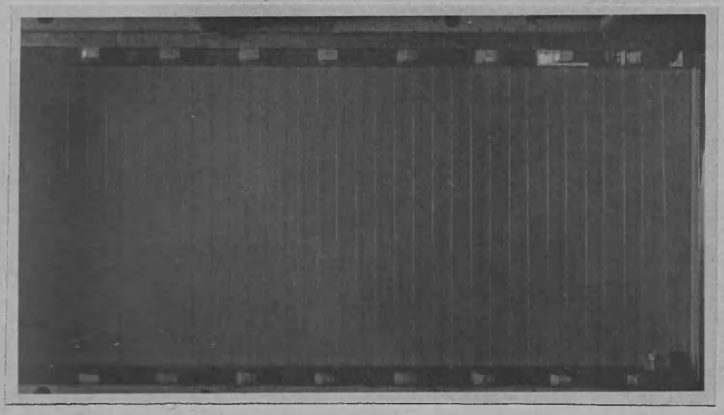

Fig. AV.12 Load = 5090lbf.

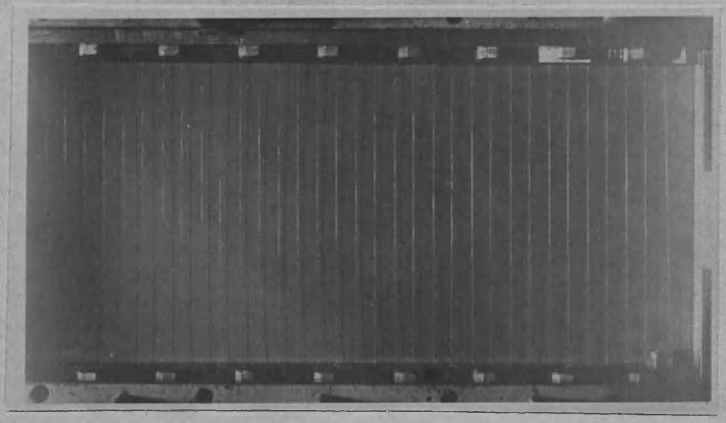

Fig. AV.13 Load = 5320lbf.

Results.

Figure AV.6 shows a specimen contour of a plate which is simply supported along one unloaded edge and fixed along the other. Figure AV.7 shows sections taken longitudinally through the plate at various loads which together with the previous figure were obtained from the sequence of photographs shown in Figures AV.8 - AV.13. Other examples of results from this method are shown in Chapters IV and V and are fully discussed in the latter.

Conclusions.

The "wire-shadow" method of deflection measure-:ment as it has been used has proved invaluable in assessing the efficacy of the experimental boundary conditions and also the mathematical analysis out-:lined in Chapters II and III. It has the advantages over more conventional method of measurement in that a plot can be obtained of the deflection over the whole surface without any contact being made with the test plate and since photographic plates form a perm-:anent record of the state of the test plate they can be reanalysed in the light of any future requirements.

The disadvantages of the method lie mainly in the

difficulties associated with the developing and measuring the fine grain photographic plates - these can be overcome with practice.

A P P E N D I X V I

APPENDIX VI.

MATERIAL PROPERTIES.

(i) Plates.

The rolled steel specimen material was supplied in 6 ft. x 3 ft. sheets which were subsequently guillotined and machined to the required test plate size. During the cutting operation pieces were taken from various locations on the plate to provide test specimens which were dimensioned according to B.S.S. 485. These were tested on a Hounsfield 2 tonf capacity tensometer; the strains being measured either by foil resist-:ance gauges or by a Huggenberger extensometer. Figure AVI.1 shows some typical Load vs. Strain curves for a 0"041 thick plate.

The range of values obtained for some forty specimens was

σ_{yield} 21.7×10^3 - 29.1×10^3 lbf/in^2

E 30.4×10^6 - 35.4×10^6 lbf/in^2

ν 0.223 - 0.280

Average values for use in the calculations were taken at

$\sigma_{yield} = 25.5 \times 10^3$ lbf/in^2 ; $E = 33 \times 10^6$ lbf/in^2 ; $\nu = 0.25$

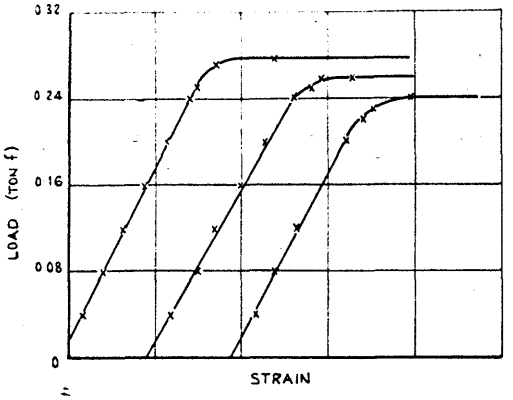

FIG. A VI. 1 PLOTS OF LOAD vs STRAIN FOR TENSILE TEST SPECIMENS

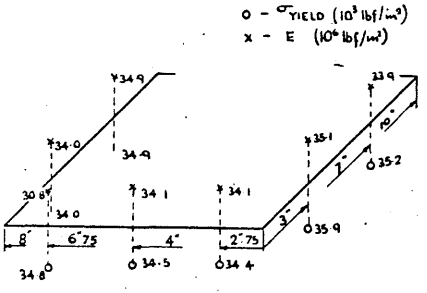

FIG A VI 2. VARIATION OF σYIELD AND E FOR A 0·071 THICK LIPPED CHANNEL

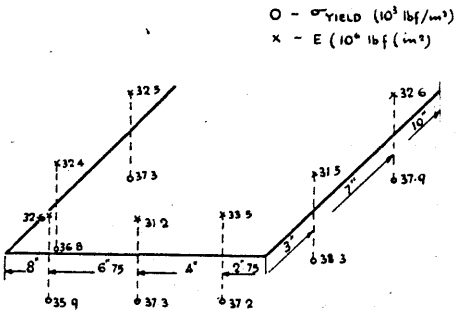

FIG. A. VI. 3 VARIATION OF σYIELD AND E FOR A 0·082 THICK PLAIN CHANNEL

(ii) Channels.

Tensile test specimens were machined from lipped and plain channel sections and Figures AVI.2 and AVI.3 show the variation of the yield stress and Young's Modulus across two such sections. A typical plot for determining Poisson's Ratio is shown in Figure AVI.4, in which the strains were obtained using foil resistance gauges bonded along and across the specimen. With one such pair on top and another bonded identically on the bottom side of the tensile test piece and wired in series any slight bending effects were eliminated.

For the channel material the range of values obtained from about twenty five specimens was

σ_{yield} 32.2×10^3 – 38.3×10^3 lbf/in²

E 30.3×10^6 – 35.3×10^6 lbf/in²

ν 0.226 – 0.272

Here the values used in the calculations were

$\sigma_{yield} = 35 \times 10^3$ lbf/in² ; $E = 33 \times 10^6$ lbf/in² ; $\nu = 0.25$

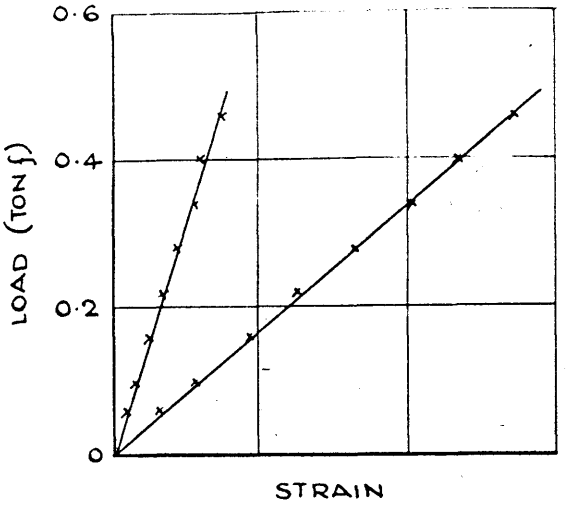

FIG A VI.4 PLOT OF LOAD Vs. STRAIN FOR DETERMINATION OF ν

x 0·0409	x 0·0416	x 0·0411	x 0·0411	x 0·0409	x 0·0412	x 0·0412
x 0·0409	x 0·0416	x 0·0412	x 0·0412	x 0·0410	x 0·0413	x 0·0411
x 0·0409	x 0·0416	x 0·0411	x 0·0412	x 0·0409	x 0·0413	x 0·0412
x 0·0409	x 0·0416	x 0·0411	x 0·0412	x 0·0409	x 0·0412	x 0·0412
x 0·0409	x 0·0415	x 0·0412	x 0·0413	x 0·0409	x 0·0412	x 0·0410

FIG. A VI 5 THICKNESS VARIATION ON A NOMINALLY 0·041" THICK PLATE

Material Thickness.

The material thickness was measured at various points on specimen plates using a ball anvil and a comparator with a ballended stylus. It was found that the thickness variation was generally within ±0".0005 and a typical distri-:bution is shown in Figure AVI.5.